Toxicokinetic Studies on the Synthetic Cannabinoid *Cumyl*-5F-P7AICA in Pigs

Dissertation

zur Erlangung des Grades

des Doktors der Naturwissenschaften

der Naturwissenschaftlich-Technischen Fakultät

der Universität des Saarlandes

von

Nadja Walle

Saarbrücken

2025

Tag des Kolloquiums:	27.01.2026
Dekan:	Prof. Dr.-Ing. Dirk Bähre
Berichterstatter:	Prof. Dr. Markus R. Meyer Prof. Dr. Thorsten Lehr
Vorsitz:	Prof. Dr. Alexandra K. Kiemer
Akad. Mitglied:	Dr. Stefan Boettcher

Vorwort

Die nachfolgende Arbeit entstand unter der Anleitung von Herrn Univ.-Prof. Dr. rer. nat. Markus R. Meyer und Herrn Univ.-Prof. Dr. med. Peter H. Schmidt in der Abteilung Experimentelle und Klinische Toxikologie der Fachrichtung Experimentelle und Klinische Pharmakologie und Toxikologie der Universität des Saarlandes in Homburg/Saar und im Institut für Rechtsmedizin der Universität des Saarlandes in Homburg/Saar von Juli 2019 bis Juli 2025.

Danksagung

An dieser Stelle möchte ich mich ganz herzlich bei all denjenigen bedanken, die mich während der Laborarbeiten und der Erstellung dieser Arbeit in jeglicher Hinsicht unterstützt und motiviert haben, diesen großen Meilenstein in meinem Leben erfolgreich abzuschließen. Ein besonderer Dank geht an die Deutsche Forschungsgemeinschaft (DFG), die durch die finanzielle Förderung eines Großteils des Projektes dieses mit ermöglicht hat.

Von Herzen möchte ich mich an erster Stelle bei meinem Doktorvater Herrn Professor Dr. Markus R. Meyer sowie Herrn Professor Dr. Peter H. Schmidt bedanken, die mir die Möglichkeit gaben, an diesem spannenden und herausfordernden Dissertationsthema zu arbeiten. Vielen Dank für das Vertrauen, das mir über die gesamte Zeit der Arbeit entgegengebracht wurde, die Diskussionsbereitschaft, die stetige Unterstützung sowie die Möglichkeit, aktiv an nationalen und internationalen Fachkongressen teilzunehmen.

Mein besonderer Dank gilt Herrn Professor Dr. Thorsten Lehr für die Übernahme des Koreferats sowie die Möglichkeit zur Durchführung der pharmakokinetischen Modellierungen.

Ein rießengroßer Dank geht an Frau Privatdozentin Dr. Nadine Schäfer für die enorme fachliche Expertise, die Ideen sowie Begleitung der Arbeit, das stets offene Ohr sowie die Umarmungen an schlechten Tagen, die stundenlangen Diskussionen sowie die grenzenlose „24/7-Unterstützung“ in sämtlichen (auch privaten) Bereichen. Ohne sie

wäre ich heute nicht da wo ich bin. Danke für die entstandene tolle Freundschaft. Danke Nadine!

Ein großes Dankeschön geht an Herrn Professor Dr. Michael D. Menger und Herrn Professor Dr. Matthias W. Laschke sowie das gesamte Team des Instituts für Klinische und Experimentelle Chirurgie in Homburg/Saar, ohne deren Unterstützung diese Arbeit nicht möglich gewesen wäre. Vielen Dank für das gesamte Know-How, die stetige Diskussionsbereitschaft sowie die experimentelle und personelle Unterstützung bei der Durchführung der Tierversuche!

Dr. Christiane Dings und Omar Zaher möchte ich für die Durchführung der pharmakokinetischen Modellierungen und die Diskussionsmöglichkeiten danken.

Ein großes Dankeschön geht auch an meine Kollegen, das gesamte Team der Rechtsmedizin Homburg, für die ständige Hilfsbereitschaft und die liebevolle „Wiederaufnahme“ im Team, selbst nach 7 Jahren Auszeit. Ein rießiges Dankeschön geht hier insbesondere auch an Adrian Dörr und Benjamin Peters, für die Unterstützung in sämtlichen Bereichen, sei es bei der Durchführung der Versuche, Diskussionen bei fachlichen Fragestellungen oder das Einbringen neuer Ideen sowie ihres technischen Know-How’s. Danke dafür, dass ihr oftmals meine Launen ertragen habt. Danke für jeden Tag, an dem ihr mich zum lachen gebracht habt, auch wenn es für mich in diesem Moment aussichtslos erschien. Ohne euch wäre alles nur halb so schön gewesen!

Ein großer Dank geht auch an meine Kollegin Nina Röhlen für die bedingungslose Unterstützung, insbesondere während der Formatierung dieser Arbeit.

Bedanken möchte ich mich auch bei meiner ehemaligen Kollegin Frau Dr. Frederike Nordmeier sowohl für die Unterstützung bei den Experimenten, das Aushalten meiner „Fragewut“ als auch das stets offene Ohr und die enorme Hilfsbereitschaft!

Danke auch an Roland Klotz für die Bereitstellung sämtlicher Materialien zur Durchführung der Experimente und die Unterstützung.

Ein rießengroßes Dankeschön geht an all meine Freunde die mich in dieser Zeit über alle Grenzen hinaus unterstützt haben, für mich da waren und auch oftmals „zurückstecken“ mussten. Danke für euer Verständnis und dass ihr so bedingungslos für mich da seid!

Danken möchte ich an dieser Stelle auch Dr. Thorben Fischer für das stetig offene Ohr und die bereits seit dem Studium entstandene Freundschaft!

Vielen Dank an Esther und Georg für die jahrelange Unterstützung, das immer offene Ohr und das Daumendrücken.

Ein rießengroßes Dankeschön geht an meinen Freund Jörg für seine grenzenlose Unterstützung und Geduld. Auch wenn es nicht immer einfache Zeiten waren, er einiges an Frust meinerseits abbekommen und es oftmals viel Kraft gekostet hat, manche Phasen zu überstehen, danke ich von Herzen dafür, dass er immer an meiner Seite stand und mich darin unterstützt hat, das zu tun, was ich liebe. Danke für unsere wundervolle Tochter Malia, die insbesondere in der Endphase meiner Dissertation mit ihren gerade einmal 1,5 Jahren so viel Geduld und Verständnis aufgebracht hat, ohne die ich jetzt nicht so weit wäre, wie ich es bin. Danke mein Sonnenschein! Ich liebe euch!

Die letzten Worte meiner Danksagung möchte ich meiner gesamten Familie widmen: Oma und Opa, Mama (die die Beendigung meiner Promotion leider nicht mehr miterleben darf) und Papa, Bruder Jonas, Patentante Tanja mit Jörg, Celine und Elias, DANKE, dass ihr bereits seit meinem Schulalter IMMER an mich geglaubt und darin unterstützt habt, das zu tun, was ich denke, was ich richtig für mich ist. Ihr habt es mir ermöglicht, diesen Weg zu gehen. Danke für euren liebevollen Zuspruch, insbesondere dann, wenn ich an mir gezweifelt habe. Ich liebe euch!

Für Oma und Opa!

„It always seems impossible until it's done."

Nelson Mandela (1918-2013)

Zusammenfassung

Synthetische Cannabinoide (SC) stellen die größte Gruppe neuer psychoaktiver Substanzen dar. Toxikokinetische (TK) Daten aus kontrollierten Studien stehen oft nicht zu Verfügung. Für die Interpretation von Befunden sind diese indes unerlässlich. Dies betrifft auch die TK in alternativen Matrices, z.B. der Ausatemluft (AAL). Daher wurde in der vorliegenden Arbeit zunächst eine *in vitro* Probenahmetechnik für AAL entwickelt, die in TK-Studien am beatmeten Schwein eingesetzt werden kann, um die TK aufzuklären. Zudem wurde der Metabolismus von *cumyl*-5F-P7AICA in *in vitro* und *in vivo* Modellen untersucht und mit Humandaten verglichen. Dabei zeigte sich, dass das Schweinemodell das humane Stoffwechselmuster am besten vorhersagt. Targets für den Nachweis eines Konsums von *cumyl*-5F-P7AICA sind neben der Muttersubstanz Metabolite, nach oxidativer Defluorierung und anschließender Carboxylierung sowie Monohydroxylierung und Sulfatierung/ Glucuronidierung. In einer Schweinestudie nach inhalativer Verabreichung ergab die Modellierung, dass ein Drei-Kompartiment-Modell die Daten am besten beschreibt, während ein Zwei-Kompartiment-Modell für den *N*-Pentansäure (NPA) Metaboliten besser geeignet ist. Die Untersuchung der Gewebeverteilung zeigte, dass, unabhängig von den Umgebungsbedingungen, Lunge, Galle sowie Duodenalinhalt geeignete Matrices für eine qualitative postmortale Analyse sind. Da das SC und der NPA nur wenig anfällig für postmortale Umverteilung sind, eignet sich auch Herzblut.

Summary

Synthetic cannabinoids (SCs) still represent the largest group of new psychoactive substances. Toxicokinetic (TK) data from controlled studies are often not available, yet indispensable to interpret toxicological findings. This also concerns to the TK in alternative matrices, e.g. exhaled breath (EB). Therefore, an *in vitro* EB sampling technique that can be used in ventilated pigs to elucidate the TK was initally developed in the present work. Furthmore, the metabolic pattern of *cumyl*-5F-P7AICA was investigated using various *in vitro* and *in vivo* models and compared with human data. The pig model was found to predict best the human metabolic pattern. In addition to the parent compound, metabolites formed by oxidative defluorination followed by carboxylation as well as monohydroxylation followed by sulfation or glucuronidation are recommended as targets to detect a consumption of *cumyl*-5F-P7AICA. In a pig study after inhalative administration, a population TK model analysis revealed that a three-compartment model describes the data best, while a two-compartment model is more appropriate for the *N*-pentanoic acid (NPA) metabolite. Investigations on the tissue distribution showed that, independent of the environmental conditions, lung, bile fluid as well as duodenum content are suitable matrices for a qualitative postmortem analysis. Since the SC as well as the NPA are only slightly susceptible to a postmortem redistribution, heart blood is also suitable.

Table of Contents

1. General Part

1.1 Synthetic Cannabinoids

Although ∆9-tetrahydrocannabinol (THC), the main ingredient of the cannabis plant (*Cannabis sativa*), has already shown auspicious effects in medicine, e.g. in pain treatment, consumption is also associated with awkward side effects, such as psychoactivity.[1,2] Hence, various research laboratories have attempted to develop novel therapeutic agents with the same biological activity as THC, but less psychoactive side effects.[2] Subsequently, a large number of structurally heterogenous substances, so-called synthetic cannabinoids (SCs), has been developed.[3,4] As shown in Fig. 1, the history of the SCs dates back to 1974 (Fig. 1). In 1974, Pfizer developed the first non-classical cannabinoid cyclohexylphenol CP 55,940.[2,5] Compared to THC, CP 55,940 structurally lacks the pyran ring structure and acts as a potent agonist at cannabinoid (CB) receptors 1 und 2.[5] In the following years, novel SCs with modified chemical structures were increasingly produced in academic laboratories, with e.g. HU-210, synthesized at the Hebrew University representing a classical cannabinoid with a similar core structure compared to THC.[5–7] In 1995, John W. Huffman (JWH) and his research group developed 1-Naphthyl-(1-pentylindol-3-yl)methanon (JWH-018), a SC with a naphtoylindole moiety showing a 4-fold affinity to the CB 1 receptor and an about 10-fold affinity to the CB 2 receptor, compared to THC.[5] In 2008, JWH-018 was also the first SC discovered in a herbal product so-called ‚Spice'.[3,5,7–9]

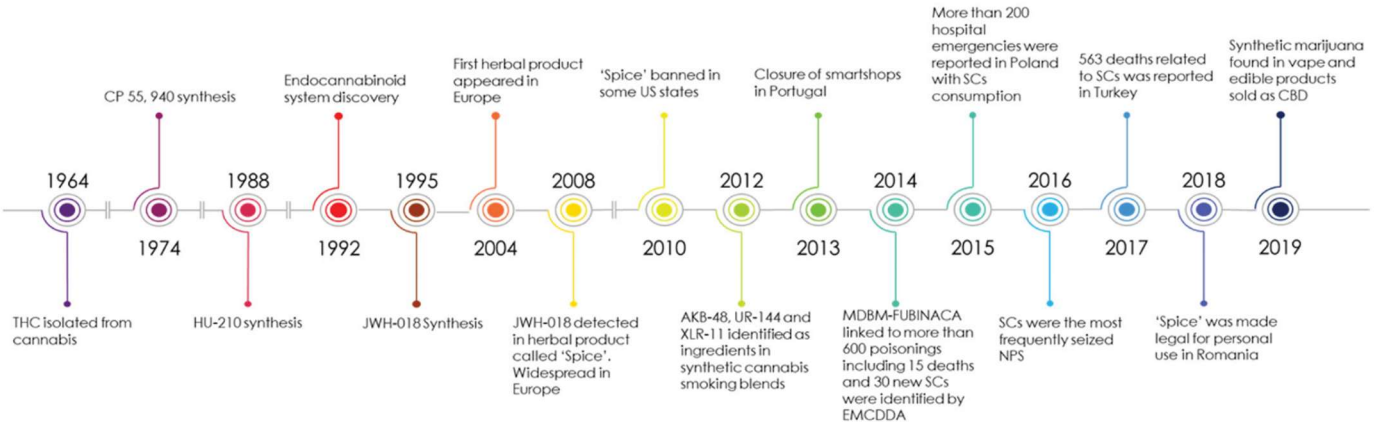

Fig. 1: Timeline of key events in the history of SCs, adopted from Alves et al.[2]

In contrast to THC, SCs typically act as full agonists on CB 1 and/ 2. Hence, they are associated with higher efficiencies, leading to unexpected physical and psychological effects.[7,9,10] As a result, interest in pharmaceutical research declined. At the same time, however, clandestine laboratories became aware of the synthesis of these novel compounds, and interest in marketing them as a 'legal' alternative to cannabis increased. Thus, the 'synthetic cannabinoid phenomenon' associated with a worldwide highly serious health problem was born.

Since then, the number of novel substances detected for the first time has increased enormously. In the period from 2008 to 2023, about 254 new SCs have been monitored by the EU Early Warning System and, alongside stimulants, they remain one of the two largest groups of new psychoactive substances (NPS) worldwide.[4,11] As depicted in Fig. 2 using the example of JWH-018, the chemical structure of SCs is modular and consists of a core structure, a tail, a bridge residue, and a linker (Fig. 2). The structural diversity and thus the high number of novel chemically modified substances arises from the multitude of variations in the respective molecular components. So, for example, a completely new compound can be created by inserting an additional nitrogen atom into the core structure or varying the number of carbon atoms in the side chain. Furthermore, the side chain can additionally be fluorinated or even cyclized and the linker or bridge residue can also be slightly altered by minor modifications.[12–16]

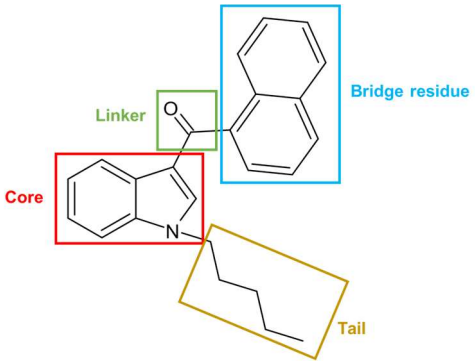

Fig. 2: Schematic representation of the modular structure of SCs using the example of JWH-018.

As isolated substances were restricted and quickly disappeared from the market again, slightly structurally modified compounds, sometimes constitutional isomers, were synthesized in order to circumvent the law. As can be seen by the example of 1-(5-fluoropentyl)-N-(2-phenylpropan-2-yl)-1H-indole-3-carboxamide *(cumyl*-5F-PICA), 1-

(5-fluoropentyl)-N-(2-phenylpropan-2-yl)-1H-indazole-3-carboxamide *(cumyl*-5F-PINACA) and 1-(5-fluoropentyl)-N-(2-phenylpropan-2-yl)-1H-pyrrolo[2,3-b]pyridine-3-carboxamide *(cumyl*-5F-P7AICA) in Fig. 3, a simple ‚scaffold hopping' led to slightly structurally modified, initially legal SCs within a very short time (Fig. 3). Hence, an insertion of a nitrogen atom into the indole core structure of the SC *cumyl*-5F-PICA resulted in the indazole containing SC *cumyl*-5F-PINACA, both being first reported in 2014.[17] Subsequently, in 2015, a simple change in the position of the nitrogen atom led to *cumyl*-5F-P7AICA with a 7-azaindole core.[18] The continuous development of structurally modified SCs has led to the fact that they still represent the largest class of new NPS monitored for the first time by the European Monitoring Centre for Drugs and Drug Addiction (EMCDDA).[4]

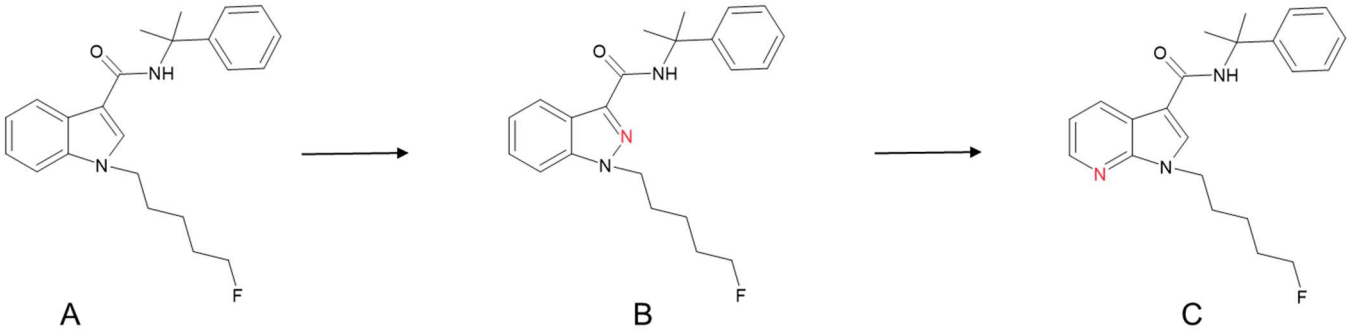

Fig. 3: Scaffold hopping for synthesis of novel synthetic cannabinoids using the example of *cumyl*-5F-PICA **(A)**, *cumyl*-5F-PINACA **(B)**, and *cumyl*-5F-P7AICA **(C)**.

Until today, SCs are still consumed as an alternative to cannabis. Without any knowledge on possible health risks, the herbal incenses are purchased as small colorful sachets or e-liquids cheap and easily accessible via the internet.[2,7,16,19] Due to the manufacturing process, the SC may be distributed inhomogeneously within the herbal product and contaminations between different batches cannot be ruled out.[2] Hence, the consumer is often unaware of the dose and exact identity of SCs actually contained. As a matter of fact, since no preclinical safety data are available for SCs, the consumer often acts as an ‘experimental subject‘. However, this does not deter users from continuing to consume these substances, resulting in increasing reports on life-threatening intoxications or even deaths attributable to the strong physical (e.g. vomiting, nausea, tachycardia, hyperglycemia, seizures) and psychological (e.g. acute psychosis, hallucinations) effects.[20–25] Appropriate toxicokinetic (TK) data are essential

for the interpretation of analytical findings related to the consumption of SCs. In forensic toxicology, this applies, for example, to the question of the driving ability of a person. Ideally, it would be possible to access human TK data for this purpose. Since systematically controlled human studies with SCs are not possible for ethical reasons, alternative *in vitro* and *in vivo* models have to be resorted. Especially regarding SCs with a carboxamide linker, a faster *in vivo* degradation by human carboxlesterases should be kept in mind which may possibly lead to altered TK properties compared to structurally different SCs, as this enzymatic pathway was already reported for several other drugs (of abuse).[26] Hence, the serum-concentration-time profiles of the SC *cumyl*-5F-P7AICA, as a representative of SCs containing a 7-azaindole-carboxamide core structure with a carboxamide linker, as well as its *N*-pentanoic acid (NPA) metabolite, should be assessed and compared to those reported for other SCs in order to clarify potentially altered TK properties attributable to the modified chemical structure (see chapter 3.4).

1.2 Biological Matrices

1.2.1 Conventional Matrices

In clinical and forensic toxicology, body fluids, such as urine and blood, as well as hair specimens still represent the most common matrices for the analytical detection of drugs (of abuse).[27–31] Forensic-analytical issues here relate in particular to the topics drug-facilitated crimes, child-custody cases, monitoring abstinence to drugs/ ethanol or driving under the influence of drugs (DUID). As each of the matrices has its particular advantages and disadvantages, the matrix used for analysis essentially depends on the respective question.

The analysis of blood samples is still considered the gold standard, especially to demonstrate the acute influence of drugs (of abuse) in drug-facilitated crimes or DUID cases.[32] However, due to the invasive sampling procedure, blood collection can not be performed at the scene of the incident or roadside and a phlebotomist has to be involved.[32] This can lead to a longer time interval between the possible offense and blood drawing.[32] Hence, the analytically proven values do not necessarily reflect the values at the time of the incident.

Due to the longer window of drug detection as compared to blood, urine still represents the matrix of choice when the consumption of exogenous substances dating back a

longer period of time has to be verified. This is commonly the case in terms of e.g. abstinence controls. Furthermore, in forensic analysis, urine is often used in cases of sexual offenses in which the administration of e.g. gamma-hydroxybutyric acid is alleged. However, to avoid adulteration, urine should be collected under supervision.[33]
Besides blood and urine, analysis of hair specimens is also implemented in forensic toxicology. Due to the plenty blood circulation of the hair root, drugs (of abuse) can be stored in hair, extending the detection window up to several months retrospectively.[34] Through a segment analysis, the examination of hair samples can also provide information about consumption behaviour and possible habituation to a substance.[35–37] Therefore, analysis of hair specimen is commonly used in the context of e.g. abstinence monitoring, child custody or special questions of drug-related fatalities.[38,39] However, acute consumption of a substance cannot be detected by hair analysis.

1.2.2 Alternative Matrices

Although conventional matrices have been implemented in forensic routine analysis for many years, there is a growing interest in alternative matrices such as oral fluid, sweat or exhaled breath (EB) in forensic toxicology, as they offer a number of advantages compared to blood or urine, comprising an easy and non-invasive sample collection, a reduced danger of adulterations as well as the possibility to test at the crime scene or roadside.[31,40,41]
Due to the high vascular perfusion of the salivary glands, oral fluid represents a valid alternative matrix for drug analysis, since, among other things, depending on the substance-specific physico-chemical properties as well as the pH value of oral fluid, numerous drugs (of abuse) can pass from the blood into saliva.[42–44] However, one disadvantage of oral fluid is the potentially drug-induced xerogenic effect, as e.g. reported after consumption of THC [45,46].
Besides oral fluid, sweat also represents an alternative option for drug analysis. However, sampling of sweat is rather difficult, as used patches can easily become contaminated. Therefore, sweat is not commonly used for routine analysis.
However, EB has been proven to be a promising alternative matrix in recent years, resulting in an increased research interest. The exchange of substances crossing the blood-air barrier between the alveolar capillary network and the air-filled space of the alveoli enables the detection of substances in EB.[47–49] These exhaled so-called

‘volatile organic compounds’ (VOCs) can be of endogenous or exogenous origin.[50,51] As endogenous VOCs represent for example respiratory biomarkers, EB is already used in clinical medicine in the field of pulmonology for diagnosis and monitoring of various lung diseases (e.g. asthma).[52–54] Furthermore, due to its easy, non-invasive and unlimited sample collection, EB also represents an alternative matrix in paediatrics, as blood collection is often difficult and stressful for children.[55]

VOCs with an exogenous origin can e.g. reflect a possible consumption of xenobiotics. The use of EB as an alternative matrix has therefore also become increasingly important in the field of forensic toxicology. Analogously to the already established use of a breath testing in the context of driving under the influence of alcohol, EB could be used as an initial rapid tool to prove an acute influence of drugs, e.g. in the context of DUID. For this reason, a lot of research has already been invested in this area, showing that several pharmaceuticals as well as drugs of abuse, such as THC, methadone, and amphetamine are detectable in EB.[56–60] However, knowledge on the respective TK properties is essential for a toxicologically reliable interpretation of the drugs or pharmaceuticals detected in the EB. Nevertheless, there are still only a few systematically controlled studies regarding the TK properties of substances in EB.[61–67] Some of these studies concerned the TK properties of THC in EB after controlled administration of smoked cannabis.[61,65–68] So far, several different sampling devices were developed to obtain EB from the test subject, for example the sampling device ExaBreath® (SensAbues®, Västerås, Schweden) and the Hound® Marijuana Breathalyzer (Hound Labs Inc., Oakland, CA, USA).[60,69] While the former one can be used to detect many different substances, the Hound® Marijuana Breathalyzer is only designed to detect THC in EB.

However, for future application of EB drug testing e.g. in the context of DUID cases, further in-depth studies on EB are required. For ethical reasons systematically controlled human studies to elucidate the TK properties of drugs of abuse are often not permitted. This also applies to SCs. Therefore, alternative models have to be used. One of these *in vivo* models that has already been proven to be suitable for elucidating the TK properties of NPS, especially SCs, is the pig model.[70–72] Using a ventilator and ventilation of the pigs via a tracheal tube, EB may therefore easily be obtained during the TK study. Thus, the pig model also represents a possibility to clarify the TK data on drugs of abuse in EB. A prerequisite for using the pig model to elucidate the TK properties of drugs of abuse in EB is that sampling of EB can be performed in a

ventilated pig in a controlled and reproducible manner. Since the aforementioned already developed sampling devices require active exhalation, they are not suitable for the *in vivo* pig model. Therefore, a new EB sampling technique for a reproducible detection of SCs, using *cumyl*-5F-P7AICA, should be developed, that can prospectively be applied in the context of TK studies using anesthetized and ventilated pigs (see chapter 3.2).

1.3 Toxicokinetics

In general, TK deals with the physiological processes that occur in the organism after consumption of a substance and affect the respective concentrations. However, in the field of TK, mostly potentially toxic substances are studied. Equivalent to the pharmacokinetics, TK comprises the following processes: liberation, absorption, distribution, metabolism, and elimination. This is also known as the 'LADME model'. However, when conducting a PK study in the field of forensic toxicology, especially regarding SCs, the sub-processes metabolism, distribution, and elimination should be examined in more detail. In particular, respective studies can provide important information on the TK properties of SCs, which can be very helpful in forensic toxicology e.g. in the context of abstinence monitoring, expert opinions in DUID or lethal intoxications.

1.3.1 Metabolism

Due to the constant emerging of novel structurally modified SCs, investigations on a possible ingestion of SCs pose a great analytical challenge in forensic toxicology, particularly applying on DUID cases, abstinence monitoring or suspected intoxications. Studies on the TK properties of SCs show that they are often extensively metabolized and eliminated in form of their metabolites, with only low or even undetectable levels of the parent compound in blood or urine specimen depending on their chemical structure.[73–76] However, if SCs consumption is suspected, urine is a promising matrix, due to its higher metabolite concentrations and longer detection window, and is commonly used for drug (of abuse) testing.[12] As SCs are structurally closely related, even in case of consumption of different SCs, the same metabolites can be formed, further complicating the interpretation of analytical data. Therefore, the knowledge of analytical targets in urine samples after consumption of SCs is essential in order to

carry out a targeted examination and reliable evaluation of urinalysis, e.g. in the context of abstinence monitoring or suspected intoxications.

In general, metabolic processes occurring in the organism convert exogenous and endogenous lipophilic substances into more hydrophilic metabolites, which can subsequently be excreted via e.g. urine. Many different organs are involved in these processes, including the lungs, kidneys and essentially the liver, representing the main organ for drug metabolism processes, especially for those catalyzed by enzymes of the cytochrome P450 monooxigenases (CYP) family.[12,77] *In vivo* metabolism usually occurs in two phases. In the phase I metabolism, functional groups are inserted into the chemical structure of a substance or existing ones are changed through enzymatic reactions, often via the CYP P450 enzyme system. These reactions can include, e.g. oxidations, hydroxylations, hydrolysis, epoxidation or dealkylation.[78,79] Subsequently, the more hydrophilic substances are conjugated with endogenous, usually highly water-soluble substances, such as glucuronic or sulfuric acid. These reactions are also catalyzed by conjugating enzymes, such as sulfotransferases or uridine 5'-diphospho-glucuronosyltransferases.[79,80] However, if a suitable binding site, e.g. a hydroxyl group, already exists, phase II reactions can also occur directly, without prior phase I reactions. Due to their highly lipophilic properties, SCs are extensively metabolized by CYP enzymes and mainly excreted into urine via their metabolites. Main phase I reactions appear to be dependent on the chemical structure of the respective SCs. As already mentioned in chapter 1.1, SCs have a modular structure (Fig. 2). Hence, aromatic and aliphatic hydroxylation, e.g. on a cumyl moiety in the bridge residue or on the carbon side chain, is one of the main metabolic pathways. The coupled aliphatic hydroxy groups can then be further oxidized to ketones or carboxylic acids.[12,81–84] Since the hydrogen atom of the terminal pentyl side chain carbon is often substituted by a fluorine atom to enhance potency of SCs, oxidative defluorination (OxF) is a typical phase I reaction of these substances, yielding to initially 5-OH-pentyl and subsequent pentanoic acids.[12,85] Further phase I reactions are N- and O-dealkylations and ester or amide hydrolysis.[12,81,82] After these initial biotransformation processes, substantial phase II reactions are glucuronidation or sulfation. However, glucuronidation seems to be the main step.[81,84,86]

There are various ways to elucidate the metabolic pattern of a substance. The best approaches are systematically controlled human studies. However, these are not ethically justifiable for clarifying the metabolic pattern of SCs. Hence, to interpret

toxicological findings, published data on authentic human urine, e.g. from clinical overdose emergency cases, can be used. However, this procedure is afflicted with the disadvantage that often neither the time and frequency, nor the dosage and type of the consumed substances are known. Thus, alternative models have to be used. For this purpose, various *in vitro* and *in vivo* assays are available so far.[87–93] Already well-established *in vitro* approaches are based on pooled human liver s9 fraction (pHS9), hepatocyte cell culture, pig liver microsomes (PLM) as well as pooled human liver microsomes (pHLM) and cytosol. The major advantages of those *in vitro* models are the simplicity, the easy handling and storage as well as the low costs.[88] On the contrary, all *in vitro* approaches act as a static model and no statement can be made on the quantity of human *in vivo* metabolites. In addition, the metabolites formed do not necessarily reflect renally eliminated substances, so that a primary analytical target for human urinanalysis cannot be determined. Therefore, *in vivo* (animal) models can be used. Examples for *in vivo* approaches are the zebrafish larvae[89,91,92,94], the rat model[12,87,95] or the chimeric mouse model[90,92]. Compared to *in vitro* models, *in vivo* experiments offer various advantages. First, substances can be administered in a systematically controlled manner. In addition, relevant physiological processes occuring after ingestion can be considered and the metabolic pattern of a substance can be elucidated depending on time. The usage of zebrafish larvae is further advantageous, as animal experiment requests can be circumvented up to 120 h post-fertilization. Even if these *in vivo* models have some advantages, they are also afflicted with various disadvantages. The rat or chimeric mouse model only provide small amounts of body fluids. Furthermore, due to possibly different enzyme patterns, the formation of metabolites may be different compared to human[12,96]. Another approach for conducting *in vivo* TK studies is the pig model.[71,93,97,98] Compared to the aforementioned models, this approach additionally offers the advantage that a repeated sampling procedure of a higher amount of body fluids and tissues is possible. As pigs are very similar to humans in terms of their physiological propertis[99,100], anatomical structure[100,101], and CYP enzymes[102,103], they have already been shown to be suitable for several metabolism studies, especially for elucidation of the TK properties of NPS.[97,104–107] To determine the best suited model for elucidation of metabolic pattern of SCs, in this study different *in vitro* and *in vivo* assays should be compared using the SC *cumyl*-5F-P7AICA, as a representative for SCs containing a 7-azaindole core structure and a carboxamide linker (see chapter 3.1).

1.3.2 Distribution and Elimination

As far as the TK of a substance is concerned, distribution begins immediately after absorption of the consumed drug into bloodstream, followed by a distribution into various body fluids, tissues, and organs. This process is necessary to ensure that the respective compound reaches the drug target in a suffient concentration. However, the extent of distribution and also the efficacy of a drug is dependent on the route of administration and thus the bioavailability, representing the percentage of the active compound that reaches the bloodstream in an unchanged form. When conducting a TK study, this should be well-considered. Pulmonary administration, e.g. by smoking a joint or more recently by vaporization of so-called ‘c-liquids’ using e-cigarettes, represents the usual route of administration for SCs.[2,10,19] However, the extent of the bioavailable fraction remains unknown, attributable to e.g. unavowed depth of puffs or frequency. Furthermore, a heat-induced pyrolytic degradation during smoking has already been reported for several SCs, leading to an unknown fraction of the active substance being inhaled.[73,108,109] As already known for THC, oral ingestion of cakes or muffins represents an alternative route of administration. This was sometimes also chosen for SCs.[81,110] However, the bioavailable fraction also remains unknown here, as nothing is known about the amount of substance passing the bio membranes, resulting in bioavailabilities of <100% after both inhalation and oral intake, although the exact level is unknown, which makes it difficult to create an adequate TK model. One possibility to determine the amount of substance reaching the lungs after inhalative administration would be the conduction of an already established *in vitro* drug delivery efficiency test after nebulization of the respective SC.[111] However, this application also bears the disadvantage that the total amount of substance reaching the systemic circulation cannot be clarified, as various ‘lung defense mechanisms’ such as a pulmonary first-pass effect and metabolism of the substance can occur.[112–115] Therefore, the only sensible way to circumvent this issue is an intravenous (i.v.) administration. As the entire dose of the substance is administered directly into the systemic circulation, this results in a 100% bioavailability and an exact quantification for the development of an TK model is possible.

As a requirement to build a TK model evaluation of concentration-time profiles of a drug is necessary. On this basis plasma or serum concentrations might be interpreted e.g. in the context of DUID cases to assess the driving ability. For this purpose, the organism is contemplated as a system of kinetic compartments. This so-called

compartmental analysis represents an extensive mathematical model, helping to predict and describe the respective concentration-time profile based on different TK parameters, such as the volumes of distribution (Vd), the area under the curve (AUC), the elimination half-lifes (t½), or the clearance (Cl).[116] Here, Vd represents an apparent volume and provides information on the extent of distribution of a drug in the body. Moreover, the AUC is proportional to the bioavailable amount of a substance and describes the integral of the concentration-time profile and t½ represents the period of time the concentration of a substance has dropped by half. The Cl is a measure of the detoxification performance of the kidneys and describes the blood volume that has been cleared of a certain substance per time.[117] When conducting a compartmental analysis as part of a TK study, various models have to be considered. In a one-compartment model, a substance is hypothetically distributed in the whole body as a single central compartment (blood and quickly equalizing tissues).[118] Within the framework of a multi-compartment model, a further distribution of a substance into one or more additional peripheral compartments, representing slowly equalizing tissues, as well as a potential redistribution between these compartments are additionally taken into consideration.[119] A distinction is made between different phases in the application of these models. Generally, a TK model consists of a distribution (α), an elimination (β), and a tissue release (γ) phase. In the α-phase, in addition to the decrease of the concentration of a substance in the central compartment, also the increase of the concentration in one or more compartments is considered. In the subsequent β-phase, both concentrations then decrease at the same rate, after a certain state of equilibrium has been reached.[116]

Two different approaches can be used for TK modeling: the individual and the population (pop) TK model. An individual TK modeling is useful, if a complete individual TK profile should be defined or a fast turnaround of the TK parameters of a substance is needed. In typical, this approach applies a non-compartmental analysis und requires extensive concentration-time data.[120] In contrast to an individual TK approach, a pop TK modeling relies on the concentration-time data from multiple individuals, often also on pooled data from several studies, applying complex mathematical and compartmental methods.[120,121] In addition to concentration-time data, this model also incorporates further data on covariates (including weight, gender, age or renal/ hepatic function), allowing to clarify the sources of interindividual variability of the TK within a population. Therefore, due to the complexity of developing a pop TK model, this is

often a time-consuming process. Moreover, pop TK modeling offers the advantage to predict the TK across populations or nonclinical species through allometric scaling, by extrapolating the TK data e.g. from adults to paediatrics or animals to human.
Thus, allometric scaling offers the possibility to clarify the TK of drugs, e.g. SCs, based on data from animal studies and is an important tool for the predicition of human data, as these cannot be collected applying human studies due to ethical reasons.
In addition to the distribution into the bloodstream, forensic toxicology also requires knowledge on the extent of tissue distribution of SCs. For example, storage in adipose tissue (AT) was already reported for several SCs, which, analogously to THC, also exhibit lipophilic properties.[122,123] Accordingly, a time-dependent redistribution from AT into the bloodstream has to be considered, resulting in a longer terminal t½ and thus a longer detection window, especially after chronic consumption. This should be considered when interpreting toxicological findings. In addition, minor modifications in the chemical structure of SCs can lead to higher potencies, as already reported for e.g. the fluorine-for-hydrogen replacement at the terminal carbon of the pentyl side chain.[124] As consumers are often unaware of the type and amount of SCs contained in a herbal blend, consumption of such slightly modified substances can lead to life-threatening intoxications or even death.[2,110,125–128] Especially in forensic toxicology, knowledge on the tissue distribution is therefore indispensable to interpret toxicological findings in fatalities involving SCs. For this, one possibility would be refering on data of published case reports. However, this is afflicted with the disadvantage that in these cases often neither the dose nor the time of consumption is known. As far as human studies are concerned, only a few self-experiments with just one or two participants are available.[10,19,129] A few systematically controlled studies using the pig model have been published so far to clarify the tissue distribution of SCs, as these animals have shown several similarities to humans in terms of their physiological properties (for more details see chapter 1.3.1). These data are based on SCs with a naphthoylindole or benzoylindole structure, such as 4-ethylnaphthalen-1-yl-(1-pentylindol-3-yl)methanone (JWH-210) or 2-(4-methoxyphenyl)-1-(1-pentylindol-3-yl)methanone (RCS-4). Regarding structurally modified SCs with the incorporation of a carboxamide moiety, such as methyl 2-{[1-(5-fluoropentyl)-1H-pyrrolo[2,3-b]pyridin-3-yl]formamido}-3,3-dimethylbutanoate (5F-MDMB-P7AICA) or *cumyl*-5F-P7AICA, a faster *in vivo* degradation by human carboxylesterases would be conceivable, as it is already known for several other drugs (of abuse).[26] This could possibly lead to changed TK properties

compared to older SCs. In the framework of an *in vitro* study on several SCs with a carboxamide moiety but various bridge residues using different isoforms of recombinant human carboxylesterases, Wagmann et al. reported on an enzymatic cleavage of ester moieties in the bridge residue, while the carboxamide linker remains stable.[130] So far, only a few systematically controlled *in vivo* studies regarding the TK properties on SCs with a carboxamide linker are available.[71,107,131] For example, a fast degradation to the respective mebabolite was reported on the SC 5F-MDMB-P7AICA, as this substance contains an ester moiety in the bridge residue in addition to the carboxamide linker.[107]

Thus, in the comprehensive TK study conducted in this work, the TK properties of the SC *cumyl*-5F-P7-AICA, as a representative for SCs containing a carboxamide linker without any further ester moiety, as well as its NPA metabolite, should be assessed in a systematically controlled manner using the pig model and should then be compared to already published data on the SCs JWH-210, RCS-4, and 5F-MDMB-P7AICA (see Chapter 3.4).

1.4 Postmortem Stability

As in postmortem (PM) cases various parameters, such as the dose and the time of ingestion, the time of death and the PM interval (PMI) are often unknown, interpretation of such analytical data poses a major challenge to forensic toxicology. For example, during the agony phase, further metabolism and elimination of the substance are possible, resulting in changes of PM drug concentrations, while the extent depends on the duration of this phase.[132] In addition, various processes occur PM in the body of the deceased, which can also significantly influence the measured substance concentration. First, a PM formation might occur, as already known for e.g. ethanol, gamma hydroxybutyrate or amitriptyline.[132,133] Additionally, due to a PM decrease of pH and a microbial colonization of the corpse, probably impacting the PM stability of the consumed drugs in the respective body fluids and tissues, a PM drug degradation is also possible.[132,133] Furthermore, a passive diffusion should be taken into account, as PM autolysis causes a disintegration of cellular membranes, allowing the substances contained in the respective body fluid or tissue specimen to diffuse into surrounding tissues.[132,134–137] Those phenomena are summarized under the term ‘PM redistribution’ (PMR), whereby the extent is dependent, on the one hand, on the physicochemical properties of a substance (e.g. lipophilicity) and its TK properties (e.g.

V_d), and, on the other hand, on the PMI or the sampling site.[132,137,138] Such site-dependent concentration changes of the drug concentration are attributable to e.g. an incomplete distribution at the time of death, protein degradation, hemolysis (decay of red blood cells) or hypostasis (sinking into lower regions of the body due to gravity), particulary if the drug shows a binding affinity to red blood cells or proteins.[132,133] To sum up, these processes should be considered, when interpreting PM toxicological findings as the drug concentrations found in PM tissue or body fluids do not directly reflect the concentrations at the time of death, quickly leading to a misinterpretation, if data on the PM TK properties of the respective drug are not available. Therefore, data on the tissue distribution, the respective susceptibility to PMR and the PM stability are indispensable for the interpretation of PM toxicological findings.

A further challenge regarding the assessment of PM analytical data arises from the prevailing state of putrefaction of a corpse, which can vary greatly depending on the respective environmental or storage conditions, such as sourrounding humidity, oxygen availability or temperature. This has already been described by Johann Ludwig Casper by means of the so-called ‚Casper-rule‘, which states that the degree of putrefaction of a corpse after one week's storage in air approximately corresponds to that of a two weeks‘ storage in water or a eight weeks’ storage in soil.[139,140] As the extent of the PMR as well as the PM stability of a drug essentially depend on the degree of putrefaction of a corpse, an environmental-dependent change of these parameters of a drug due to a delayed onset of autolysis should also be considered, e.g. if the corpse is stored under oxygen-deficient conditions. Regarding SCs, data on the PM time- and temperature-dependent TK properties were published for JWH-210, RCS-4, as well as their metabolites, whereby a change of concentration could especially be observed for RCS-4 and HO-RCS-4.[70] However, until now, data on the PMR and PM stability of SCs in body fluids and tissues stored under oxygen-deficient conditions, such as water storage, are lacking.

Therefore, the time- and oxygen-dependent PM stability as well as the susceptibility to PMR of *cumyl*-5F-P7AICA and its NPA metabolite under different storage conditions (air vs. water) should be investigated and compared to the perimortem distribution using the pig model (see chapter 3.3).

2. Aims and Scopes

Continuous modifications in the chemical structure of SCs, resulting in 'novel' compounds, pose a major challenge for a profound interpretation of toxicological findings, e.g. in DUID cases or abstinence control monitoring. During the last few years, alternative matrices, such as EB, have gained increasing attention, as they are often easily and readily accessible without any physical interventions or interferences with the personality of an individual. In the context of DUID cases, breath testing is already well-established to prove an acute influence of alcohol. Furthermore, several studies have already shown that various drugs (of abuse) are detectable in EB. However, TK data are essential for a reliable forensic toxicological interpretation of the analytical data obtained, but are often not available, particularly concerning NPS. As human studies are not allowed for ethical reasons, alternative models must be developed to obtain respective data.

Hence, the aim of the present dissertation was to elucidate the TK properties of SCs with a 7-azaindole core structure and a carboxamide linker in a systematically and controlled manner using the pig model after inhalative and i.v. administration. For a comprehensive knowledge on the TK, the metabolic fate of *cumyl*-5F-P7AICA, a representative for this class, should initially be investigated using different *in vitro* and *in vivo* assays. Subsequently, the results should be compared with already published data in order to find the most suitable and practicable assay for the investigation of new NPS. In addition, the time-dependent distribution of *cumyl*-5F-P7AICA in serum, blood and tissue specimens, its kinetic properties as well as the time- and environmental-dependent PM stability should be assessed. In order to expand the possibilities of clarifying the TK properties of SCs in EB, a sampling technique should be developed for future application in anesthetized and ventilated pigs to collect EB in a systematically controlled and reproducible manner.

For these purposes, the following steps had to be carried out:

- Development of a new sampling technique in an *in vitro* pig lung model to collect EB in a systematically controlled and reproducable manner, that can prospectively be applied to anaesthetized and ventilated pigs for the detection of SCs, using *cumyl*-5F-P7AICA as a representative for SCs containing a 7-azaindole core structure

- Development of an analytical liquid chromatography-tandem mass spectrometry (LC-MS/MS) method for the detection and quantification of *cumyl*-5F-P7AICA in EB

- Determination of the metabolic pattern of *cumyl*-5F-P7AICA in pig urine using LC-high resolution (HR)-MS/MS, identication of its targets using different *in vitro* and *in vivo* assays and comparison with each other as well as with already published *in vitro* and human data

- Elucidation of concentration-time profiles of SCs containing a carboxamide moiety, using *cumyl*-5F-P7AICA as a representative, after i.v. and inhalative administration to pigs and comparison with those already published for JWH-210 and RCS-4

- Modeling of the concentration-time profiles and evaluation, if this model can be used to predict human data

- Determination of the perimortem distribution pattern of *cumyl*-5F-P7AICA, a representative for SCs containing a 7-azaindole core structure, as well as its NPA metabolite in a representative set of specimens, such as relevant tissues, organs and body fluids, after inhalative administration using the pig model

- Investigations on the time- and oxygen-dependent PM concentration changes of *cumyl*-5F-P7AICA and its NPA metabolite in the organ, tissue, and body fluid specimens already selected to determine the perimortem distribution and comparison with those found in perimortem specimens

3. Results

The results of the studies were published in the following articles:

3.1 Comparison of *in vitro* and *in vivo* models for the elucidation of metabolic patterns of 7-azaindole-derived synthetic cannabinoids exemplified using *cumyl*-5F-P7AICA[141]

(DOI: 10.1002/dta.2899)

Author Contributions:

Nadja Walle conducted and evaluated the experiment as well as composed the manuscript; Frederike Nordmeier, Adrian A. Doerr, and Benjamin Peters assisted with the execution of the in vitro and animal experiments; Matthias W. Laschke and Michael D. Menger carried out and enabled the animal experiments and assisted with scientific discussions; Peter H. Schmidt, Markus R. Meyer, and Nadine Schaefer assisted with scientific discussions and supervised the research.

Received: 19 May 2020 | Revised: 6 July 2020 | Accepted: 11 July 2020

DOI: 10.1002/dta.2899

RESEARCH ARTICLE

WILEY

Comparison of *in vitro* and *in vivo* models for the elucidation of metabolic patterns of 7-azaindole-derived synthetic cannabinoids exemplified using cumyl-5F-P7AICA

Nadja Walle[1] | Frederike Nordmeier[1] | Adrian A. Doerr[1] | Benjamin Peters[1] | Matthias W. Laschke[2] | Michael D. Menger[2] | Peter H. Schmidt[1] | Markus R. Meyer[3] | Nadine Schaefer[1]

[1]Institute of Legal Medicine, Saarland University, Homburg, Germany

[2]Institute for Clinical and Experimental Surgery, Saarland University, Homburg, Germany

[3]Department of Experimental and Clinical Toxicology, Center for Molecular Signaling (PZMS), Saarland University, Homburg, Germany

Correspondence
Nadine Schaefer, Institute of Legal Medicine, Saarland University, Building 49.1, 66421 Homburg, Germany.
Email: nadine.schaefer@uks.eu

Abstract

Due to the dynamic market involving synthetic cannabinoids (SCs), the determination of analytical targets is challenging in clinical and forensic toxicology. SCs usually undergo extensive metabolism, and therefore their main metabolites must be identified for the detection in biological matrices, particularly in urine. Controlled human studies are usually not possible for ethical reasons; thus, alternative models must be used. The aim of this work was to predict the *in vitro* and *in vivo* metabolic patterns of 7-azaindole-derived SCs using 1-(5-fluoropentyl)-*N*-(2-phenylpropan-2-yl)-1*H*-pyrollo[2,3-*b*]pyridin-3-carboxamide (cumyl-5F-P7AICA) as an example. Different *in vitro* (pooled human liver S9 fraction, pooled human liver microsomes, and pig liver microsomes) and *in vivo* (rat and pig) systems were compared. Monooxygenase isoenzymes responsible for the most abundant phase I steps, namely oxidative defluorination (OF) followed by carboxylation, monohydroxylation, and ketone formation, were identified. In both *in vivo* models, OF/carboxylation and *N*-dealkylation/monohydroxylation/sulfation could be detected. Regarding pHS9 and pig urine, monohydroxylation/sulfation or glucuronidation was also abundant. Furthermore, the parent compound could still be detected in all models. Initial monooxygenase activity screening revealed the involvement of CYP2C19, CYP3A4, and CYP3A5. Therefore, in addition to the parent compound, the OF/carboxylated and monohydroxylated (and sulfated or glucuronidated) metabolites can be recommended as urinary targets. In comparison to literature, the pig model predicts best the human metabolic pattern of cumyl-5F-P7AICA. Furthermore, the pig model should be suitable to mirror the time-dependent excretion pattern of parent compounds and metabolites.

KEYWORDS

cumyl-5F-P7AICA, pigs, 7-azaindolesynthetic cannabinoidsurinary excretion pattern

1 | INTRODUCTION

In the past few years, new psychoactive substances (NPS), especially synthetic cannabinoids (SCs), appeared on the market via the Internet or head shops as a "legal" alternative to Δ^9-tetrahydrocannabinol (THC), because they were initially not controlled. In the following years, the number of different SCs on the market increased steadily.[1] According to the published European Drug Report 2018 of the European Monitoring Centre for Drugs and Drug Addiction (EMCDDA), SCs represent the largest group of NPS.[2] In addition to being the legal alternative to common drugs, the easy accessibility, the cheap availability, and the fact that SCs can hardly be detected in toxicological routine screenings are the main consumption motives. As they act as full agonists at cannabinoid receptors (CB1 and CB2),[2–5] compared to THC higher potencies such as psychoactive effects are expected, leading to an increasing number of intoxications, mass intoxications, and even deaths.[1,6–10] Therefore, they gained increased attention in forensic toxicological analytics. Data on the toxicokinetic (TK) and toxicodynamic properties of SCs are necessary for the interpretation of clinical and forensic toxicological results, but for ethical reasons, human studies are often not possible.

One of the so-called new-generation SCs is 1-(5-fluoropentyl)-*N*-(2-phenylpropan-2-yl)-1*H*-pyrollo[2,3-*b*]pyridin-3-carboxamide (cumyl-5F-P7AICA), first reported in 2015. Since April 2018, cumyl-5F-P7AICA has been subject to the narcotic law in Germany. Concerning its toxicodynamic properties, Asada et al reported that cumyl-5F-P7AICA acts as a nonselective cannabinoid receptor agonist at CB1 and CB2 receptors.[5] Until today, only little is known about the TK property of cumyl-5F-P7AICA.[11–14]

In general, *in vitro* and *in vivo* assays are available for the elucidation of TK properties. As described elsewhere,[15–17] already-established *in vitro* assays are based on pooled human liver microsomes (pHLM) and cytosol, hepatocyte cell cultures, and pig liver microsomes (PLMs) as well as the pooled human liver S9 fraction (pHS9). Staeheli et al first reported on the *in vitro* metabolism of cumyl-5F-P7AICA using pHLM.[13] The benefits of those *in vitro* assays are low cost and easy handling/storage.[17] Nevertheless, the disadvantage of all *in vitro* models is that they act as a static and the only qualitative model. In contrast, *in vivo* models allow one to consider relevant physiological processes of the body.

As far as cumyl-5F-P7AICA is concerned, *in vivo* data regarding major metabolic pathways have already been published using human urine.[11] The interpretation of the findings was limited, because nothing was known about the time of consumption, the dose, and user habits.[11] Therefore, alternative systematic studies under controlled conditions must be performed for better interpretation and assessment of human TK properties. Common *in vivo* systems to determine the metabolic patterns of drugs are the zebrafish larvae,[18] the rat model after oral administration,[15] the chimeric mouse model after oral administration,[19] and the pig model.[20–22] Zebrafish larvae are a new *in vivo* model to circumvent an animal experiment request up to 120 h post-fertilization. Yet post-mortem studies are not possible. Rats are comparably easy to handle and maintain, but only small volumes of body fluids are available. Due to the transplantation of human hepatocytes, the chimeric mouse model has already proven to be suitable as an alternative animal model for human administration studies.[19] In analogy to the rat model, chimeric mice are also limited by the small amount of body fluids, resulting in a long sample interval of 24 or 48 h. In comparison, the amount of available body fluids and tissues is higher in pigs. Therefore, repeated sampling is possible, enabling the elucidation of metabolic excretion patterns. In addition, pigs have a great similarity to humans in terms of anatomical structure[23,24] and isoenzymes[25,26] as well as physiological properties, and they have already proven to be suitable in TK studies of other SCs as well as synthetic opioids,[16,20–22,27,28] thus justifying the difficult and laborious experimental procedure for research purposes.

To determine which system is best suited and most practicable to investigate new NPS, different assays should be compared. Cumyl-5F-P7AICA was particularly chosen to study the different *in vitro* and *in vivo* metabolism assays, because certain *in vitro* (pHLM[13]) and human[11] metabolism data have already been published and may be compared with our results. Thus, in the present work, the metabolic pattern of cumyl-5F-P7AICA was determined and its targets were identified using different *in vitro* (pHLM, PLM, pHS9 fraction) and *in vivo* (rat/pig) assays. The obtained results were compared with each other as well as with already-published *in vitro* and *in vivo* data.[11,13] In addition, the main enzyme cytochrome P450 isoenzymes (CYP) was identified.

2 | MATERIALS AND METHODS

2.1 | Chemicals and reagents

Cumyl-5F-P7AICA (purity 99.72%) was provided by the German Federal Criminal Police Office (Wiesbaden, Germany). HPLC-grade ethanol was purchased from Fisher Scientific (Loughborough, United Kingdom). Glucuronidase (EC no. 3.2.1.32)/arylsulfatase (EC no. 3.1.6.1) from *Helix pomatia* L, LC-MS-grade methanol, analytical-grade ammonium formate, LC-MS-grade formic acid, LC-MS-grade acetonitrile, potassium chloride (KCl), ethylenediaminetetraacetic acid disodium salt (Na_2EDTA), and all other analytical-grade chemicals and reagents were obtained from Merck (Darmstadt, Germany). pHLM from 25 individual donors with 20-mg microsomal protein per milliliter and 330 pmol of total CYP P450 per milligram protein, pHS9 from 30 individual donors with 20-mg protein per milliliter, baculovirus-infected insect cell microsomes (Supersomes)-

containing 1 nmol/mL of human complementary DNA (cDNA)-expressed cytochrome P450 monooxygenases (CYP) CYP1A2, CYP2A6, CYP2B6, CYP2C8, CYP2C9, CYP2C19, CYP2D6, CYP2E1 (2 nmol/mL), CYP3A4, CYP3A5 (2 nmol/mL), or flavin-containing monooxygenase (FMO) 3 (5 mg protein per milliliter) as well as the UGT (uridine diphosphate [UDP]-glucuronosyltransferase) reaction mix solutions A (25 mM UDP-glucuronic acid) and B (250 mM Tris–HCl, 40 mM $MgCl_2$, and 0.125 mg/mL of alamethicin) were provided by Corning (Amsterdam, the Netherlands). Nicotinamide adenine dinucleotide phosphate ($NADP^+$) was purchased from Biomol (Hamburg, Germany), and superoxide dismutase (SOD), isocitrate, isocitrate dehydrogenase (IDH), dithiotreitol (DTT), reduced glutathione (GSH), acetyl coenzyme A (AcCoA), acetyl carnitine, 3′-phosphoadenosine-5′-phosphosulfate (PAPS), *S*-(5′-adenosyl)-L-methionine (SAM), and phenylmethylsulfonylfluoride were obtained from Sigma-Aldrich (Taufkirchen, Germany). The Pierce BCA Protein Assay Kit was purchased from ThermoFisher Scientific (Schwerte, Germany).

All enzyme solutions, microsomes, and CYPs were thawed at 37°C. Then they were snap-frozen in liquid nitrogen and stored at −80°C for further analysis.

2.2 | Preparation of PLM

For the preparation of PLM, the liver of one drug-free Swabian Hall strain pig, obtained from Emil Faerber GmbH & Co. KG (Zweibrücken, Germany), was used.[16] The liver was stored at −80°C for further analysis. As previously described,[16] 12.5 g of liver was cut into small pieces. After the addition of homogenization buffer (0.154 M KCl, 1 mM Na_2EDTA) in a ratio of 15%–20% tissue/volume and phenylmethylsulfonylfluoride (10 μg/mL), the liver was homogenized and centrifuged at 10 000*g* for 15 min. Then, the supernatant was filled in the centrifugation tubes and ultra-centrifuged at 3°C–4°C and 100 000*g* for 1.15 h. The pellet (microsomes) was resuspended in washing buffer (0.154 M KCl) and centrifuged again at 3°C–4°C and 100 000*g* for 1.15 h. After the pellet (microsomes) was resuspended in storing buffer (0.154 M KCl, 0.1 mM Na_2EDTA), the microsomes were aliquoted and stored at −80°C for further analysis.

For the determination of the obtained protein concentration, a Pierce BCA Protein Assay Kit was used. A mixture of reagent A: reagent B (50:1) was mixed with a part of the produced protein solution. After the mixture was shaken and incubated for 30 min at 60°C, the protein concentration was determined by a photometric measurement (540 nm) of the absorption using a bovine serum albumin calibration curve.

2.3 | Incubation conditions and sample preparation for identification of phase I and II metabolites using pHS9 fraction

According to the experimental design published by Richter et al[17] and other published studies,[15,29] 100 U/mL of SOD, 0.1 mM AcCoA, 2.3 mM acetyl carnitine, 2.5 mM isocitrate, 0.8 U/mL of IDH, 0.6 mM $NADP^+$, 2.5 mM Mg^{2+}, 25 μg/mL of alamethicin (UGT reaction mix solution B) and 90 mM phosphate buffer (pH 7.4) were initially preincubated for 10 min at 37°C with a final protein concentration of 2 mg/mL of pHS9. Then, 40 μM aqueous PAPS, 1 mM DTT, 2.5 mM UDP-glucuronic acid (UGT reaction mix solution A), 1.2 mM SAM, and 10 mM GSH were added to the previously produced and preincubated solution. To start the reactions, 25 μM cumyl-5F-P7AICA in phosphate buffer (substrate) was added. All concentrations stated earlier are final concentrations. After the solution was incubated for 60 min at 37°C, 60 μL of the mixture was transferred into a reaction tube, and the reaction was stopped by adding 20 μL of ice-cold acetonitrile. The remaining mixture was further incubated for 5 h. The reactions were stopped by adding 30 μL of ice-cold acetonitrile, and the solutions were cooled at −18°C for 30 min and then centrifuged at 14 000 rpm for 2 min. After the supernatant was transferred into autosampler vials, 5 μL of the solution was injected into a liquid chromatography (LC)–high-resolution mass spectrometry (HRMS) system described later, which is based on an Orbitrap. To remove impurities and possibly interfering compounds, additional blank (without pHS9) and control samples (without substrate) were prepared and incubated.

2.4 | Incubation conditions and sample preparation for initial CYP activity screening and identification of phase I metabolites using pHLM/PLM

The samples were incubated according to already-published standard incubation conditions, containing 25 μM cumyl-5F-P7AICA (substrate) and 50 pmol/mL of each CYP isoenzyme (CYP1A2, CYP2A6, CYP2B6, CYP2C8, CYP2C9, CYP2C19, CYP2D6, CYP2E1, CYP3A4, or CYP3A5), 0.25 mg protein per milliliter FMO3, or 1 mg protein per milliliter of pHLM or PLM.[16,17,29,30] All incubation mixtures had a final volume of 50 μL and contained 200 U/mL of SOD, the $NADP^+$ regenerating system (containing 5 mM isocitrate, 0.5 U/mL of IDH, 5 mM Mg^{2+}, 1.2 mM $NADP^+$), 90 mM phosphate buffer (pH 7.4), and the substrate as well as the respective enzymes. According to the manufacturer's manual, phosphate buffer was replaced with 90 mM Tris buffer (pH 7.4) in incubations with CYP isoenzymes CYP2A6 and CYP2C9. After preincubation for 10 min, the $NADP^+$ regenerating system was added to start the reactions. All mixtures were incubations at 37°C. After 30 min the incubation was stopped by the addition of 50 μL of ice-cold acetonitrile. Then, the mixtures were centrifuged for 2 min at 14 000 rpm. After 50 μL of the supernatant was transferred into autosampler vials, 5 μL of the solution was injected into an LC–HRMS/MS system. According to the already-described sample preparation using pHS9, additional control samples (without substrate) were prepared and incubated.

2.5 | *In vivo* studies

2.5.1 | Rat

As already described elsewhere,[30–32] the experiment was performed using urine samples from one male Wistar rat (Charles River, Sulzfeld,

Germany) for toxicological diagnostic reasons according to German law. First, one blank rat urine sample was collected before drug administration for removing possible interfering compounds. Then, a single dose of 0.6 mg/kg body weight (BW) of cumyl-5F-P7AICA was orally administered in an aqueous suspension via a gastric intubation. The urine sample of the rat was collected separately from feces over a period of 24 h. The animal was housed in a metabolism cage and had water ad libitum. The urine samples were aliquoted and stored at −20°C for further analysis.

2.5.2 | Pig

The *in vivo* experiment was performed in accordance with the German legislation on protection of animals and the National Institutes of Health Guide for the Care and Use of Laboratory Animals (permission number: 44/2019). According to already-published studies,[16,20–22,27] one domestic male pig of the Swabian Hall strain with a BW of 43.2 kg was used. During the housing, the pig had free access to tap water and daily standard chow. For 12 h before the experiment, the animal had free access to water but was kept fasting.

Surgical procedures

The surgical procedures were performed in accordance with previous studies.[16,20–22,27,28] First, the animal received an intramuscular injection of 30 mg/kg BW of ketamine hydrochloride (Ursotamin, Serumwerke Bernburg, Bernburg, Germany), 2.5 mg/kg BW of xylazine hydrochloride (Rompun, Bayer, Leverkusen, Germany), and 1 mg of atropine (Braun, Melsungen, Germany) as premedication. For maintenance of analgosedation, 2%–4% of isoflurane (Forene, AbbVie, Ludwigshafen, Germany) was administered through inhalation. During the whole experiment, the animal was mechanically ventilated with a 1:2 v/v mixture of oxygen and air (FiO_2 of 0.30, Respirator ABV-U, F. Stephan GmbH, Gackenbach, Germany) and volume cycled with a tidal volume of 10–12 mL/kg BW. To ensure sufficient fluid replacement with 0.9% of sodium chloride (8 mL/kg/h, Braun), the left ear vein was catheterized. For blood sampling and monitoring of the mean central venous pressure, a triple-lumen 7F (Certofix Trio, Braun) central venous catheter was placed in the jugular vein. In addition, a suprapubic catheter (Cystofix, Braun) was placed in the bladder for collecting urine. Following the aforementioned measures, the animal was then allowed to stabilize for 10–15 min.

Study design

First, 2 mL of a stock solution containing 5 mg/mL of cumyl-5F-P7AICA in ethanol was prepared. To obtain the desired dose of 200 μg/kg BW, the required volume of the stock solution (1728 μL) was filled with ethanol (272 μL) to a volume of 2 mL. Analogous to previous studies,[27,28] the prepared solution was administered within 12 min by nebulization of cumyl-5F-P7AICA applying the inspiration-triggered mode (<0.2 mL/min) of the M-neb flow$^+$ ventilation ultrasonic nebulizer MN-300/7 (Nebutec, Elsenfeld, Germany). Through the inspiratory limb and the tracheal tube, the aerosol was delivered into the ventilated lung of the pig. The urine samples were collected hourly (t_1 = 0–1 h, t_2 = 1–2 h, t_3 = 2–3 h, t_4 = 3–4 h, t_5 = 4–5 h, t_6 = 5–6 h, t_7 = 6–7 h, and t_8 = 7–8 h) after the beginning of inhalative administration. In addition, one urine sample was collected before administration (t_0). All collected urine samples were stored at −20°C for further analysis.

2.6 | Preparation of rat and pig urine samples for identification of phase I and II metabolites

According to published procedures,[15,30,33] phase I and II metabolites in urine samples were identified after protein precipitation with acetonitrile. Therefore, 100 μL of urine was mixed with 500 μL of acetonitrile. After shaking, the mixture was centrifuged for 2 min at 14 000 rpm. The supernatant was transferred into new vials and then evaporated to dryness under a gentle stream of nitrogen at 60°C. Subsequently, the residue was dissolved in 50 μL of a mixture of eluents A and B (1:1, v/v). The composition of the eluents is described in the next section. The solution was transferred into autosampler vials, and 1 μL of the solution was injected into an LC–HRMS/MS system.

2.7 | LC–HRMS/MS apparatus

As already described in other studies,[15,16] the extracts were analyzed using a Dionex UltiMate 3000 RS pump consisting of a degaser, a quaternary pump, and an UltiMate autosampler (ThermoFisher Scientific, Dreieich, Germany). The used LC system was coupled to a TF Q-Exactive Plus system equipped with a heated electrospray ionization (HESI)-II source.

The gradient elution of the LC system was performed using a TF Accucore Phenylhexyl column (100 × 2.1 mm, 2.6 μm), with mobile phases consisting of 2 mM aqueous ammonium formate plus 0.1% (v/v) formic acid and 0.1% (v/v) acetonitrile (pH 3, eluent A) and 2 mM ammonium formate solution with acetonitrile/methanol (50:50, v/v) plus 0.1% (v/v) formic acid and 1% (v/v) water (eluent B). The column oven temperature was set to 60°C. The settings of the gradient and the flow rate of the eluents were as follows: 0–1.0 min 99% A (0.5 mL/min flow rate), 1–10 min to 1% A (0.5 mL/min flow rate), 10–11.5 min hold 1% A (0.8 mL/min flow rate), 11.5–13.5 min hold 99% A (0.8 mL/min flow rate).

The settings for the HESI-II-source were as follows: spray voltage, 3.00 kV; heater temperature, 320°C; sheath gas, 60 arbitrary units (AU); auxiliary gas, 10 AU; and S-lens RF level, 60.0.

The mass spectrometer was operated in positive-ionization mode with full scan (FS) and a subsequent data-dependent acquisition (DDA) mode. According to the manufacturer's recommendations, mass calibration was done before analysis using external mass calibrators. For FS mode, the following settings were defined: maximum injection time (IT), 120 ms; resolution, 35.000; scan range, *m/z* 200–650; microscans, 1; and automatic gain control (AGC) target,

TABLE 1 Identification (ID), cumyl-5F-P7AICA and its metabolites, elemental composition, exact masses, accurate masses, characteristic product ions, mass errors, and retention time (RT) of the compounds detected in pooled human liver microsome, pig liver microsome, pooled human liver S9 fraction incubations, rat urine after oral administration, and pig urine after inhalative administration

ID	Cumyl-5F-P7AICA and its metabolites	Elemental composition	Monoisotopic exact masses	Monoisotopic accurate masses	Error (ppm)	Accurate fragment masses (*m/z*)								
						Product 1	Error (ppm)	Product 2	Error (ppm)	Product 3	Error (ppm)	Product 4	Error (ppm)	RT (min)
	Cumyl-5F-P7AICA	**$C_{22}H_{26}ON_3F$**	**368.2132**	**368.2129**	**−0.9399**	**250.1349**	**−0.5776**	**233.1083**	**−0.8213**	**145.0395**	**−0.7159**	**119.0857**	**1.7179**	**7.63**
M0	Carboxamide	$C_{13}H_{16}ON_3F$	250.1350	250.1346	−1.8586	233.1082	−1.3450	207.1289	−1.3604	145.0394	−1.3471	119.0604	0.6122	7.63
M1	Oxidative defluorinated (OF) and carboxylated	$C_{22}H_{25}O_3N_3$	380.1968	380.1965	−0.9613	262.1183	−1.1492	244.1078	−0.9611	201.1021	−0.7871	119.0857	1.6538	6.71
M2	Monohydroxylated[1]	$C_{22}H_{26}O_2N_3F$	384.2081	384.2075	−1.7238	250.1348	−0.9436	145.0397	0.6518	135.0804	−0.2051	107.0494	2.7750	7.32
M3	Monohydroxylated[2]	$C_{22}H_{26}O_2N_3F$	384.2081	384.2078	−1.0883	266.1297	−0.8710	145.0396	−0.6107	119.0857	1.6538	91.0547	5.4784	6.71
M4	Ketone	$C_{22}H_{24}O_2N_3F$	382.1925	382.1915	−2.6255	264.1140	−0.8983	247.0876	−0.5328	221.1081	−1.6940	119.0857	1.5898	7.06
M5	*N*-Dealkylated	$C_{17}H_{17}ON_3$	280.1444	280.1442	−0.8681	162.0662	−0.1625	119.0606	1.6374	–	–	–	–	6.13
M6	Dihydroxylated[1]	$C_{22}H_{26}O_3N_3F$	400.2030	400.2030	−0.3098	250.1350	0.0934	233.1084	−0.2322	151.0754	0.4505	123.0443	1.6426	6.53
M7	Dihydroxylated[2]	$C_{22}H_{26}O_3N_3F$	400.2030	400.2030	−0.1573	282.1247	−0.4281	239.1184	−2.6030	162.0658	−2.5163	119.0858	2.1023	6.32
M8	OF-monohydroxylated[2]	$C_{22}H_{27}O_3N_3$	382.2125	382.2123	−0.4629	264.1342	−0.4266	203.1181	1.0505	119.0857	1.8460	91.0549	7.8245	6.14
M9	Carboxamide-monohydroxylated[2]	$C_{13}H_{16}O_2N_3F$	266.1299	266.1298	−0.6417	223.1241	−0.0813	174.0663	0.5500	145.0397	0.1258	119.0606	2.0860	6.79
M10	Monohydroxylated[3]	$C_{22}H_{26}O_2N_3F$	384.2081	384.2066	−4.1067	266.1301	0.5050	223.1240	−0.5600	161.0346	0.1395	135.0553	0.0625	7.19
M11	*N*-Dealkylated-monohydroxylated[3]	$C_{17}H_{17}O_2N_3$	296.1393	296.1383	−3.5378	178.0608	−0.8954	161.0348	1.6556	135.0553	0.2885	–	–	5.38
M12	*N*-Dealkylated-monohydroxylated[1]	$C_{17}H_{17}O_2N_3$	296.1393	296.1399	1.8209	162.0658	−2.2338	145.0395	−1.2419	135.0804	−0.5440	119.0604	0.1636	5.04
M13	OF-carboxamide and carboxylated	$C_{13}H_{15}O_3N_3$	262.1186	262.1183	−1.3821	244.1077	−1.5237	201.1020	−1.2424	145.0395	−1.2419	119.0605	1.2529	6.56
M14	OF-carboxamide	$C_{13}H_{17}O_2N_3$	248.1393	248.1393	−0.1636	231.1126	−0.7751	205.1335	−0.1977	145.0396	−0.1898	131.0604	0.2650	6.74
M15	OF	$C_{22}H_{27}O_2N_3$	366.2176	366.2172	−1.1197	248.1391	−0.9015	231.1125	−1.2372	205.1334	−0.5697	119.0857	1.5898	6.73
M16	OF-monohydroxylated[1]	$C_{22}H_{27}O_3N_3$	382.2125	382.2133	2.0921	248.1394	0.3283	205.1334	−0.5697	135.0805	0.5856	107.0495	3.7728	6.02
M17	Dihydroxylated[1 + 2]	$C_{22}H_{26}O_3N_3F$	400.2030	400.2020	3.3504	266.1285	−5.4579	223.1242	0.5341	135.0808	2.5059	107.0500	7.6214	5.88
M18	*N*-Dealkylated-monohydroxylated[1] and sulfated	$C_{17}H_{17}O_5N_3S$	376.0961	376.0956	−1.3979	296.1393	−0.0340	162.0659	−1.7630	135.0810	3.9744	119.0605	0.7403	4.86
M19	Monohydroxylated[1] and sulfated	$C_{22}H_{26}O_5N_3FS$	464.1649	464.1661	2.3275	384.2087	1.4534	250.1354	1.4355	233.1088	1.5352	135.0807	2.0541	6.18
M20	Monohydroxylated[1] and glucuronidated	$C_{28}H_{34}O_8N_3F$	560.2402	560.2398	−0.8256	384.2081	−0.2940	250.1349	−0.5776	135.0805	0.4726	107.0495	3.1314	6.09
M21	Dihydroxylated[1 + 2] and sulfated	$C_{22}H_{26}O_6N_3FS$	480.1599	480.1604	1.0194	400.2032	0.2239	266.1301	0.6197	135.0806	1.0374	119.0609	4.1365	5.62
M22	Dihydroxylated[1 + 1] and sulfated	$C_{22}H_{26}O_6N_3FS$	480.1599	480.1607	1.6550	400.2019	−2.9788	250.1350	−0.1506	151.0755	1.0565	123.0443	−0.0936	6.55
M23	*N*-Dealkylated-monohydroxylated[1] and glucuronidated	$C_{23}H_{25}O_8N_3$	472.1714	472.1718	0.6602	296.1385	−2.8164	162.0658	−2.5163	135.0800	−3.5940	119.0608	3.6239	4.34
M24	Monohydroxylated[2] and glucuronidated	$C_{28}H_{34}O_8N_3F$	560.2402	560.2360	−7.5802	384.2092	2.6449	266.1302	1.1931	174.0665	1.9526	119.0860	4.0243	6.43

Note. 1, aryl-monohydroxylated; 2, 5-fluoropentyl-monohydroxylated; 3, 7-azaindole-monohydroxylated.

1e6. The DDA mode was used, with the addition of an inclusion list containing the *m/z* values of expected compounds. The following settings were programmed for DDA mode: maximum IT, 250 ms; resolution, 17 500; AGC target, 2e5; loop count, 5; isolation window, 1.0 *m/z*; dynamic exclusion, off; spectrum data type, profile; underfill ratio, 0.5%; option "do not pick others," enabled; microscans, 1; high collision dissociation with stepped normalized collision energy, 17.5%, 35%, and 52.5%. For data handling, TF Xcalibur Qual Browser software version 3.0.63 was used.

3 | RESULTS AND DISCUSSION

3.1 | Dosage

A 0.6 mg/kg BW dose was administered orally to the rat. For the study of pigs, a 200 μg/kg BW dose was inhalatively administered, resulting in a total dose of ∼8.64 mg. These doses were calculated based on reports of common drug users, recommending a dose of SC in the range of 0.5 – 20 mg, depending on the route of administration.[34] In addition, comparable dosages have already been established in previous studies on NPS.[16,21,22,27,28]

3.2 | General findings

The aim of the study was to identify the *in vitro* and *in vivo* metabolic patterns of cumyl-5F-P7AICA and compare the results with already-published pHLM and human data. In all blank and control samples of the *in vitro* assays as well as in all rat and pig urine specimens collected before drug administration, neither the parent compound nor any metabolite could be found. In all blank samples as well as in pHS9-, pHLM-, and PLM incubations, a compound with a mass of *m/z* 250.1346 could be detected. The mass difference of *m/z* 118.0786 to the precursor mass (PM) of the parent compound (*m/z* 368.2132) indicated a cleavage of the cumyl moiety. The resulting carboxamide M0 (Table 1; Figure S1 [supporting information]) was identified by the product ion (PI) at *m/z* 233.1082 representing hydrolysis of the amide moiety, *m/z* 207.1289 indicating the cleavage of the complete amide residue, and the PI at *m/z* 145.0394 and *m/z* 119.0604 corresponding to an unaltered 7-azaindole core structure. Therefore, M0 has been identified as an impurity, but interfering substances could be excluded.

Metabolites of cumyl-5F-P7AICA could clearly be identified in all *in vitro* as well as in all *in vivo* assays using LC–HRMS/MS fragmentation. The parent compound (Table 1; Figure 1) could still be observed in all *in vitro* assays and in rat urine, as well as in the early pig urinary samples.

Cumyl-5F-P7AICA (protonated mass, PM of *m/z* 368.2132, Table 1; Figure 1) was identified by the PI at *m/z* 233.1083 and *m/z* 250.1349, indicating a cleavage at the amide moiety. Furthermore, the PI at *m/z* 145.0395 and *m/z* 174.0661 represented an unaltered 7-azaindole core structure. The additional presence of *m/z* 119.0857 has resulted from an unaltered cumyl moiety, whereas *m/z* 91.0548 exhibited cumyl moiety after the cleavage of the methyl units. The fragmentation pattern of the parent compound is consistent with the findings of Bovens et al.[14]

The respective metabolites were identified by comparison of their MS^2 spectra with the MS^2 spectra of the parent compound cumyl-5F-P7AICA. An overview of all tentatively identified phase I and II metabolites using *in vitro* and *in vivo* assays is presented in Table 1. The table includes elemental composition, exact masses, accurate masses, mass error, characteristic fragment ions, and retention time. Due to the high number of metabolites found, not all are discussed in detail in the following section.

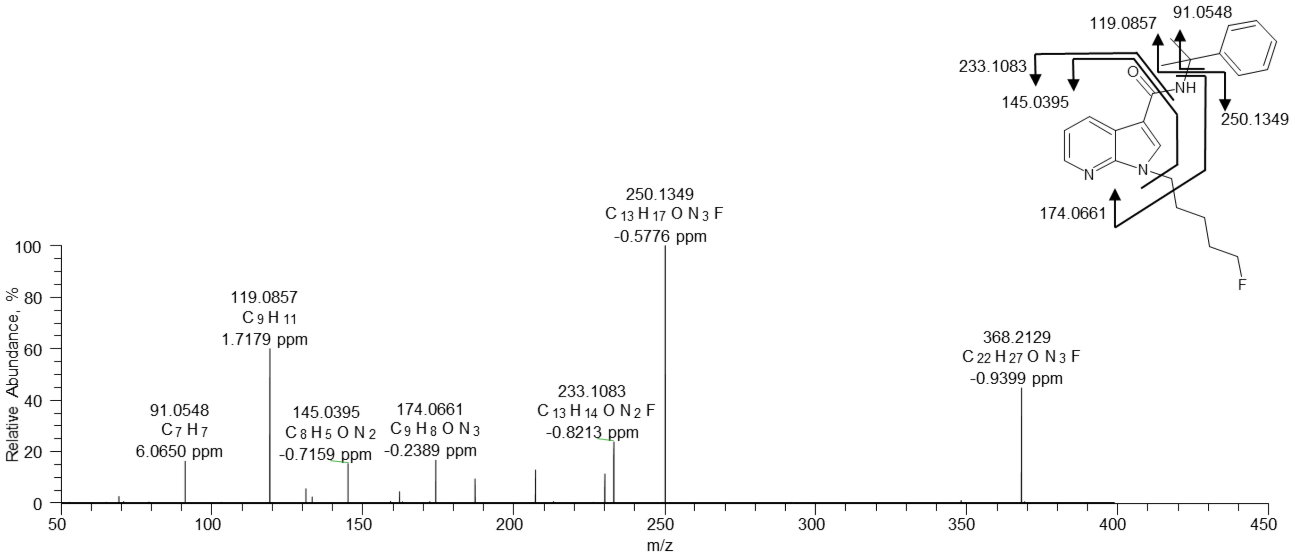

FIGURE 1 HRMS/MS spectra of cumyl-5F-P7AICA identified in pooled human liver S9 fraction incubation containing 25 μM cumyl-5F-P7AICA [Colour figure can be viewed at wileyonlinelibrary.com]

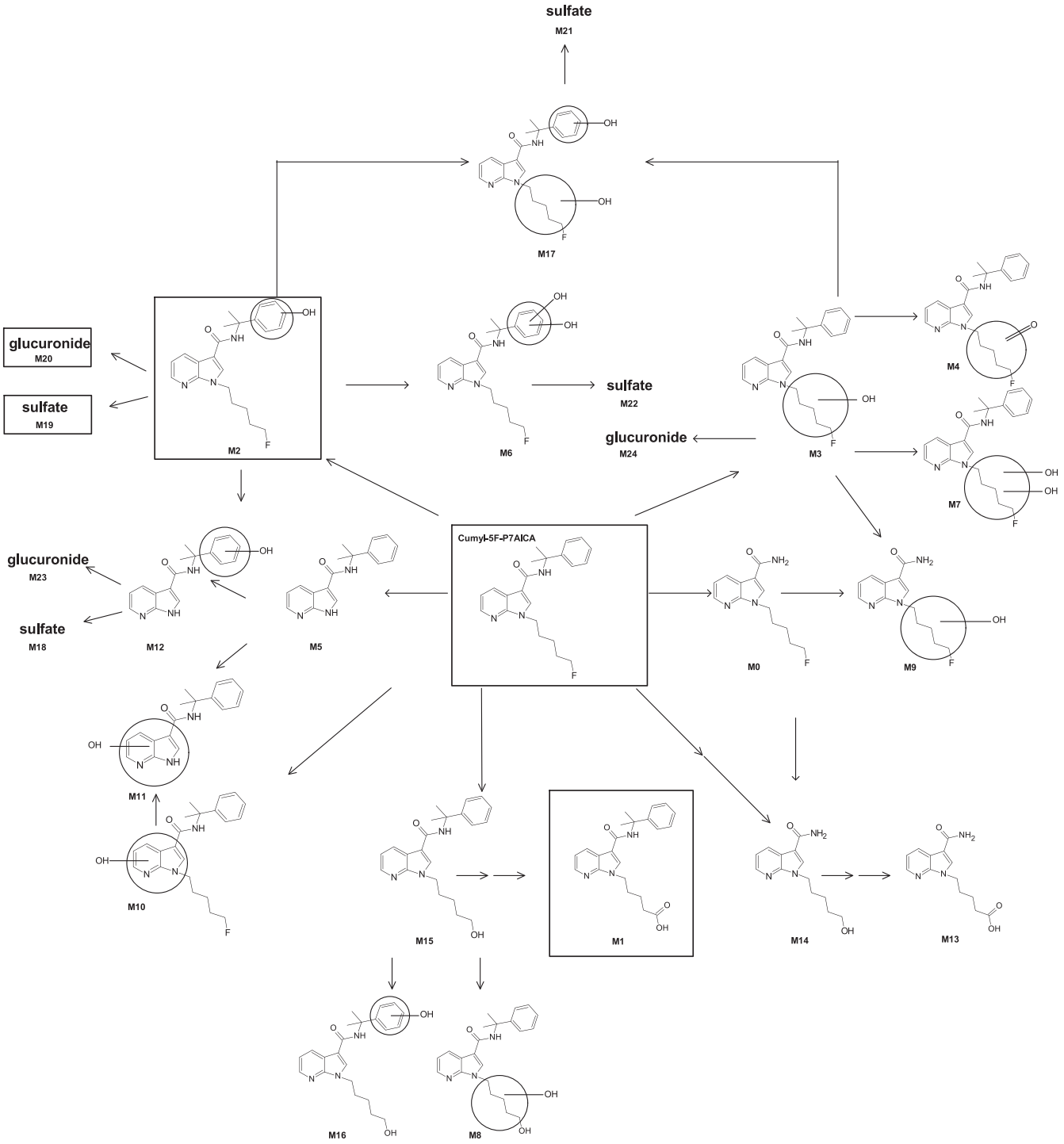

FIGURE 2 Metabolic patterns of cumyl-5F-P7AICA (M0–M24) elucidated in pooled human liver S9 fraction, pooled human liver microsomes/published data using pHLM,[9] pig liver microsomes, rat urine, pig urine, and/or human urine (HU).[7] Urinary targets are marked in boxes

3.3 | LC–HRMS/MS fragmentation and identification of cumyl-5F-P7AICA and its *in vitro* phase I and II metabolites using pHLM, PLM, and pHS9

3.3.1 | pHLM/PLM

Eleven phase I metabolites could be detected in pHLM and PLM incubation samples (Figure 2). In addition to the already-described presence of the parent compound, major metabolic pathways of cumyl-5F-P7AICA seemed to be oxidative defluorination (OF) followed by carboxylation, aryl-monohydroxylation, 5-fluoropentyl-monohydroxylation, and ketone formation, as well as *N*-dealkylation in both *in vitro* incubation assays. In addition, aryl-dihydroxylation could be detected in pHLM incubation.

The OF/carboxylated metabolite (M1, PM of *m/z* 380.1968, Table 1; Figure 3) was identified by the most abundant and characteristic PI at *m/z* 119.0857 and *m/z* 262.1183, indicating the cleavage of the cumyl moiety. As already shown in the fragmentation pattern of cumyl-5F-P7AICA, the PI at *m/z* 91.0548 suggested the cumyl moiety after the cleavage of the methyl units. The unaltered 7-azaindole core structure was identified by the PI at *m/z* 145.0396. The cleavage of the C–O bond of the carboxyl unit resulted in the PI at *m/z* 244.1078 and *m/z* 201.1021, whereas the amide moiety is still present at *m/z* 244.1078.

The aryl-monohydroxylated metabolite (M2, PM of *m/z* 384.2081, Table 1; Figure 4A) was identified by the PI at *m/z* 135.0804 and *m/z* 107.0494, which can be explained by a mass shift of +16 u of the fragmentation pattern of the unaltered cumyl moiety of cumyl-5F-P7AICA with *m/z* 119.0857 and *m/z* 91.0548. The PI at *m/z* 250.1348 indicated the cleavage of the hydroxylated cumyl moiety. The additional presence of the PI at *m/z* 145.0397 and *m/z* 174.0660 resulted from an unaltered 7-azaindole core structure.

In comparison, the 5-fluoropentyl-monohydroxylated metabolite (M3, PM of *m/z* 384.2081, Table 1; Figure 4B) was identified by the PI at *m/z* 266.1297, *m/z* 119.0857, and *m/z* 91.0547, indicating the cleavage of the cumyl moiety. The PI at *m/z* 266.1297 exhibited a hydroxylation at the 5-fluoropentyl or 7-azaindole moiety. The additional presence of the PI at *m/z* 145.0396 and *m/z* 174.0661 suggested an unaltered 7-azainole core structure. Therefore, hydroxylation was formed at the 5-fluoropentyl moiety.

Ketone formation resulting in M4 (PM of *m/z* 382.1925, Table 1; Figure S2 [supporting information]) was identified by the PI at *m/z* 264.1140 and *m/z* 119.0857, indicating the cleavage of the cumyl moiety. Hydrolysis of the amide unit was identified by the PI at *m/z* 247.0876, whereas *m/z* 221.1081 exhibited the cleavage of the bond between the amide and the 7-azaindole core.

The *N*-dealkylated metabolite (M5, PM of *m/z* 280.1444, Table 1; Figure 5A) was identified by the presence of the most abundant and characteristic PI at *m/z* 162.0662, representing cleavage of the cumyl moiety. The unaltered 7-azaindole core structure formed the PI at *m/z* 119.0606.

The aryl-dihydroxylated metabolite (M6, PM at *m/z* 400.2030, Table 1; Figure S3A [supporting information]) was identified by the presence of the PI at *m/z* 250.1350, which could also be found in HRMS/MS spectra of the aryl-monohydroxylated metabolite, as well as the parent compound, indicating no hydroxylation at the 7-azaindole or 5-fluoropentyl moiety. The cleavage of the dihydroxylated aryl moiety was also characterized by the PI at *m/z* 151.0754 and *m/z* 123.0443, which can be explained by a mass shift of +32 u to the PI at *m/z* 119.0857 and *m/z* 91.0548 of the unaltered cumyl moiety or +16 u to the PI at *m/z* 135.0804 and *m/z* 107.0494 of the aryl-monohydroxylated part.

Furthermore, the 5-fluoropentyl-dihydroxylated metabolite (M7, PM at *m/z* 400.2030, Table 1; Figure 3B) was identified by the PI at *m/z* 119.0858, indicating the cleavage of the cumyl moiety. The PI at *m/z* 282.1247 and *m/z* 239.1184, indicating the hydroxylation at the 7-azaindole core or 5-fluoropentyl chain, and the additional presence of *m/z* 162.0658 resulted from an unaltered 7-azaindole core.

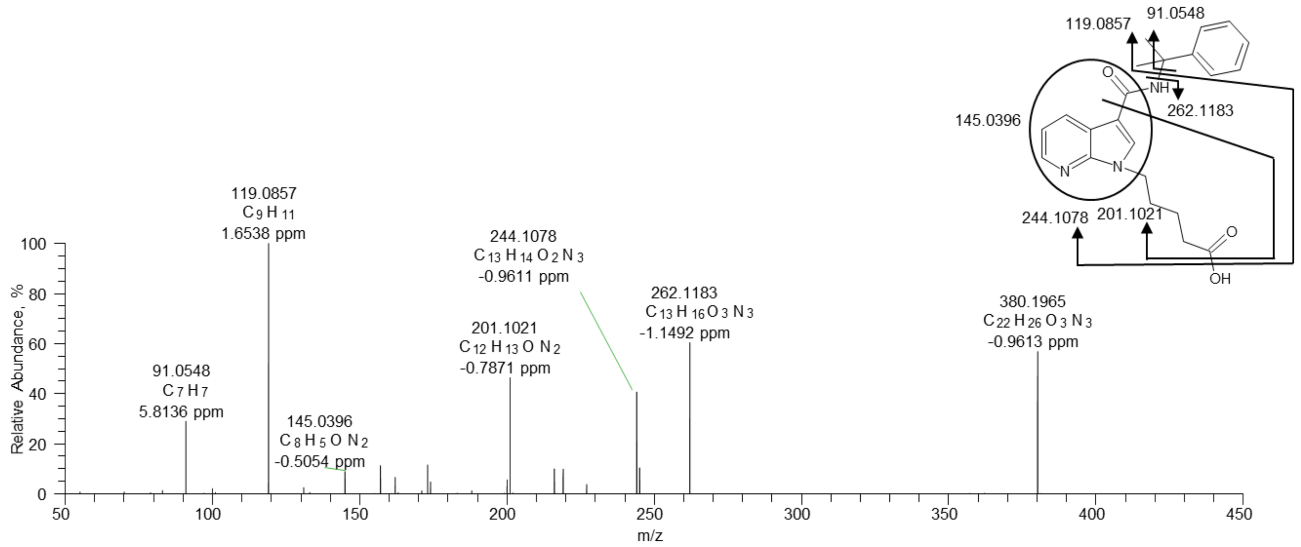

FIGURE 3 HRMS/MS spectra of the oxidative defluorinated and carboxylated metabolite M1 identified in pooled human liver S9 fraction incubation containing 25 μM cumyl-5F-P7AICA [Colour figure can be viewed at wileyonlinelibrary.com]

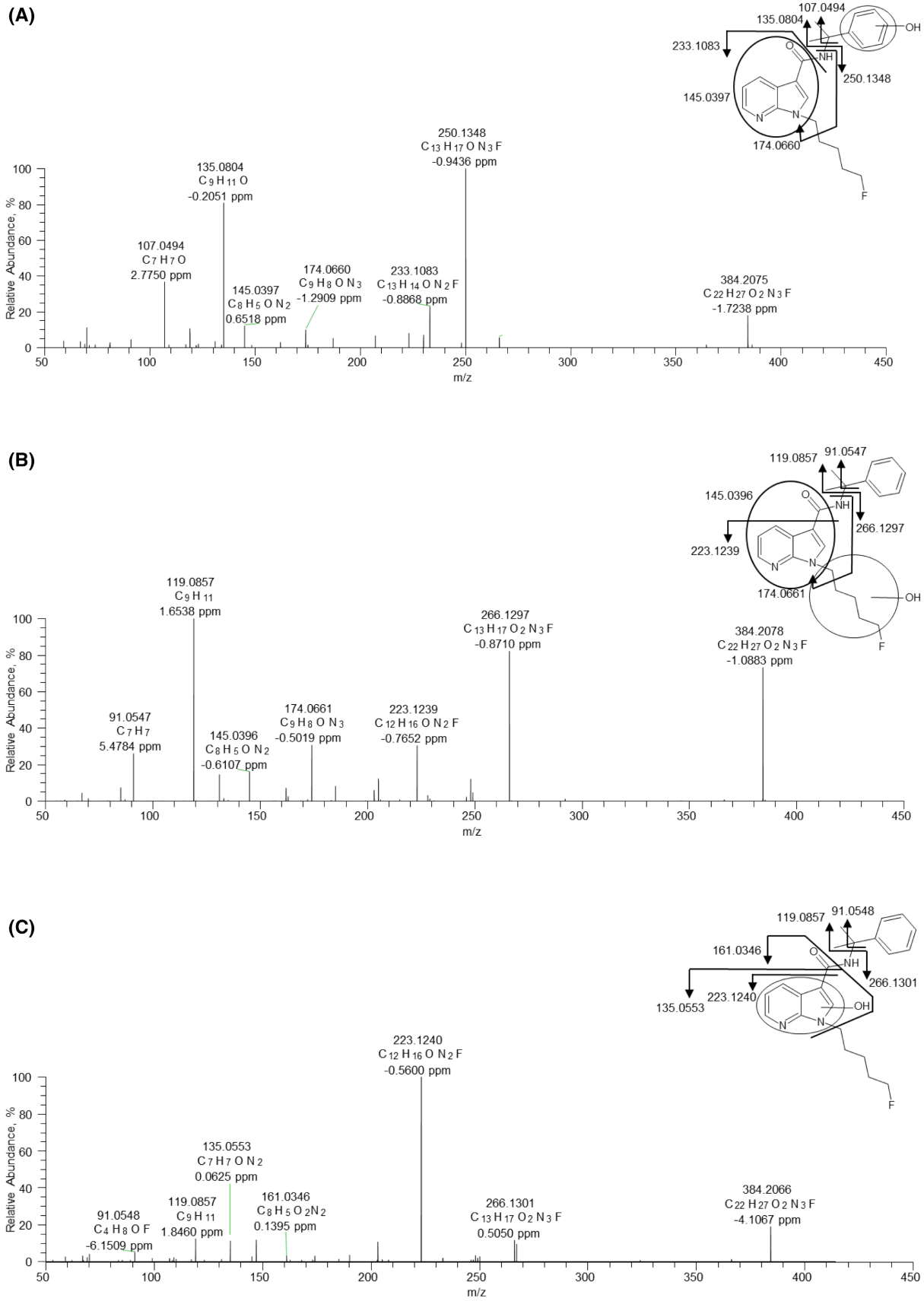

FIGURE 4 HRMS/MS spectra of A, aryl-monohydroxylated (M2); B, 5-fluoropentyl-monohydroxylated (M3); and C, 7-azaindole-monohydroxylated (M10) metabolites of cumyl-5F-P7AICA identified in pooled human liver S9 fraction incubation containing 25 μM cumyl-5F-P7AICA [Colour figure can be viewed at wileyonlinelibrary.com]

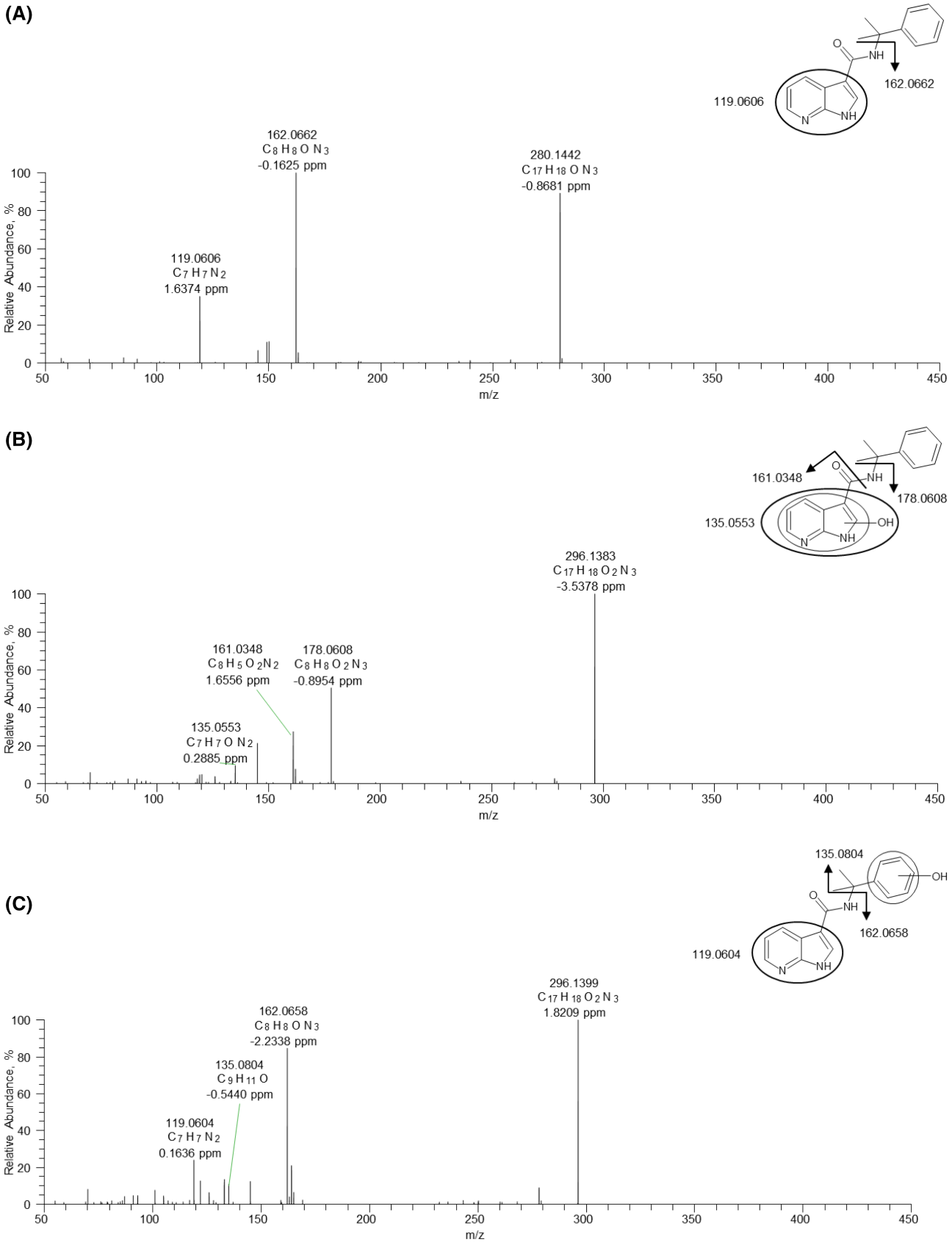

FIGURE 5 HRMS/MS spectra of A, *N*-dealkylated (M5); B, *N*-dealkylated-7-azaindole-monohydroxylated (M11); and C, *N*-dealkylated-aryl-monohydroxylated (M12) metabolites of cumyl-5F-P7AICA identified in rat urine following a single oral administration of 0.6 mg/kg body weight dose of cumyl-5F-P7AICA [Colour figure can be viewed at wileyonlinelibrary.com]

The OF/5-fluoropentyl-monohydroxylated metabolite (M8, PM at *m/z* 382.2125, Table 1; Figure S4A [supporting information]) was identified by the presence of the PI at *m/z* 119.0857, representing the cleavage of the cumyl moiety. The PI at *m/z* 264.1342, indicating the hydroxylation at the 7-azaindole core or 5-fluoropentyl chain, and the additional presence of *m/z* 174.0666 and *m/z* 145.0401 represented an unaltered 7-azaindole core.

The carboxamide/5-fluoropentyl-monohydroxylated metabolite (M9, PM at *m/z* 266.1299, Table 1; Figure S5 [supporting information]), not detected in pHLM, was identified by the presence of the PI at *m/z* 223.1241, indicating a hydroxylation at the 7-azaindole core or 5-fluoropentyl chain, and the additional presence of *m/z* 145.0397, *m/z* 174.0663, and *m/z* 119.0606 representing an unaltered 7-azaindole core. However, the exact position of the hydroxylation at the aryl or 5-fluoropentyl moiety could not be identified by the methods applied.

3.3.2 | pHS9 fraction

As far as pHS9 incubations are concerned, phase II metabolites could be identified in addition to phase I metabolites due to the addition of cofactors. In total, 14 phase I and 6 phase II metabolites were found (Figure 2).

The major metabolic pathways in pHS9 incubation seemed to be those found in pHLM and PLM incubations, extended by mono- and dihydroxylation followed by glucuronidation and sulfation. The metabolites described later could additionally be identified in pHS9 incubation samples.

The 7-azaindole-monohydroxylated metabolite (M10, PM at *m/z* 384.2081, Table 1; Figure 4C) was identified by the PI at *m/z* 223.1240 and *m/z* 266.1301, indicating a hydroxylation at the 7-azaindole core or 5-fluoropentyl chain. The PI at *m/z* 119.0857 and *m/z* 91.0548 indicated the cleavage of the unaltered cumyl moiety, and the additional presence of the PI at *m/z* 135.0553 and *m/z* 161.0346 represented a hydroxylated 7-azaindole core structure.

Phase II metabolites were mainly formed by glucuronidation or sulfation of the monohydroxylated, dihydroxylated, and *N*-dealkylated/aryl-monohydroxylated compounds. The *N*-dealkylated/aryl-monohydroxylated/sulfated metabolite (M18, PM at *m/z* 376.0961, Table 1) was identified by the aglycone at *m/z* 296.1393, as well as the PI at *m/z* 135.0810 represented by a hydroxylated cumyl unit, and *m/z* 162.0659 indicated an unaltered 7-azaindole core structure.

The aryl-monohydroxylated/sulfated metabolite (M19, PM at *m/z* 464.1649, Table 1) was identified by the corresponding aglycone at *m/z* 384.2087. The PI at *m/z* 250.1354 and *m/z* 233.1088 indicated an unaltered 7-azaindole core and 5-fluoropentyl chain, and *m/z* 135.0807 formed by hydroxylation at the cumyl moiety. The aryl-monohydroxylated/glucuronidated metabolite (M20, PM at *m/z* 560.2402, Table 1) was identified by the corresponding aglycone at *m/z* 384.2081, as well as the PI at *m/z* 135.0805 and *m/z* 107.0495 representing a hydroxylation at the aryl moiety, and *m/z* 250.1349 suggesting an unaltered 7-azaindole core and 5-fluoropentyl chain.

The aryl- and 5-fluoropentyl-dihydroxylated/sulfated metabolite (M21, PM at *m/z* 480.1599, Table 1) was identified by the aglycone at *m/z* 400.2032, and the PI at *m/z* 266.1301 and *m/z* 223.1239 formed by hydroxylation at the 7-azaindole core or 5-fluoropentyl chain. The concurrent presence of *m/z* 135.0806 indicated a hydroxylation at the cumyl moiety, as well as the PI at *m/z* 119.0609, *m/z* 174.0666, and *m/z* 145.0398 representing an unaltered 7-azaindole core. It was not possible to determine whether sulfation occurred at the aryl- or 5-fluoropentyl hydroxylation, because corresponding fragments without cleavage of the sulfate group could not be detected in the spectra.

In contrast to M21 (Table 1), the aryl-dihydroxylated/sulfated metabolite (M22, PM at *m/z* 480.1599, Table 1) was identified by the corresponding aglycone at *m/z* 400.2019. The cleavage of the dihydroxylated cumyl moiety was characterized by the PI at *m/z* 151.0755 and *m/z* 123.0443. An unaltered 7-azaindole core was identified by the PI at *m/z* 174.0662, whereas *m/z* 250.1350 and *m/z* 233.1089 characterized an unaltered 5-fluoropentyl chain. The spectra of the formed phase II metabolites differed only in the higher precursor mass, caused by the additional presence of a sulfate or glucuronide, from the corresponding phase I metabolite.

3.4 | LC–HRMS/MS fragmentation and identification of cumyl-5F-P7AICA and its *in vivo* phase I and II metabolites using rat and pig urine

3.4.1 | Rat urine

In total, eight phase I and two phase II metabolites could be detected (Figure 2) and were found only in low abundances. The major metabolic pathways in rats seemed to be OF/carboxylation, *N*-dealkylation/monohydroxylation/glucuronidation or sulfation, and monohydroxylation, as well as dihydroxylation. The metabolites described later could be found only in rat urine sample. In analogy to the *in vitro* results, the parent compound (PM at *m/z* 368.2132, Table 1; Figure 1) could also be detected in rat urine.

The *N*-dealkylated/7-azaindole-monohydroxylated metabolite (M11, PM at *m/z* 296.1393, Table 1; Figure 5B) was identified by the PI at *m/z* 178.0608, *m/z* 161.0348, and *m/z* 135.0553 formed by a hydroxylated 7-azaindole core. In comparison to the unhydroxylated core, there is a mass shift of +16 u of *m/z* 162.0662 and *m/z* 119.0606. The *N*-dealkylated/aryl-monohydroxylated metabolite (M12, PM at *m/z* 296.1393, Table 1; Figure 5C) was identified by *m/z* 162.0658 and *m/z* 119.0604, representing an unaltered 7-azaindole core, and the additional presence of *m/z* 135.0804 formed by a hydroxylated aryl moiety.

The *N*-dealkylated/aryl-monohydroxylated/glucuronidated metabolite (M23, PM at *m/z* 472.1714, Table 1) was identified by the aglycone at *m/z* 296.1385. The PI at *m/z* 135.0800 was formed by a hydroxylated aryl moiety, and the PI at *m/z* 162.0658 and *m/z* 119.0608 represented an unaltered 7-azaindole core. The OF carboxamide/carboxylated metabolite (M13, PM at *m/z* 262.1186, Table 1; Figure S6 [supporting information]) was identified by the PI at *m/z*

244.1077 and *m/z* 201.1020, indicating the cleavage of the C–O bond of the carboxyl unit, as well as the PI at *m/z* 119.0605 and *m/z* 145.0395, representing an unaltered 7-azaindole core.

3.4.2 | Pig urine

In total, one phase I and four phase II metabolites were identified in the analyzed pig urine specimens (Figure 2). The major metabolic pathways of cumyl-5F-P7AICA in pig seemed to be OF/carboxylation, *N*-dealkylation/monohydroxylation/sulfation, and monohydroxylation/glucuronidation or sulfation. The PIs used for the identification of the metabolites (Table 1) were in accordance with those that have already been described in pHS9 incubation results.

In addition, the 5-fluoropentyl-monohydroxylated/glucuronidated metabolite (M24, PM at *m/z* 560.2402, Table 1) could be detected only in pig urine specimens and was identified by the aglycone at *m/z* 384.2092. The PI at *m/z* 119.0860 suggested an unaltered cumyl moiety, *m/z* 266.1302 indicated a hydroxylation at the 7-azaindole core or 5-fluoropentyl chain, and *m/z* 174.0665 represented an unaltered 7-azaindole core.

3.5 | CYP initial screening

To elucidate the main metabolic steps in pigs as compared to humans, and the responsible CYP isoenzymes, a CYP activity screening, using human CYP isoenzymes, was performed. All initial steps for cumyl-5F-P7AICA, consisting of *N*-dealkylation, *N*-dealkylation/hydroxylation, OF, OF/carboxylation, ketone formation, monohydroxylation, and dihydroxylation, could be confirmed. As shown in Table 2, cumyl-5F-P7AICA was predominantly metabolized by CYP2C19, CYP3A4, and CYP3A5. The important metabolic steps in pigs and humans, that is, OF followed by carboxylation as well as monohydroxylation, were catalyzed mainly by these three CYP isoenzymes. In addition, *N*-dealkylation, catalyzed by CYP1A2, CYP3A4, and CYP3A5 followed by monohydroxylation through CYP1A2, CYP2C8, CYP2C9, CYP2C19, CYP3A4, and CYP3A5, could be the main metabolic step in pigs, considering that human CYP isoenzymes were used.

Note. The main metabolizing enzymes are marked in boxes.

Consistent with these findings, the fact that the isoenzymes CYP3A4 and CYP2C19 are involved in the metabolism of SCs, specifically monohydroxylation and dealkylation, has already been demonstrated for different SCs, such as XLR-11, UR-11, AM-2201, RCS-4, and JWH-210.[20,35–37] Oxidative metabolism catalyzed by CYP3A5 could also be observed for several SCs, such as 5F-AKB-48 and EAM-2201.[38]

3.6 | Comparison of the metabolic pattern in the different metabolizing systems with human data

3.6.1 | *In vitro* metabolic pattern using pHLM, PLM, and pHS9

The parent compound (Table 3; Figure 1) could be detected in high abundances in all *in vitro* incubation samples. In general, the detected phase I metabolites (Table 3; Figure 2) in the three *in vitro* assays were consistent. The metabolic reactions observed in all three *in vitro* models were OF, OF/carboxylation, OF/aryl-monohydroxylation, *N*-dealkylation, aryl- and 5-fluoropentyl-monohydroxylation, and ketone formation, as well as aryl-dihydroxylation, 5-fluoropentyl-dihydroxylation, and a combination of both. M0 (Table 3; Figure S1 [supporting information]) was detected as an impurity in pHS9, pHLM, and PLM incubations.

In contrast to the results obtained from pHS9 and pHLM incubation samples, OF/5-fluoropentyl-monohydroxylation (M8, Table 3; Figure S4A [supporting information]) could not be identified in PLM incubation. In pHLM, the carboxamide/5-fluoropentyl-monohydroxylated metabolite M9 (PM at *m/z* 266.1299, Table 3; Figure S5 [supporting information]) could not be detected. Due to the fact that M8 (Table 3; Figure S4A [supporting information]) was not found in pig urine as well as in human urine samples, the formation of M8 seems to be species dependent. In addition, M8 (Table 3; Figure S4A [supporting information]) and M9 (Table 3; Figure S5 [supporting information]) were only minor metabolites. Because M0 (Table 3; Figure S1 [supporting information]) could be found

TABLE 2 Overview of the detected metabolites of cumyl-5F-P7AICA in cytochrome P450 monooxygenase (CYP) initial screening

	CYP										
	1A2	2A6	1B6	2C8	2C9	2C19	2D6	2E1	3A4	3A5	FMO3
N-dealkylation	+								+	+	
N-dealkylation-hydroxylation									+		
Oxidative defluorination (OF)				+	+	+	+			+	
OF-carboxylation						+	+		+	+	
Ketone formation						+			+	+	
Monohydroxylation	+			+	+	+			+	+	
Dihydroxylation						+			+	+	

TABLE 3 Overview and comparison of cumyl-5F-P7AICA and its phase I and II metabolites detected in different *in vitro* (pooled human liver S9 fraction [pHS9], pooled human liver microsome [pHLM], and pig liver microsome [PLM] incubation) and *in vivo* models (rat urine [RU] after oral administration and pig urine [PU] after inhalative administration) with already-published pHLM incubation[13] and human urine (HU)[11] data

		pHS9	pHLM	PLM	RU	PU	pHLM[13]	HU[11]
	Cumyl-5F-P7AICA	X	x	x	x	x	x	
M0	Carboxamide	X	x	x				
M1	Oxidative defluorinated (OF) and carboxylated	X	x	x	x	x	x	x
M2	Monohydroxylated[1]	X	x	x	x		x	x
M3	Monohydroxylated[2]	X	x	x			x	
M4	Ketone	X	x	x			x	
M5	*N*-Dealkylated	X	x	x	x		x	
M6	Dihydroxylated[1]	X	x	x			x	
M7	Dihydroxylated[2]	x	x	x	x			
M8	OF-monohydroxylated[2]	x	x					
M9	Carboxamide-monohydroxylated[2]	x		x				
M10	Monohydroxylated[3]	x						x
M11	*N*-Dealkylated-monohydroxylated[3]				x		x	
M12	*N*-Dealkylated-monohydroxylated[1]				x			
M13	OF-carboxamide and carboxylated				x			
M14	OF-carboxamide	x						
M15	OF	x	x	x			x	
M16	OF-monohydroxylated[1]	x	x	x			x	
M17	Dihydroxylated[1 + 2]	x	x	x	x		x	
M18	*N*-Dealkylated-monohydroxylated[1] and sulfated	x			x	x		
M19	Monohydroxylated[1] and sulfated	x				x		x
M20	Monohydroxylated[1] and glucuronidated	x				x		x
M21	Dihydroxylated[1 + 2] and sulfated	x						
M22	Dihydroxylated[1 + 1] and sulfated	x						
M23	*N*-Dealkylated-monohydroxylated[1] and glucuronidated				x			
M24	Monohydroxylated[2] and glucuronidated					x		

Note. 1, aryl-monohydroxylated; 2, 5-fluoropentyl-monohydroxylated; 3, 7-azaindole-monohydroxylated.

in all *in vitro* samples as an impurity, it is possible that M9 (Table 3; Figure S5 [supporting information]) was formed from M0 (Table 3; Figure S1 [supporting information]) by monohydroxylation at the 5-fluoropentyl chain.

In PLM and pHLM incubations, comparable phase I metabolites were detected. The 7-azaindole-monohydroxylated metabolite (M10, Table 3; Figure 4C) could be detected only in pHS9 incubation samples in low abundances. Due to the presence of the carboxamide linker and the 5-fluoropentyl tail in its chemical structure, steric hinderance could be the reason why monohydroxylation at the 7-azaindole core, resulting in M10 (Table 3; Figure 4C), was seen only in pHS9. In addition, the compound at PM *m/z* 248.1393 (M14, Table 3; Figure S7 [supporting information]) was identified as a carboxamide and OF compound and observed only in pHS9 incubation. As mentioned earlier, this substance could have resulted from the impurity M0 (Table 3; Figure S1 [supporting information]) with a subsequent phase I reaction.

In addition, phase II reactions, that is, sulfation and glucuronidation of mono- and dihydroxylated as well as *N*-dealkylated/monohydroxylated compounds, were detected in pHS9 incubation, whereas sulfated compounds were observed more often (Table 3; Figure 2).

In general, the identified phase I metabolic reactions of cumyl-5F-P7AICA in pHLM incubation of the present work were consistent with those published by Staeheli et al,[13] also using pHLM, identifying dihydroxylation, OF/carboxylation, and monohydroxylation as the three major metabolic pathways. In addition, ketone formation (M4, Table 3; Figure S2 [supporting information]), *N*-dealkylation (M5, Table 3; Figure 5A), OF (M15, Table 3; Figure S8 [supporting information]), and OF/aryl-monohydroxylation (M16, Table 3; Figure S4B

[supporting information]) were observed as metabolic reactions in both pHLM incubations.

In contrast to the already-published data by Staeheli et al,[13] describing an OF followed by methylation as well as an OF compound in the blank pHLM incubation samples due to the storage of cumyl-5F-P7AICA in methanol, none of those metabolites could be detected as an impurity in the present study. Except for M0 (Table 3; Figure S1 [supporting information]) as an impurity, an OF/5-fluoropentyl-monohydroxylated (M8, Table 3; Figure S4A [supporting information]) and a 5-fluoropentyl-dihydroxylated metabolite (M7, Table 3; Figure S3B [supporting information]) were additionally identified in the present study, but no *N*-dealkylated/monohydroxylated metabolite[13] could be found.

3.6.2 | *In vivo* metabolic pattern using rat and pig urine

First, it must be mentioned that the metabolites excreted into rat and pig urine, as well as their abundances, can hardly be compared to each other, as the applied dosages and routes of administrations were different. Nevertheless, if the metabolites detected in rat and pig urine should be compared, it means that, in general, in addition to the parent compound, only a small number of similar phase I and II metabolites were found in rat and pig urine. Although SCs are generally known to be extensively metabolized,[20,39] the excretion of the parent compound into urine has already been reported for other 7-azaindole-derived SCs,[40] as well as, for example, SCs containing an indazole-core structure.[41]

The OF/carboxylated (M1, Table 3; Figure 2) as well as the *N*-dealkylated/aryl-monohydroxylated/sulfated (M18, Table 3; Figure 2) metabolites were detected in high abundances in both rat and pig urine. On the contrary, the metabolites M2, M5, M7, M11, M13, M17, and M23 (Table 3; Figure 2) were detected only in rat urine. In addition, M12 formed by *N*-dealkylation/aryl-monohydroxylation could be found using only this animal model. However, the corresponding phase II metabolites of the aryl-monohydroxylated metabolite (M2) formed by sulfation (M19) or glucuronidation (M20), as well as the 5-fluoropentyl-monohydroxylated/glucuronidated (M24, Table 3) metabolite, could be detected only in pig urine specimens but not in rat urine (Table 3).

The intensive *N*-dealkylation in rats not observed in pig urine samples could be due to differences in CYP isoenzymes.[42] The absence of M2, M7, M12, and M17 (Table 3) in pig urine can be explained by the fact that the monohydroxylated compounds underwent conjugation in pigs, preventing further hydroxylation. This finding is in accordance with results published by Schaefer et al,[20] describing an intensive phase II metabolism in pigs.

In conclusion, the rat model seems to be less suitable for the elucidation of metabolic patterns of 7-azaindole-containing SCs as compared to the pig model. Due to its highly lipophilic properties, cumyl-5F-P7AICA may not have been sufficiently absorbed after oral administration, thus probably explaining the low abundances of the detected metabolites in rat urine.

3.6.3 | Comparison of *in vitro* and *in vivo* metabolism

Comparing *in vitro* and *in vivo* assays, many of the *in vitro* identified phase I metabolites could not be found *in vivo*, except for M1, M2, M5, M7, and M17 (Table 3) also being detected in rat urine. The ketone formation, resulting in M4 (Table 3), as a major metabolic pathway of *in vitro* assays, could not be identified *in vivo*.

Comparing the results of PLM incubation with the elucidated metabolites in pig urine, more phase I metabolites, such as monohydroxylations and dihydroxylations, could be detected. This difference is not surprising, as monohydroxylated compounds undergo conjugation *in vivo*. The metabolites M15 and M16 were identified in PLM but not in pig urine (Table 3). Furthermore, M5 was identified in PLM incubations; however, *N*-dealkylated compounds could not be found in pig urine. A subsequent monohydroxylation of the aryl moiety and conjugation with a sulfate resulting in M18 might be the reason (Table 3).

Based on the high abundances of the formed phase II metabolites *in vivo*, one might conclude that pHS9 is more appropriate for the elucidation of the metabolic pattern of 7-azaindole-derived SCs as compared to pHLM and PLM.

3.6.4 | Comparison of metabolism in pig with human data

Consistent with the already-published study by Staeheli et al,[11] phase I and II metabolites detected in pig urine were in good accordance with those found in authentic human urine samples. OF/carboxylation (M1) and aryl-monohydroxylation/sulfation (M19) or glucuronidation (M20) were detected in pig urine as well as in human urine specimens (Table 3) as the main metabolic reactions.

High abundances of the phase I metabolite M1 were observed in pig urine as well as in human urine samples. Regarding this metabolite, no other phase II metabolite could be detected. Therefore, M1 does not appear to be further metabolized by phase II reactions (Table 3). This finding indicates that the intensive formation of an OF/carboxylated metabolite seems to be a major metabolic pathway for cumyl-5F-P7AICA, as already described in a previous study.[11] In addition, this result is consistent with those found for other fluorinated SCs.[43–45]

Furthermore, no dihydroxylated/glucuronidated/sulfated compounds were identified in human and pig urine, which suggests that monohydroxylated compounds undergo a fast phase II conjugation.

On the contrary, some differences between pig and human data were found. To begin with, cumyl-5F-P7AICA was detected in pig urine for 3 h after inhalative administration, but no parent compound could be found in authentic human urine samples by Staeheli et al[11] (Table 3). As in the casework by Staeheli et al,[11] nothing is known about the time of consumption as well as the consumed dosage; a consumption of cumyl-5F-P7AICA far before urine sampling may offer an explanation for the fact that no parent compound was found. On the contrary, again in line with our results, the urinary excretion of the

parent compound of 7-azaindole-derived SCs after oral administration was already reported by Giorgetti et al.[40]

M18 and M24 could additionally be detected as phase II metabolites in pig urine but not in human urine (Table 3). This intensive formation of phase II metabolites in pigs is in accordance with already-published metabolism data in pigs by Schaefer et al.[20] This issue could be attributed to species-dependent differences in the formation of these metabolites, because differences in the primary structure of CYP forms, as well as in the gene expression, have already been reported.[42]

On the contrary, the monohydroxylated phase I metabolites M2 and M10 (Table 3) were detected only in studies on human urine performing enzymatic hydrolysis during sample preparation but as mixed spectra.[11] The absence of these metabolites in pig urine samples in our study is not surprising, as no enzymatic hydrolysis was carried out.

In sum, despite minor differences, the metabolic pattern of the *in vivo* pig model was consistent with the already-identified metabolites in human urine samples. In conclusion, the pig is a suitable animal model for the elucidation of recommended urinary targets of 7-azaindole-derived SCs in forensic toxicology.

3.7 | Urinary excretion pattern in pig and recommendation of analytical targets

In the present work, the parent compound, cumyl-5F-P7AICA, was detectable in the collected pig urine specimens for 3 h after drug administration, with the abundance decreasing time dependently. Regarding the LC–HRMS/MS data, M20 (Table 3) was the most abundant metabolite for 8 h after administration in our experiment. M19 (Table 3) was also initially predominantly present but disappeared after 7 h. M1 (Table 3; Figure 3), M18 (Table 3), and M24 (Table 3) were found in all collected samples for 8 h but displayed lower abundances.

Assessing the metabolic pattern of other 7-azaindole-derived SCs, such as 5F-MDMB-P7AICA, in pig urine[46]—in contrast to the results obtained in our study of pig—no sulfated phase II metabolites were detected. In addition, the parent compound, 5F-MDMB-P7AICA, was detectable only for 1 h after inhalative administration,[46] whereas in the present study, cumyl-5F-P7AICA could be found for 3 h. This observation could be explained by differences in the chemical structures. Despite an identical 5-fluoropentyl tail, 7-azaindole core, and carboxamide linker, the linked group is different. Whereas cumyl-5F-P7AICA contains a cumyl moiety as a linked group, 5F-MDMB-P7AICA has an ester structure, undergoing a fast degradation due to ester hydrolysis.[46] Regarding indazole-derived SCs, such as 5F-MDMB-PINACA, no parent compound could be detected in urinary specimens;[47,48] however, no systematic controlled studies were conducted.

Based on the aforementioned results and despite the fact that cumyl-5F-P7AICA could not be detected in human urine samples, the parent compound might be a high-specific urinary target to prove the recent consumption of 7-azaindole-derived SCs.

Due to its high abundances in urine samples, M1 (Table 3; Figure 3) might be used as a marker for consumption of cumyl-5F-P7-AICA, as already described by Staeheli et al.[11] Nevertheless, when interpreting the findings, one must consider that the OF/carboxylated metabolite M1 contains the full parent structure but is not fully specific, because it could also originate by the consumption of, for example, cumyl-5F-PINACA or cumyl-PINACA.[49] Due to the intensive phase II metabolism of cumyl-5F-P7AICA *in vivo*, we further recommend to use the aryl-monohydroxylated/sulfated (M19, Table 3) or glucuronidated (M20, Table 3) metabolites as consumption markers if no enzymatic hydrolysis is performed. To improve the specificity, enzymatic hydrolysis of urine samples could be carried out. In accordance with the study by Staeheli et al, the aryl-monohydroxylated metabolite should also be used as a urinary target to prove consumption, as it includes the full parent structure.[11] This recommendation is confirmed by the fact that monohydroxylation is an already-published common metabolic pathway for SCs.[20,45,50,51]

Due to the high number of structurally similar SCs with common metabolites, high sensitivity and specificity of recommended urinary targets are necessary. To draw a conclusion from the findings of this study and those published by Staeheli et al,[11] urinary targets for the confirmation of a consumption of cumyl-5F-P7AICA should be the parent compound (seemed to be detectable only for a few hours after inhalation), OF/carboxylated as well as the aryl-monohydroxylated metabolite M2 (after enzymatic hydrolysis), and the corresponding sulfated (M19) and glucuronidated (M20) metabolites (Table 3).

4 | CONCLUSIONS

The present work elucidated the metabolic patterns of cumyl-5F-P7AICA using different *in vitro* (pHS9, pHLM, and PLM incubations) and *in vivo* (rat and pig) models. In this context, the major metabolic pathways were OF/carboxylation, aryl-monohydroxylation, and aryl-monohydroxylation/glucuronidation or sulfation. CYP2C19, CYP3A4, and CYP3A5 were predominantly involved in the metabolism of cumyl-5F-P7AICA. To prove the consumption of cumyl-5F-P7AICA, the parent compound and the OF/carboxylated, the aryl-monohydroxylated/glucuronidated, or sulfated metabolites should be used as urinary targets. After the enzymatic hydrolysis of urine samples, the aryl-monohydroxylated metabolite might be preferentially used as a urinary marker instead of the glucuronidated or sulfated phase II metabolites. In contrast to the rat model, the pig formed metabolites comparable to those found in human urine specimens except for the parent compound, detected only in pig urine samples for 3 h but not in human urine. Considering all the results of the present study, the pig model is the most suitable animal model for the elucidation of the metabolic pattern of 7-azaindole-derived SCs. In particular, the pig model allows for the elucidation of the time-dependent urinary excretion pattern, because repeated collection of multiple samples is possible.

ACKNOWLEDGMENTS

We thank the staff of the Institute of Experimental and Clinical Toxicology at Saarland University and the Institute for Clinical and

Experimental Surgery at Saarland University for their support and help during the study. We acknowledge the EU-funded project ADEBAR (IZ25-5793-2016-27).

ORCID

Nadine Schaefer https://orcid.org/0000-0002-5589-9370

REFERENCES

1. European Monitoring Centre for Drugs and Drug Addiction (EMCDDA). Perspectives on Drugs: Synthetic Cannabinoids in Europe 2017. www.emcdda.europa.eu/system/files/publications/2753/POD_Synthetic%20cannabinoids_0.pdf. Accessed April 6, 2020.
2. European Monitoring Centre for Drugs and Drug Addiction (EMCDDA). European Drug Report 2018: Trends and Developments. http://www.emcdda.europa.eu/system/files/publications/8585/20181816_TDAT18001ENN_PDF.pdf. Accessed April 6, 2020.
3. Tai S, Fantegrossi WE. Pharmacological and toxicological effects of synthetic cannabinoids and their metabolites. *Curr Top Behav Neurosci*. 2017;32:249-262.
4. Karila L, Benyamina A, Blecha L, Cottencin O, Billieux J. The synthetic cannabinoids phenomenon. *Curr Pharm Des*. 2016;22(42):6420-6425.
5. Asada A, Doi T, Tagami T, et al. Cannabimimetic activities of cumyl carboxamide-type synthetic cannabinoids. *Forensic Toxicol*. 2018;36(1):170-177.
6. Trecki J, Gerona RR, Schwartz MD. Synthetic cannabinoid–related illnesses and deaths. *New Engl J Med*. 2015;373(2):103-107.
7. Kraemer M, Boehmer A, Madea B, Maas A. Death cases involving certain new psychoactive substances: a review of the literature. *Forensic Sci Int*. 2019;298:186-267.
8. Giorgetti A, Busardò FP, Tittarelli R, Auwärter V, Giorgetti R. Post-mortem toxicology: a systematic review of death cases involving synthetic cannabinoid receptor agonists. *Front Psych*. 2020;11:464–486.
9. Darke S, Duflou J, Farrell M, Peacock A, Lappin J. Characteristics and circumstances of synthetic cannabinoid-related death. *Clin Toxicol (Phila)*. 2020;58(5):368-374.
10. Alipour A, Patel PB, Shabbir Z, Gabrielson S. Review of the many faces of synthetic cannabinoid toxicities. *Ment Health Clin*. 2019;9(2):93-99.
11. Staeheli SN, Steuer AE, Kraemer T. Identification of urinary metabolites of the synthetic cannabinoid 5F-CUMYL-P7AICA in human casework. *Forensic Sci Int*. 2019;294:76-79.
12. Banister SD, Adams A, Kevin RC, et al. Synthesis and pharmacology of new psychoactive substance 5F-CUMYL-P7AICA, a scaffold- hopping analog of synthetic cannabinoid receptor agonists 5F-CUMYL-PICA and 5F-CUMYL-PINACA. *Drug Test Anal*. 2019;11(2):279-291.
13. Staeheli SN, Poetzsch M, Veloso VP, et al. In vitro metabolism of the synthetic cannabinoids CUMYL-PINACA, 5F–CUMYL-PINACA, CUMYL-4CN-BINACA, 5F–CUMYL-P7AICA and CUMYL-4CN-B7AICA. *Drug Test Anal*. 2018;10(1):148-157.
14. Bovens M, Bissig C, Staeheli SN, Poetzsch M, Pfeiffer B, Kraemer T. Structural characterization of the new synthetic cannabinoids CUMYL-PINACA, 5F-CUMYL-PINACA, CUMYL-4CN-BINACA, 5F-CUMYL-P7AICA and CUMYL-4CN-B7AICA. *Forensic Sci Int*. 2017;281:98-105.
15. Nordmeier F, Richter LHJ, Schmidt PH, Schaefer N, Meyer MR. Studies on the in vitro and in vivo metabolism of the synthetic opioids U-51754, U-47931E, and methoxyacetylfentanyl using hyphenated high-resolution mass spectrometry. *Sci Rep*. 2019;9(1):13774–13791.
16. Nordmeier F, Doerr A, Laschke MW, et al. Are pigs a suitable animal model for in vivo metabolism studies of new psychoactive substances? A comparison study using different in vitro/in vivo tools and U-47700 as model drug. *Toxicol Lett*. 2020;329:12-19.
17. Richter LHJ, Flockerzi V, Maurer HH, Meyer MR. Pooled human liver preparations, HepaRG, or HepG2 cell lines for metabolism studies of new psychoactive substances? A study using MDMA, MDBD, butylone, MDPPP, MDPV, MDPB, 5-MAPB, and 5-API as examples. *J Pharm Biomed Anal*. 2017;143:32-42.
18. Richter LHJ, Herrmann J, Andreas A, et al. Tools for studying the metabolism of new psychoactive substances for toxicological screening purposes - a comparative study using pooled human liver S9, HepaRG cells, and zebrafish larvae. *Toxicol Lett*. 2019;305:73-80.
19. De Brabanter N, Esposito S, Tudela E, et al. In vivo and in vitro metabolism of the synthetic cannabinoid JWH-200. *Rapid Commun Mass Spectrom*. 2013;27(18):2115-2126.
20. Schaefer N, Helfer AG, Kettner M, et al. Metabolic patterns of JWH-210, RCS-4, and THC in pig urine elucidated using LC-HR-MS/MS: do they reflect patterns in humans? *Drug Test Anal*. 2017;9(4):613-625.
21. Schaefer N, Kettner M, Laschke MW, et al. Distribution of synthetic cannabinoids JWH-210, RCS-4 and Δ 9-tetrahydrocannabinol after intravenous administration to pigs. *Curr Neuropharmacol*. 2017;15(5):713-723.
22. Schaefer N, Wojtyniak JG, Kettner M, et al. Pharmacokinetics of (synthetic) cannabinoids in pigs and their relevance for clinical and forensic toxicology. *Toxicol Lett*. 2016;253:7-16.
23. Swindle MM, Makin A, Herron AJ, Clubb FJ, Frazier KS. Swine as models in biomedical research and toxicology testing. *Vet Pathol*. 2011;49(2):344-356.
24. Meurens F, Summerfield A, Nauwynck H, Saif L, Gerdts V. The pig: a model for human infectious diseases. *Trends Microbiol*. 2012;20(1):50-57.
25. Anzenbacher P, Soucek P, Anzenbacherová E, et al. Presence and activity of cytochrome P450 isoforms in minipig liver microsomes. *Drug Metab Dispos*. 1998;26(1):56-59.
26. Soucek P, Zuber R, Anzenbacherová E, Anzenbacher P, Guengerich FP. Minipig cytochrome P450 3A, 2A and 2C enzymes have similar properties to human analogs. *BMC Pharmacol*. 2001;1(1):11–16.
27. Schaefer N, Kroll AK, Korbel C, et al. Distribution of the (synthetic) cannabinoids JWH-210, RCS-4, as well as 9-tetrahydrocannabinol following pulmonary administration to pigs. *Arch Toxicol*. 2019;93(8):2211-2218.
28. Schaefer N, Wojtyniak JG, Kroell AK, et al. Can toxicokinetics of (synthetic) cannabinoids in pigs after pulmonary administration be upscaled to humans by allometric techniques? *Biochem Pharmacol*. 2018;155:403-418.
29. Manier SK, Richter LHJ, Schaper J, Maurer HH, Meyer MR. Different in vitro and in vivo tools for elucidating the human metabolism of alpha-cathinone-derived drugs of abuse. *Drug Test Anal*. 2018;10(7):1119-1130. https://doi.org/10.1002/dta.2355
30. Wagmann L, Hempel N, Richter LHJ, Brandt SD, Stratford A, Meyer MR. Phenethylamine-derived new psychoactive substances 2C-E-FLY, 2C-EF-FLY, and 2C-T-7-FLY: investigations on their metabolic fate including isoenzyme activities and their toxicological detectability in urine screenings. *Drug Test Anal*. 2019;11(10):1507-1521.
31. Meyer MR, Vollmar C, Schwaninger AE, Wolf E, Maurer HH. New cathinone-derived designer drugs 3-bromomethcathinone and 3-fluoromethcathinone: studies on their metabolism in rat urine and human liver microsomes using GC-MS and LC-high-resolution MS and their detectability in urine. *J Mass Spectrom*. 2012;47(2):253-262.
32. Michely JA, Helfer AG, Brandt SD, Meyer MR, Maurer HH. Metabolism of the new psychoactive substances N,N-diallyltryptamine (DALT) and 5-methoxy-DALT and their detectability in urine by GC-MS, LC-MSn, and LC-HR-MS-MS. *Anal Bioanal Chem*. 2015;407(25):7831-7842.

33. Caspar AT, Brandt SD, Stoever AE, Meyer MR, Maurer HH. Metabolic fate and detectability of the new psychoactive substances 2-(4-bromo-2,5-dimethoxyphenyl)-N-[(2-methoxyphenyl)methyl] ethanamine (25B-NBOMe) and 2-(4-chloro-2,5-dimethoxyphenyl)-N-[(2-methoxyphenyl)methyl]ethanamine (25C-NBOMe) in human and rat urine by GC-MS, LC-MS(n), and LC-HR-MS/MS approaches. *J Pharm Biomed Anal*. 2017;134:158-169.
34. EVE and Rave. - The Swiss Drug Forum 2012. https://www.eve-rave.ch/Forum/viewtopic.php?t=28044. Accessed April 06, 2020.
35. Holm NB, Nielsen LM, Linnet K. CYP3A4 mediates oxidative metabolism of the synthetic cannabinoid AKB-48. *AAPS J*. 2015;17(5):1237-1245.
36. Stout SM, Cimino NM. Exogenous cannabinoids as substrates, inhibitors, and inducers of human drug metabolizing enzymes: a systematic review. *Drug Metab Rev*. 2014;46(1):86-95.
37. Nielsen LM, Holm NB, Olsen L, Linnet K. Cytochrome P450-mediated metabolism of the synthetic cannabinoids UR-144 and XLR-11. *Drug Test Anal*. 2016;8(8):792-800.
38. Yarbrough AL, Pinson A, Prather PL, et al. Oxidative metabolism and comparative analysis of synthetic cannabinoid N-(1-adamantyl)-1-(5-fluoropentyl)indazole-3-carboxamide (5F-AKB-48) and the unfluorinated analog AKB-48. *FASEB J*. 2019;33(1_supplement): 469.466–469.466.1–1.
39. Mogler L, Halter S, Wilde M, Franz F, Auwärter V. Human phase I metabolism of the novel synthetic cannabinoid 5F-CUMYL-PEGACLONE. *Forensic Toxicol*. 2019;37(1):154-163.
40. Giorgetti A, Mogler L, Haschimi B, et al. Detection and phase I metabolism of the 7-azaindole-derived synthetic cannabinoid 5F-AB-P7AICA including a preliminary pharmacokinetic evaluation. *Drug Test Anal*. 2020;12(1):78-91.
41. Yeter O, Ozturk YE. Metabolic profiling of synthetic cannabinoid 5F-ADB by human liver microsome incubations and urine samples using high-resolution mass spectrometry. *Drug Test Anal*. 2019;11(6): 847-858.
42. Turpeinen M, Ghiciuc C, Opritoui M, Tursas L, Pelkonen O, Pasanen M. Predictive value of animal models for human cytochrome P450 (CYP)-mediated metabolism: a comparative study in vitro. *Xenobiotica*. 2007;37(12):1367-1377.
43. Watanabe S, Kuzhiumparambil U, Nguyen MA, Cameron J, Fu S. Metabolic profile of synthetic cannabinoids 5F-PB-22, PB-22, XLR-11 and UR-144 by Cunninghamella elegans. *AAPS J*. 2017;19(4):1148-1162.
44. Wohlfarth A, Gandhi AS, Pang S, Zhu M, Scheidweiler KB, Huestis MA. Metabolism of synthetic cannabinoids PB-22 and its 5-fluoro analog, 5F-PB-22, by human hepatocyte incubation and high-resolution mass spectrometry. *Anal Bioanal Chem*. 2014;406(6): 1763-1780.
45. Wohlfarth A, Pang S, Zhu M, et al. First metabolic profile of XLR-11, a novel synthetic cannabinoid, obtained by using human hepatocytes and high-resolution mass spectrometry. *Clin Chem*. 2013;59(11): 1638-1648.
46. Doerr A, Nordmeier F, Walle N, et al. Can a recently developed pig model be used for in vivo metabolism studies of 7-azaindole derived synthetic cannabinoids? A study using 5F-MDMB-P7AICA as example. *J Anal Toxicol*. 2020. submitted
47. Barceló B, Pichini S, López-Corominas V, et al. Acute intoxication caused by synthetic cannabinoids 5F-ADB and MMB-2201: a case series. *Forensic Sci Int*. 2017;273:e10-e14.
48. McCain KR, Jones JO, Chilbert KT, Patton AL, James LP, Moran JH. Impaired driving associated with the synthetic cannabinoid 5f-Adb. *J Forensic Sci Criminol*. 2018;6(1):105-112.
49. Angerer V, Franz F, Moosmann B, Bisel P, Auwärter V. 5F-Cumyl-PINACA in 'e-liquids' for electronic cigarettes: comprehensive characterization of a new type of synthetic cannabinoid in a trendy product including investigations on the in vitro and in vivo phase I metabolism of 5F-Cumyl-PINACA and its non-fluorinated analog Cumyl-PINACA. *Forensic Toxicol*. 2019;37(1):186-196.
50. Mogler L, Wilde M, Huppertz LM, Weinfurtner G, Franz F, Auwarter V. Phase I metabolism of the recently emerged synthetic cannabinoid CUMYL-PEGACLONE and detection in human urine samples. *Drug Test Anal*. 2018;10(5):886-891.
51. Erratico C, Negreira N, Norouzizadeh H, et al. In vitro and in vivo human metabolism of the synthetic cannabinoid AB-CHMINACA. *Drug Test Anal*. 2015;7(10):866-876.

SUPPORTING INFORMATION

Additional supporting information may be found online in the Supporting Information section at the end of this article.

How to cite this article: Walle N, Nordmeier F, Doerr AA, et al. Comparison of *in vitro* and *in vivo* models for the elucidation of metabolic patterns of 7-azaindole-derived synthetic cannabinoids exemplified using cumyl-5F-P7AICA. *Drug Test Anal*. 2021;13:74–90. https://doi.org/10.1002/dta.2899

Supporting information

Comparison of in vitro and in vivo models for the elucidation of metabolic patterns of 7-azaindole-derived synthetic cannabinoids exemplified using cumyl-5F-P7AICA

Nadja Walle[1], Frederike Nordmeier[1], Adrian Doerr[1], Benjamin Peters[1], Matthias W. Laschke[2], Michael D. Menger[2], Peter H. Schmidt[1], Markus R. Meyer[3] and Nadine Schaefer[1*]

---

[*]Correspondence to: Nadine Schaefer, Institute of Legal Medicine, Saarland University, Building 49.1, 66421 Homburg, Germany.

Email: nadine.schaefer@uks.eu

[1]Institute of Legal Medicine, Saarland University,

Building 49.1, 66421 Homburg, Germany

[2]Institute for Clinical & Experimental Surgery, Saarland University,

Building 65/66, 66421 Homburg, Germany

[3]Department of Experimental and Clinical Toxicology, Center for Molecular Signaling (PZMS), Saarland University,

Building 46, 66421 Homburg, Germany

Legend to figures

Supplementary Figure 1. HR-MS/MS spectrum of the carboxamide (M0) metabolite of cumyl-5F-P7AICA identified in pooled human liver S9 fraction incubation containing 25 µM cumyl-5F-P7AICA

Supplementary Figure 2. HR-MS/MS spectrum of the ketone (M4) metabolite of cumyl-5F-P7AICA identified in pooled human liver S9 fraction incubation containing 25 µM cumyl-5F-P7AICA

Supplementary Figure 3. HR-MS/MS spectra of the

A: aryl-dihydroxylated (M6)

B: 5-fluoropentyl-dihydroxylated (M7)

C: aryl-and 5-fluoropentyl-dihydroxylated (M17)

metabolite of cumyl-5F-P7AICA identified in pooled human liver microsome (M6) and pooled human liver S9 fraction (M7, M17) incubations containing 25 µM cumyl-5F-P7AICA each

Supplementary Figure 4. HR-MS/MS spectra of the

A: oxidative defluorinated-5-fluoropentyl-monohydroxylated (M8)

B: oxidative defluorinated-aryl-monohydroxylated (M16)

metabolite of cumyl-5F-P7AICA identified in pooled human liver S9 fraction (M8) and pig liver microsome (M16) incubations containing 25 µM cumyl-5F-P7AICA each

Supplementary Figure 5. HR-MS/MS spectrum of carboxamide-5-fluoropentyl-monohydroxylated (M9) metabolite of cumyl-5F-P7AICA identified in pig liver microsome incubation containing 25 µM cumyl-5F-P7AICA

Supplementary Figure 6. HR-MS/MS spectrum of the oxidative defluorinated-carboxamide and carboxylated (M13) metabolite of cumyl-5F-P7AICA identified in rat urine following a single oral administration of 0.6 mg/kg body weight dose of cumyl-5F-P7AICA

Supplementary Figure 7. HR-MS/MS spectrum of the oxidative defluorinated-carboxamide (M14) metabolite of cumyl-5F-P7AICA identified in pooled human liver S9 fraction incubation containing 25 µM cumyl-5F-P7AICA

Supplementary Figure 8. HR-MS/MS spectrum of the oxidative defluorinated (M15) metabolite of cumyl-5F-P7AICA identified in pooled human liver S9 fraction incubation containing 25 µM cumyl-5F-P7AICA

Supplementary Figure 1.

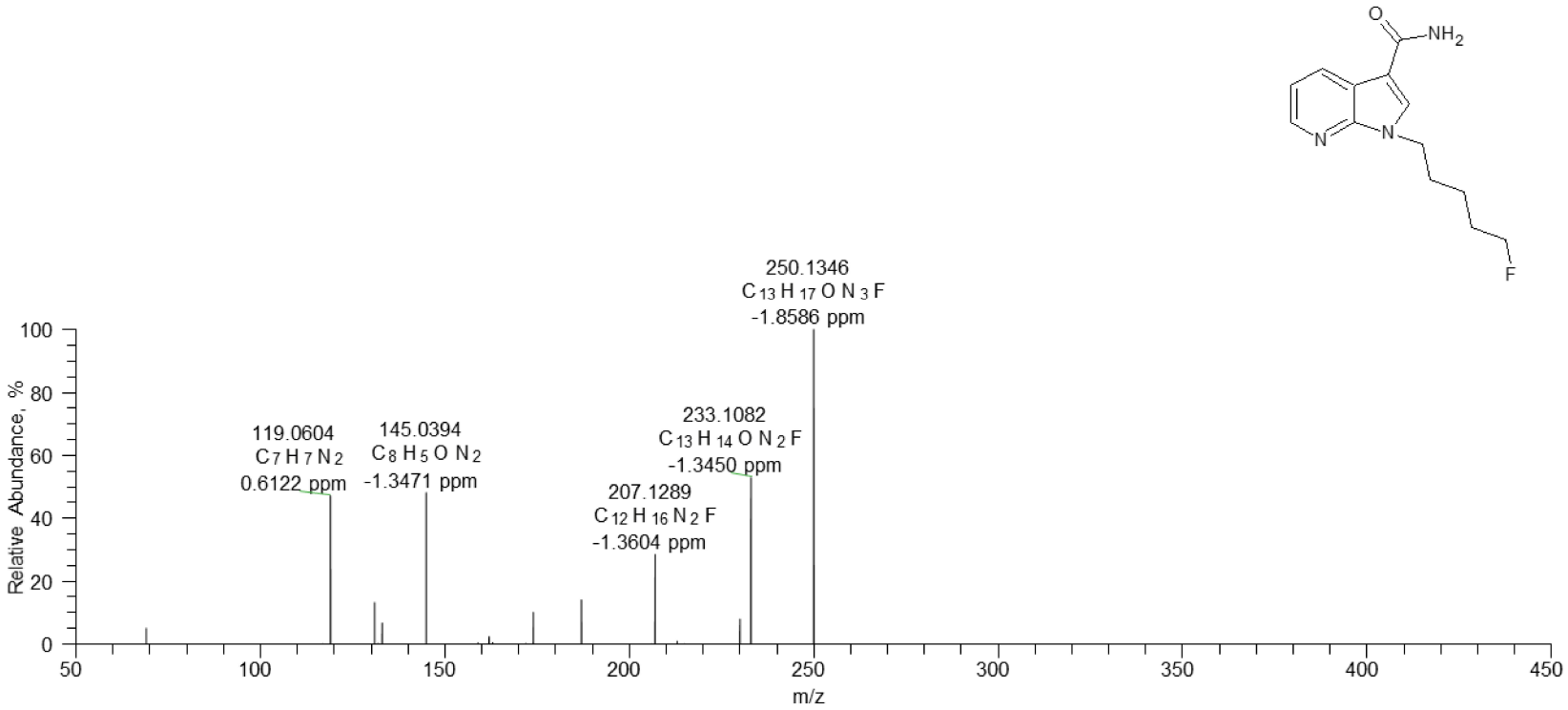

Supplementary Figure 2.

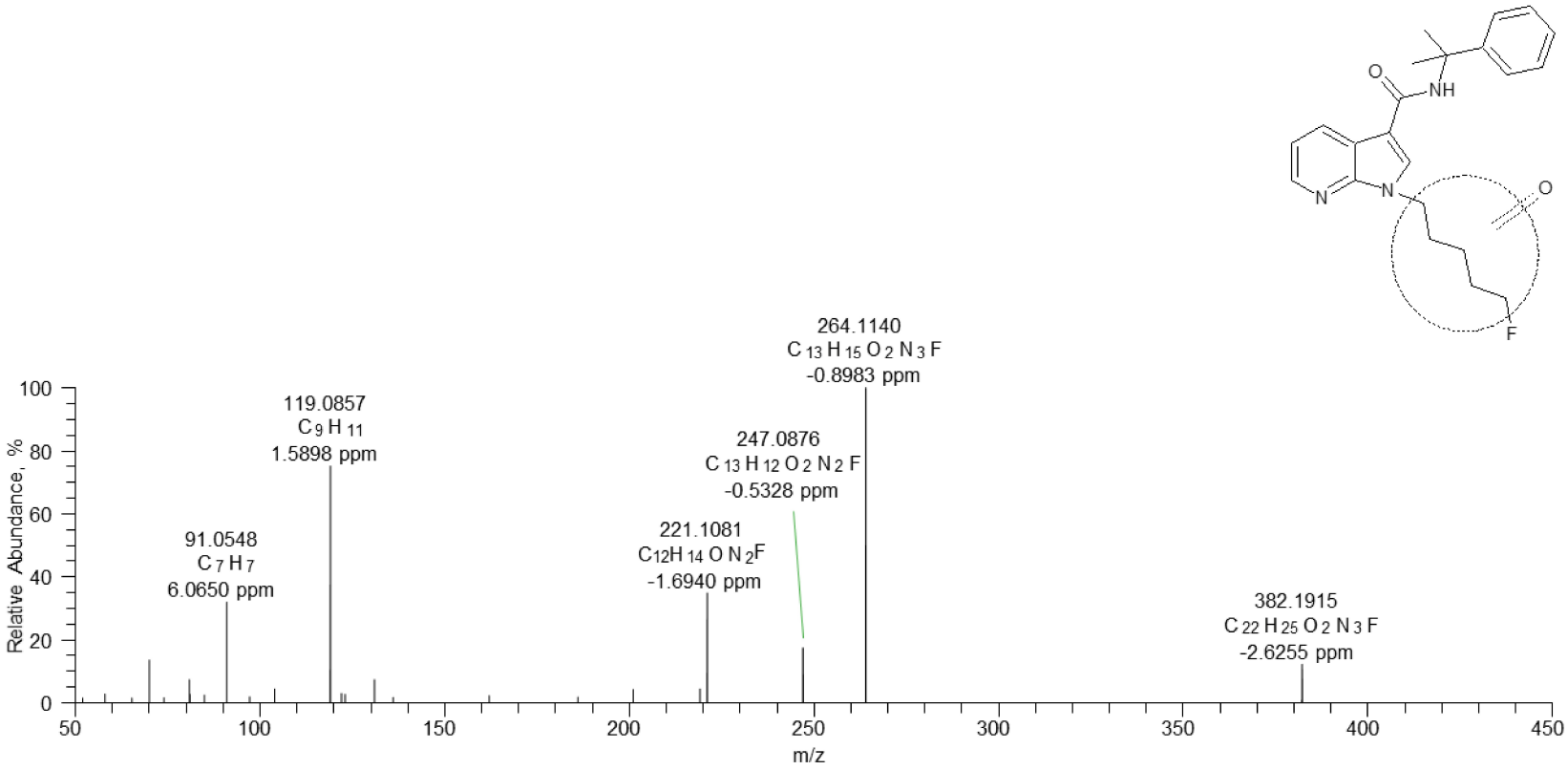

Supplementary Figure 3.

A

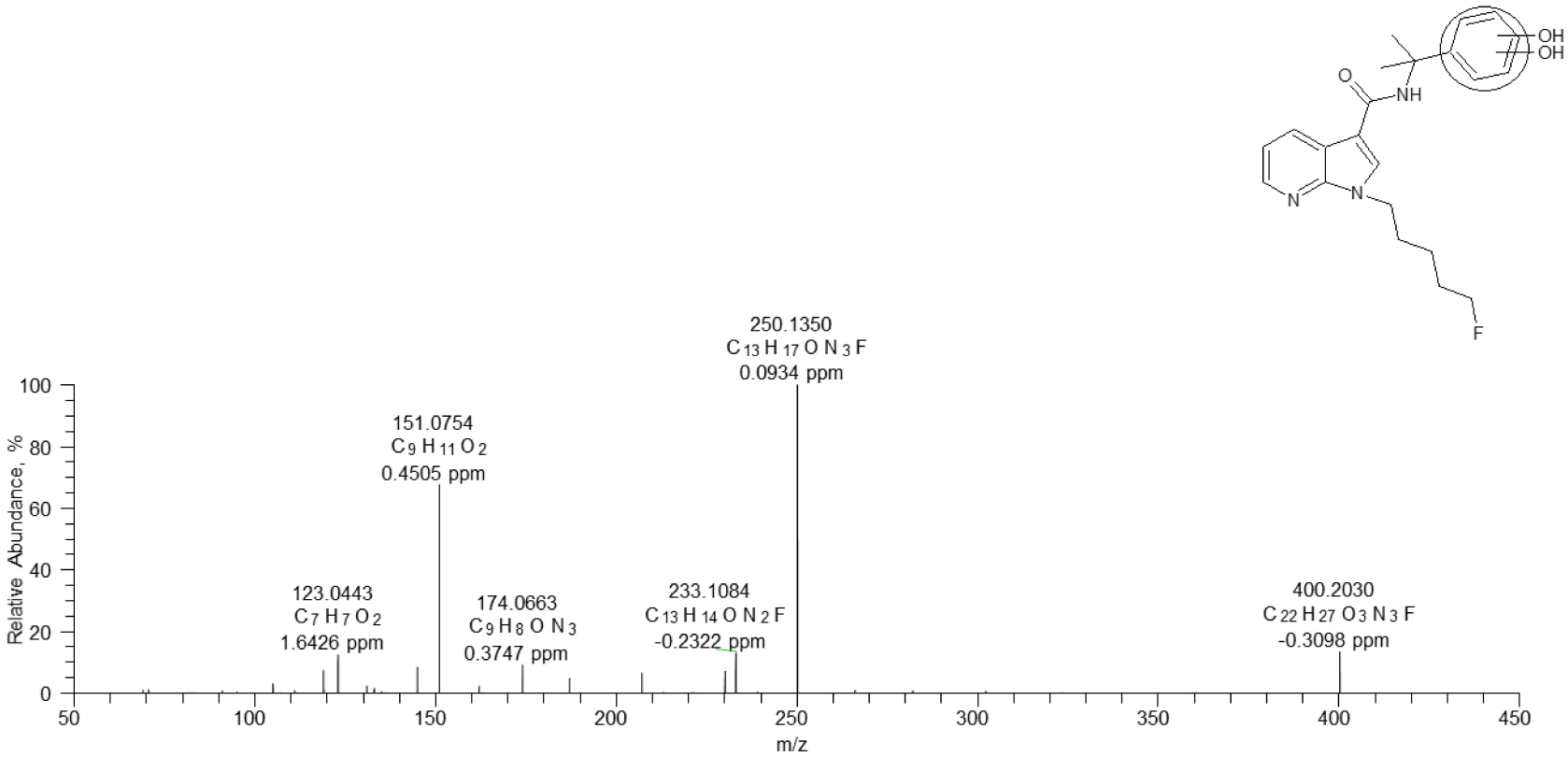

Supplementary Figure 4.

A

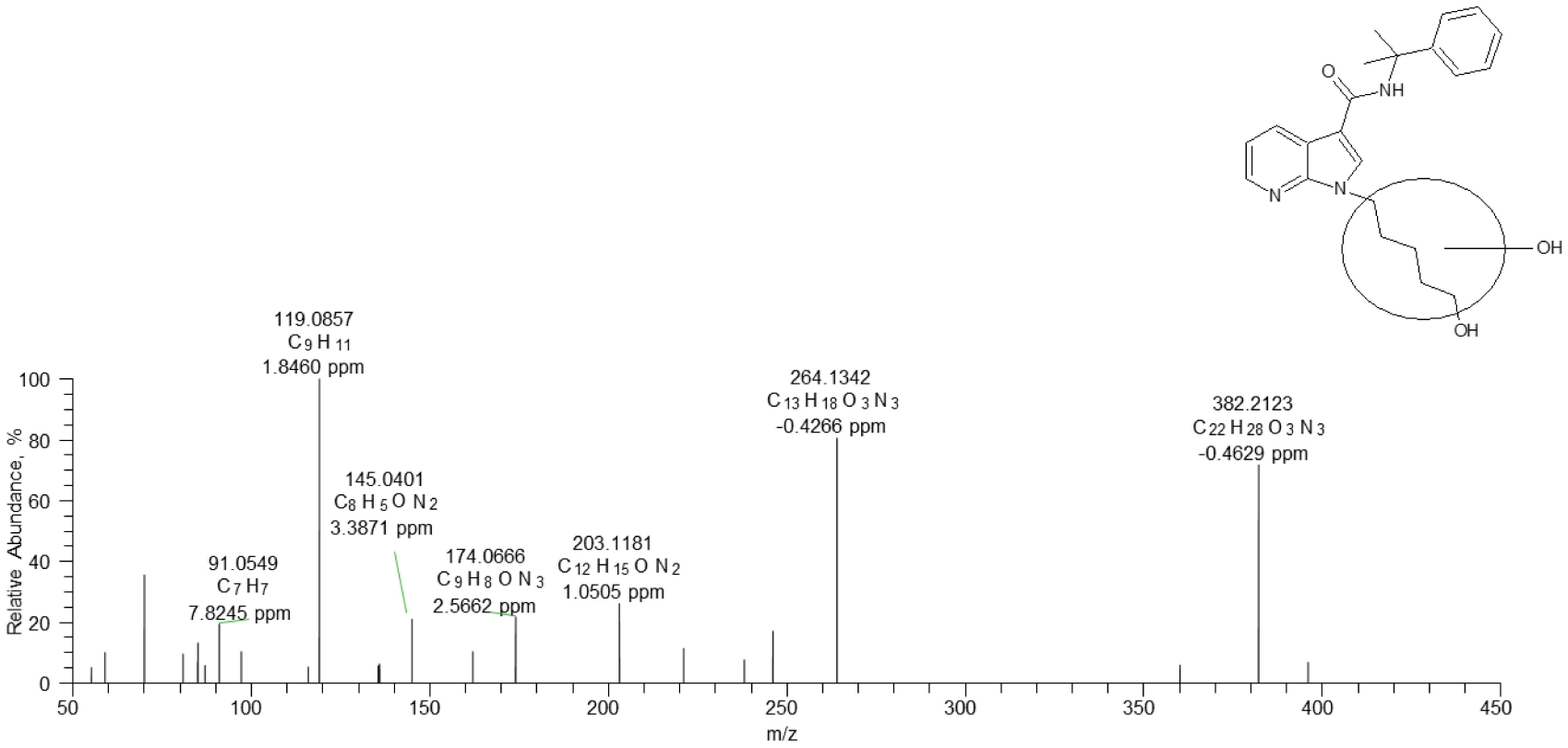

Supplementary Figure 5.

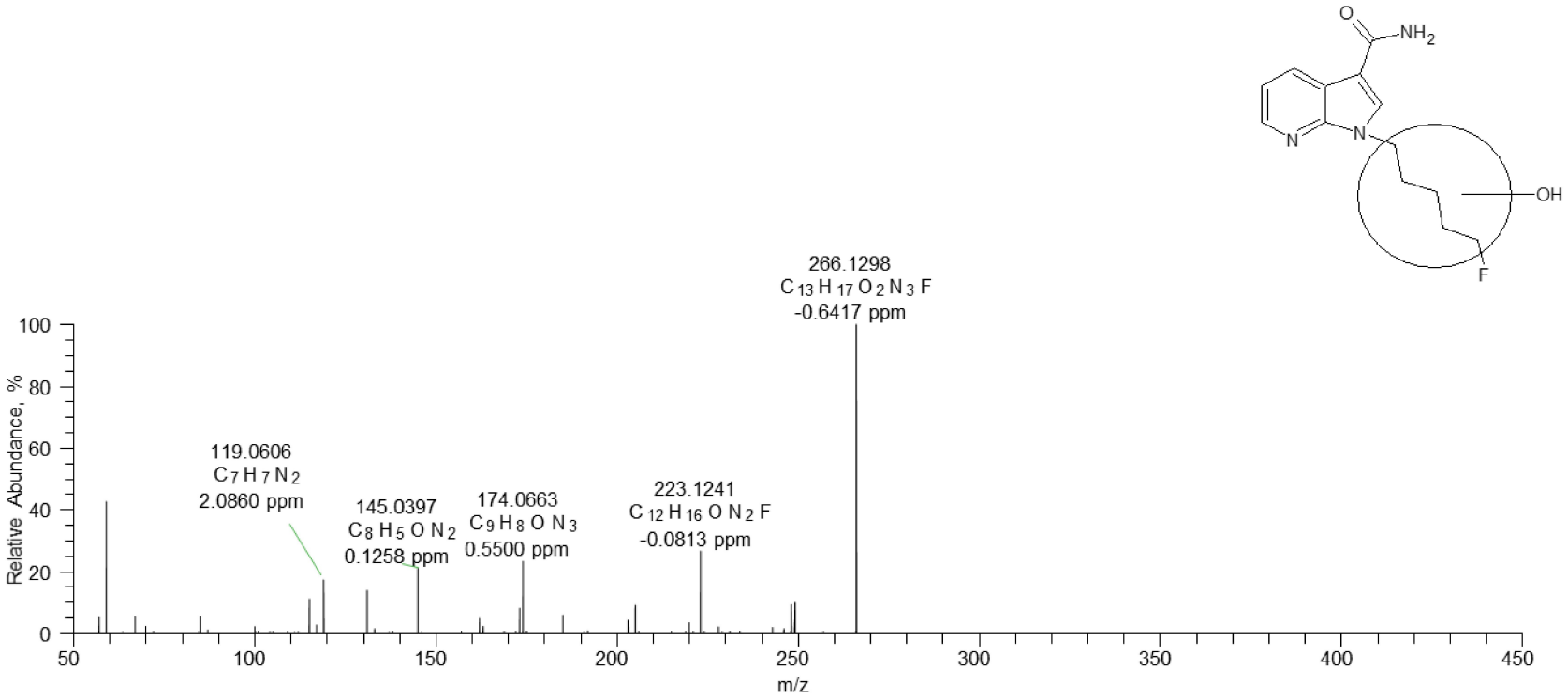

Supplementary Figure 6.

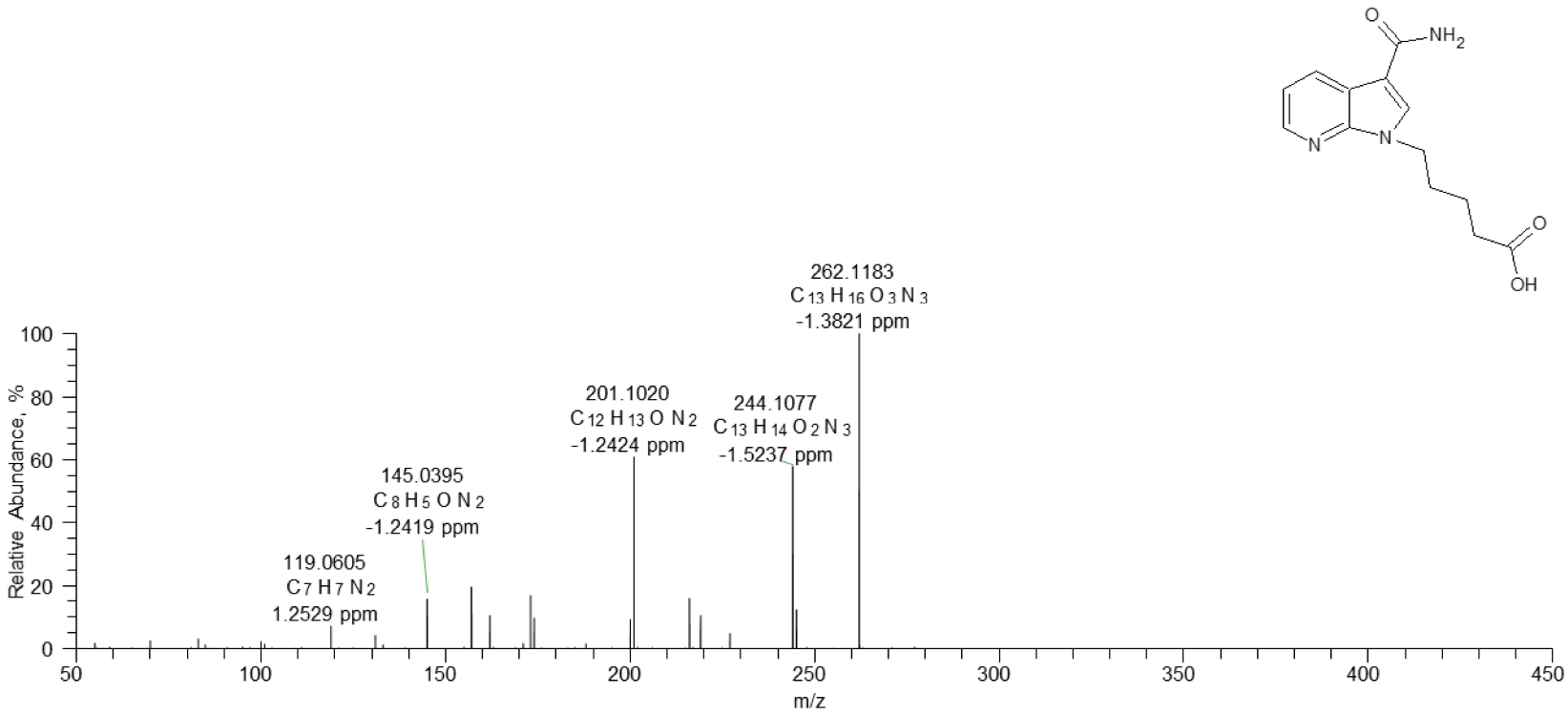

Supplementary Figure 7.

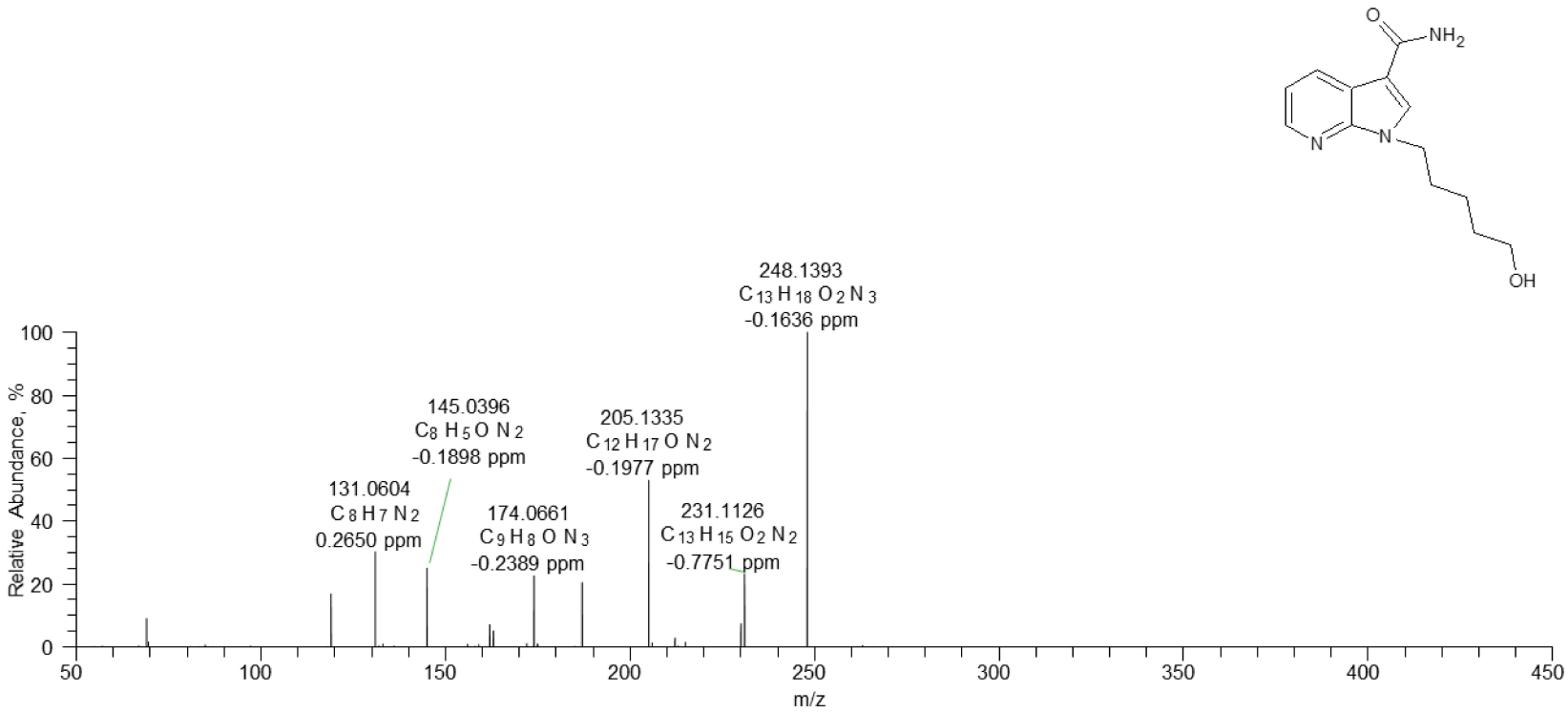

Supplementary Figure 8.

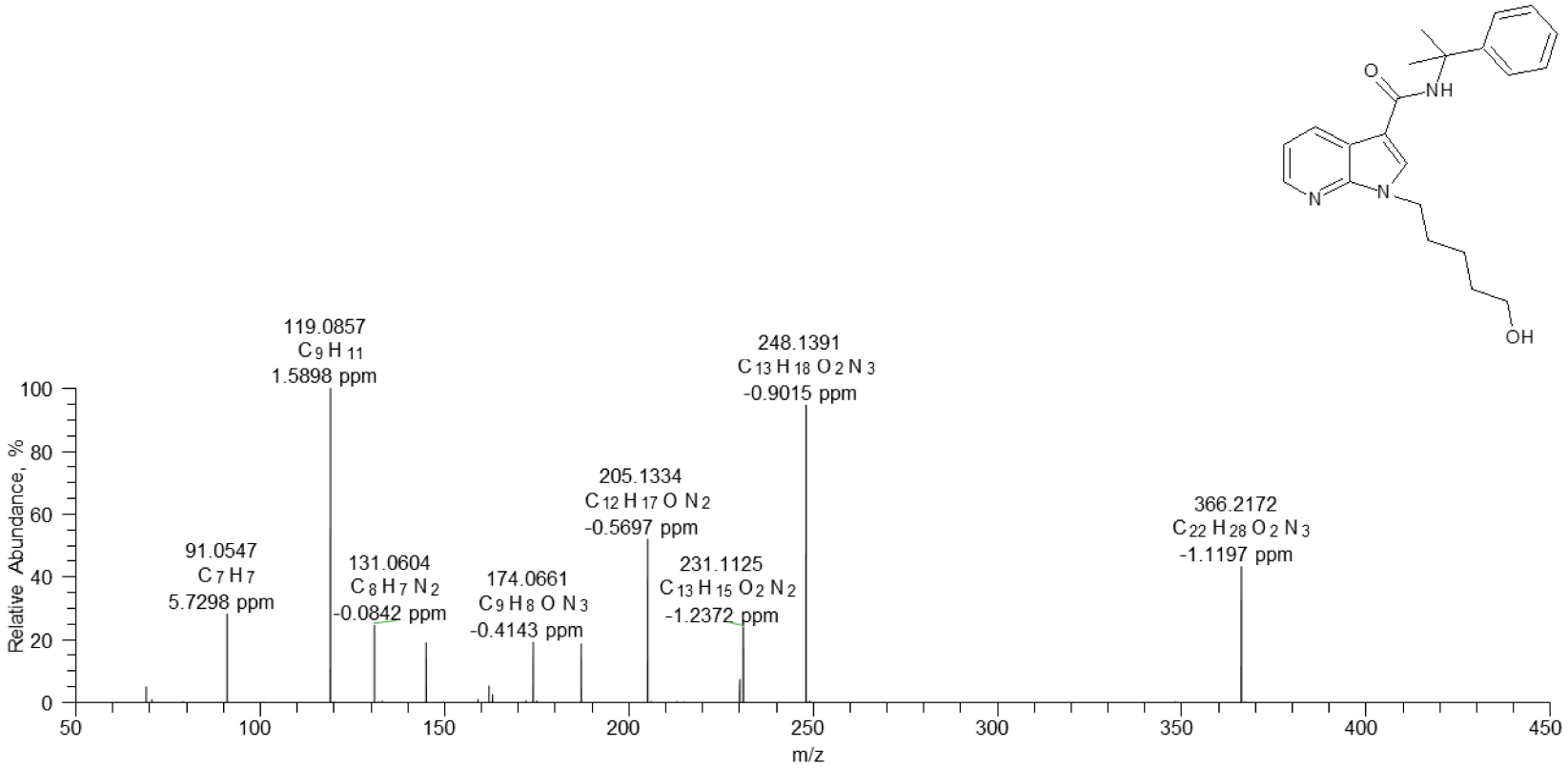

3.2 Development and method validation of a sampling technique for a reproducible detection of synthetic cannabinoids in exhaled breath using an *in vitro* pig lung model[142]

This is a pre-copyedited, author-produced version of an article accepted for publication in Journal of Analytical Toxicology following peer review. The version of record[142] and the Electronic Supplement Material is available online at:

(DOI: 10.1002/dta.2899)

Authors Contributions:

Nadja Walle conducted and evaluated the experiment as well as composed the manuscript; Adrian A. Doerr and Benjamin Peters assisted with the execution of the experiment; Matthias W. Laschke and Michael D. Menger assisted with the practical execution of the experiment and assisted with scientific discussions; Peter H. Schmidt, Markus R. Meyer, and Nadine Schaefer assisted with scientific discussions and supervised the research.

OXFORD UNIVERSITY PRESS | Journal of Analytical Toxicology

Development and method validation of a sampling technique for a reproducible detection of synthetic cannabinoids in exhaled breath using an in vitro pig lung model

Journal:	*Journal of Analytical Toxicology*
Manuscript ID	JAT-24-4235.R2
Manuscript Type:	Article
Keywords:	Exhaled breath, synthetic cannabinoids, cumyl-5F-P7AICA, pig model, sampling technique, LC-MS/MS, method validation

ABSTRACT

Alternative matrices, especially exhaled breath (EB), have gained increasing attention for a few years. To interpret toxicological findings, knowledge on the toxicokinetic (TK) properties of a substance in EB is indispensable. Whilst such data are already accessible for various drugs (e.g. Δ^9-tetrahydrocannabinol), they are still not available for new psychoactive substances, particularly synthetic cannabinoids (SCs). As SCs raise a high public health concern, the aim of this study was to assess these data in future TK studies in pigs. For this purpose, an in vitro sampling technique of EB was initially developed, being prospectively applied to anesthetized and ventilated pigs for the detection of SCs in a controlled and reproducible manner as exemplified by *cumyl*-5F-P7AICA. Furthermore, a method for the qualitative and quantitative detection of *cumyl*-5F-P7AICA in EB using glass fiber filters (GFF) was established und fully validated. Therefore, *cumyl*-5F-P7AICA (0.5 mg/mL in ethanol abs.) was initially nebulized using a ventilation machine and a breathing tube, as they are also used in surgeries. The aerosol was delivered into a simulated pig lung. To collect EB, a pump was connected to that part of the breathing tube, that contains EB (expiratory limb), and sampling was performed repeatedly (n=6) for 15 min (2 L EB/min) each using GFF. For extraction of the substance, the GFF were macerated with acetone and the remaining experimental components were rinsed with ethanol. After sample preparation, the extracts were analyzed by LC-MS/MS. In the complete experimental setup, about 40% of the initially nebulized *cumyl*-5F-P7AICA dose was found with 3.6 ± 1.3% being detected in the GFF. Regarding the comparably high loss of substance, the open ventilation system and a conceivable adsorption of the SC in the ventilator have to be considered. However, the herein introduced approach is promising to determine the TK properties of *cumyl*-5F-P7AICA in EB.

KEYWORDS Exhaled breath, synthetic cannabinoids, c*umyl*-5F-P7AICA, pig model, sampling technique, LC-MS/MS, method validation.

Introduction

Blood sample analysis is generally considered the gold standard for demonstrating impairment while driving under the influence of illicit substances (1). Urine drug testing also has a long history in clinical and forensic toxicology given the longer window of drug detection with most parent and metabolite compounds compared to blood. Hence, urine represents a commonly used matrix, e.g. in terms of abstinence controls within the scope of verifying the fitness to drive. Nevertheless, both commonly used matrices are afflicted with various disadvantages. On the one hand, sampling of blood (or urine) cannot be performed roadside (1). Furthermore, blood collection must be carried out by a phlebotomist (1), usually leading to a longer time interval between driving and blood drawing. Hence, the drug concentrations found in blood do not necessarily correspond to the concentrations at the time of participating in road traffic. Recently, the use of alternative matrices, e.g. oral fluid, dried blood spots and exhaled breath (EB), have gained increasing attention, as they offer several advantages as compared to blood and urine.

As EB is readily, easily, and unlimitedly available (2, 3), this specimen has emerged as a promising alternative matrix in various fields in the last few years. In clinical medicine, analysis of biomarkers in EB could be used for diagnosis and monitoring of different lung diseases (e.g. asthma) (4). Additionally, Thevis et al. (5) showed that EB aerosol analysis seems to be a promising approach at drug testing in sports, as selected model substances used in doping scenes were found in EB collected from patients who received the drug in the framework of their regular therapeutic setting. Last not least, interest in EB analysis has also increased recently in the field of clinical and forensic toxicology, to prove the acute influence of pharmaceuticals or drugs of abuse (DOA) in the context of intoxications or in road traffic, comparably to breath testing for alcohol. Several studies have shown that various pharmaceuticals and DOA (e.g. amphetamine, methadone, Δ^9-tetrahydrocannabinol (THC) are

detectable in EB (6–10). Thus, for promising future application in DOA testing, e.g. in road traffic, further investigations on EB are necessary.

To interpret toxicological findings of DOA in EB, knowledge on their toxicokinetic (TK) properties are necessary. Until now, only a few TK studies in EB have been conducted (3, 11–16). For THC, several data on its TK properties in EB have already been published (3, 14–17). As a 'legal' alternative to THC, synthetic cannabinoids (SCs) are still consumed without having underwent any previous toxicity study. However, data on their TK properties in EB are still lacking and have to be determined in systematic and controlled studies. Due to ethical reasons, human studies are not possible. Thus, alternative models have to be used. Previous studies have shown that the pig model seems to be suitable for the conduction of TK studies on new psychoactive substances, especially SCs (18–21). Hence, the pig model could also be a useful approach for the elucidation of the TK properties of drugs of abuse in EB, because this matrix can easily be obtained during a TK study. As already reported in previous studies, the pigs are anesthetized and given artificial respiration during the in vivo experiment (18–25). To apply the pig model in future TK EB studies, a prerequisite would be that EB can be collected in vivo in the ventilated pig in a controlled and reproducible manner.

Therefore, the aim of the present study was to develop a new sampling technique for EB in an in vitro pig lung model that can be applied prospectively to anesthetized and ventilated pigs for the detection of SCs, using *cumyl*-5F-P7AICA (Supplementary Figure S1A) as a representative for SCs containing a 7-azaindole core structure. Recently, this structural class of SCs have become more important, because by minimal structural modifications of already illegal derivatives, isomeric compounds were synthesized resulting in new, legal SCs, containing a e.g. 7-azaindole core structure, initially not regulated in most countries at this time. As a consequence, intoxications and fatal cases have increasingly been reported after the

consumption of such SCs (26–29). Additionally, an analytical method for a qualitative and quantitative detection of *cumyl*-5F-P7AICA in EB samples was developed and fully validated.

Materials and methods

Chemicals and reagents

The respective chemicals and reagents used for this study are listed in the Supplementary data.

EB sampling technique design using an in vitro pig lung model

Assessment of extraction efficiency

For the determination of the extraction efficiency, a reference solution of *cumyl*-5F-P7AICA (0.1 mg/mL each) was spiked onto glass fiber filters (GFF; 1.6 µm pore size, Sartorius AG, Goettingen, Germany; n=24). Subsequently, extraction of the drug was carried out by adding 5 mL of different extraction solvents (n=4 each; Table I), respectively. After ultrasonication for 10 min and centrifugation at 1,476 x *g* for 15 min, the solutions over the GFF were filtrated into new tubes using chromafil filters (1.0 µm pore size, Macherey-Nagel, Düren, Germany). Following, 1 mL of the solution was transferred into a new vial and evaporated to dryness under a gentle stream of nitrogen at 60 °C. The residues were dissolved in 1 mL ethanol and the solution was diluted 1:50 using a mixture (50:50, *v/v*) of mobile phases A (0.1% (v/v) formic acid in water) and B (0.1% (v/v) formic acid in acetonitrile). After the addition of 20 µL of a stable isotope-labeled internal standard (SIL-IS, AB-FUBINACA-d_4, 2 µg/20 µL), 5 µL of the extracts were injected onto the liquid chromatography tandem mass spectrometry (LC-MS/MS) system.

The examination of the drug concentrations was carried out using a one-point calibration, containing the same concentrations (2 µg/mL) of *cumyl*-5F-P7AICA and SIL-IS. For this, 20 µL each of a stock solution containing 100 µg/mL of *cumyl*-5F-P7AICA or SIL-IS was drawn

and diluted with 960 µL mobile phases A and B to a final volume of 1 mL. The one-point calibrator was prepared in triplicate and analysed over the entire sequence. For analysis, the mean value of the respective ratios was used.

Assessment of the EB sampling techniques efficiency

In order to collect the EB from anesthetized and ventilated pigs, the published and already applied setup for inhalative administration of SCs (22) was modified, as seen in Figure 1A. For this purpose, a pump was interposed at the expiratory limb to collect EB during expiration using GFF as adsorbens for *cumyl*-5F-P7AICA (Figure 1B).

Following, *cumyl*-5F-P7AICA (0.5 mg in 1 mL ethanol abs.) was nebulized under ventilation by the M-neb flow$^+$ nebulizer (Nebutec, Elsenfeld, Germany) applying the inspiration-triggered mode (< 0.2 mL/min). The settings of the ventilator were in accordance with the in vivo conditions of TK studies (18, 20, 21): 500 mL tidal volume, respiratory rate 12/min, 2% isoflurane (Forene, AbbVie, Ludwigshafen, Germany), mixture of oxygen and air (1:2 vol/vol; FiO_2 0.30; Respirator ABV-U; F. Stephan, Gackenbach, Germany). The heat and moisture exchanger (HME)-filter were removed in advance to prevent an adsorption of *cumyl*-5F-P7AICA to the internal components and only the box of the HME-filter was used to initiate nebulization. During inspiration, the aerosol was delivered through the tracheal tube into a simulated pig lung (n=6; SelfTestLung, Dräger, Germany; Figure 1B). During expiration, the EB passed the box of the HME-filter and was reverted via the expiratory limb into the ventilator. Additionally, a pump originating from environmental analysis (BiVOC2V2, Umweltanalytik Holbach GmbH, Wadern, Germany) was connected to the expiratory limb to collect a part of EB (Figure 1B). The pump was connected proximally to the tracheal tube and was set as follows: 2 L EB/min for 15 min. In order to collect *cumyl*-5F-P7AICA contained in EB, a GFF (n=6) as described in the previous section was placed between the expiratory limb

and the pump (Figure 1B). Subsequently, *cumyl*-5F-P7AICA was extracted from the GFF according to the already described procedure with a few modifications. First of all, acetone was used as extraction solvent. In addition, 25 µL SIL-IS (AB-FUBINACA-d_4, 50 ng/20 µL) was added as part of the 1:50 dilution.

Determination of the EB sampling techniques' efficiency was performed using a one-point calibration containing 50 ng/mL of *cumyl*-5F-P7AICA and SIL-IS, respectively. Preparation of the one-point calibrator was performed by diluting the respective stock solutions of *cumyl*-5F-P7AICA (1 µg/mL) and SIL-IS (2 µg/mL) with the required volume of a solution of mobile phases A and B. The one-point calibrator was prepared four times and was analysed over the entire sequence. For analysis, the mean value of the respective ratios was used.

Determination of drug residue in the reservoir of the nebulizer

Extraction of the drug from the drug reservoir was carried out in accordance to a previous study by Schaefer et al. (22). For this, the drug reservoir of the nebulizer device (n=6) was rinsed with approximately (approx.) 10 mL ethanol. Afterwards, the solution was diluted 1:50 using ethanol. Then, the obtained solution was diluted 1:5 with a mixture of mobile phases A and B (50:50, *v/v)* with addition of 25 µL SIL-IS (50 ng/25 µL). Analysis of the extracts was carried out by LC-MS/MS. The amount of the drug contained in the drug reservoir was determined using a one-point calibration (50 ng/mL) as described previously.

Determination of drug deposition in the tracheal tube

In accordance to a previous study (22), the drug deposition of *cumyl*-5F-P7AICA was determined after the tracheal tube (n=6) was cut into small pieces by adding approx. 80 mL of ethanol. After maceration for 10 min, the solution was diluted 1:20 with a mixture of mobile phases A and B (50:50, *v/v)*. After the addition of 25 µL SIL-IS (50 ng/25 µL), the extracts

were analyzed by LC-MS/MS. Evaluation of the results was performed in analogy to the previously described procedure.

Determination of drug deposition in the ventilation bag, box of the HME-filter and the breathing tube

In addition to the procedure described by Schaefer et al. (22) the amount of drug deposition in the ventilation bag, the box of the HME-filter and the expiratory limb of the breathing tube were determined. Initially, the ventilation bag (n=6) was chopped up with scissors. the addition of approx. 150 mL ethanol the solution was macerated for 10 min. The box of the HME-filter as well as the expiratory limb were rinsed with approx. 10 mL and 50 mL ethanol respectively. The subsequent procedure was in accordance to the approaches already described.

Calibration standards, and quality control (QC) solutions

In a first step, *cumyl*-5F-P7AICA as well as the SIL-IS RCS-4-d_9 and AB-FUBINACA-d_4 were dissolved in ethanol to get standard stock solutions with final concentrations of 1000 µg/mL each. Following, the prepared solutions were further diluted with ethanol to receive working standard solutions containing 0.01, 0.1, 1, and 10 µg/mL.

For preparation of the calibration standards containing final concentrations of 0.1, 2, 4, 6, 8, and 10 ng/filter of *cumyl*-5F-P7AICA, the prepared working standard solutions were dissolved with ethanol. Furthermore, QC solutions low and high containing final concentrations of 1.5 and 7 ng/filter of *cumyl*-5F-P7AICA were prepared analogously. All prepared solutions were stored at -20 °C until use.

Blank EB samples

Blank EB samples for method validation and preparation of QC samples were collected from drug-free pigs in the context of conducted TK studies and were performed in accordance with the German legislation on protection of animals and the National Institutes of Health Guide for the Care and Use of Laboratory Animals (permission number: 44/2019). The respective surgical procedures were in accordance to already published TK studies on SCs (18, 19, 21, 30), with the modification, that in addition carprofen (5 mg/kg body weight; Rimadyl; Zoetis, Berlin, Germany) was given to the animals as pain medication.

For this purpose, sixteen domestic male pigs of the Swabian Hall strain were used. Blank EB samples were collected prior to the in vivo TK studies using the BiVOC2V2 pump, being connected to the expiratory limb. Sampling of blank EB was performed over 2 h using GFF as adsorbent and 2 L of EB were collected for 15 min each, resulting in 8 blank EB samples per pig. Until use, the blank EB samples were stored at -20 °C.

Method validation

The method validation for EB was carried out in analogy to the guidelines of the Society of Toxicological and Forensic Chemistry (GTFCh) (31) and international guidelines (32) and included the parameter linearity, intra- and interday accuracy and precision tests, recovery (RE), matrix effects (ME), process efficiency (PE), selectivity, limit of detection (LOD), lower limits of quantification (LLOQ), freeze/ thaw, long-term, and processed sample stability and carryover effects.

Initially, 20 µL of a respective calibration solution (final concentrations: 0.1, 2, 4, 6, 8, and 10 ng/filter of *cumyl*-5F-P7AICA) were added to GFF without matrix to check for linearity of the calibration. Additionally, 20 µL of QC low and high solutions (final concentrations: 1.5 and 7 ng/filter of *cumyl*-5F-P7AICA) were spiked onto GFF without matrix as well as GFF containing blank EB in duplicates, respectively. Extraction was performed as already described

in the section 'Assessment of extraction efficiency' with a few modifications. First, acetone and RCS-4-d_9 were used as extraction solvent and SIL-IS (0.25 µg/20 µL), respectively. In addition, 20 µL SIL-IS were added to 1 mL acetone prior to evaporation without a further solution step with ethanol and the residues were dissolved in 100 µL of a mixture of mobile phases A and B. Analyses were performed in replicates at 8 different days. Linearity of the calibration was evaluated by plotting the analyte/SIL-IS peak area ratios against the respective concentration of the calibrator. A daily calibration curve was used to calculate the respective QC concentration.

Investigation of ME, PE, and RE was in analogy to the approach already published by Matuszewski et al. (33). In brief, for approach 1, blank EB GFF were spiked with QC low or high. For approach 2 the respective QC low or high solutions were added to 1 mL acetone after the extraction procedure. Approach 3 only consisted of the neat QC standards. Extraction was performed in accordance to the procedure described previously. To evaluate ME, the peak areas of *cumyl*-5F-P7AICA of approach 2 were set into correlation with the peak areas of the neat standards (approach 3), and for PE those of approach 1 and 3. Regarding RE, the absolute peak areas of the spiked blank EB GFF were compared to those of approach 2.

For the exclusion of possible interfering signals at the multiple reaction monitoring (MRM) transitions of *cumyl*-5F-P7AICA as well as the SIL-IS RCS-4-d_9 respectively, three different approaches were prepared. First, six blank EB GFF collected from different pigs were used and analyzed (blank samples). Additionally, two blank EB GFF were analyzed after the addition of SIL-IS (zero samples). Third, 25 µL of a solution containing different possibly interfering substances (JWH-015, JWH-081, JWH-122, JWH-182, JWH-200, JWH-203, JWH-210, JWH-250, AB-005, AM-694, AM-697, AM-1220, AM-1248, AM-2201, AM-2232, AM-2233, PB-22, 5F-PB-22, AB-FUBINACA, EAM-2201, RCS-4, RCS-8, MAM-2201, UR-144, XLR-11, THC, 11-THC-OH, THC-COOH, cannabidiol, cannabinol, pravadoline, 5F-MDMB-

PINACA, and 5F-MDMB-P7AICA; final concentration of 6.25 ng/filter each) were spiked onto a blank EB GFF.

LOD was evaluated by spiking blank EB GFF from drug-free pigs as well as GFF without matrix with *cumyl*-5F-P7AICA in final concentrations of 0.01, 0.02, 0.03, 0.04, 0.05, 0.06, 0.07, 0.08, 0.09, and 0.1 ng/filter respectively and was defined as the lowest concentration at which the signal to noise ratios of the respective qualifier and quantifier MRM transitions were at least 3:1.

For examination of the processed sample stability of *cumyl*-5F-P7AICA, 8 GFF without matrix were spiked with 20 µL QC low or high solution respectively and extraction was performed using the standard extraction method described previously. After the residues were dissolved in mobile phases A and B (50:50, *v/v)*, the solutions of each QC level were pooled and aliquoted to evenly distribute the analysis over an authentic LC-MS/MS sequence of about 10 h with time intervals of approx. 80 min. Evaluation of the results was performed by comparing the absolute peak area of *cumyl*-5F-P7AICA at each QC level against the time of injection and linear regression was performed. To investigate the freeze-thaw stability, GFF with matrix were spiked with 20 µL QC low or high solution (n=6 each) and stored at -20 °C. After three freeze-thaw cycles (20 h freezing followed by thawing of about 1 h at room temperature per cycle), extraction and analysis of the samples was performed. Preparation of the long-term stability samples was performed analogously and was determined after storage at -20 °C for 2 weeks. For evaluation of the results, an additional daily extraction without any prior treatment was performed (n=6 each). Quantification of *cumyl*-5F-P7AICA was carried out using a daily calibration curve.

Carry-over effects were examined during a LC-MS/MS analysis by measuring one blank sample between two highly concentrated extracts.

During the method validation, statistical tests were performed using Valistat 2.0.

LC-MS/MS conditions

For analysis, an Exion (AB SCIEX, Concord, USA) high pressure LC system was used. The LC system consisted of two AD pumps, an AD autosampler and an AD column oven. Separation of the analyte was achieved using a Macherey-Nagel (Dueren, Germany) nucleoshell PFP column (100x2 mm, 2.7 µm). The temperature of the column oven was set to 40 °C. Elution was carried out using mobile phases A (0.1% (*v/v*) formic acid in water) and B (0.1% (*v/v*) formic acid in acetonitrile) configured as a gradient elution as follows: 0-1 min 95% A, 1-6 min to 5% A, 6-9 min hold 5% A, 9-12 min hold 95% A, resulting in a total runtime of about 12 min. The flow rate was set to 0.5 mL/min. The SCIEX QTrap 5500+ mass spectrometer (MS) was provided with an electrospray ionization (ESI) source, run in positive mode and was set as follows: curtain gas, 40 arbitrary units (AU); ion source gas 1, 60 AU; ion source gas 2, 60 AU; ion spray voltage, 5.500 V; collision gas, 9 AU; ESI temperature, 550 °C; entrance potential, 10 V. The detection was carried out in the MRM mode using three transitions for the precursor ion of *cumyl*-5F-P7AICA and two transitions for the precursor ion of AB-FUBINACA-d_4 and RCS-4-d_9, respectively. The analysis conditions, the masses of the precursor ions as well as their respective product ions are listed in Supplementary Table SI. Analyst 1.7.2 was used for data analysis. Evaluation of the results was performed in accordance to national guidelines (34).

Results

Assessment of extraction efficiency

For the determination of the EB sampling technique efficiency, various extraction solvents were used to evaluate the best extraction procedure for *cumyl*-5F-P7AICA adsorbed at GFF. After spiking GFF with a reference solution of *cumyl*-5F-P7AICA (0.1 mg/mL in ethanol) the

extraction efficiencies of the various solvents were determined. The respective values are shown in Table I.

Assessment of the EB sampling technique efficiency

To assess the efficiency of the EB sampling technique, the respective ratios of the extracted drug from the GFF were compared with those obtained by extracted spiked drugs. Hence, in GFF approx. 3.6 ± 1.3% *cumyl*-5F-P7AICA could be found based on a nebulized dose of 0.5 mg (Figure 2).

Determination of drug residue in the reservoir of the nebulizer and drug deposition in the tracheal tube/ventilation bag/box of the HME-filter/breathing tube

The percentages of the nebulized dose found in the respective experimental components are shown in Figure 2. Comparing the results, highest values were found in the drug reservoir of the nebulizer device containing approx. 11 ± 4.2% of the initially nebulized drug dose followed by the breathing tube with approx. 8.4 ± 2.5% and the ventilation bag with approx. 7.9 ± 0.8%. The percentages found in the tracheal tube as well as in the box of the HME-filter amounted to approx. 3.7 ± 1.0% and 3.6 ± 0.3% respectively. In summary, about 40% of the nebulized SC dose could be found in the whole in vitro experimental setup.

Method development

In the context of the method development, RCS-4-d_9 as well as AB-FUBINACA-d_4 were tested as SIL-IS. Therefore, EB was collected during an in vivo TK study following pulmonary administration of *cumyl*-5F-P7AICA. Here, only a very low amount of *cumyl*-5F-P7AICA (pg

range) could be found in EB specimens. However, during the LC-MS/MS analysis of these authentic specimens it could be observed, that the internal standard AB-FUBINACA-d4 showed high signal intensities, even at low concentrations. As a result, the calculated ion ratios were in a very low range and the values could not be evaluated based on these ratios. Hence, RCS-4-d_9 appeared to be more suitable for quantification of *cumyl*-5F-P7AICA in GFF than AB-FUBINACA-d_4 and RCS-4-d_9 was used as SIL-IS for further method validation.

Method validation

The LC-MS/MS method was successfully validated with all sample matrices. All validation criteria were met for linearity, precision, accuracy, ME, PE, RE, selectivity, LOD, LLOQ, processed sample stability, freeze-thaw stability, long-term stability as well as carry-over effects (Table II).

The method validation has shown that all QC samples (with and without blank EB) could successfully be evaluated using a calibration curve without matrix. So, in future, evaluation of the results can therefore be carried out using calibration curves prepared without matrix.

Accuracy was demonstrated with QC bias ranging from -0.080% to -5.5% and repeatability RSD (relative standard deviation) from 2.9% to 7.3% (Table II). Intermediate precision RSD ranged from 4.1% to 8.1% demonstrating an acceptable reproducibility as the bias values lay within 15% of the nominal QC concentration and the RSD values are ≤15% (31).

ME ranged from 97% to 103%, being acceptable within ±25% when using a non-matched SIL-IS (31).

Concerning the selectivity, no interferences were detected at the MRM transitions of *cumyl*-5F-P7AICA and RCS-4-d_9 when analyzing blank pig EB samples as well as after spiking

with a solution containing various possibly interfering substances as already described in the section 'materials and methods' paragraph 'method validation'.

During validation, a value of 0.017 ng/filter was set as LOD for *cumyl*-5F-P7AICA in blank EB GFF of drug-free pigs and 0.022 ng/filter for blank GFF without matrix. Additionally, the lowest calibrator (0.1 ng/filter) was set as LLOQ.

Processed sample stability for 10h at 5 °C (4 – 6 °C), long-term frozen stability (2 weeks; -10 to -30 °C) and freeze-thaw stability was demonstrated with peak areas remaining within 10% of the original untreated concentration and the 90% confidence interval within 20% of the untreated concentration (31).

Finally, no carry over effects were detected.

Discussion

To elucidate the TK properties of SCs in EB, an already established pig model represents an appropriate tool, as EB can easily be obtained during an in vivo TK study. However, this application requires a sampling technique that can be used in anesthetized and ventilated pigs.

In order to obtain EB, Beck et al. developed a sampling device (ExaBreath®, SensAbues®, Västerås, Schweden) containing a polymer filter made of electret material (10, 35). Additionally, a handheld device, namely Hound® Marijuana Breathalyzer (Hound Labs Inc., Oakland, California, USA) is available to detect EB THC. Main advantages of the aforementioned devices are the easy applicability and transportability. Moreover, a substantial benefit is the sample delivery, with 100% of the EB and therefore also 100% of the substance contained in EB of the subject being delivered through the sampling device. However, the sampling devices require active exhalation of the subject. Therefore, these applications would not be suitable for use in an in vivo pig model.

For this reason, a new EB sampling technique has been developed in the present study applying an in vitro set up for implementation in the context of future TK studies on the SC *cumyl*-5F-P7AICA in anesthetized and ventilated pigs.

First of all, determination of the extraction efficiency using different extraction solvents revealed the highest amount and best extraction efficiency of *cumyl*-5F-P7AICA using acetone (90 ± 3.2%; Table I). Based on this finding, this extraction solvent was used for further extraction procedures in the context of the in vitro setup development for sampling EB in the present study.

Regarding the development of the EB sampling technique design, a total of about 40% of the nebulized dose of *cumyl*-5F-P7AICA was retained in the various components of the experimental setting (Figure 2). The comparably high 'loss' of substance (approx. 60%) may be influenced by several issues. First, as already seen for other SCs, they have a high affinity to plastic surfaces (22, 36, 37). Therefore, the comparably high amounts regarding the drug deposition at the expiratory limb, the box of the HME-filter, the tracheal tube as well as the ventilation bag are not surprising. Considering that these experimental components are also components of the authentic in vivo setup of the pulmonary TK study of SCs using the pig model (18–21), the observed adsorption of *cumyl*-5F-P7AICA might be neglected, as it could also be transferred to the in vivo experiment, at least in part.

Concerning the low amount of about 3.6 ± 1.3% (18 ± 6.5 µg/filter) *cumyl*-5F-P7AICA detected in GFF some issues have to be discussed. First of all, the pump is only capable of collecting a maximum EB volume of 2 L EB/min. Considering the aforementioned set up of the ventilator with a tidal volume of 500 mL and a respiratory rate of 12/min, this capacity results in only approx. 33% of the EB collected by the BiVOC2V2 pump. Consequently, only a maximum of about 33% of the amount of *cumyl*-5F-P7AICA contained in EB could be withheld by the used GFF. As a result, approx. 67% of the simulated EB/ contained substance

is transported back into the ventilator or is deposited on the components of the experimental setup (Figure 1B). Considering the nebulized dose (0.5 mg *cumyl*-5F-P7AICA) during the development of the in vitro sampling technique, a maximum quantity of approx. 165 µg of the substance can therefore be collected by the GFF. Hence, 11 ± 3.8% of the maximum detectable amount of *cumyl*-5F-P7AICA was found in the GFF. Compared to the sampling devices ExaBreath® and Hound® Marijuana Breathalyzer, with EB completely passing through the device, the lower passage represents a limiting factor in the sampling technique presented in the present study. This issue leads to lower drug concentrations retained in the GFF and the need of a more sensitive analytical procedure, especially for in vivo application. However, in a possible future application in authentic human clinical scenarios, the low amount of the total dose detected in EB may possibly lead to an undetectability of the ingested SC. This could especially be the case if, on the one hand the consumption took place a longer time before EB analysis and on the other hand only small quantities have been consumed. This should be considered when interpreting such data.

Additionally, the ventilator used in the present study constitutes an open ventilation system. Therefore, an additional adsorption of *cumyl*-5F-P7AICA in the ventilator resulting in a relevant loss of the SC should also be considered. However, as the ventilator also represents a component of the in vivo TK setup, this aspect can be transferred to the in vivo experiment.

Even if only small amounts of the nebulized SC have been detected in EB in the experimental setup, the comparably low standard deviations indicate that the technique allows for controlled and reproducible sampling of SCs in EB using the in vitro pig lung model for the detection of *cumyl*-5F-P7AICA in the framework of future TK studies after inhalative administration using pigs.

As a consequence, an analytical method for the qualitative and quantitative detection of *cumyl*-5F-P7AICA in EB was successfully developed and fully validated, so that it can be used

prospectively in the framework of proof-of-concept studies using the in vivo pig model.

Even if the method is suitable for the collection of EB using the pig model it should be considered, that the ventilation as well as the collection system limit the amount of EB collected. Therefore, the high 'loss' of approx. 67% of EB should be taken into account in the context of future studies and the respective methods adapted.

Conclusion

A controlled and reproducible sampling technique of EB in an in vitro pig lung model for the detection of the SC *cumyl*-5F-P7AICA as well as an analytical method for a qualitative and quantitative detection of this SC were successfully developed and fully validated in the present study. The comparatively high loss of the initial dose may be attributed to an adsorption of the substance to the ventilator. Nevertheless, the low standard deviation of the measurements indicates a good reproducibility of the technique and offers a promising approach for future application to anesthetized and ventilated pigs to assess the TK properties of *cumyl*-5F-P7AICA in EB.

Data availability

The data underlying this article are available in the article and in its online supplementary material.

References

1. Beck O, Ullah S, Kronstrand R. First evaluation of the possibility of testing for drugged driving using exhaled breath sampling. *Traffic Inj Prev* 2019;**20**:238–243. https://doi.org/10.1080/15389588.2019.1584397.
2. Arvidsson M, Ullah S, Franck J, et al. Drug abuse screening with exhaled breath and oral fluid in adults with substance use disorder. *Drug Test Anal* 2019;**11**:27–32. https://doi.org/10.1002/dta.2384.
3. Kintz P, Mura P, Jamey C, et al. Detection of Δ9-tetrahydrocannabinol in exhaled breath after cannabis smoking and comparison with oral fluid. *Forensic Toxicol* 2017;**35**:173–178. https://doi.org/10.1007/s11419-016-0333-x.
4. van Velzen P, Brinkman P, Knobel HH, et al. Exhaled breath profiles before, during and after exacerbation of COPD: a prospective follow-up study. *COPD* 2019;**16**:330–337. https://doi.org/10.1080/15412555.2019.1669550.
5. Thevis M, Krug O, Geyer H, et al. Expanding analytical options in sports drug testing: Mass spectrometric detection of prohibited substances in exhaled breath. *Rapid Commun Mass Spectrom* 2017;**31**:1290–1296. https://doi.org/10.1002/rcm.7903.
6. Beck O, Sandqvist S, Eriksen P, et al. Method for determination of methadone in exhaled breath collected from subjects undergoing methadone maintenance treatment. *J Chromatogr B Analyt Technol Biomed Life Sci* 2010;**878:**2255–2259. https://doi.org/10.1016/j.jchromb.2010.06.035.
7. Beck O, Leine K, Palmskog G, et al. Amphetamines detected in exhaled breath from drug addicts: A new possible method for drugs-of-abuse testing. *J Anal Toxicol* 2010;**34**:233–237. https://doi.org/10.1093/jat/34.5.233.
8. Beck O, Sandqvist S, Dubbelboer I, et al. Detection of Δ9-tetrahydrocannabinol in exhaled breath collected from cannabis users. *J Anal Toxicol* 2011;**35**:541–544. https://doi.org/10.1093/anatox/35.8.541.
9. Beck O, Stephanson N, Sandqvist S, et al. Detection of drugs of abuse in exhaled breath from users following recovery from intoxication. *J Anal Toxicol* 2012;**36:**638–646. https://doi.org/10.1093/jat/bks079.
10. Beck O, Stephanson N, Sandqvist S, et al. Detection of drugs of abuse in exhaled breath using a device for rapid collection: comparison with plasma, urine and self-reporting in 47 drug users. *J Breath Res* 2013;**7**:26006. https://doi.org/10.1088/1752-7155/7/2/026006.
11. Arvidsson M, Dahl M-L, Beck O, et al. Pharmacokinetics of methylphenidate and ritalinic acid in plasma correlations with exhaled breath and oral fluid in healthy volunteers. *Eur J Clin Pharmacol* 2020;**76**:229–237. https://doi.org/10.1007/s00228-019-02787-x.
12. Meyer MR, Rosenborg S, Stenberg M, et al. First report on the pharmacokinetics of tramadol and O-desmethyltramadol in exhaled breath compared to plasma and oral fluid after a single oral dose. *Biochem Pharmacol* 2015;**98:**502–510. https://doi.org/10.1016/j.bcp.2015.09.008.
13. Ellefsen KN, Concheiro M, Beck O, et al. Quantification of cocaine and metabolites in exhaled breath by liquid chromatography-high-resolution mass spectrometry following controlled administration of intravenous cocaine. *Anal Bioanal Chem* 2014;**406:**6213–6223. https://doi.org/10.1007/s00216-014-8051-x.
14. Himes SK, Scheidweiler KB, Beck O, et al. Cannabinoids in exhaled breath following controlled administration of smoked cannabis. *Clin Chem* 2013;**59**:1780–1789. https://doi.org/10.1373%2Fclinchem.2013.207407.

15. Coucke L, Massarini E, Ostijn Z, et al. Δ(9)-Tetrahydrocannabinol concentrations in exhaled breath and physiological effects following cannabis intake - A pilot study using illicit cannabis. *Clini Biochem* 2016;**49**:1072–1077. https://doi.org/10.1016/j.clinbiochem.2016.06.003.
16. Lynch KL, Luo YR, Hooshfar S, et al. Correlation of breath and blood Δ(9)-tetrahydrocannabinol concentrations and release kinetics following controlled administration of smoked cannabis. *Clin Chem* 2019;**65:**1171–1179. https://doi.org/10.1373/clinchem.2019.304501.
17. Manolis A, McBurney LJ, Bobbie BA. The detection of Δ9-tetrahydrocannabinol in the breath of human subjects. *Clin Biochem* 1983;**16:**229–233. https://doi.org/10.1016/S0009-9120(83)90070-X.
18. Doerr, AA, Nordmeier F, Walle N, et al. Can a recently developed pig model be used for in vivo metabolism studies of 7-azaindole-derived synthetic cannabinoids? A study using 5F-MDMB-P7AICA. *J Anal Toxicol* 2021;**45:**593–604. https://doi.org/10.1093/jat/bkaa122.
19. Schaefer N, Kroell A-K, Koerbel C, et al. Time- and temperature-dependent postmortem concentration changes of the (synthetic) cannabinoids JWH-210, RCS-4, as well as Δ9-tetrahydrocannabinol following pulmonary administration to pigs. *Arch Toxicol* 2020;**94:**1585–1599. https://doi.org/10.1007/s00204-020-02707-4.
20. Schaefer N, Kroell A-K, Koerbel C, et al. Distribution of the (synthetic) cannabinoids JWH-210, RCS-4, as well as Δ9-tetrahydrocannabinol following pulmonary administration to pigs. *Arch Toxicol* 2019;**93:**2211–2218. https://doi.org/10.1007/s00204-019-02493-8.
21. Walle N, Nordmeier F, Doerr AA, et al. Comparison of in vitro and in vivo models for the elucidation of metabolic patterns of 7-azaindole-derived synthetic cannabinoids exemplified using cumyl-5F-P7AICA. *Drug Test Anal* 20;**13:**74–90. https://doi.org/10.1002/dta.2899.
22. Schaefer N, Kroell AK, Laschke MW, et al. Development of an in-vitro drug delivery efficiency test for a pulmonary toxicokinetic pig study. *Curr Drug Deliv* 2018;**15:**1167–1171. http://dx.doi.org/10.2174/1567201815666180214130014.
23. Schaefer N, Wojtyniak J-G, Kettner M, et al. Pharmacokinetics of (synthetic) cannabinoids in pigs and their relevance for clinical and forensic toxicology. *Toxicol Lett* 2016;**253:**7–16. https://doi.org/10.1016/j.toxlet.2016.04.021.
24. Schaefer N, Kettner M, Laschke MW, et al. Distribution of synthetic cannabinoids JWH-210, RCS-4 and Δ 9-tetrahydrocannabinol after intravenous administration to pigs. *Curr Neuropharmacol* 2017;**15**:713–723. https://doi.org/10.2174/1570159x15666161111114214.
25. Schaefer N, Wojtyniak J-G, Kroell A-K, et al. Can toxicokinetics of (synthetic) cannabinoids in pigs after pulmonary administration be upscaled to humans by allometric techniques? *Biochem Pharmacol* 2018;**155:**403–418. https://doi.org/10.1016/j.bcp.2018.07.029.
26. Oberhofer E. Tödlicher Rauch aus der Eimer-Bong. *MMW - Fortschritte der Medizin* 2018;**160:**14. https://doi.org/10.1007/s15006-018-0960-8.
27. Walle N, Doerr AA, Schmidt PH, et al. 'Flying high?'-Jump from a height in a 'Spice' high?: A case report on the synthetic cannabinoid 5F-MDMB-P7AICA. *Drug Test Anal* 2023;**15**:368–373. https://doi.org/10.1002/dta.3401.
28. Halter S, Angerer V, Roehrich J, et al. Cumyl-PEGACLONE: A comparatively safe new synthetic cannabinoid receptor agonist entering the NPS market? *Drug Test Anal* 2019;**11**:347–349. https://doi.org/10.1002/dta.2545.

29. Zawadzki M, Chłopaś-Konowałek A, Nowak K, et al. Quantification of 5F-CUMYL-P7AICA in blood and urine from an authentic fatality associated with its consumption by UHPLC–MS/MS. *Forensic Toxicol* 2021;**39**:240–247. http://dx.doi.org/10.1007/s11419-020-00555-6.
30. Schaefer N, Nordmeier F, Kroell A-K, et al. Is adipose tissue suitable for detection of (synthetic) cannabinoids? A comparative study analyzing antemortem and postmortem specimens following pulmonary administration of JWH-210, RCS-4, as well as Δ9-tetrahydrocannabinol to pigs. *Arch Toxicol* 2020;**94:**3421–3431. https://doi.org/10.1007%2Fs00204-020-02843-x.
31. Peters FT, Hartung M, Herbold M, et al. Anhang B zur Richtlinie der GTFCh zur Qualitätssicherung bei forensisch-toxikologischen Untersuchungen - Anforderungen an die Validierung von Analysenmethoden. *Toxichem Krimtech* 2009;**76:**185–208.
32. Peters FT, Drummer OH, Musshoff F. Validation of new methods. *Forensic Sci Int* 2007;**165:**216–224. http://dx.doi.org/10.1016/j.forsciint.2006.05.021.
33. Matuszewski BK, Constanzer ML, Chavez-Eng CM. Strategies for the assessment of matrix effect in quantitative bioanalytical methods based on HPLC-MS/MS. *Anal Chem* 2003;**75:**3019–3030. https://doi.org/10.1021/ac020361s.
34. Paul LD, Musshoff F, Becker J, et al. Richtlinie der GTFCh zur Qualitätssicherung bei forensisch-toxikologischen Untersuchungen. *Toxichem Krimtech* 2018;**85**:2-6.
35. Tinglev ÅD, Ullah S, Ljungkvist G, et al. Characterization of exhaled breath particles collected by an electret filter technique. *J Breath Res* 2016;**10:**26001. https://doi.org/10.1088/1752-7155/10/2/026001.
36. Christophersen AS. Tetrahydrocannabinol stability in whole blood: plastic versus glass containers. *J Anal Toxicol* 1986;**10:**129–131. https://doi.org/10.1093/jat/10.4.129.
37. Kneisel S, Speck M, Moosmann B, et al. Stability of 11 prevalent synthetic cannabinoids in authentic neat oral fluid samples: glass versus polypropylene containers at different temperatures. *Drug Test Anal* 2013;**5**:602–606. https://doi.org/10.1002/dta.1497.

Table I. Extraction efficiencies [EE; %] of *cumyl*-5F-P7AICA from glass fiber filter using different solvents.
(RSD = relative standard deviation)

Solvent	EE ± RSD
Acetone	90 ± 3.2
Ethyl acetate	87 ± 3.1
Acetonitrile	84 ± 1.0
Methanol	84 ± 6.3
Ethanol	83 ± 2.5
N-hexane/ethyl acetate (9:1)	54 ± 1.6

544

Table II. Calibration range (ng/filter), limit of detection (LOD; ng/filter), lower limits of quantification (LLOQ; ng/filter), nominal concentration (conc.; ng/filter), matrix effect (ME), recovery (RE), process efficiency (PE), accuracy, repeatability, as well as intermediate precision values of *cumyl*-5F-P7AICA after quality control (QC) solutions low and high were spiked on GFF with pig blank EB (matrix) and GFF without matrix, respectively.
(RSD = relative standard deviation; ./. = not tested)

	Matrix	**Without matrix**
Calibration range	0.1 - 10	0.1 - 10
LOD	0.017	0.022
LLOQ	0.10	0.10

	QC low		**QC High**	
	Matrix	**Without matrix**	**Matrix**	**Without matrix**
Nominal conc.	1.5	1.5	7	7
ME % (RSD %)	103 (4.2)	./.	97 (5.2)	./.
RE % (RSD %)	85 (8.3)	./.	85 (4.9)	./.
PE % (RSD %)	87 (8.5)	./.	83 (3.6)	./.
Accuracy bias [%]	-5.5	-3.5	-2.4	-0.080
Repeatability RSD [%]	2.9	7.3	2.9	4.4
Intermediate precision RSD [%]	8.1	7.3	4.1	4.4

Legend to figures

Figure 1. In vivo **(A)** and in vitro **(B)** setup for the collection of exhaled breath (EB) in the context of future toxicokinetic studies using a pig model after inhalative administration of synthetic cannabinoids (SC) (EB = exhaled breath; HME = heat and moisture; * = possible adhesion of the SC (approx. 67%); [1)] = sampling of 2 L EB/min, i.e. a maximum of approx. 33% of EB can be collected by the pump, resulting in a maximum of 33% of the initial SC dose that can be retained in the glass fiber filter if the ventilator settings are considered (tidal volume and respiratory rate)).

Figure 2. Percentages of *cumyl*-5F-P7AICA found in the respective experimental components (nebulizer device (pink); breathing tube (yellow); ventilation bag (gray); tracheal tube (red); box of the heat and moisture /HME)-filter (blue) and glass fiber filter (green)) based on a nebulized dose of 0.5 mg. (* = approx. 11 ± 3.8% of the maximum amount of substance (33% of 0.5 mg = 165 µg)).

Table I. Extraction efficiencies [EE; %] of *cumyl*-5F-P7AICA from glass fiber filter using different solvents.
(RSD = relative standard deviation)

Solvent	EE ± RSD
Acetone	90 ± 3.2
Ethyl acetate	87 ± 3.1
Acetonitrile	84 ± 1.0
Methanol	84 ± 6.3
Ethanol	83 ± 2.5
N-hexane/ethyl acetate (9:1)	54 ± 1.6

Table II. Calibration range (ng/filter), limit of detection (LOD; ng/filter), lower limits of quantification (LLOQ; ng/filter), nominal concentration (conc.; ng/filter), matrix effect (ME), recovery (RE), process efficiency (PE), accuracy, repeatability, as well as intermediate precision values of *cumyl*-5F-P7AICA after quality control (QC) solutions low and high were spiked on GFF with pig blank EB (matrix) and GFF without matrix, respectively.
(RSD = relative standard deviation; ./. = not tested)

	Matrix	**Without matrix**
Calibration range	0.1 - 10	0.1 - 10
LOD	0.017	0.022
LLOQ	0.10	0.10

	QC low		**QC High**	
	Matrix	**Without matrix**	**Matrix**	**Without matrix**
Nominal conc.	1.5	1.5	7	7
ME % (RSD %)	103 (4.2)	./.	97 (5.2)	./.
RE % (RSD %)	85 (8.3)	./.	85 (4.9)	./.
PE % (RSD %)	87 (8.5)	./.	83 (3.6)	./.
Accuracy bias [%]	-5.5	-3.5	-2.4	-0.080
Repeatability RSD [%]	2.9	7.3	2.9	4.4
Intermediate precision RSD [%]	8.1	7.3	4.1	4.4

Figure 1.

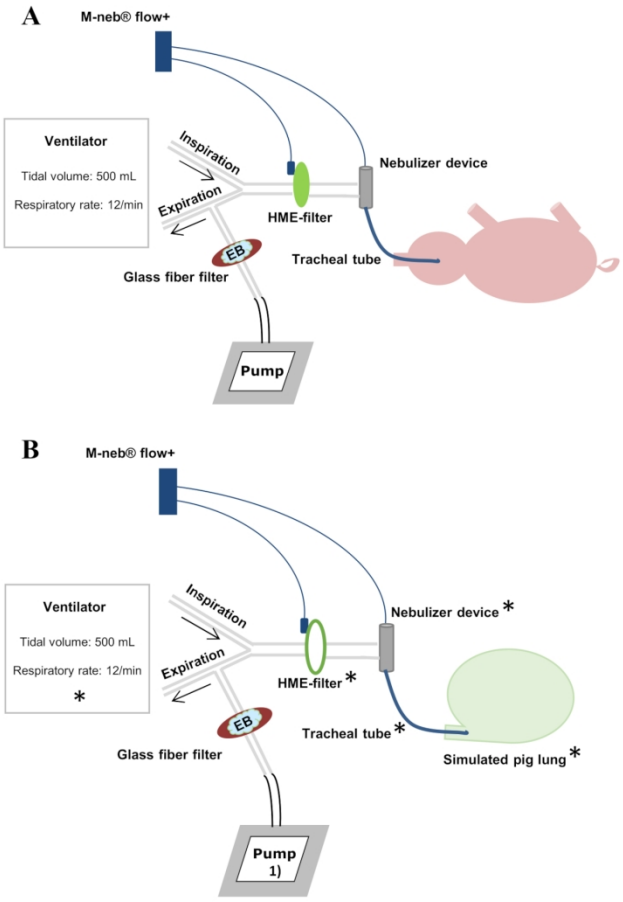

173x176mm (300 x 300 DPI)

Figure 2.

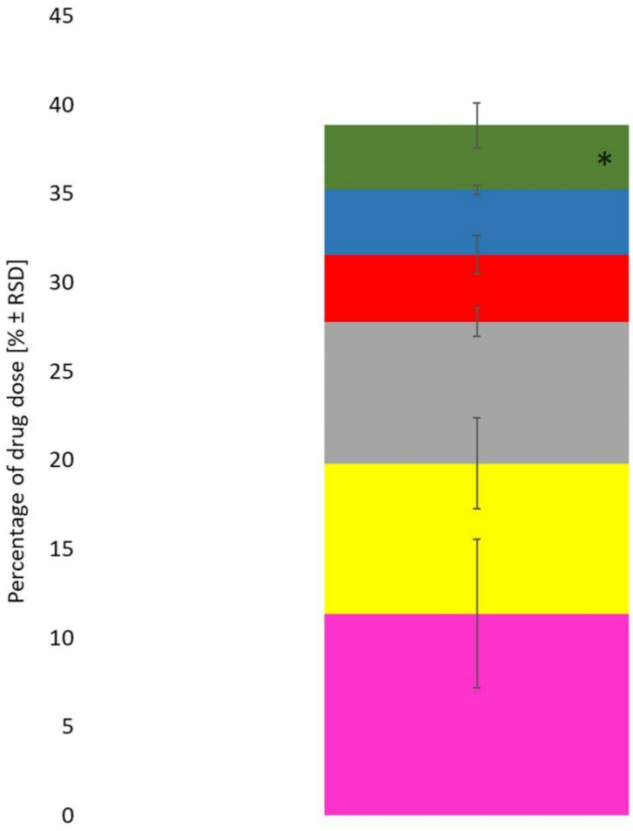

173x163mm (300 x 300 DPI)

Figure S1.

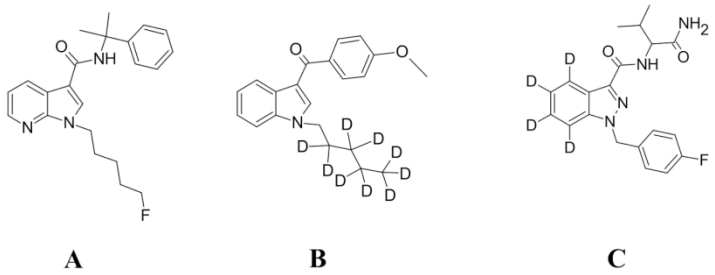

A **B** **C**

173x90mm (300 x 300 DPI)

Journal of Analytical Toxicology

Supplementary Data

Development and method validation of a sampling technique for a reproducible detection of synthetic cannabinoids in exhaled breath using an in vitro pig lung model

Materials and methods

Chemicals and reagents

Ethanol p.a., methanol p.a., acetonitrile (HPLC grade), water (HPLC grade), and acetone (analytical grade) were obtained from Fisher Scientific (Loughborough, United Kingdom), ethyl acetate, n-hexane as well as formic acid (98-100%) from Merck (Darmstadt, Germany). *Cumyl*-5F-P7AICA (purity 99.72 %) was provided by the German Federal Criminal Police Office (Wiesbaden, Germany). JWH-015, JWH-081, JWH-122, JWH-182, JWH-200, JWH-203, JWH-210, JWH-250, AB-005, AM-694, AM-697, AM-1220, AM-1248, AM-2201, AM-2232, AM-2233, PB-22, 5F-PB-22, AB-FUBINACA, EAM-2201, RCS-4, RCS-8, MAM-2201, UR-144, XLR-11, 5F-MDMB-PINACA, Pravadoline, 5F-MDMB-P7AICA (solid; 1 mg) as well as the standards RCS-4-d_9 (solid; 1 mg, Supplementary Figure S1B) and AB-FUBINACA-d_4 (solid; 1 mg, Supplementary Figure S1C) were purchased from Cayman Europe (Tallinn, Estonia). JWH-018 was provided from THC Pharm (Frankfurt/Main, Germany) and cannabinol, cannabidiol, Δ9-tetrahydrocannabinol (THC), 11-hydroxy-THC (11-HO-THC), as well as 11-nor-9-carboxy-THC (THC-COOH) were from Sigma-Aldrich (Munich, Germany).

Table S1. MRM transitions of c*umyl*-5F-P7AICA, AB-FUBINACA-d_4, and RCS-4-$d_9$as well as the respected retention time.
(* = target ion)

Analyte	Precursor ion [*m/z*]	Product ions [*m/z*]	Retention time [*min*]	Dwell time [*msec*]	Declustering potential [*V*]	Collision energy [*V*]	Cell exit potential [*V*]
Cumyl-5F-P7AICA	368.06	250.20* 174.10 230.20	4.60	20	106	37* 47 41	14* 10 14
AB-FUBINACA-d_4	373.18	328.20* 257.10	4.20	20	66	23* 35	12* 16
RCS-4-d_9	331.08	135.10 77.10	5.08	20	100	33* 69	6* 10

Legend to figures

Figure S1. Molecular structures of *cumyl*-5F-P7AICA **(A)**, and RCS-4-d_9 **(B)**, and AB-FUBINAC-d_4 **(C)**.

3.3 Are the postmortem concentration changes of the synthetic cannabinoid *cumyl*-5F-P7AICA and its *N*-pentanoic acid metabolite dependent on the environmental conditions? – A systematic study following pulmonary administration to pigs[143]

(DOI: 10.1016/j.toxlet.2024.10.006)

Authors Contributions:

Nadja Walle conducted and evaluated the experiment as well as composed the manuscript; Adrian A. Doerr and Benjamin Peters assisted at the execution of the animal experiments; Matthias W. Laschke and Michael D. Menger carried out and enabled the animal experiments and assisted with scientific discussions; Peter H. Schmidt, Markus R. Meyer, and Nadine Schaefer assisted with scientific discussions, the development of the experiment and supervised the research.

Toxicology Letters 401 (2024) 170–180

Contents lists available at ScienceDirect

Toxicology Letters

journal homepage: www.journals.elsevier.com/toxicology-letters

Are the postmortem concentration changes of the synthetic cannabinoid *cumyl*-5F-P7AICA and its *N*-pentanoic acid metabolite dependent on the environmental conditions? – A systematic study following pulmonary administration to pigs

Nadja Walle [a], Adrian A. Doerr [a], Benjamin Peters [a], Matthias W. Laschke [b], Michael D. Menger [b], Peter H. Schmidt [a], Markus R. Meyer [c], Nadine Schaefer [a,*]

[a] *Institute of Legal Medicine, Saarland University, Building 49.1, Homburg 66421, Germany*
[b] *Institute for Clinical & Experimental Surgery, Saarland University, Building 65/66, Homburg 66421, Germany*
[c] *Department of Experimental and Clinical Toxicology, Center for Molecular Signaling (PZMS), Saarland University, Building 46, Homburg 66421, Germany*

ARTICLE INFO

Keywords:
Synthetic cannabinoids
cumyl-5F-P7AICA
7-azaindole
Pigs
Postmortem redistribution

ABSTRACT

The number of fatal cases involving synthetic cannabinoids (SCs) is increasing. However, interpretation of postmortem (PM) toxicological findings is challenging, due to unknown PM intervals and possible redistribution processes or instabilities. Only sparse data on SCs are available. Therefore, a controlled pig study was performed to determine the PM stability of *cumyl*-5F-P7AICA under different environmental conditions. Ten pigs inhalatively received 200 µg/kg body weight *cumyl*-5F-P7AICA each. Six hours later, they were euthanized and biopsies of the main tissues and body fluids were taken. Animals were stored in air or water (n=5 each) and samples were repeatedly taken for three days. Quantification of *cumyl*-5F-P7AICA and its *N*-pentanoic acid metabolite (NPA) was performed using standard addition or a fully validated method (blood) followed by LC-MS/MS. Time-dependent concentration changes of *cumyl*-5F-P7AICA were observed in liver, bile fluid and muscle specimens at both conditions. Concentrations of NPA only changed considerably in duodenum content of animals stored in air. Environment-dependent concentrations changes were only observed for *cumyl*-5F-P7AICA in kidney and the NPA metabolite in duodenum content. Overall, *cumyl*-5F-P7AICA and its metabolite seem to be quite stable in PM specimens. Hence, also central blood might be analyzed, if no peripheral blood is available.

1. Introduction

In addition to ‘common‘ drugs, such as cocaine or heroin, numerous fatal intoxications related to the use of synthetic cannabinoids (SCs) have been reported in the literature worldwide (Boland et al., 2020; Doerr et al., 2022; Ferrari Júnior et al., 2022; Giorgetti et al., 2020; Schaefer et al., 2013; Walle et al., 2023). In the last years, several new initially legal SCs with slightly modified chemical structures, e.g., with a 7-azaindole core structure, emerged on the drug market to circumvent legal restrictions. However, such modifications can lead to higher potencies, resulting in life-threatening intoxications or even death (Oberhofer, 2018; Walle et al., 2023; Zawadzki et al., 2021). Accordingly, also these substances were covered by law in Germany. In this context knowledge of the toxicokinetic (TK) properties, especially the postmortem (PM) stability as well as a possible PM redistribution (PMR), is essential for the interpretation of toxicological PM findings, as a degradation or new formation of ingested substances can occur PM. Well-known examples of a PM formation are ethanol or gamma hydroxybutyrate as, on the contrary, a PM degradation was reported, e.g. for cocaine or diacetylmorphine (Skopp, 2010). Until now, only sparse data on PM tissue distribution of SCs as well as their PM stability are available in the literature. However, these data are usually based on case reports, where neither the dose and the time of consumption nor the PM interval (PMI) is known (Adamowicz, 2016; Boland et al., 2020; Doerr et al., 2022; Giorgetti et al., 2020; Kraemer et al., 2019; Walle et al., 2023). In addition, PM autolysis leading to a disintegration of membrane functions, resulting in a passive diffusion of substances into surrounding tissues has to be considered for example (Brockbals et al., 2018;

* Corresponding author.
E-mail address: nadine.schaefer@uks.eu (N. Schaefer).

https://doi.org/10.1016/j.toxlet.2024.10.006
Received 18 April 2024; Received in revised form 13 September 2024; Accepted 7 October 2024
Available online 10 October 2024

Drummer and Gerostamoulos, 2002; Gerostamoulos et al., 2012; Skopp, 2010). Moreover, the extent of this redistribution is dependent on the physicochemical (e.g. lipophilicity) as well as the TK properties of the respective substances (Pélissier-Alicot et al., 2003; Skopp, 2010). Furthermore, due to a PM decrease of pH and a microbial colonization of the corpse, a further degradation of substances can occur, influencing the PM stability of drugs in tissue and body fluid samples (Skopp, 2010).

In order to prove a possible intoxication after ingestion of drugs (of abuse) as the cause of death in a putrefied corpse, all these processes must be considered when interpreting PM toxicological findings, as the measured analytical values are not necessarily reflecting the ante-mortem situation, which can quickly lead to a misinterpretation, if the PM properties of the respective substance are unknown.

Several systematically controlled pig studies on the perimortem tissue distribution as well as the PM stability, respectively tendency for PMR have been successfully performed on SCs with an indole core structure (Schaefer et al., 2017, 2019, 2020a) and structurally modified SCs with a 7-azaindole core (Doerr et al., 2024)after intravenous or inhalative administration.

Comparison of the perimortem and PM TK data of a SC with a 7-azaindole core structure reported by Doerr et al. (2024) with the data obtained by Schaefer et al. (2017), (2019), (2020a) for SCs with an indole core indicates that the tissue distribution, the PM stability and the tendency for PMR of SCs seem to be significantly affected by the changes of their physicochemical properties resulting from modifications in the chemical structure.

Hence, in the present study, already published data on the perimortem tissue distribution of SCs with a 7-azaindole core structure (Doerr et al., 2024) should initially be supplemented by data on the structurally modified SC *cumyl*-5F-P7AICA as well as its *N*-pentanoic acid (NPA) metabolite in the framework of a systematically controlled study after pulmonary administration using the pig model.

Additionally, as already mentioned above, putrefaction of a corpse can vary greatly depending on prevailing storage or environmental conditions, such as temperature, oxygen availability or humidity. This principle was already elucidated by Johann Ludwig Casper by means of the so-called ‚Casper-rule', which describes the degree of putrefaction and, thus, also of the autolytic processes as a function of the prevailing ambient conditions (Dettmeyer et al., 2014; Vennemann and Brinkmann, 2003). Accordingly, the degree of putrefaction of a corpse after 1-week in air corresponds approximately to that of a 2-week water storage or a 8-week storage in soil (Dettmeyer et al., 2014; Vennemann and Brinkmann, 2003). Therefore, a change of the PMR degree as well PM stability of SCs may also be expected due to a delayed onset of the autolytic processes, if the corpse is stored under oxygen-deficient conditions, e.g. in water. In a previous study, Schaefer et al. found PM time- and temperature-dependent concentration (conc.) changes especially of RCS-4 and HO-RCS-4 (Schaefer et al., 2020a). Data on the PM stability and PMR of SCs in tissues and body fluids under different environmental conditions, e.g. water storage, are not availableso far. Therefore, in a second step of the present study the time- and oxygen-dependent conc. changes of *cumyl*-5F-P7AICA and its main metabolite were compared under different storage conditions, at air and in water, for the first time. The PM data obtained should further be compared with those found in perimortem specimens.

2. Materials and methods

2.1. Chemicals, reagents and blank whole blood samples

Detailed information on the chemicals and reagents used for the study, their origin and the preparation of blank whole blood samples can be found in the Electronic Supplementary Material (ESM).

2.2. Preparation of stock solutions, quality control (QC) samples, calibration standards, and calibrators for standard addition

Standard stock solutions (1000 µg/mL) were prepared by dissolving the obtained solid substances in ethanol. To obtain working standard solutions (0.01 µg/mL, 0.1 µg/mL, 1 µg/mL, and 10 µg/mL), the stock solutions were diluted with ethanol, respectively. For preparation of the QC low (final conc. of 5 ng/mL *cumyl*-5F-P7AICA and 0.2 ng/mL NPA) and high (final conc. of 35 ng/mL *cumyl*-5F-P7AICA and 0.8 ng/mL NPA) samples, the respective working standard solution was diluted with ethanol. Furthermore, the spiking solutions for calibration standards were also prepared by diluting the working solutions with ethanol to obtain solutions for final blood conc. of 0.5, 10, 20, 30, 40, and 50 ng/mL as well as 0.1, 0.3, 0.5, 0.7, 0.9, and 1.1 ng/mL of *cumyl*-5F-P7AICA and NPA, respectively. Calibrators for standard addition were also prepared by dissolving working standard solutions with ethanol. The respective conc. of the calibrators used for the different specimens are depicted in Table 1. All prepared solutions were stored at −20 °C.

2.3. Preparation of buffer solutions

The preparation of the buffer solutions is described in detail in the ESM.

2.4. In vivo study

2.4.1. Animals

As described previously (Walle et al., 2021) the in vivo experiment performed in the present study was conducted in accordance with the German legislation on protection of animals and the National Institutes of Health Guide for the Care and Use of Laboratory Animals (permission number: 44/2019).

Ten domestic male pigs (Swabian Hall strain) with a body weight (BW) between 44 and 64 kg were used. The pigs had free access to tap water, daily standard chow and were kept fasting for 12 h before the experiment, while they still had free access to water.

2.4.2. Surgical procedures and study design

The surgical procedures and the study design were in accordance to those already published elsewhere (Doerr, 2024). A detailed description

Table 1
Calibrator concentrations (conc.) of *cumyl*-5F-P7AICA and its *N*-pentanoic acid (NPA) metabolite used for the standard addition approach divided between the different approaches as well as the various specimens in ng/g tissue/ body fluid specimen. (./. = not added).

Perimortem specimens						
Specimen	**Calibrator conc. of *cumyl*-5F-P7AICA [ng/g]**			**Calibrator conc. of NPA [ng/g]**		
	1	**2**	**3**	**1**	**2**	**3**
Brain/ liver/ kidney/ muscle tissue	0.5	1	1.5	0.5	1	1.5
Lung	5	10	15	0.1	0.2	0.3
Bile fluid/ duodenum content	5	10	15	5	10	15
Adipose tissue	10	20	30	./.	./.	./.
Postmortem specimens						
Specimen	**Calibrator conc. of *cumyl*-5F-P7AICA [ng/g]**			**Calibrator conc. of NPA [ng/g]**		
	1	**2**	**3**	**1**	**2**	**3**
Brain/ liver/ kidney/ muscle tissue	1	2	3	0.2	0.4	0.6
Lung	3	6	9	0.2	0.4	0.6
Bile fluid	1.5	3	4.5	5	10	15
Duodenum content	5	10	15	2	4	6
Adipose tissue	10	20	30	./.	./.	./.

on the surgical procedures can be found in the ESM.

Regarding the study design, a stock solution of *cumyl*-5F-P7AICA (5000 μg/mL) was prepared by dissolving the solid substance in ethanol as already described in a previous study (Walle et al., 2021). In order to achieve the desired 200 μg/kg BW dose, the required volume of the stock solution was taken or diluted with ethanol, respectively. The dilution was subsequently administered inhalatively within 12 min by nebulization applying the inspiration-triggered mode (< 0.2 mL/min) of the M-neb flow+ ventilation ultrasonic nebulizer MN-300/7 (Nebutec, Elsenfeld, Germany) in accordance to the administration setup already published by Schaefer et al. (Schaefer et al., 2018).

After sampling of approximately 10 mL peripheral blood (PB) from the jugular vein (t=360 min),the pigs were euthanized by administering 0.12 mL/kg BW T61 (Intervet Deutschland GmbH, Unterschleißheim, Germany) six hours after drug administration. A small piece of muscle was collected from the inner thigh during the removal of the catheter from the left artery. Following, the abdominal cavity was opened and samples of different body fluids, organs, and tissues were drawn (PMI 0) as follows: subcutaneous (s.c.) adiposetissue (AT) was sampled from the inside of the incision. Depending on the amount contained, approximately 1–2 mL of bile fluid were removed from the gall bladder using a syringe. The puncture site was closed with a clamp to prevent leaking. A piece of liver (approximately 10 g) was then cut out while the cut surface was cauterized to stop bleeding. To obtain duodenum content, the upper part of the small intestine (duodenum) was divided into 4 sections of approximately 30 cm each using stitches. The first section, starting at the pylorus, was opened and the duodenum content squeezed out. The other parts were put back for PM sampling. Subsequently, the renal capsule was opened to take some perirenal AT as well as cut off a piece of kidney tissue (approximately 10 g). In order to access the lung tissue and central blood (CB), the diaphragm was first severed with a scalpel. Sampling of lung tissue and CB was carried out inside the chest cavity. Therefore, a piece of lung tissue was initially cut off. Following, CB was collected by puncturing the heart using a syringe and a 14 G cannula. A total of about 10 g was sampled from each tissue specimen. The respective organs and tissues were left in situ and the abdominal cavity was sutured. Subsequently, a small incision was made in the neck of the pig to obtain dorsal AT. Finally, the skull was opened using a head saw and some cerebrum tissue was sampled. The skullcap was put on again and the skin was sutured.

Subsequently, one group of the animals (n=5) was stored at room temperature (RT), whilst the other part (n=5) was kept in approximately 50 L water lying in a bathtub, with the water not being replaced over the entire duration of the experiment. Further specimens of the above-mentioned organs and body fluids were drawn after 24 h (PMI 1), 48 h (PMI 2), and 72 h (PMI 3) in analogy to the previously described procedure with a few modifications. In brief, PB was drawn from the femoral or the brachiocephalic vein at PMI 1–3, after the veins have been exposed with a scalpel. To obtain muscle specimens, the clamps at the inner thigh were removed. After sampling, the skin was sutured again using stitches. S.c. AT was also taken at the incision site during the opening of the abdominal cavity. Bile fluid was removed from the gall bladder in accordance to the procedure described above. A piece of liver was cut off, while a cauterization of the cut surface was no longer necessary. For duodenum content, the respective separated section of the small intestine was opened and the content was pressed out. Regarding kidney tissue, sampling was performed by cutting off small pieces of tissue specimens after the collection of perirenal AT. However, the sampling site was switched to the second kidney at PMI 2 or 3. Lung tissue and CB were sampled in accordance to the previously described procedure. However, at PMI 3, sampling of CB was performed after the heart has been removed from the chest and opened. Dorsal AT was collected as previously described. For sampling of brain tissue, the skullcap was initially removed. After the skull was closed again, the skin was sutured with stitches. However, brain specimens of the animals stored in water were only collected after 72 h. The respective organs and tissues were left in situ and the abdominal cavity was sutured after each time point. Analogously to the perimortem sampling procedure, a total of about 10 g was sampled from each PM tissue specimen.

Regarding the perimortem and PM sampling procedure of lung, liver and kidney tissue, no exact sampling location could be maintained. All specimens were stored at −20 °C until analysis.

2.5. Preparation of blood specimens

Since the volume of PM PB and CB samples was very low and no standard addition could be performed, *cumyl*-5F-P7AICA as well as its NPA were quantified using a fully validated method (unpublished data) based on a solid phase extraction (SPE) in analogy to the procedure already published by Schaefer et al. for the (synthetic) cannabinoids JWH-210, RCS-4, and THC (Schaefer et al., 2019, 2020a). The limit of detection was set at 0.06 ng/mL for *cumyl*-5F-P7AICA and 0.006 ng/mL for the NPA metabolite, the lower limits of quantification were defined as the lowest calibrator in blood (0.5 ng/mL for *cumyl*-5F-P7AICA, 0.1 ng/mL for the NPA). Analysis was performed by a liquid chromatography (LC) quadrupole time-of-flight (TOF)-mass spectrometer (MS) system. A detailed description of the blood sample preparation can be found in the ESM.

2.6. Preparation of tissue and body fluid specimens

The preparation of perimortem as well as PM tissue and body fluid specimens was performed in accordance to previous published studies (Schaefer et al., 2020a, 2020b). In brief, 2 g of the solid tissue (lung, liver, kidney, brain, muscle tissue) or 1 g bile fluid and duodenum content was homogenized with water in a ratio of 1 amount tissue + 4 amounts water or 1 amount body fluid + 9 amounts water, respectively. For quantification of *cumyl*-5F-P7AICA and its NPA metabolite, a standard addition approach was performed. For this purpose, the homogenates were first divided into four 0.5 g portions. Subsequently, to create a stand addition curve, one of those aliquots was prepared without and the others with the addition of 25 μL of different analyte conc. Thereafter, 20 μL of an ethanolic stable-isotope-labeled internal standard mixture solution (SIL-IS;1 ng/20 μL RCS-4-d_9), 0.5 mL acetate buffer (pH 4), and 50 μL β-glucuronidase/arylsulfatase was added and after vortexing, incubation for enzymatic hydrolysis was performed at 60 °C for 2 h. The hydrolysis was stopped by the addition of 0.5 mL acetonitrile. After vortexing and centrifugation at 3500 *g* for 8 min the supernatants were fortified with 1.5 mL phosphate buffer (pH 9). After an additional vortexing step, the mixtures were loaded on conditioned solid phase cartridges. After thee washing steps with 3 mL phosphate buffer (pH 9), 3 mL acetic acid (0.25 M), and 3 mL water, 60 μL acetone were added and the cartridges were dried under a maximum vacuum of 10 inHg. Subsequently, 1.5 mL of a methanol-acetone mixture (1:1, *v/v*) was added for elution of the substances. After evaporation of the eluates at 60 °C under a gentle stream of nitrogen, the dry residues were dissolved by the addition of 50 μL of a mixture (50:50, *v/v*) of mobile phases A (0.1 % aqueous formic acid) and B (0.1 % formic acid in acetonitrile). For analysis, 5 μL of the solutions were injected onto a LC-triple quadrupole-MS system.

Regarding AT specimens, 2 g AT was homogenized with acetonitrile (1 amount AT + 5 amounts acetonitrile). After centrifugation at 3500 *g* for 8 min, four 0.5 mL portions were prepared with and without different conc. of *cumyl*-5F-P7AICA to perform a standard addition approach. Subsequently, 20 μL SIL-IS (1 ng/20 μL RCS-4-d_9) was added. After evaporation under nitrogen at 60 °C, the dry residues were dissolved in 100 μL of a mixture of mobile phases A and B (50:50, *v/v*). Finally, 20 μL of the respective extracts were injected onto a LC-triple-quadrupole-MS system.

2.6.1. Standard addition approach

In the present study, a standard addition approach was performed to

quantify the conc. of *cumyl*-5F-P7AICA and its NPA metabolite in different tissues and body fluids respectively, with the exception of blood specimens. For this purpose, four portions of the homogenates with and without the addition of different analyte conc. were prepared (Table 1). Evaluation of the conc. in tissues and body fluids was performed using Microsoft Office Excel 2003 (Redmond, WA, USA). Therefore, by plotting the respective calibrator conc. against the analyte/SIL-IS ratio, a linear regression was performed to create standard addition calibration equations as follows: $y = a\,x + b$. Calculation was performed depending on the slope (a) as well as the intercept (b), while the negative point of interception of the x-axis represents the unknown drug conc.

2.7. LC-MS/MS apparatus

Instrumentation, chromatographic, and mass spectrometric conditions of the LC-triple quadrupole-MS as well as the LC-quadrupole TOF-MS used for the analysis of the respective extracts are described in detail in the ESM. Furthermore, detailed information on the respective precursor and product ions, the retention time as well as the analysis conditions can be found in Supplementary Table 1.

2.8. Evaluation of drug conc. changes and statistical tests

Calculation of the PM median drug conc. changes of *cumyl*-5F-P7AICA and its NPA metabolite was performed in accordance to previous published studies (Nordmeier et al., 2022; Schaefer et al., 2020a). Analogously, the conc. ascertained at PMI 1–3 were compared with the

Table 2
Mean and median concentrations (conc.) ± standard deviations (SD) of *cumyl*-5F-P7AICA and its *N*-pentanoic acid metabolite in ng/mL or ng/g measured in different tissue and body fluid specimens collected six hours after drug administration defined as the postmortem interval (PMI) 0 as well as 24 h (PMI 1), 48 h (PMI 2), and 72 h (PMI 3) after euthanasia of five pigs and a following storage at room temperature (RT) or water, respectively. Brain specimens were only taken at PMI 3 when stored in water. Median conc. are depicted in square brackets. All stated concentrations are approximated. Deviations in the number of samples tested are indicated accordingly.

***Cumyl*-5-P7AICA**								
	RT				**Water**			
	PMI 0	PMI 1	PMI 2	PMI 3	PMI 0	PMI 1	PMI 2	PMI 3
Lung	19 ± 9.1[15]	9.5 ± 8.4[9.3]	20 ± 11[9.3]	25 ± 7.0[12]	4.5 ± 3.8[3.1]	12 ± 17[2.4]	16 ± 9.1[15]	10 ± 7.4[8.6]
Liver	1.4 ± 0.95 [1.6]	2.2 ± 0.86[2.1]	3.5 ± 1.5*[3.5]	5.1 ± 6.4[3.3]	0.95 ± 0.78 [0.90]	1.6 ± 1.1[1.2]	2.3 ± 1.3[2.2]	4.6 ± 4.0[2.2]
Kidney	2.0 ± 2.1[1.4]	3.0 ± 1.5[3.1]	3.4 ± 1.9[2.6]	3.4 ± 1.4[2.3]	1.2 ± 0.69[1.2]	1.6 ± 0.73[1.5]	2.4 ± 1.4[1.7]	2.4 ± 1.3[2.0]
Brain	0.58 ± 0.12 [0.55]	0.97 ± 0.36 [0.91]	6.1 ± 7.8[1.2](n = 4)	1.7 ± 0.92[0.99]	0.54 ± 0.47 [0.41] (n = 4)			10 ± 11[6.4]
Muscle	1.8 ± 1.6 [0.87](n = 4)	1.1 ± 0.46[1.1]	1.0 ± 0.52[1.0]	1.7 ± 0.65[1.8]	0.42 ± 0.36 [0.34]	0.92 ± 0.59 [0.76]	0.90 ± 0.31 [0.80]	1.5 ± 0.96*[1.1]
AT dorsal	8.4 ± 4.8[7.4] (n = 4)	10 ± 10[8.5]	4.4 ± 2.5[3.6]	6.2 ± 1.4[5.9]	7.7 ± 4.1[7.7]	4.8 ± 3.0[5.3]	4.0 ± 3.4[3.7]	6.4 ± 1.1[6.4]
AT s.c.	11 ± 7.5[10]	10 ± 7.4[12]	12 ± 11[7.7]	8.9 ± 4.4[9.7]	11 ± 5.3[10]	8.3 ± 2.2[8.3]	9.3 ± 4.7[7.6]	9.2 ± 4.6[9.4]
AT perirenal	15 ± 7.8[12]	16 ± 12[13]	12 ± 6.6[10]	11 ± 8.8[6.6]	14 ± 5.8[13]	12 ± 3.2[12]	8.7 ± 1.6[9.0]	9.6 ± 2.5[10]
Bile fluid	6.7 ± 3.0[5.2]	5.1 ± 1.6[3.3]	2.4 ± 1.1*[2.2] (n = 3)	3.6 ± 1.1*[3.6] (n = 2)	6.7 ± 4.8[7.2]	4.5 ± 0.52[4.4]	3.2 ± 0.43[3.2]	2.8 ± 0.77[3.0]
Duodenum	2.5 ± 1.4[1.7] (n = 3)	3.1 ± 1.6[2.0](n = 3)	3.4 ± 2.5[2.3]	2.5 ± 1.4[1.9]	3.5 ± 3.3[0.0] (n = 2)	1.8 ± 1.1[1.4]	1.4 ± 0.77[1.4] (n = 4)	2.2 ± 0.70[2.0] (n = 4)
PB	0.47 ± 0.15 [0.47]	0.46 ± 0.12 [0.32](n = 3)	0.46 ± 0.21 [0.15](n = 2)	0.30(n = 1)	0.34 ± 0.11 [0.33]	0.49 ± 0.14 [0.35](n = 3)	0.40 ± 0.004 [0.20](n = 2)	0.46(n = 1)
CB	0.20 ± 0.11 [0.18]	0.21 ± 0.084 [0.17]	0.37 ± 0.31 [0.28](n = 4)	0.26 ± 0.059 [0.26]	0.22 ± 0.084 [0.21]	0.26 ± 0.14 [0.21]	0.25 ± 0.064 [0.27](n = 4)	0.28 ± 0.16 [0.28]
***Cumyl*−5-P7AICA N-pentanoic acid**								
	RT				**Water**			
	PMI 0	PMI 1	PMI 2	PMI 3	PMI 0	PMI 1	PMI 2	PMI 3
Lung	neg.	neg.	1.0 ± 0.042[0.0] (n = 2)	0.81(n = 1)	neg.	neg.	neg.	neg.
Liver	0.71 ± 0.70 [0.61]	1.0 ± 0.52[0.59] (n = 3)	1.5 ± 0.10[0.0] (n = 2)	1.9 ± 2.3[1.2]	0.61 ± 0.23 [0.67]	0.39(n = 1)	0.72 ± 0.87[0.0] (n = 2)	0.71 ± 0.64 [0.42](n = 4)
Kidney	0.84 ± 0.63 [0.69]	0.59 ± 0.15 [0.61](n = 4)	1.2 ± 0.52 [0.97](n = 3)	0.89 ± 0.41 [0.71](n = 4)	0.78 ± 0.50 [0.56]	1.3 ± 1.9[0.42] (n = 4)	0.87 ± 0.37 [0.76]	0.31 ± 0.30 [0.33](n = 3)
Brain	neg.	neg.	neg.	neg.	neg.			neg.
Muscle	neg.	neg.	neg.	neg.	neg.	neg.	neg.	neg.
AT dorsal	neg.	neg.	neg.	neg.	neg.	neg.	neg.	neg.
AT s.c.	neg.	neg.	neg.	neg.	neg.	neg.	neg.	neg.
AT perirenal	neg.	neg.	neg.	neg.	neg.	neg.	neg.	neg.
Bile fluid	37 ± 17[23] (n = 4)	8.0 ± 3.7[9.0]	18 ± 13[13](n = 3)	22 ± 16[22](n = 2)	29 ± 46[7.1](n = 4)	16 ± 7.2[13](n = 4)	21 ± 17[11](n = 4)	6.7 ± 2.9[6.1](n = 4)
Duodenum	8.4 ± 3.2[8.7]	5.2 ± 3.3[4.1](n = 4)	3.6 ± 3.2[1.5]	2.4 ± 1.0*[2.5]	2.1 ± 2.3[1.4]	1.0 ± 1.0[0.36] (n = 3)	1.0 ± 0.25[0.77] (n = 3)	1.9 ± 1.3[0.54] (n = 3)
PB	0.10 ± 0.084 [0.060]	0.067 ± 0.008 [0.060](n = 3)	0.053 ± 0.023 [0.040](n = 3)	0.047 ± 0.003 [0.045](n = 3)	0.060 ± 0.012 [0.060]	0.055 ± 0.030 [0.040](n = 4)	0.050 ± 0.014 [0.020](n = 2)	0.041 ± 0.009 [0.040](n = 4)
CB	0.046 ± 0.048 [0.050]	0.035 ± 0.025 [0.037]	0.036 ± 0.026 [0.017](n = 4)	0.027 ± 0.015 [0.025]	0.038 ± 0.015 [0.030](n = 4)	0.026 ± 0.007 [0.029]	0.024 ± 0.015 [0.020]	0.019 ± 0.012 [0.010]

AT = adipose tissue; s.c. = subcutaneous; PB = peripheral blood; CB = central blood; neg.=negative
* = statistically significant concentration changes ($p<0.05$)).

respective conc. at PMI 0 (Table 2). For this purpose, the following equation was used:

$$\Delta c(\%) = \frac{c(PMI1-3)-c(PMI0)}{c(PMI0)} x100$$

$\Delta c > 0$: *increase*

$\Delta c < 0$: *decrease*

Thereby, a value of $\Delta c > 0$ means an increase and a value of $\Delta c < 0$ a decrease of the respective PM conc. at the sampling time compared to the perimortem conc. at PMI 0.

Statistical tests were performed using GraphPad Prism 5.00 (GraphPad Software, San Diego, CA, USA). Additionally, to examine the respective conc. changes of the analytes in the tissue and body fluid specimens at different points of time, a non-parametric Friedman-test ($p<0.05$) followed by the Dunn's multiple comparison post-hoc test was applied.

Furthermore, for comparison of the obtained conc. after storage at RT with those obtained after storage in water, a non-parametric Mann-Whitney U test ($p < 0.05$) was used.

3. Results

3.1. Standard addition approach

In the present study, a standard addition approach was successfully applied for quantification of *cumyl*-5F-P7AICA and its NPA metabolite in different tissue und body fluid specimens. The regression coefficients (r^2) ranged between 0.90 and 1.0 for *cumyl*-5F-P7AICA and between 0.90 and 0.99 for the NPA metabolite, respectively.

3.2. Perimortem distribution

To determine the perimortem distribution of *cumyl*-5F-P7AICA and its NPA metabolite, various tissue and body fluid samples were drawn six hours after inhalative drug administration (PMI 0). In general, the respective conc. of the analytes showed high interindividual variations in the different analyzed specimens. The mean conc. as well as the corresponding standard deviations of both substances at PMI 0 are listed in Table 2. As far as *cumyl*-5F-P7AICA is considered, the highest conc. was found in lung and bile fluid, followed by kidney and duodenum content, if AT is initially disregarded. On the other hand, lowest conc. were observed in PB and CB (Table 2).

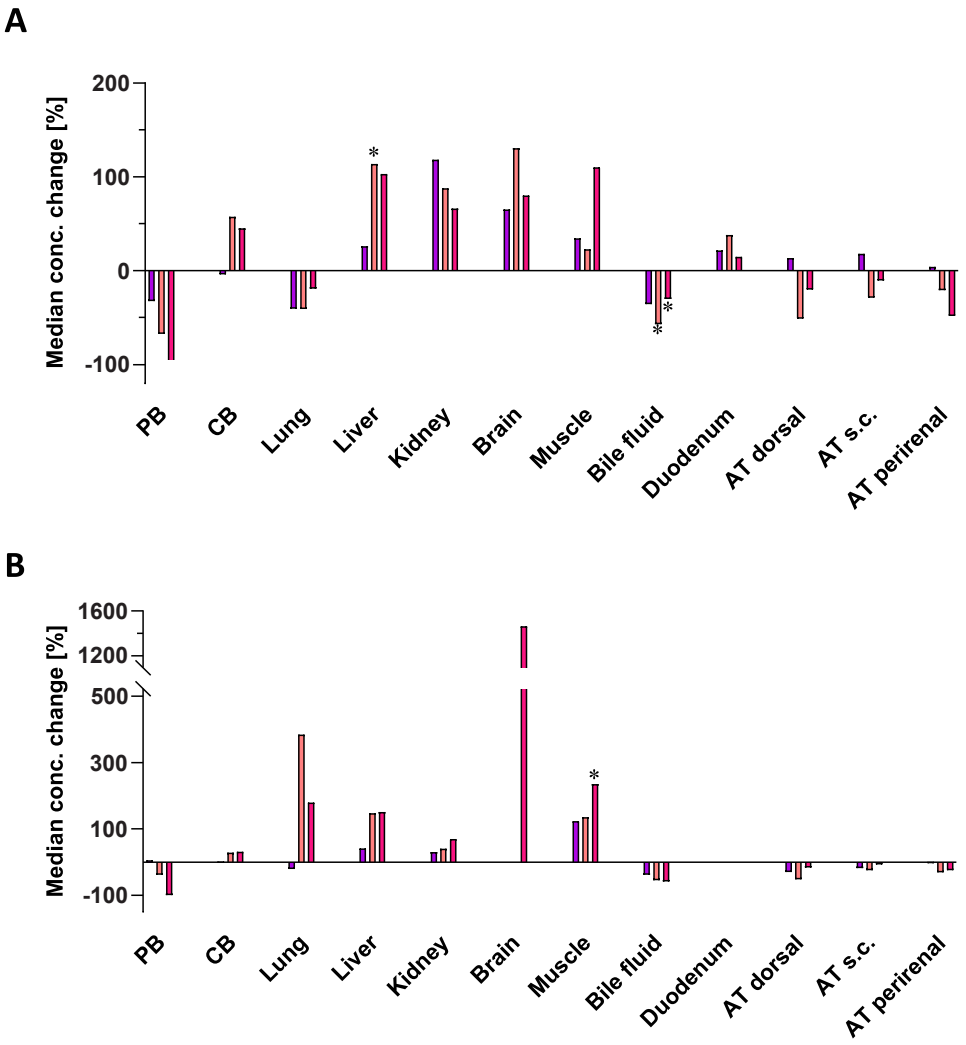

Fig. 1. Median time- and environmental-dependent postmortem concentration (conc.) changes [%] of *cumyl*-5F-P7AICA in different tissues and body fluids stored at air **(A)** and water **(B)** collected 24 h (postmortem interval (PMI) 1;), 48 h (PMI 2;), and 72 h (PMI 3;) after pulmonary administration of a 200 μg/kg body weight dose to pigs compared to PMI 0. (* = statistically significant concentration changes ($p<0.05$); PB = peripheral blood, CB = central blood, AT = adipose tissue, s.c. = subcutaneous).

Regarding the NPA metabolite, the highest conc. could primarily be assessed in bile fluid and duodenum content, followed by liver and kidney. In analogy to the parent compound *cumyl*-5F-P7AICA, lowest conc. of the metabolite were also detected in PB and CB (Table 2). Analysis of lung, brain, and muscle specimens yielded negative results.

Concerning AT specimens, highest conc. of *cumyl*-5F-P7AICA were found in perirenal AT, followed by subcutaneous AT, with lowest conc. detected in dorsal AT. The NPA metabolite could not be found in any AT specimen.

3.3. PM conc. changes

3.3.1. Storage in air

The mother substance *cumyl*-5F-P7AICA could be determined in every solid tissue specimen sampled at PMI 1 – 3 stored at RT, with the exception of brain at PMI 2 (n=4). As for the body fluids, the parent substance could only be detected in a few samples of bile fluid (n=3 at PMI 2 and n=2 at PMI 3), duodenum content (n=3 at PMI 1), CB (n=4 at PMI 2), and PB (n=3 at PMI 1, n=2 at PMI 2 and n=1 at PMI 3).

Overall, in the examined specimens only few to rarely conc. changes could be observed during the entire experiment (Fig. 1a; Table 2). For example, compared to PMI 0, the median conc. of *cumyl*-5F-P7AICA slightly increased in liver, kidney, muscle, and brain specimens. On the contrary in perirenal AT and bile fluid the median PM conc. slightly decreased, especially from PMI 2 to PMI 3. Furthermore, PM conc. in lung, duodenum content, CB and dorsal as well as s.c. AT were found to be rather stable over the observed period. For PB, a continuous decrease of the median conc. could be observed until PMI 3.

Overall, as depicted in Fig. 1a, statistically significant conc. changes ($p<0.05$) were observed for *cumyl*-5F-P7AICA in liver between PMI 0 and PMI 2 as well as in bile fluid between PMI 0 and PMI 2 or PMI 3.

Regarding the NPA metabolite, analysis of muscle, brain, s.c., dorsal as well as perirenal AT were negative over the observed period of time. Highest conc. of the metabolite could be found in bile fluid and duodenum content at each sampling time (Table 2). First of all, it has to be stated that in lung, compared to PMI 0, the NPA metabolite could only be detected in isolated samples at PMI 2 and 3 (n=2 at PMI 2; n=1 at PMI 3). Compared to the median conc. at PMI 0, the conc. of the NPA metabolite remained comparably stable in kidney tissue until 72 h (Fig. 2a, Table 2). Regarding bile fluid no clear tendency was recognizable. In liver specimens, a slight decrease of the conc. could be found from PMI 1 to PMI 2, increasing again from PMI 2 to PMI 3. However, in duodenum content, the conc. of the NPA metabolite declined over time. Regarding PB and CB, PM conc. remained comparably stable until PMI 3.

Statistically significant conc. changes ($p<0.05$) were only found for

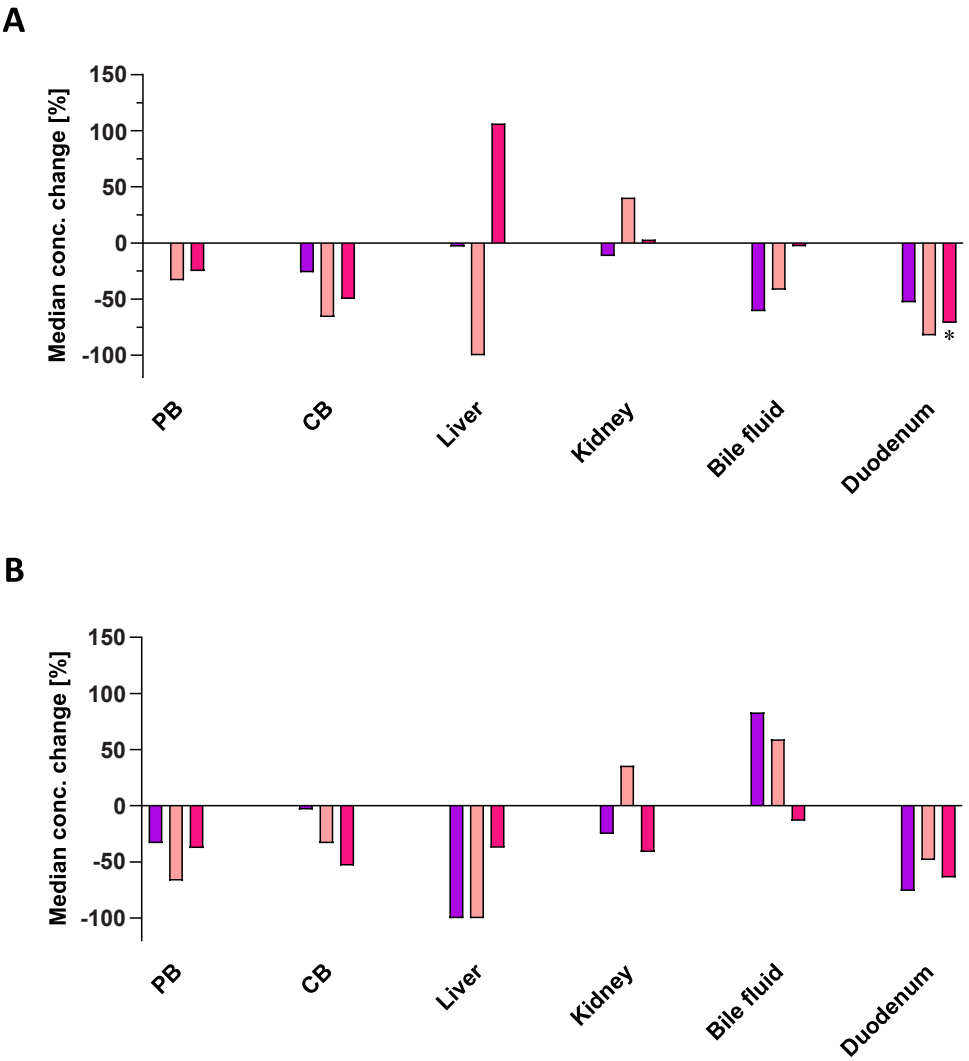

Fig. 2. Median time- and environmental-dependent postmortem concentration (conc.) changes [%] of *cumyl*-5F-P7AICA *N*-pentanoic acid in different tissues and body fluids stored at air **(A)** and water **(B)** collected 24 h (postmortem interval (PMI) 1;), 48 h (PMI 2;), and 72 h (PMI 3;) after pulmonary administration of a 200 μg/kg body weight dose to pigs compared to PMI 0 (PB = peripheral blood, CB = central blood).

duodenum content between PMI 0 and PMI 3 (Fig. 2a).

3.3.2. Storage in water

In tissues and body fluids stored in water (group 2), *cumyl*-5F-P7AICA could be quantified in every specimen, with the exception of PB (n=3 at PMI 1; n=2 at PMI 2 and n=1 at PMI 3), CB (n=4 at PMI 2), and duodenum content (n=4 at PMI 2 and 3 each). However, in accordance to a storage at air, only occasional and minor conc. changes were found when stored in water (Fig. 1b; Table 2).

Compared to PMI 0 (Fig. 1b, Table 2) a strong increase of the conc. could be noted especially in brain. However, brain specimens were only taken at PMI 3. In lung specimens, an increase of the conc. could be observed from PMI 1 to PMI 2 with a following slight decrease at PMI 3. Regarding PB and CB specimens, conc. of *cumyl*-5F-P7AICA remained relatively stable until PMI 3.

Statistically significant conc. changes ($p<0.05$) of *cumyl*-5F-P7AICA were found in muscle between PMI 0 and PMI 3 when stored in water.

Regarding the NPA metabolite, analysis of muscle, lung, brain and every AT specimen yielded negative results. In the samples, the NPA metabolite could only be detected in about half of all analyzed specimens. In terms of duodenum content, no clear trend could be observed over 72 h. In liver, kidney, bile fluid, CB as well as PB specimens, the PM median conc. of the NPA remained comparably stable for the entire period of the experiment (Fig. 2b, Table 2).

All in all, no significant conc. changes of the NPA metabolite could be found in tissues and body fluids stored in water.

4. Discussion

4.1. Dosage

In the present study, a dose of 200 μg/kg BW *cumyl*-5F-P7AICA was administered inhalatively to the pigs, resulting in total doses of 8.8 – 12.8 mg. This dosage of *cumyl*-5F-P7AICA was chosen, as, on the one hand, it has already been proven to be well tolerated by the animals in a previous metabolism study (Walle et al., 2021). On the other hand, comparable doses were successfully administered to the pigs in the context of previous TK studies on SC (Doerr et al., 2021, 2024; Schaefer et al., 2019, 2020a). Furthermore, depending on the administration route, the dosage used in the current work is a recommended dose of SC reported by drug addicts in drug fora.

4.2. Standard addition approach

In the current study, the standard addition approach was used for the qualitative and quantitative determination of *cumyl*-5F-P7AICA as well as its NPA metabolite in body fluids and tissue specimens. Analyzing PM tissue specimens, quantification based on a calibration curve using blood as matrix is not recommended, as this might considerably increase the variability. Hence, the standard addition approach was chosen deliberately, as it has the advantage that matrix effects are minimized, since each calibration curve is adapted on the respective matrix. Especially in PM toxicology, matrix effects can complicate or even falsify the interpretation of analytical results, in particular in the case of putrefied specimens. However, in the context of a common method validation procedure, different parameters must be evaluated using different blank matrices. However, PM tissues are prone to a high interindividual biological variance that leads to the question, if representative results can be obtained. Therefore, for quantification of drugs (of abuse) in PM tissue and body fluid specimens, national and international guidelines recommend the use of the standard addition approach (GTFCh, 2018; Jickells and Negrusz, 2008; Peters et al., 2007; Skopp, 2010; SOFT/AAFS, 2006).

4.3. Perimortem distribution pattern

First of all, it has to be noted that the perimortem body fluid and tissue specimens were drawn shortly after death and thus before separation into the different environmental conditions. Nevertheless, measurements of the respective specimens drawn at PMI 0 revealed partially different median conc. (Table 2) of *cumyl*-5F-P7AICA, especially in lung (15 ng/g vs. 3.1 ng/g), liver (1.6 ng/g vs. 0. 90 ng/g) and duodenum (1.7 ng/g vs. 0.0 ng/g), as well as its NPA metabolite in bile fluid (23 ng/g vs. 7.1 ng/g) and duodenum (8.4 ng/g vs. 1.5 ng/g). However, several issues have to be taken into account. Overall, it should first be noted that there are high inter-individual TK differences between the individual animals. Therefore, reduced or increased absorption, metabolism, distribution or excretion of the substances may have already occurred during the in vivo study, whereby the extent of the individual steps depends on the respective animal. This may therefore result in higher or lower conc. of the respective substances at PMI 0. Differences in the measured conc. may also be due to an inhomogeneous distribution of the substances. However, it was not possible to always ensure the same collection site. These issues should be considered, when interpreting the respective conc. at PMI 0.

However, as already described above, with few exceptions *cumyl*-5F-P7AICA was found in every tissue or body fluid specimen sampled 6 h after drug administration. On the contrary, the NPA metabolite could only be detected in liver, kidney, duodenum content, bile fluid, CB, and PB. The mean as well as median conc. of the examined substances at PMI 0 are shown in Table 2. As easily can be seen, besides AT, the highest mean conc. of *cumyl*-5F-P7AICA could be found in lung and bile fluid, whereas lowest conc. were detected in CB and PB specimens, respectively. For interpretation, the route of administration must be considered. As *cumyl*-5F-P7AICA was inhalatively administered, it is not surprising, that high conc. were found in the lung. Furthermore, the findings of the present study are in line with those already reported by Schaefer et al. in the framework of a perimortem TK study regarding the SCs JWH-210 and RCS-4, which display more or less pronounced lipophilic properties, as also highest conc. of the SC were found among other locations in lung specimens after inhalative administration (Schaefer et al., 2019). This observation of sequestration of drugs in lung tissue was already described for some liphophilic drugs a few years ago and is called ‘pulmonary first-pass uptake and metabolism’ (Bakhle, 1990; Bend et al., 1985; Boer, 2003). However, compared to the studies by Schaefer et al. (Schaefer et al., 2019, 2020a), generally lower conc. of *cumyl*-5F-P7AICA were found in the different perimortem specimens in the present study. For explanation, on the one hand, *cumyl*-5F-P7AICA contains a carboxamide unit in its chemical structure, as, compared to JWH-210 and RCS-4, possibly leading to a certain instability and, thus, a faster in vivo degradation. Furthermore, the lower lipophilicity of *cumyl*-5F-P7AICA (LogP = 4.20) compared to e.g. JWH-210 (LogP = 7.5) or RCS-4 (LogP = 5.6) (Schaefer et al., 2019) might also contribute to the comparably lower drug conc. in e.g. lung. Additionally, Doerr et al. published data on the perimortem and PM distribution of 5F-MDMB-P7AICA, a SC also containing a 7-azaindole core structure, after inhalative administration to pigs (Doerr et al., 2024). Here, the authors reported on highest perimortem concentrations of the parent substance in AT, duodenum content and bile fluid, while in lung specimens only a low amount of 5F-MDMB-P7AICA was found. Regarding the PM specimens, highest conc. of 5F-MDMB-P7AICA were found in AT followed by bile fluid. While the conc. in PB, CB and bile fluid measured by Doerr et al. were approximately in the same range as those found for *cumyl*-5F-P7AICA in the present study, lower perimortem and PM values were found for 5F-MDMB-P7AICA in the remaining tissue and body fluids (AT excluded) as compared to those found for *cumyl*-5F-P7AICA. In this context, it should be considered that in contrast to *cumyl*-5F--P7AICA, 5F-MDMB-P7AICA additionally contains an ester structure in the linked group of its chemical structure, which may lead to a fast degradation to its corresponding metabolite, as it was also reported by

Krotulski et al. in a stability study for such classes of SCs (Krotulski et al., 2021).

Herein, euthanasia of the animals and sample collection was already performed 6 h after drug administration, whereas, in the aforementioned studies (Schaefer et al. 2019, 2020a; Doerr et al. 2024), the pigs were put to death only after 8 h. This longer period of metabolic degredation should not be neglected, and might also be another explanatory reason for the comparatively lower tissue and body fluid conc. reported by Doerr et al. (2024).

Two markers are described in the literature to predict a possible PMR. On the one hand a central-to-peripheral blood (*C/P*) conc. ratio > 1, and on the other hand a liver-to-peripheral blood (*L/P*) ratio > 5 or 20–30 indicate the occurrence of PMR (Han et al., 2012; McIntyre, 2014). Considering the respective mean conc. detected in the present work for *cumyl*-5F-P7AICA (Table 2), *C/P* ratios lower than 1 could be calculated, speaking rather less for a redistribution from the peripheral to the central compartment. In contrast, for both storage conditions *L/P* ratios> 5 were especially found at PMI 2 and 3, suggesting that *cumyl*-5F-P7AICA may underlie a slight time-dependent PMR into surrounding tissues. This should be considered, when interpreting PM toxicological findings.

Regarding the NPA metabolite, besides in PB and CB specimens, it could especially be detected in organs involved in metabolism and elimination (liver, kidney, bile fluid, and duodenum content), with highest conc. in bile fluid followed by duodenum content (Table 2). This is not surprising and was also reported in previous TK studies conducted by Schaefer et al. for the SCs JWH-210 and RCS-4 (Schaefer et al., 2019). The higher conc. in bile fluid and duodenum content as compared to liver and kidney specimens suggest an enterohepatic circulation, as it has already been reported for other SCs (Schaefer et al., 2017, 2019). Analogously to the parent substance, substantially lower conc. of the NPA were detected in bile fluid and duodenum as compared to those reported by Schaefer et al. for e.g. RCS-4-COOH (Schaefer et al., 2019). On the other hand, comparing the NPA conc. of the present work with those reported by Doerr et al. for the dimethyl butanoic acid (DBA) metabolite of the SC 5F-MDMB-P7AICA, higher DBA conc. were found in bile fluid and duodenum content (Doerr et al., 2024). This might also be caused by the high instability of 5F-MDMB-P7AICA due to its ester structure, leading to higher conc. of the DBA metabolite. In addition, as previously mentioned, a longer duration of the in vivo experiment (8 h vs. 6 h in the present study) may be another reason for the higher DBA conc. measured by Doerr et al. (2024).

Comparison of the tissue distribution pattern of *cumyl*-5F-P7AICA and its NPA metabolite obtained in the present work with data from authentic fatal cases is not possible, as such data are lacking in the literature. Until now, only one fatal case with a contribution of *cumyl*-5F-P7AICA to the occurrence of death was published by Zawadzki et al. (2021). Indeed, in this fatal case, only PM blood and urine conc. of *cumyl*-5F-P7AICA were reported with conc. of 2.8 ng/mL in blood and 3.1 ng/mL in urine, respectively. Although the PMI is unknown in the case reported by Zawadzki et al., comparison with the PB conc. obtained in the present study at PMI 1–3 shows that the reported conc. in the fatal case are much higher. However, it should be borne in mind that such single case reports are subject to strong uncertainties, as usually neither the consumed dose and time of consumption nor the PMI are known. Accordingly, these data are difficult to compare with those from systematically controlled studies. Furthermore, comparison of the PM TK properties of different SCs also represents a difficulty due to their structural modifications, as shown by the aforementioned comparison of the SCs *cumyl*-5F-P7AICA and 5F-MDMB-P7AICA, both containing a 7-azaindole core structure but different linked groups, possibly resulting in a fast in vivo degradation and metabolism.

To sum up, the perimortem distribution pattern of JWH-210 and RCS-4 as well as of its metabolites is comparable to that of ‚newer' SCs with a 7-azaindole core structure. However, considerably lower conc. were detected in tissues and body fluids, possibly resulting from unstable units within the chemical structure, as also seen for the SC 5F-MDMB-P7AICA which contains a 7-azaindole core. In order to investigate a possible impact of *cumyl*-5F-P7AICA on the occurrence of fatal intoxications, lung samples as well as bile fluid and duodenum content should included in the standard specimens collected during autopsy in addition to the common matrices CB and PB, especially in the case of an extended PMI.

4.4. Comparison of the PM conc. changes at different storage conditions

In the present study, the PM time-dependent conc. changes of *cumyl*-5F-P7AICA and its NPA metabolite were investigated in various tissue and body fluid specimens stored at two different ambient conditions. Comparing the results obtained after storage at air and in water, *cumyl*-5F-P7AICA and its metabolite consistently showed only slight conc. changes throughout the observed time period.

As already described by Johann Ludwig Casper by means of the ‚Casper-rule' (Dettmeyer et al., 2014; Vennemann and Brinkmann, 2003), the extent of putrefaction varies largely depending on the prevailing storage or environmental conditions (e.g. temperature, availability of oxygen). Accordingly, the degree of putrefaction of a corpse after 1-week in air corresponds approximately to that of a 2-week storage in water or an 8-week storage in soil (Dettmeyer et al., 2014; Vennemann and Brinkmann, 2003). Hence, due to a delayed onset of the autolytic processes when stored under oxygen-deficient conditions (e.g. water), less PMR would be expected as compared in air. Contrary to the expectations, this difference could not be confirmed in the present work, as the conc. changes were comparable and statistical tests showed only two significant conc. changes. Regarding *cumyl*-5F-P7AICA, a statistically significant conc. change was only observed at PMI 1 in kidney samples and concerning the NPA metabolite a respective change was only found at PMI 2 in duodenum content.

However, it should be considered that the specimens examined were sampled postmortem and the extent of putrefaction does not only depend on the ambient temperature and can vary widely between different individuals. For example, some animals showed a strong green putrefaction already after 48 h, while others were still in a good condition even after 72 h. This difference can lead to strong interindividual variations of the conc. of the substances measured in tissues and body fluids. Additionally, in particular PM specimens also pose a great challenge to the analytical methods. High interindividual fluctuations have been observed when determining drug conc. in PM tissues and blood specimens, even if the method was fully validated (Brunet et al., 2010; Gleba and Kim, 2020; Nagasawa et al., 2016; Saar et al., 2012). Taken together, all these factors can lead to a high standard deviation, as also found in the present study (Table 2). Therefore, the results of statistical tests, which are generally based on the mean conc., should be regarded with great caution.

In terms of *cumyl*-5F-P7AICA, only minor conc. changes (less than 200 % conc. change) were observed in most specimens at both storage conditions (Fig. 1a and b). This finding might also be attributable to analytical or interindividual deviations. In general, a PMR is essentially characterized by a redistribution of a substance from an organ with high conc. (drug reservoir) into the surrounding tissues with lower conc. (Skopp, 2010). This process depends on various factors, including the physicochemical properties of the respective substance, but also interindividual factors, such as the degree of putrefaction. For example, a PM increase of the pH value or a microbial colonization can lead to a degradation of the respective substances, a release from a protein bound form or a possible cleavage of glucuronides (Butzbach, 2010).

However, when interpreting the PM conc. changes observed for *cumyl*-5F-P7AICA in brain specimens, especially when stored in water, with regard to a possible PMR it should first be noted that brain specimens were only sampled at PMI 3, as a repeated opening of the skull during storage should be avoided. Since the brain represents a closed compartment, similar to e.g. vitreous fluid, a redistribution from other

organs containing higher conc. of the substance seems to be rather unlikely. Attempting to explain the increase of conc., it should be noted that it was not possible to take samples exactly from the same region of the brain, because among other things, the tissue had also already begun to liquefy. As a large amount of cannabinoid receptors 1 are located in the cerebellum (Pertwee, 1997; Svízenská et al., 2008), another plausible explanation for the comparably high PM conc. at PMI 3 in brain when stored in water might be a PMR of *cumyl*-5F-P7AICA from the cerebellum into the cerebrum during the period from PMI 0 to PMI 3. In terms of the blood specimens, PM conc. of CB specimens remained relatively stable in a low conc. range, whereas the median conc. of *cumyl*-5F-P7AICA in PB decreased over 72 h at both storage conditions. Interpreting this difference, it should be kept in mind that the parent substance could only be detected in single PB samples, resulting in low median conc., especially at PMI 3. Regarding this issue, it should furthermore be noted that PB specimens were collected from different veins (femoral or brachiocephalic vein), so that the sampling procedure was not standardized. Finally, due to the PM coagulation of blood and the increasing putrefaction of the corpses, only small amounts of PB could be obtained. In the context of the further analytical process, the blood specimens therefore had to be strongly diluted with blank whole blood. This procedure may have led to very low conc. of the analyte, also possibly below the LOD. Taken together, conc. changes in PB and CB specimens should be regarded with caution, as in most of the cases, the values were lower than the LLOQ (0.5 ng/mL) and sometimes nearby the LOD (0.06 ng/mL), possibly resulting in high analytical deviations. Therefore, in cases of PM toxicology, determined conc. of *cumyl*-5F--P7AICA in blood specimens should be regarded with caution, especially if there has been a prolonged PMI.

In summary, only a slight tendency for PMR was shown for *cumyl*-5F-P7AICA under both storage conditions. Due to the comparatively stable conc. of *cumyl*-5F-P7AICA during the whole experimental period of 72 h, CB also appears to be suitable for PM quantification, if no PB can be obtained. Regarding the NPA metabolite, only minor conc. changes (less than 100 %) in tissue and body fluid specimens were determined at both storage conditions, if detectable at all. This observation might potentially also be attributable to interindividual or analytical deviations. Compared to PMI 0, only a slight decrease in conc. of the NPA metabolite was observed in duodenum content at both storage conditions, with statistically significant changes of the conc. at PMI 2. A tendency for a PMR of the metabolite could not be shown in the present study, regardless of the respective storage condition.

To sum up, bile fluid and duodenum content as well as lung tissue appear to be suitable specimens for a qualitative PM detection of a previous consumption of *cumyl*-5F-P7AICA of the decedent, independent of the storage conditions. If PB is not available for quantification, e.g. due to a PM alteration of the corpse, CB appears to be a useful alternative specimen, as no relevant PMR was observed for *cumyl*-5F-P7AICA in the present study.

Taken together, the data obtained in the present work support the interpretation of PM toxicological cases as knowledge on the PM stability as well as the tendency on a PMR of *cumyl*-5F-P7AICA under different environmental conditions is gained. In addition, specific instructions are given for a correct sampling procedure over a PMI of 3 days in order to be able to detect potentially fatal intoxications after consumption of the SC *cumyl*-5F-P7AICA even in putrefied corpses.

4.5. Limitations

One limitation of the study is posed by the permanent re-opening of the abdominal cavity of the animals to take PM specimens, because this procedure may have led to a stronger contamination with microorganisms as well as a more aerobic environment inside the body, possibly resulting in a faster advanced putrefaction. Due to the storage in water and the associated changes of the skin condition, an absolutely tight seal of the abdominal cavity was not always possible. Thus, it should be considered that a small amount of the water may have entered the abdominal cavity, inducing e.g. a further contamination with microorganisms.

Furthermore, the lack of insect activity represents a further limitation of the present study, as the presence of insects has a significant influence on the extent of decomposition of a corpse. However, even without insect activity, a clear difference in the degree of putrefaction could be observed macroscopically during storage at different environmental conditions. So, an influence on the PM stability of exogenous substances might be expected. In practice, corpses are always colonized to varying degrees with insects. Whilst some corpses are not exposed to insect activity, others can be very heavily infested, e.g. found at home vs. in the forest or in the bathtub vs. in the river). A varying degree of decomposition is therefore expected depending on the environmental conditions, resulting in a different PM stability of substances. However, as no insect activity was tested in the context of the current study, the data obtained are only transferable to authentic human cases with no relevant insect activity to ensure comparability.

In addition, due to repetitive sampling, tissue and body fluid specimens were collected from different veins or sites of the organs, respectively. As the substances may have been inhomogenously distributed within the tissues, the difference may have led to an adulteration of the respective conc.

Last not least it has to be considered that the process of putrefaction was accompanied by the production of putrefactive liquid was produced during the examined time period of 72 h. In particular, this liquid was also located inside of the corpse, so that an impact on PMR cannot completely be excluded.

5. Conclusions

In a first part of the present study, the perimortem distribution patterns of *cumyl*-5F-P7AICA and its NPA metabolite after inhalative administration to pigs was investigated. In a second part of the study, the PM distribution patterns as well as the time- and oxygen-dependent conc. changes were determined. In general, both substances could primarily be detected in tissues involved in TK, such as absorption, metabolism and excretion (lung, liver, kidney, bile fluid/ duodenum content), even though in very low conc. If no standard specimens, such as PB and CB, are available due to an extended PMI, bile fluid and duodenum content and lung are suitable for PM toxicological analysis of the SC *cumyl*-5F-P7AICA. Statistically significant conc. changes associated with the storage conditions (in air vs water) were only observed for *cumyl*-5F-P7AICA in kidney at PMI 1 and the NPA metabolite in duodenum content at PMI 2.

Ethical approval

All experiments were performed in accordance with the German legislation on protection of animals and the National Institutes of Health Guide for the Care and Use of Laboratory Animals (permission number: 44/2019).

Funding

This work was supported by the Deutsche Forschungsgemeinschaft (DFG, German Research Foundation, grant number 508380150).

CRediT authorship contribution statement

Nadja Walle: Writing – original draft, Project administration, Methodology, Investigation, Formal analysis. **Benjamin Peters:** Project administration, Methodology, Investigation. **Adrian Doerr:** Software, Resources, Project administration. **Michael Menger:** Resources, Conceptualization. **Matthias Laschke:** Resources, Project administration, Conceptualization. **Peter Schmidt:** Writing – review & editing,

Supervision, Conceptualization. **Nadine Schaefer:** Writing – review & editing, Supervision, Methodology, Funding acquisition, Conceptualization. **Markus Meyer:** Writing – review & editing, Conceptualization.

Declaration of Competing Interest

The authors declare that they have no known competing financial interests or personal relationships that could have appeared to influence the work reported in this paper.

Acknowledgements

The authors would like to thank Nicole Hoffmann and the staff of the Institute for Clinical & Experimental Surgery at Saarland University for their support and help during the study. We acknowledge the EU funded project ADEBAR (IZ25–5793–2016–27).

Appendix A. Supporting information

Supplementary data associated with this article can be found in the online version at doi:10.1016/j.toxlet.2024.10.006.

Data Availability

Data will be made available on request.

References

Adamowicz, P., 2016. Fatal intoxication with synthetic cannabinoid MDMB-CHMICA. Forensic Sci. Int. 261, e5–e10. https://doi.org/10.1016/j.forsciint.2016.02.024.
Bakhle, Y.S., 1990. Pharmacokinetic and metabolic properties of lung. Br. J. Anaesth. 65, 79–93. https://doi.org/10.1093/bja/65.1.79.
Bend, J.R., Serabjit-Singh, C.J., Philpot, R.M., 1985. The pulmonary uptake, accumulation, and metabolism of xenobiotics. Annu. Rev. Pharmacol. Toxicol. 25, 97–125.
Boer, F., 2003. Drug handling by the lungs. Br. J. Anaesth. 91, 50–60. https://doi.org/10.1093/bja/aeg117.
Boland, D.M., Reidy, L.J., Seither, J.M., Radtke, J.M., Lew, E.O., 2020. orty-three fatalities involving the synthetic cannabinoid, 5-Fluoro-ADB: forensic pathology and toxicology implications. J. Forensic Sci. 65, 170–182. https://doi.org/10.1111/1556-4029.14098.
Brockbals, L., Staeheli, S.N., Gascho, D., Ebert, L.C., Kraemer, T., Steuer, A.E., 2018. Time-dependent postmortem redistribution of opioids in blood and alternative matrices. J. Anal. Toxicol. 42, 365–374. https://doi.org/10.1093/jat/bky017.
Brunet, B., Hauet, T., Hébrard, W., Papet, Y., Mauco, G., Mura, P., 2010. Postmortem redistribution of THC in the pig. Int. J. Leg. Med. 124, 543–549. https://doi.org/10.1007/s00414-009-0403-2.
Butzbach, D.M., 2010. The influence of putrefaction and sample storage on post-mortem toxicology results. Forensic Sci. Med. Pathol. 6, 35–45. https://doi.org/10.1007/s12024-009-9130-8.
Dettmeyer, R.B., Schütz, H.F., Verhoff, M.A., 2014. Thanatologie. In: Schuetz, Verhoff, Dettmeyer (Ed.), Rechtsmedizin, 2nd edn. Springer-Verlag, Berlin Heidelberg, p. 19.
Doerr, A.A., Nordmeier, F., Walle, N., Laschke, M.W., Menger, M.D., Schmidt, P.H., Schaefer, N., Meyer, M.R., 2021. Can a recently developed pig model be used for in vivo metabolism studies of 7-azaindole-derived synthetic cannabinoids? A study using 5F-MDMB-P7AICA. J. Anal. Toxicol. 45, 593–604. https://doi.org/10.1093/jat/bkaa122.
Doerr, A.A., Walle, N., Heinbuch, S., Potente, S., Schmidt, P.H., Schaefer, N., 2022. P-TX-1 Tödliche Monointoxikation nach Konsum des synthetischen Cannabinoids 4F-MDMB-BICA. Rechtsmedizin 32, 347. https://doi.org/10.1007/s00194-022-00580-2.
Doerr, A.A., Nordmeier, F., Walle, N., Laschke, M.W., Menger, M.D., Meyer, M.R., Schmidt, P.H., Schaefer, N., 2024. Does a postmortem redistribution affect the concentrations of the 7 azaindole-derived synthetic cannabinoid 5F-MDMB-P7AICA in tissues and body fluids following pulmonary administration to pigs? Arch. Toxicol. https://doi.org/10.1007/s00204-024-03815-1.
Drummer, O.H., Gerostamoulos, J., 2002. Postmortem drug analysis: analytical and toxicological aspects. Ther. Drug Monit. 24, 199–209.
Ferrari Júnior, E., Leite, B.H.M., Gomes, E.B., Vieira, T.M., Sepulveda, P., Caldas, E.D., 2022. Fatal cases involving new psychoactive substances and trends in analytical techniques. Front. Toxicol. 4, 1–18. https://doi.org/10.3389/ftox.2022.1033733.
Gerostamoulos, D., Beyer, J., Staikos, V., Tayler, P., Woodford, N., Drummer, O.H., 2012. The effect of the postmortem interval on the redistribution of drugs: a comparison of mortuary admission and autopsy blood specimens. Forensic Sci. Med. Pathol. 8, 373–379. https://doi.org/10.1007/s12024-012-9341-2.
Giorgetti, A., Busardò, F.P., Tittarelli, R., Auwärter, V., Giorgetti, R., 2020. Post-mortem toxicology: a systematic review of death cases involving synthetic cannabinoid receptor agonists. Front. Psychiatry 11, 1–22. https://doi.org/10.3389/fpsyt.2020.00464.
Gleba, J., Kim, J., 2020. A mechanism-based forensic investigation into the postmortem redistribution of morphine. J. Anal. Toxicol. 44, 256–262. https://doi.org/10.1093/jat/bkz093.
GTFCh, 2018. Empfehlungen zur Asservierung von Obduktionsmaterial für forensisch-toxikologische Untersuchungen und spezielle Aspekte der Postmortem-Analytik. Toxichem Krimtech 85(1):14–28.
Han, E., Kim, E., Hong, H., Jeong, S., Kim, J., In, S., Chung, H., Lee, S., 2012. Evaluation of postmortem redistribution phenomena for commonly encountered drugs. Forensic Sci. Int. 219, 265–271. https://doi.org/10.1016/j.forsciint.2012.01.016.
Jickells, S., Negrusz, A., 2008. Clarke's analytical forensic toxicology. Pharm. Press, Lond.
Kraemer, M., Boehmer, A., Madea, B., Maas, A., 2019. Death cases involving certain new psychoactive substances: a review of the literature. Forensic Sci. Int. 298, 186–267. https://doi.org/10.1016/j.forsciint.2019.02.021.
Krotulski, A.J., Bishop-Freeman, S.C., Mohr, A.L.A., Logan, B.K., 2021. Evaluation of synthetic cannabinoid metabolites in human blood in the absence of parent compounds: a stability assessment. J. Anal. Toxicol. 45, 60–68. https://doi.org/10.1093/jat/bkaa054.
McIntyre, I.M., 2014. Liver and peripheral blood concentration ratio (L/P) as a marker of postmortem drug redistribution: a literature review. Forensic Sci. Med. Pathol. 10, 91–96. https://doi.org/10.1007/s12024-013-9503-x.
Nagasawa, S., Katagiri, N., Nara, A., Chiba, F., Kubo, Y., Torimitsu, S., Yajima, D., Akutsu, M., Iwase, H., 2016. Postmortem redistribution mechanism of donepezil in the rat. Forensic Sci. Int. 266, 1–7. https://doi.org/10.1016/j.forsciint.2016.04.017.
Nordmeier, F., Doerr, A.A., Potente, S., Walle, N., Laschke, M.W., Menger, M.D., Schmidt, P.H., Meyer, M.R., Schaefer, N., 2022. Are the (new) synthetic opioids U-47700, tramadol and their main metabolites prone to time-dependent postmortem redistribution? - A systematic study using an in vivo pig model. J. Anal. Toxicol. 47, 236–244. https://doi.org/10.1093/jat/bkac082.
Oberhofer, E., 2018. Toedlicher Rauch aus der Eimer-Bong. MMW - Fortschr. der Med. 160, 14. https://doi.org/10.1007/s15006-018-0960-8.
Pélissier-Alicot, A.L., Gaulier, J.-M., Champsaur, P., Marquet, P., 2003. Mechanisms underlying postmortem redistribution of drugs: a review. J. Anal. Toxicol. 27, 533–544. https://doi.org/10.1093/jat/27.8.533.
Pertwee, R.G., 1997. Pharmacology of cannabinoid CB1 and CB2 receptors. Pharmacol. Ther. 74, 129–180. https://doi.org/10.1016/s0163-7258(97)82001-3.
Peters, F.T., Drummer, O.H., Musshoff, F., 2007. Validation of new methods. Forensic Sci. Int. 165 (2), 216–224.
Saar, E., Beyer, J., Gerostamoulos, D., Drummer, O.H., 2012. The time-dependant post-mortem redistribution of antipsychotic drugs. Forensic Sci. Int. 222, 223–227. https://doi.org/10.1016/j.forsciint.2012.05.028.
Schaefer, N., Peters, B., Bregel, D., Kneisel, S., Auwärter, V., Schmidt, P.H., Ewald, A.H., 2013. A fatal case involving several synthetic cannabinoids. Toxichem. Krimtech. 80, 248–251.
Schaefer, N., Kettner, M., Laschke, M.W., Schlote, J., Ewald, A.H., Menger, M.D., Maurer, H.H., Schmidt, P.H., 2017. Distribution of synthetic cannabinoids JWH-210, RCS-4 and Δ 9-tetrahydrocannabinol after intravenous administration to pigs. Curr. Neuropharmacol. 15, 713–723. https://doi.org/10.2174/1570159X15666161111114214.
Schaefer, N., Kroell, A.-K., Laschke, M.W., Menger, M.D., Maurer, H.H., Meyer, M.R., Schmidt, P.H., 2018. Development of an in-vitro drug delivery efficiency test for a pulmonary toxicokinetic pig study. Curr. Drug Deliv. 15, 1167–1171. https://doi.org/10.2174/1567201815666180214130014.
Schaefer, N., Kroell, A.-K., Koerbel, C., Laschke, M.W., Menger, M.D., Maurer, H.H., Meyer, M.R., Schmidt, P.H., 2019. Distribution of the (synthetic) cannabinoids JWH-210, RCS-4, as well as Δ9-tetrahydrocannabinol following pulmonary administration to pigs. Arch. Toxicol. 93, 2211–2218. https://doi.org/10.1007/s00204-019-02493-8.
Schaefer, N., Kroell, A.-K., Koerbel, C., Laschke, M.W., Menger, M.D., Maurer, H.H., Meyer, M.R., Schmidt, P.H., 2020a. Time- and temperature-dependent postmortem concentration changes of the (synthetic) cannabinoids JWH-210, RCS-4, as well as Δ9-tetrahydrocannabinol following pulmonary administration to pigs. Arch. Toxicol. 94, 1585–1599. https://doi.org/10.1007/s00204-020-02707-4.
Schaefer, N., Nordmeier, F., Kroell, A.-K., Koerbel, C., Laschke, M.W., Menger, M.D., Maurer, H.H., Meyer, M.R., Schmidt, P.H., 2020b. Is adipose tissue suitable for detection of (synthetic) cannabinoids? A comparative study analyzing antemortem and postmortem specimens following pulmonary administration of JWH-210, RCS-4, as well as Δ9-tetrahydrocannabinol to pigs. Arch. Toxicol. 94, 3421–3431. https://doi.org/10.1007/s00204-020-02843-x.
Skopp, G., 2010. Postmortem toxicology. Forensic Sci. Med. Pathol. 6, 314–325. https://doi.org/10.1007/s12024-010-9150-4.
SOFT/AAFS, 2006. Forensic toxicology laboratory guidelines. ⟨http://www.the-ltg.org/data/uploads/guidelines/soft-guidelines_2006.pdf⟩. Accessed September 2024.
Svízenská, I., Dubový, P., Sulcová, A., 2008. Cannabinoid receptors 1 and 2 (CB1 and CB2), their distribution, ligands and functional involvement in nervous system structures–a short review. Pharmacol. Biochem. Behav. 90, 501–511. https://doi.org/10.1016/j.pbb.2008.05.010.
Vennemann, B., Brinkmann, B., 2003. Der Tod im Wasser. Rechtsmedizin 13, 201–215. https://doi.org/10.1007/s00194-003-0212-8.
Walle, N., Nordmeier, F., Doerr, A.A., Peters, B., Laschke, M.W., Menger, M.D., Schmidt, P.H., Meyer, M.R., Schaefer, N., 2021. Comparison of in vitro and in vivo models for the elucidation of metabolic patterns of 7-azaindole-derived synthetic

cannabinoids exemplified using cumyl-5F-P7AICA. Drug Test. Anal. 13, 74–90. https://doi.org/10.1002/dta.2899.
Walle, N., Doerr, A.A., Schmidt, P.H., Schaefer, N., 2023. 'Flying high?'-Jump from a height in a "Spice" high?: A case report on the synthetic cannabinoid 5F-MDMB-P7AICA. Drug Test. Anal. 15, 368–373. https://doi.org/10.1002/dta.3401.
Zawadzki, M., Chłopaś-Konowałek, A., Nowak, K., Wachełko, O., Szpot, P., 2021. Quantification of 5F-CUMYL-P7AICA in blood and urine from an authentic fatality associated with its consumption by UHPLC–MS/MS. Forensic Toxicol. 39, 240–247. https://doi.org/10.1007/s11419-020-00555-6.

Electronic Supplementary Material

Are the postmortem concentration changes of the synthetic cannabinoid *cumyl*-5F-P7AICA and its *N*-pentanoic acid metabolite dependent on the environmental conditions? – A systematic study following pulmonary administration to pigs

Nadja Walle[1], Adrian A. Doerr[1], Benjamin Peters[1], Matthias W. Laschke[2], Michael D. Menger[2], Peter H. Schmidt[1], Markus R. Meyer[3] and Nadine Schaefer[1*]

---

[*]Correspondence to: Nadine Schaefer, Institute of Legal Medicine, Saarland University, Building 49.1, 66421 Homburg, Germany

Email: nadine.schaefer@uks.eu

[1]Institute of Legal Medicine, Saarland University, Building 49.1, 66421 Homburg, Germany

[2]Institute for Clinical & Experimental Surgery, Saarland University, Building 65/66, 66421 Homburg, Germany

[3]Department of Experimental and Clinical Toxicology, Center for Molecular Signaling (PZMS), Saarland University, Building 46, 66421 Homburg, Germany

Materials and Methods

Chemicals, reagents and blank whole blood samples

Di-potassium hydrogen phosphate, aqueous potassium hydroxide solution (1 M), glacial acetic acid and β-glucuronidase/arylsulfatase (from Helix pomatia) were purchased by Merck (Darmstadt, Germany). Water (Optima), methanol (HPLC grade), ethanol (HPLC grade), aceton p.a., acetonitrile (Optima), and formic acid (Optima) were obtained from Fisher Scientific (Loughborough, United Kingdom). Na_2EDTA was purchased from Sigma-Aldrich (Steinheim, Germany). *Cumyl*-5F-P7AICA was provided by the German Federal Criminal Police Office (Wiesbaden, Germany) with a purity of 99.72 % for research purpose. The *N*-pentanoic acid (NPA) metabolite (1 mg; solid), AB-FUBINACA-d_4 (1 mg; solid) as well as RCS-4-d_9 (1 mg; solid) were from Cayman Europe (Tallinn, Estonia).

Blank whole blood specimens for preparation of quality control (QC) samples as well as calibrators were obtained from drug free pigs (Swabian Hall strain, Emil Faerber GmbH & Co. KG, Zweibruecken, Germany). Upon receipt, Na_2EDTA (1.64 mg/mL) was added to the blank whole blood specimens to prevent clotting. Subsequently, the samples were stored at -20 °C until analysis.

Preparation of buffer solutions

The preparation of the buffer solutions was in accordance to previously published data (Doerr et al., 2021; Schaefer et al., 2015, 2017, 2019; Walle et al., 2023). Accordingly, preparation of acetate buffer (0.1 M, pH 4) was performed by diluting 16 mL aqueous potassium hydroxide solution (1M) and 5.7 mL glacial acetic acid with HPLC grad water ad 1 L. For the phosphate buffer (0.1 M, pH 9), 22.82 di-potassium hydrogen phosphate was dissolved in 1 L HPLC grade water.

Surgical procedures

In accordance to other studies (Doerr et al., 2021; Nordmeier et al., 2022a, b; Schaefer et al., 2017, 2019, 2020; Walle et al., 2021), 30 mg/kg body weight (BW) ketamine hydrochloride (Ursotamin; Serumwerke Bernburg, Bernburg, Germany), 1 mg atropine (Braun, Melsungen, Germany), and 2.5 mg/kg BW xylazine hydrochloride (Rompun; Bayer, Leverkusen, Germany) were administered intramuscularly to the animal as a premedication. As a slight modification to the aforementioned studies, 5 mg/kg BW carprofen (Rimadyl; Zoetis, Berlin, Germany) was additionally administered to the animal in the present study, to relieve possible pain. Subsequently, 2-4 % of isoflurane (Forene, AbbVie, Ludwigshafen, Germany) was administered inhalatively to maintain anesthesia. The pigs were mechanically ventilated during the whole experiment with a 1:2 v/v mixture of oxygen and air (FiO_2 of 0.30, Respirator ABV-U; F. Stephan GmbH, Gackenbach, Germany) and volume cycled with a tidal volume of 10-12 mL/kg BW. A catheter was placed in the left ear vein to ensure sufficient fluid replacement with 0.9 % sodium chloride (8 mL kg^{-1} h^{-1}, Braun, Melsungen, Germany). Additionally, a triple-lumen 7F (Certofix Trio, Braun, Melsungen, Germany) central venous catheter was placed into the jugular vein for monitoring of the mean central venous pressure and blood sampling. Additionally, to monitor the arterial blood pressure an additional catheter (Leadercath Expert 14G, Vygon, Aachen, Germany) was placed in the left femoral artery. Finally, for urine collection a suprapubic catheter (Cystofix, Braun, Melsungen, Germany) was placed into the bladder. After the aforementioned preparations, the animal was allowed to stabilize for 10-15 min.

Preparation of blood specimens

For blood preparation, a solid phase extraction was performed using Strata C18 endcapped cartridges (200 mg/3 mL). For this purpose, an aliquot of the respective postmortem (PM) peripheral blood (PB) and central blood (CB) specimens was firstly diluted with blank blood.

Afterwards, 500 µL of the dilution was added to a mixture of 20 µL of an ethanolic stable-isotope-labeled internal standard mixture solution (SIL-IS, 1 ng/20 µL RCS-4-d_9, and 0.25 ng/20 µL AB-FUBINACA-d_4), 25 µL ethanol and 2.5 mL phosphate buffer (pH 9). Calibrators and QC samples were prepared analogously, with the change that blank blood was used and ethanol was replaced by 25 µL QC or calibration spiking solutions. Following, the specimens were vortexed and centrifuged at 3500 g for 8 min. After a conditioning step of the cartridges with 2x3 mL methanol and 3 mL phosphate buffer (pH 9), the prepared solutions were loaded. Three washing steps were carried out using 3 mL phosphate buffer (pH 9), 3 mL acetic acid (0.25 M), and 3 mL water. After the addition of 60 µL acetone, the cartridges were dried under a maximum vacuum of 10 inHg. Subsequently, elution of the analytes was achieved by adding 1.5 mL of a methanol-acetone mixture (1:1, *v/v*) and the eluates were evaporated under a gentle stream of nitrogen at 60 °C. The dry residues were dissolved in 50 µL of a mixture (50:50, *v/v*) of mobile phases A (0.1% aqueous formic acid) and B (0.1% formic acid in acetonitrile). The solution was transferred into an autosampler vial and 5 µL were injected onto a liquid chromatography (LC) quadrupole time-of-flight (TOF)-mass spectrometer (MS) system.

LC-MS/MS apparatus

LC-triple quadrupole-MS

Analysis of the tissue, body fluid and adipose tissue specimens was performed using a Thermo Fisher (Dreieich, Germany) LC. In brief, the LC was furnished with one Allegro pump as well as an HTC PAL autosampler and chromatography was achieved by a Gravity C18 column (150 x 2 mm, 5 µm, Macherey-Nagel, Dueren, Germany) with a gradient elution using mobile phases A and B. The runtime was set to 10 min and gradient settings were configured as follows: start with mobile phase B (25%) with a flow rate of 0.5 mL/min, 1 min holding, increase of mobile phase B within 4 min to 100%, hold for 4 min, restore the starting conditions, held for 1 min. A TF TSQ Quantum Ultra Accurate Mass triple stage MS with an electrospray ionization

(ESI) run in positive mode was coupled to the LC for detection of the analytes. The settings of the MS were set as follows: capillary temperature 290 °C; spray voltage 4.000 V; ion sweep gas 5 arbitrary units (AU); sheath gas 40 AU; auxiliary gas 20 AU; collision cell pressure 1.5 mTorr; vaporizer temperature 380 °C.

Subsequently, detection and quantification of the analytes was performed in the multiple-reaction monitoring mode with three transitions per precursor ion of *cumyl*-5F-P7AICA and the NPA and two transitions for RCS-4-d_9 (Supplementary Table 1). The TF Xcalibur Version 2.0.7 SP 1 software was used.

LC-quadrupole time-of-flight-MS

Additionally, analysis of the perimortem and PM PB and CB specimens was performed using a SCIEX TripleTOF 6600+ (AB SCIEX, Concord, USA) system, which was connected to an Exion LC system (AB SCIEX). The system consisted of an AD autosampler, an AD column oven, and 2 AD pumps. For chromatographic separation a nucleoshell PFP column (100x2 mm, 2.7 µm) by Macherey-Nagel (Dueren, Germany) was used, applying a gradient elution set as follows: 25% mobile phase B (flow rate: 0.5 mL/min) kept for 1 min, increase to 99% mobile phase B over 3 min, hold for 3 min, restore starting conditions, hold for 2 min. Total runtime was 10 min. The column oven temperature was set to 40 °C. The coupled MS was equipped with a DuoSpray source running in positive ESI mode for sample analysis. The respective settings were as follows: capillary temperature, 450 °C; ion spray voltage, 4.500 V; curtain gas, 30 AU; ion source gas 1, 45 AU; ion source gas 2, 57 AU; collision energy spread, 15 V; collision energy, 35 V; declustering potential, 80 V. The system was mass calibrated every 5 runs using a calibrant delivery system. Detection and quantification of the analytes were carried out in the product ion scan mode. For detection, the recorded spectra were compared in terms of accurate mass as well as fragment abundance. For quantification, the area ratio of one

fragment ion of the respective substance and the SIL-IS was used applying the calibration equation. Data handling was achieved using Sciex OS version 1.6.1.29803 software.

References

Doerr, A.A., Nordmeier, F., Walle, N., Laschke, M.W., Menger, M.D., Schmidt, P.H., Schaefer, N., Meyer, M.R., 2021. Can a recently developed pig model be used for in vivo metabolism studies of 7-azaindole-derived synthetic cannabinoids? A study using 5F-MDMB-P7AICA. J. Anal. Toxicol. 45, 593–604. https://doi.org/10.1093/jat/bkaa122.

Nordmeier, F., Doerr, A.A., Potente, S., Walle, N., Laschke, M.W., Menger, M.D., Schmidt, P.H., Meyer, M.R., Schaefer, N., 2022a. Perimortem distribution of U-47700, tramadol and their main metabolites in pigs following intravenous administration. J. Anal. Toxicol. 46, 479–486. https://doi.org/10.1093/jat/bkab044.

Nordmeier, F., Doerr, A.A., Potente, S., Walle, N., Laschke, M.W., Menger, M.D., Schmidt, P.H., Meyer, M.R., Schaefer, N., 2022b. Are the (new) synthetic opioids U-47700, tramadol and their main metabolites prone to time-dependent postmortem redistribution? - A systematic study using an in vivo pig model. J. Anal. Toxicol. 47,236-244. https://doi.org/10.1093/jat/bkac082

Schaefer, N., Kettner, M., Laschke, M.W., Schlote, J., Peters, B., Bregel, D., Menger, M.D., Maurer, H.H., Ewald, A.H., Schmidt, P.H., 2015. Simultaneous LC-MS/MS determination of JWH-210, RCS-4, Δ9-tetrahydrocannabinol, and their main metabolites in pig and human serum, whole blood, and urine for comparing pharmacokinetic data. Anal. Bioanal. Chem. 407, 3775–3786. https://doi.org/10.1007/s00216-015-8605-6.

Schaefer, N., Kettner, M., Laschke, M.W., Schlote, J., Ewald, A.H., Menger, M.D., Maurer, H.H., Schmidt, P.H., 2017. Distribution of synthetic cannabinoids JWH-210, RCS-4 and Δ 9-tetrahydrocannabinol after intravenous administration to pigs. Curr. Neuropharmacol. 15, 713–723. https://doi.org/10.2174/1570159X15666161111114214.

Schaefer, N., Kroell, A.-K., Koerbel, C., Laschke, M.W., Menger, M.D., Maurer, H.H., Meyer, M.R., Schmidt, P.H., 2019. Distribution of the (synthetic) cannabinoids JWH-210, RCS-4, as well as Δ9-tetrahydrocannabinol following pulmonary administration to pigs. Arch. Toxicol. 93, 2211–2218. https://doi.org/10.1007/s00204-019-02493-8.

Schaefer, N., Kroell, A.-K., Koerbel, C., Laschke, M.W., Menger, M.D., Maurer, H.H., Meyer, M.R., Schmidt, P.H., 2020. Time- and temperature-dependent postmortem concentration changes of the (synthetic) cannabinoids JWH-210, RCS-4, as well as Δ9-tetrahydrocannabinol following pulmonary administration to pigs. Arch. Toxicol. 94, 1585–1599. https://doi.org/10.1007/s00204-020-02707-4.

Walle, N., Nordmeier, F., Doerr, A.A., Peters, B., Laschke, M.W., Menger, M.D., Schmidt, P.H., Meyer, M.R., Schaefer, N., 2021. Comparison of in vitro and in vivo models for the elucidation of metabolic patterns of 7-azaindole-derived synthetic cannabinoids exemplified using cumyl-5F-P7AICA. Drug Test. Anal. 13, 74–90. https://doi.org/10.1002/dta.2899.

Walle, N., Doerr, A.A., Schmidt, P.H., Schaefer, N., 2023. 'Flying high?'-Jump from a height in a "Spice" high?: A case report on the synthetic cannabinoid 5F-MDMB-P7AICA. Drug Test. Anal. 15, 368–373. https://doi.org/10.1002/dta.3401.

Supplementary Table S1. Multiple reaction monitoring transitions, the respected retention times as well as the analysis conditions adjusted for the qualitative and quantitative analyses of c*umyl*-5F-P7AICA, its *N*-pentanoic acid metabolite and the internal standards AB-FUBINACA-d_4, and RCS-4-d_9 in tissue/ body fluid (liquid chromatography (LC) tandem mass spectrometry (MS)) and blood specimens (LC quadrupole time-of-flight-MS system).
(* = target ion)

LC-MS/MS (Tissue/ body fluid specimens)						
Analyte	**Precursor ion** [*m/z*]	**Product ions** [*m/z*]	**Retention time** [*min*]	**Scan time** [*msec*]	**Tube lens** [*V*]	**Collision energy** [*V*]
Cumyl-5F-P7AICA	368.20	250.20* 119.25 233.20	3.98	40	54	16* 33 26
N-pentanoic acid	380.20	262.11* 201.10 244.10	3.04	40	80	17* 25 21
RCS-4-d_9	331.10	135.06* 77.10	4.96	40	82	25* 45

LC-TOF-MS (Blood specimens)						
Analyte	**Precursor ion** [*m/z*]	**Product ions** [*m/z*]	**Retention time** [*min*]	**Scan time** [*msec*]	**Declustering potential** [*V*]	**Collision energy** [*V*]

Cumyl-5F-P7AICA	368.21	174.06	3.34	35	80	44
N-pentanoic acid	380.19	262.11	2.72	35	80	21
AB-FUBINACA-d_4	373.19	257.10	2.95	35	80	29
RCS-4-d_9	331.23	135.04	3.92	35	80	32

3.4 Does a carboxamide moiety alter the toxicokinetics of synthetic cannabinoids? A study after pulmonary and intravenous administration of *cumyl*-5F-P7AICA to pigs[144]

(DOI: 10.1007/s00204-024-03906-z)

Authors Contributions:

Nadja Walle conducted and evaluated the experiment as well as composed the manuscript; Christiane Dings, Omar Zaher, and Thorsten Lehr assisted with the calculation and modulation of the pharmacokinetic data; Adrian A. Doerr and Benjamin Peters assisted with the execution of the animal experiments; Matthias W. Laschke and Michael D. Menger carried out and enabled the animal experiments and assisted with scientific discussions; Peter H. Schmidt, Markus R. Meyer, and Nadine Schaefer assisted with scientific discussions, the development of the experiment and supervised the research.

Archives of Toxicology (2025) 99:633–643
https://doi.org/10.1007/s00204-024-03906-z

TOXICOKINETICS AND METABOLISM

Does a carboxamide moiety alter the toxicokinetics of synthetic cannabinoids? A study after pulmonary and intravenous administration of *cumyl*-5F-P7AICA to pigs

Nadja Walle[1] · Christiane Dings[2] · Omar Zaher[2] · Adrian A. Doerr[1] · Benjamin Peters[1] · Matthias W. Laschke[3] · Thorsten Lehr[2] · Michael D. Menger[3] · Peter H. Schmidt[1] · Markus R. Meyer[4] · Nadine Schaefer[1]

Received: 15 October 2024 / Accepted: 20 November 2024 / Published online: 4 December 2024

Abstract

Synthetic cannabinoids (SCs) are consumed as an alternative to cannabis. Novel compounds are developed by minor modifications in their chemical structure, e.g. insertion of a carboxamide moiety as a linker, which can potentially lead to altered toxicokinetics (TK). Knowledge on the TK data of SCs, especially structural modified substances, is scarce. Hence, interpretation of toxicological results is challenging. Therefore, the aim of the present study was to evaluate the TK of *cumyl*-5F-P7AICA in a pig model, which was shown to be suitable for TK studies of SCs. A 200 µg/kg body weight dose of *cumyl*-5F-P7AICA was administered intravenously (n = 6) or inhalatively (n = 10) via an ultrasonic nebulizer to pigs. Blood specimens were repeatedly drawn over 6 h and the concentrations of *cumyl*-5F-P7AICA as well as its *N*-pentanoic acid (NPA) metabolite were determined using a fully validated LC–MS/MS method. Based on the concentration–time profiles, a population TK analysis yielded a three-compartment model for the TK of *cumyl*-5F-P7AICA, whilst a two-compartment model described the NPA best. The incorporation of transit compartments accounts for the time delay between the appearance of *cumyl*-5F-P7AICA and NPA in serum. Finally, the model was upscaled to humans using allometric scaling. In comparison to older SCs, a higher volume of distribution was determined for *cumyl*-5F-P7AICA. No further relevant differences of the TK properties were observed. Insertion of a carboxamide moiety into the chemical structure of SCs does not appear to have only minor influence on the TK.

Keywords Synthetic cannabinoids · *cumyl*-5F-P7AICA · Carboxamide · Pigs · Toxicokinetics · Allometric scaling

Introduction

For several years, new psychoactive substances (NPS) have emerged on the drug market as synthetically produced variants of conventional drugs. These substances are included in herbal mixtures, bath salts or plant food (Elliott and Evans 2014) in forms of herbal smoking mixtures, powders or even liquids (Shafi et al. 2020). Due to the absence of clinical safety studies (Guirguis 2017), they are consumed without the understanding of potential consequences. Furthermore, consumers are unaware of the specific dose or the exact SCs involved, involuntarily becoming the 'experimental subjects'. This can lead to unexpected and severe side effects, including e.g. nausea, vomiting, tachycardia, hallucinations and psychosis, which may result in life-threatening conditions (Hermanns-Clausen et al. 2013; Meyer 2016; Kraemer et al. 2019).

Even when isolated SCs and entire chemical structure elements are restricted, these regulations are circumvented by slight modifications in the chemical structures. Such modified SCs, e.g. those containing a carboxamide moiety, have gained increased attention since several years, as numerous intoxications and fatalities following their consumption

✉ Nadine Schaefer
nadine.schaefer@uks.eu

1 Institute of Legal Medicine, Saarland University, Building 49.1, 66421 Homburg, Germany

2 Department of Clinical Pharmacy, Saarland University, Building C5 3, 66123 Saarbrücken, Germany

3 Institute for Clinical and Experimental Surgery, Saarland University, Building 65/66, 66421 Homburg, Germany

4 Department of Experimental and Clinical Toxicology, Center for Molecular Signaling (PZMS), Saarland University, Building 46, 66421 Homburg, Germany

have been reported (Oberhofer 2018; Kraemer et al. 2019; Giorgetti et al. 2020; Kleis et al. 2020; Zawadzki et al. 2021; Ferrari Júnior et al. 2022; de Oliveira et al. 2023; Walle et al. 2023; Houston et al. 2023).

Cumyl-5F-P7AICA (Fig. 1A) is one of those modified SCs and was first identified by the European Monitoring Centre for Drugs and Drug Addiction (EMCDDA) in 2015 (European Monitoring Centre for Drugs and Drug Addiction 2016). Besides a 7-azaindole core structure, *cumyl*-5F-P7AICA contains a carboxamide moiety as a linker between the core and the bridge residue and represents a further structurally modification of the SCs 5F-CUMYL-PICA and 5F-CUMYL-PINACA containing an indole or indazole core structure besides the carboxamide moiety (Banister et al. 2019). As a faster in vivo degradation via human carboxylesterases has been reported for various drugs (of abuse) containing amide moieties (Di 2018), structural modifications of SCs with incorporation of a carboxamide moiety could conceivably lead to altered toxicokinetic (TK) properties compared to 'older' SC containing e.g. a benzoyl moiety as a linker between the core and the bridge residue. However, in an in vitro metabolism study using various isoforms of recombinant human carboxylesterases with carboxamide containing SCs with different bridge residues, Wagmann et al. reported the degradation of SCs containing an ester moiety in the bridge residue, while the carboxamide linker remained stable (Wagmann et al. 2022).

In forensic toxicology, interpretation of plasma or serum concentrations is fundamental, e.g. for the evaluation of the driving ability of a person. For this purpose, human TK data of SCs are essential. However, due to ethical reasons, systematically controlled human studies are not possible. Therefore, TK data are predominantly available from in vitro studies, self-experiments or case reports, often lacking precise information on dose and time of intake or involving only a small number of participants (Castaneto et al. 2015; Meyer 2016; Houston et al. 2023). Furthermore, only limited TK data from systematically controlled animal studies have been published so far (Schaefer et al. 2015, 2016, 2017a, b, 2019; Castaneto et al. 2015; Walle et al. 2021, 2024; Doerr et al. 2021, 2024a, b). Thus, Schaefer et al. have successfully developed a pig model that can be used for the determination of the TK properties of (synthetic) cannabinoids and opioids after inhalative or intravenous (i.v.) administration (Schaefer et al. 2016, 2017a, b, 2018, 2019; Nordmeier et al. 2021). Compared to other in vivo setups, such as the zebrafish larvae or the rat model, the pig model offers various advantages: The larger blood volume enables a repeated sampling to study the TK. Additionally, pigs are considered to be very similar to humans with regard to the anatomical structures, isoenzymes, and physiological properties (Anzenbacher et al. 1998; Soucek et al. 2001; Meurens et al. 2012; Swindle et al. 2012).

In particular, only sparse in vivo TK data from systematically controlled studies on structurally modified SCs are available. Recently, Doerr et al. reported on the TK properties of the SC 5F-MDMB-P7AICA, which contains an ester moiety in the bridge residue in addition to a carboxamide linker (Doerr et al. 2024a).

Therefore, the aim of the present study was to elucidate the TK of *cumyl*-5F-P7AICA (Fig. 1A) after inhalative and i.v. administration using a sophisticated pig model. This drug was chosen as a representative for SCs containing a carboxamide moiety. In this study. the obtained data were used for the development of a TK model in order to predict human concentration–time profiles using allometric scaling. Subsequently, the results were compared with those previously published for the SCs JWH-210 (Fig. 1B) and RCS-4 (Fig. 1C) (Schaefer et al. 2016, 2018), which contain an indole core structure, to identify potential different TK properties due to the modified chemical structures.

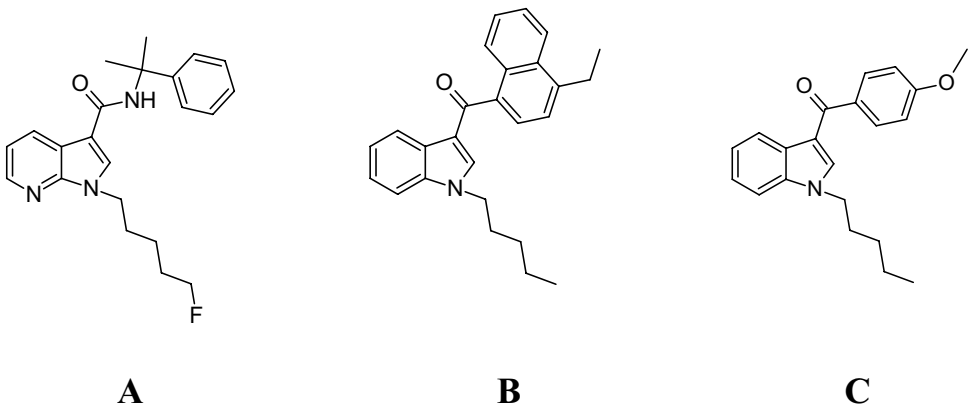

Fig. 1 Molecular structures of *cumyl*-5F-P7AICA (**A**), JWH-210 (**B**), and RCS-4 (**C**)

Materials and methods

Chemicals, reagents, and preparations

A detailed list of the used chemicals and reagents as well as a description of the respective preparations (buffer solution, stock solutions, calibration standards, quality control samples as well as blank pig whole blood and serum) can be found in the Supplementary Information (SI).

In vivo study

Animals

Analogous to previous studies (Walle et al. 2021, 2024), the in vivo experiments conducted in the present study were performed in accordance with the German legislation on protection of animals and the National Institutes of Health Guide for the Care and Use of Laboratory Animals (permission number: 44/2019).

Sixteen domestic male pigs of the Swabian Hall strain were used. The body weight (BW) of the pigs varied between 44 and 64 kg. In accordance to previous studies (Schaefer et al. 2018, 2019; Walle et al. 2021; Doerr et al. 2021; Nordmeier et al. 2022a, b), the animals had free access to tap water and daily standard chow up to 12 h before the start of the experiment. Then, they were kept fasting with still free access to water.

Surgical procedures

All surgical procedures were in accordance with already published previous studies (Schaefer et al. 2018, 2019, 2020; Walle et al. 2021; Doerr et al. 2021; Nordmeier et al. 2022a, b) and are described in detail in the SI.

Study design

The study included two different routes of administering the drug, i.v. or inhalative. First, six pigs received an i.v. dose of 200 µg/kg BW of *cumyl*-5F-P7AICA. For preparation of a solution with a concentration of 5 mg/mL, the SC was first diluted in ethanol. Following, to obtain the required dose of 200 µg/kg BW, the respective volume of the solution was withdrawn, fortified with 1 mL Polysorbat 80 for solubilization, and filled up with 0.9% sodium chloride to a final volume of 10 mL. Subsequently, the final solution was administered intravenously via the jugular vein over 30 s. Then, the venous catheter was washed for 30 s using 10 mL of 0.9% sodium chloride in order to remove possible retained substance (t = 0 min). After the washing step, blood samples were drawn 1, 2, 5, 10, 15, 30, 45, 60, 90, 120, 180, 240, 300, and 360 min after administration. Additionally, a control sample was taken before the administration of *cumyl*-5F-P7AICA.

Additional ten pigs received a 200 µg/kg BW dose of *cumyl*-5F-P7AICA via inhalative administration. For this purpose, *cumyl*-5F-P7AICA was initially dissolved in ethanol to obtain a stock solution of 5 mg/mL. The required volume to obtain a 200 µg/kg BW dose was diluted with ethanol to receive a final volume of 2 mL. The applied setup as well as the subsequent inhalative administration of *cumyl*-5F-P7AICA were in accordance to previous studies (Walle et al. 2021, 2024). Briefly, the prepared solution was nebulized and administered inhatively. For nebulization, the M-neb flow + ventilation ultrasonic nebulizer MN-300/7 (Nebutec, Elsenfeld, Germany) was used, applying the inspiration-triggered mode (< 0.2 mL/min). Blood samples were drawn prior to the administration as well as 1, 2, 5, 6, 7, 8, 9, 10, 15, 30, 45, 60, 90, 120, 180, 240, 300, and 360 min after the start of nebulization.

To obtain serum specimens, the blood specimens sampled during the experiment were centrifuged at 1476×*g* for 15 min. Blood and serum samples were stored at − 20 °C until analysis.

Sample preparation

For qualitative and quantitative determination of *cumyl*-5F-P7AICA and its *N*-pentanoic acid (NPA) metabolite in pig blood and serum specimens, a solid phase extraction using Strata C18 endcapped cartridges (200 mg/3 mL; Phenomenex LTD, Aschaffenburg, Germany) was performed, following the procedure previously successfully applied for other SCs by Schaefer et al. (2015, 2016, 2018). If measured concentrations were above the calibration range, samples were diluted 1:10 and analyzed again. A detailed description of the sample preparation and method validation can be found in the SI.

Liquid chromatography (LC)-quadrupole time of flight (TOF)–mass spectrometry (MS) apparatus

The settings of the LC-quadrupole TOF–MS used for detection and quantification of the substances in pig blood and serum samples were in accordance with a recent study (Walle et al. 2024) and can be found in detail in the SI.

Non-compartmental analysis

A non-compartmental analysis (NCA) was performed using the Software R (Version 4.3.0, The R Foundation for Statistical Computing, Vienna, Austria) and R package 'PKNCA' (Version 0.10.2) (Denney et al. 2015). Mean values and standard deviations (SD) were calculated using the available

parent drug and metabolite concentration measurements in serum and whole blood. The areas under the curve (AUCs) were derived from the concentration–time profiles using the linear up/log down method.

Population TK modeling

A population (pop) TK model was developed using nonlinear mixed-effects modelling techniques, facilitated by the software NONMEM (Version 7.4.3, ICON Development Solutions, Ellicott City, MD, USA). This approach enables the concurrent estimation of population medians for the model parameters alongside inter-individual (IIV) and residual variability. The model development process comprised three sequential phases: (I) Initial establishment of a TK model for *cumyl*-5F-P7AICA serum concentration after i.v. administration, involving exploration of various structural models (1-, 2-, 3- and 4 compartment models) and different elimination kinetics (i.e. linear and saturable processes); (II) subsequent integration of the metabolite formation into the parent model through an additional clearance rate from parent to metabolite, considering diverse structural models, metabolite formation and elimination kinetics; and (III) eventual extension of the model to incorporate parent and metabolite profiles following pulmonary administration by evaluating different absorption models. BW was incorporated as an exponential covariate on all clearance and volume of distribution parameters with an exponent of 0.75 to facilitate allometric scaling to human subjects (Schaefer et al. 2018).

For parameter estimation, the first-order conditional estimation algorithm with interaction was used. Model selection was based on visual inspection of goodness-of-fit plots (Karlsson and Savic 2007), precision of parameter estimates in the form of relative standard errors (Upton and Mould 2014), visual predictive checks (VPCs) and the objective function value (OFV) provided by NONMEM. Here, a nested model was considered superior if the difference of OFVs was > 3.84 points (chi^2, $p < 0.05$, 1 df). For the VPC, 1000 simulations of the dataset were performed including random effects with the final model. Based on the simulation results, median serum concentration–time profiles and 90% prediction intervals were calculated and compared with the observed serum concentration. The software R (Version 4.3.0, The R Foundation for Statistical Computing) was used for the generation of the NONMEM dataset and graphics.

Prediction of human exposure

The final pig model was upscaled to humans, using a reference BW of 70 kg and following allometric principles (Schaefer et al. 2018). Simulated scenarios included single-dose administrations of 0.5, 2 and 14 mg as well as multiple dose application of 2 mg every 60 min, for both i.v. and pulmonary application and with a fixed inhalation duration of 10 min. Each scenario underwent 1000 simulations including random effects. Subsequently, median simulated serum concentration–time profiles were plotted along with their corresponding 90% prediction intervals.

Results

Concentration–time profiles

The respective mean drug concentration of *cumyl*-5F-P7AICA and its NPA metabolite in pig serum and blood sampled during the experiment over 360 min after i.v. and inhalative administration are depicted in Fig. 2. Six pigs received *cumyl*-5F-P7AICA intravenously, yielding 83 measurements each for *cumyl*-5F-P7AICA and NPA. Ten pigs received *cumyl*-5F-P7AICA via pulmonary application, resulting in 180 and 156 measurements for *cumyl*-5F-P7AICA and NPA, respectively.

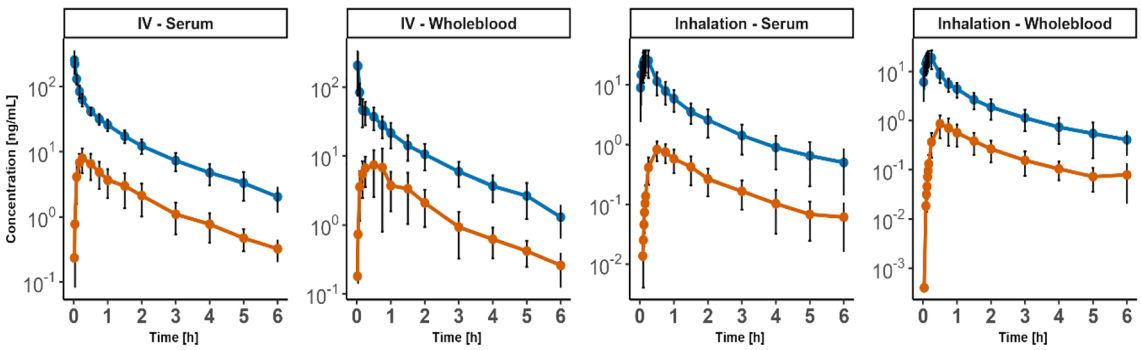

Fig. 2 Mean serum and whole blood concentration–time profiles of *cumyl*-5F-P7AICA (blue lines) and its *N*-pentanoic acid metabolite (orange lines). Whiskers indicate standard deviations (color figure online)

After i.v. administration of a 200 µg/kg BW dose of *cumyl*-5F-P7AICA, the maximum concentration (C_{max}) of the parent substance in serum samples was found immediately after administration (t_{max} = 1 min) with 260 ± 99 ng/mL (mean ± SD; Fig. 2). Following, the concentrations declined rapidly to approximately 25 ± 5.1 ng/mL after 60 min. Afterwards, concentrations decreased slowly until the end of the experiment at 360 min. At this point of time, lowest concentrations (C_{last}) were observed with 2.0 ± 0.87 ng/mL in serum specimens. Concerning the NPA metabolite, following a continuous increase, C_{max} was reached 15 to 30 min after administration with concentrations of 7.9 ± 3.2 ng/mL in serum. Afterwards, concentrations declined again to C_{last} of 0.32 ± 0.12 ng/mL in serum samples at 360 min.

On the other hand, after inhalative administration of the same dosage of *cumyl*-5F-P7AICA, C_{max} of 28 ± 11 ng/mL was reached after 10 min (t_{max}) in serum samples (Fig. 2). Afterwards, concentrations fell rapidly to a mean concentration of 5.8 ± 2.3 ng/mL after 60 min. Subsequently, concentrations continued to decline, albeit to a lesser extent as after 360 min C_{last} was found to be 0.5 ± 0.36 ng/mL in serum. Regarding the NPA metabolite, maximum concentrations of 0.83 ± 0.30 ng/mL were reached in serum samples 30–50 min after drug administration (t_{max}), declining to final concentrations at t = 360 min of 0.060 ± 0.050 ng/.

Figure 2 presents the mean concentration–time profiles after i.v. and pulmonary administration, which shows a three-phasic course for the parent, consisting of a tissue distribution (α) phase, with following elimination (β) phase, passing into a tissue release (γ) phase, and a two-phasic course for the metabolite.

The NCA revealed a half-life ($t_{1/2}$) of 1.9 ± 0.52 h in serum for *cumyl*-5F-P7AICA after i.v. application. After inhalation, $t_{1/2}$ amounted to 1.7 ± 0.36 h in serum. Bioavailability (F) in serum was 17 ± 13%.

For the NPA metabolite, $t_{1/2}$ after i.v. administration was 1.4 ± 0.36 h and 1.7 ± 0.59 h after pulmonary administration for serum. All TK parameters obtained from the NCA are summarized in Table 1.

PopTK model

A popTK model was developed to examine serum concentration–time profiles of *cumyl*-5F-P7AICA and its NPA

Table 1 Non-compartmental analysis summary

Parameter	Serum		Whole blood	
	I.V.	Inhalation	I.V.	Inhalation
	n = 6	n = 10	n = 6	n = 10
Body weight [kg]	51 ± 4.9	52 ± 6.3	51 ± 4.9	52 ± 6.3
***Cumyl*-5F-P7AICA**				
AUC_{last} [ng h/mL/kg]	99 ± 16	22 ± 10	75 ± 18	15 ± 5.8
AUC_{inf} [ng h/mL/kg]	104 ± 21	20 ± 9.0	80 ± 20	16 ± 6.2
C_{max} [ng/mL]	242 ± 90	26 ± 11	199 ± 137	20 ± 7.6
CL/F[a] [L/min/kg]	0.030 ± 0.010	0.16 ± 0.060	0.040 ± 0.010	0.21 ± 0.070
V_z/F[a] [L/kg]	5.0 ± 1.2	23 ± 8.2	65 ± 4.2	33 ± 19
V_{ss}/F[a][L/kg]	3.2 ± 0.60	14 ± 5.2	3.9 ± 1.1	20 ± 8.6
$t_{1/2}$ [h]	1.9 ± 0.52	1.7 ± 0.36	1.6 ± 0.70	2.0 ± 0.93
t_{max} [h]	0.020 ± 0.010	0.17 ± 0.040	0.030 ± 0.010	0.18 ± 0.040
F [%]	–	17 ± 13	–	21 ± 8.0
NPA metabolite				
AUC_{last} [ng h/mL/kg]	10 ± 4.7	1.3 ± 0.64	10 ± 5.5	1.3 ± 0.62
AUC_{inf} [ng h/mL/kg]	12 ± 4.5	1.5 ± 0.70	11 ± 5.5	1.5 ± 0.73
C_{max} [ng/mL]	7.9 ± 3.2	0.83 ± 0.30	8.8 ± 5.0	0.80 ± 0.44
CL/F[a] [L/min/kg]	0.31 ± 0.16	2.3 ± 1.5	0.31 ± 0.20	2.5 ± 1.5
V_z/F[a] [L/kg]	37 ± 31	310 ± 249	36 ± 35	351 ± 235
V_{ss}/F[a] [L/kg]	34 ± 21	329 ± 246	33 ± 25	370 ± 306
$t_{1/2}$ [h]	1.4 ± 0.36	1.7 ± 0.59	1.4 ± 0.38	1.8 ± 0.34
t_{max} [h]	0.25 ± 0.00	0.84 ± 0.30	0.56 ± 0.52	0.53 ± 0.11

AUC_{last} area under the curve calculated from zero to last observation, *AUC_{inf}* area under the curve from zero to infinity, *CL* clearance, *C_{max}* maximum observed concentration, *F* bioavailability, *n* number of animals, *$t_{1/2}$* elimination half-life; results are presented as mean (± standard deviation)

[a]Apparent clearance and apparent volume of distributions (CL/F, V_z/F, V_{ss}/F) for parameters derived after inhalation

metabolite following pulmonary or i.v. application. The modeling analysis revealed that a three-compartment model with linear clearance provided the best description of the serum concentration–time profiles of *cumyl*-5F-P7AICA, while a two-compartment model was optimal for describing the profiles of the NPA metabolite. For pulmonary application, the dose was administered as a bolus to an absorption compartment, which was emptied after the individually recorded inhalation duration. The bioavailability was estimated to be 48%. However, considering the emptying of the inhalation compartment, the actual bioavailable fraction is lower.

Due to insufficient knowledge regarding the fraction of the parent metabolized to NPA, it was not possible to simultaneously determine the fraction of the parent metabolized to NPA and the volume of distribution of NPA. Consequently, the central volume of distribution of NPA (VM) was fixed to that of *cumyl*-5F-P7AICA (V). The clearance rate to the metabolite NPA was expressed as a fraction of the total clearance rate. With these assumptions, the fraction metabolized to NPA after i.v. and inhalative administration revealed 24 vs. 12%, respectively. Transit compartments were incorporated to account for the delay between the appearance of *cumyl*-5F-P7AICA and NPA in serum. Here, one transit compartment sufficed to describe the data after i.v. administration whereas two compartments were required after pulmonary application, resulting in mean transit times of 6.4 and 12 min after i.v. and pulmonary application, respectively. A schematical representation of the model can be found in Fig. SI 1.

Model parameters were estimated with sufficient precision (RSE < 45.9%). IIV was observed in various parameters, comprising the bioavailable fraction after inhalation (F), *cumyl*-5F-P7AICA clearance (CL), the fraction metabolized to NPA (f_{MET}), the transit rate (ktr), the central volume of distribution (V) and intercompartmental clearances of *cumyl*-5F-P7AICA and NPA (Q1, Q2, QM). All parameter estimates can be found in Table 2. The associated differential equations can be found in the SI.

Goodness-of-fit plots (Fig. SI 2) demonstrate a good agreement between observed data and model predictions, while VPCs (Fig. 3) confirm the model's descriptive performance for both application forms without bias and with appropriate variability. Observed and predicted individual serum concentration–time profiles further illustrate the accurate depiction of observed concentrations (Fig. SI 3).

Prediction of human exposure

The human exposure to *cumyl*-5F-P7AICA and its NPA metabolite was predicted based on the popTK model developed for pigs using allometric scaling for BW. Figure 4 depicts serum concentration–time profiles for a 70 kg human after the i.v. application and inhalation of 0.5, 2 and 14 mg *cumyl*-5F-P7AICA as a single dose and 2 mg as a multiple dose every 60 min. Inhalation duration was set to 10 min.

Discussion

Dosage

In the present TK study, a dose of 200 µg/kg BW *cumyl*-5F-P7AICA was given i.v. or inhalatively to the animals. Depending on the respective BW of the pigs, the administered dose resulted in a total administered quantity of 8.8–12.8 mg *cumyl*-5F-P7AICA. This dosage was chosen based on previous TK studies demonstrating that a 200 µg/kg BW dose of *cumyl*-5F-P7AICA as well as other various SCs is well tolerated by pigs (Schaefer et al. 2016, 2018; Walle et al. 2021; Doerr et al. 2021). Additionally, 200 µg/kg BW is within the range of SC doses suggested by drug users in drug fora (Eve & Rave 2012). Thus, the dose administered in the present work reflects an authentic setting.

Concentration–time profiles of *cumyl*-5F-P7AICA and its NPA metabolite

After i.v. administration, substantially higher concentrations of *cumyl*-5F-P7AICA as well as its NPA metabolite were detected compared to inhalative administration. As anticipated, C_{max} of the parent compound was observed immediately following i.v. administration, whereas with inhalative administration C_{max} was reached after a 10 min delay. The bioavailable fraction after inhalative administration obtained from the NCA amounted to 17 and 21% based on serum and whole blood data, respectively. A number of reasons are responsible for this low estimation: For one, an in vitro drug delivery efficiency test revealed that only 74 ± 10% of the nebulized SC dose reaches the lungs. Furthermore, several 'lung defense mechanisms', such as mechanical or chemical barriers (e.g. surfactant, proteolytic enzymes), as well as a pulmonary first-pass effect and metabolism of the inhaled substances can occur (Bend et al. 1985; Bakhle 1990; Boer 2003; Newman 2017).

The obtained serum concentration–time profiles as well as the TK properties of *cumyl*-5F-P7AICA are similar to other SCs after i.v. or inhalative administration of JWH-210 and RCS-4 to pigs (Schaefer et al. 2016, 2018). C_{max} (260 ± 99 ng/mL) and C_{last} (0.32 ± 0.12 ng/mL) obtained in the present work for *cumyl*-5F-P7AICA were slightly lower compared with RCS-4 (316 ± 60 ng/mL (C_{max}) and 3.8 ± 1.1 ng/mL (C_{last})) after i.v. administration (Schaefer et al. 2016). For JWH-210, substantial higher C_{max} values (1600 ± 362 ng/mL) were determined after i.v. administration (Schaefer et al. 2016). After inhalative administration of

Table 2 Model parameter estimates

Parameter	Description	Unit	Estimate	RSE
***cumyl*-5F-P7AICA**				
Ka	First-order absorption rate from lung compartment	min^{-1}	0.051	19%
F	Bioavailable fraction after inhalation	–	0.48	16%
CL	Clearance from central compartment	$L/min/kg^{0.75}$	0.092	6.9%
V	Volume of the central compartment	$L/kg^{0.75}$	1.5	16%
V_{P1}	Volume of the peripheral compartment	$L/kg^{0.75}$	4.4	5.8%
Q1	Intercompartmental clearance	$L/min/kg^{0.75}$	0.030	16%
V_{P2}	Volume of the peripheral compartment	$L/kg^{0.75}$	3.3	4.5%
Q2	Intercompartmental clearance	$L/min/kg^{0.75}$	0.21	18%
V_{ss}	Volume of distribution at steady-state	$L/kg^{0.75}$	9.2	
$t_{1/2\alpha}$	Elimination half-life during the alpha phase	min	2.6	–
$t_{1/2\beta}$	Elimination half-life during the beta phase	min	32	–
$t_{1/2\gamma}$	Elimination half-life during the gamma phase	min	146	–
IIV F	Interindividual variability F	%CV	64	36%
IIV CL	Interindividual variability CL	%CV	24	18%
IIV V	Interindividual variability V	%CV	60	17%
IIV Q1	Interindividual variability Q1	%CV	49	12%
IIV V2	Interindividual variability V2	%CV	69	19%
PRE	Proportional residual error	%	9.0	9.2%
ARE	Additive residual error (fixed)	ng/mL	0.010	–
***N*-pentanoic acid metabolite**				
f_{MET}	Fraction metabolized from cumyl-5F-P7AICA to NPA	–	0.24	24%
f_{APP}	Fractional change of f_{MET} for pulmonary application	–	−0.48	22%
ktr	Transit rate between cumyl-5F-P7AICA and NPA	min^{-1}	0.15	20%
CL_M	Clearance from central compartment	$L/min/kg^{0.75}$	0.18	19%
V_{PM}	Volume of the peripheral compartment	$L/kg^{0.75}$	8.2	27%
QM	Intercompartmental clearance	$L/min/kg^{0.75}$	0.024	45%
IIV f_{MET}	Interindividual variability f_{MET}	%CV	43	12%
IIV ktr	Interindividual variability ktr	%CV	66	18%
IIV QM	Interindividual variability QM	%CV	126	25%
PRE	Proportional residual error	%	18	12%
ARE	Additive residual error (fixed)	ng/mL	0.010	–

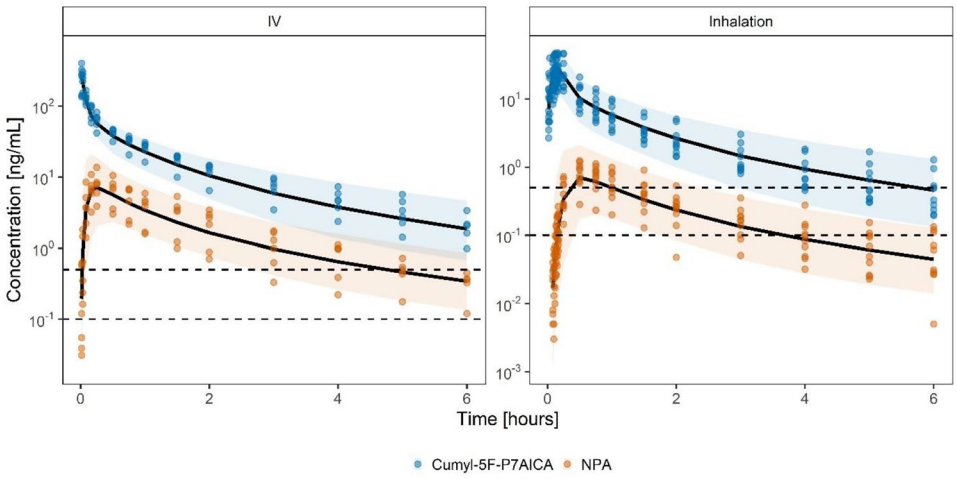

Fig. 3 Visual predictive checks (VPCs) stratified by analyte and application. Observed serum concentrations are represented as circles. Lines represent the simulation median. Bands represent the simulated 90% prediction intervals. Dashed lines represent the LLOQ

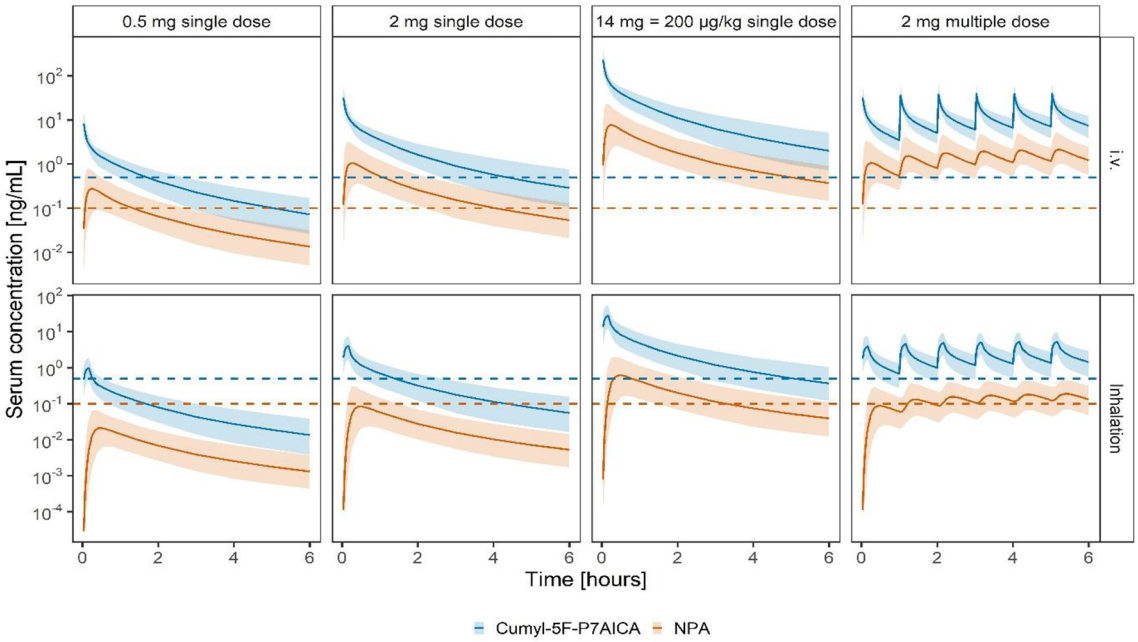

Fig. 4 Prediction of human serum concentration–time profiles after i.v. application and inhalation of various doses. Full lines represent the simulation median. Bands represent the simulated 90% prediction intervals. Dashed lines represent the LLOQ

200 µg/kg BW of JWH-210 and RCS-4 to pigs, mean C_{max} values of 34–66 ng/mL 10–15 (t_{max}) after start of nebulization were reported (Schaefer et al. 2018). Furthermore, 8 h after substance administration, mean concentrations of 0.87–1.5 ng/mL of the investigated parent substances were determined. Regarding the metabolites, Schaefer et al. reported on a C_{max} range between < 1.0–11 ng/mL with t_{max} between 5–60 min depending on the respective metabolite after inhalative administration (Schaefer et al. 2018). The data obtained in the current study for *cumyl*-5F-P7AICA and the NPA metabolite is in a good agreement with these values, with 28 ± 11 ng/mL and 0.83 ± 0.30 ng/mL (C_{max}) 10 min and 30–50 min (t_{max}) after drug administration as well as C_{last} values of 0.5 ± 0.36 ng/mL and 0.060 ± 0.050 ng/mL, respectively. Nevertheless, C_{last} of *cumyl*-5F-P7AICA in serum is considerably lower than those of JWH-210 and RCS-4 suggesting a faster in vivo elimination. In comparison, the C_{max} and t_{max} values of the NPA metabolite are in the same range as those reported by Schaefer et al. (Schaefer et al. 2018) for the metabolites of JWH-210 and RCS-4.

In addition, Doerr et al. recently reported on the TK properties of the SC 5F-MDMB-P7AICA after inhalative administration using the pig model (Doerr et al. 2024a). This substance also represents a structurally modified SC, containing a carboxamide moiety in the linker as well as an ester moiety in the bridge residue (Doerr et al. 2024a). Additionally, an NCA as well as a popTK analysis were performed for 5F-MDMB-P7AICA analogously to the present study. A similar serum concentration–time course was found for 5F-MDMB-P7AICA compared to the data obtained for *cumyl*-5F-P7AICA, with C_{max} values of 63 ± 18 ng/mL 6–10 min after start of nebulization. Additionally, a transit compartment was included for 5F-MDMB-P7AICA after inhalative administration in analogy to the present study. Taken together, the TK properties of structurally modified SCs with a carboxamide moiety appear to be very similar. However, in contrast to *cumyl*-5F-P7AICA, a four-compartment model describes the data for 5F-MDMB-P7AICA best.

Only limited data on fatal and non-fatal human intoxications involving the SC *cumyl*-5F-P7AICA have already been reported (Halter et al. 2019; Kleis et al. 2020; Zawadzki et al. 2021). These cases have in common that additional SCs or exogenous substances were found besides *cumyl*-5F-P7AICA. This finding could at least in parts be anticipated due to the manufacturing process of such herbal mixtures, which often contain various different SCs in one package. Consequently, the specific SC composition and quantity remain unknown for the consumer potentially leading to mixed intoxications. Halter et al. published data on several intoxications primarily associated with the consumption of the SC *cumyl*-PEGACLONE (Halter et al. 2019). In three cases, *cumyl*-5F-P7AICA was additionally detected with concentrations of 2.5 ng/mL and approximately 0.03 ng/mL in serum, as well as 0.23 ng/mL in femoral blood. Furthermore, a series of several (fatal) intoxications after consumption of the SC 5F-MDMB-PICA included one fatality related to a combination of various other SCs and *cumyl*-5F-P7AICA with < 0.1 ng/mL of *cumyl*-5F-P7AICA

detected in femoral blood (Kleis et al. 2020). To date, only one fatal mono intoxication with *cumyl*-5F-P7AICA has been reported (Zawadzki et al. 2021). Upon the toxicological examination, 2.8 and 3.1 ng/mL of *cumyl*-5F-P7AICA were found in blood and urine specimens, respectively. Taken together, the data already published up to now correspond well with the data obtained in the current TK study, suggesting in non-fatal intoxications that *cumyl*-5F-P7AICA had been consumed a considerable time before blood sampling. However, several issues must be taken into account. For one, the ingested dose of *cumyl*-5F-P7AICA remains unclear in these cases and a more recent consumption of a lower dose might also be conceivable. Furthermore, the route of consumption (inhalative vs. oral) must be taken into account, resulting in possibly lower substance concentration in vivo. As SCs are commonly smoked by consumers in the form of a joint, a heat-related pyrolytic degradation must be considered, as already reported for other SCs (Kaizaki-Mitsumoto et al. 2017; Franz et al. 2017). Whilst *cumyl*-5F-P7AICA was administered without any heat treatment inhalatively to pigs in the present study, a possible heat-related pyrolytic degradation might have led to lower serum concentrations in the context of human (fatal) intoxications. Regarding *cumyl*-5F-P7AICA, respective data are lacking. Nevertheless, this mechanism should be kept in mind when interpreting toxicological findings. On the other hand, some blood specimens were collected postmortem. In cases of a prolonged agony, further metabolism of the consumed substance might have occurred, leading to lower substance levels at the time of death as compared to C_{max}. Finally, the postmortem interval is often unknown and a possible instability of *cumyl*-5F-P7AICA must be considered. Therefore, interpretation of such postmortem analytical results using the TK data obtained in the present study should be regarded with caution.

Population TK model

A TK model was developed describing *cumyl*-5F-P7AICA and its metabolite NPA. Overall, parameters derived from the modeling analysis (Table 2) are comparable with those previously identified for JWH-210 and RCS-4 (Schaefer et al. 2016, 2018). Regarding the volume of distribution (V_{ss}) calculated in the present study for *cumyl*-5F-P7AICA (9.2 L/kg$^{0.75}$), similar values were reported by Schaefer et al. for JWH-210 and RCS-4 (4.91 and 15.97 L/kg$^{0.75}$, respectively). Comparison of these results shows that V_{ss} of *cumyl*-5F-P7AICA lay between the values of JWH-210 and RCS-4 and therefore correspond very well with those of the 'older' SCs. Furthermore, the calculated half-lifes of 2.6 min ($t_{1/2\alpha}$), 32 min ($t_{1/2\beta}$), and 146 min ($t_{1/2\gamma}$) for *cumyl*-5F-P7AICA are also in agreement with those reported for JWH-210 and RCS-4 ($t_{1/2\alpha}$: 1.2 and 1.8 min, $t_{1/2\beta}$: 8.9 and 11.3 min, $t_{1/2\gamma}$: 160 and 162 min, respectively). This finding indicates that in vivo, no relevant cleavage of the incorporated carboxamide moiety in the chemical structure of *cumyl*-5F-P7AICA occurs. This is also consistent with the in vitro results reported by Wagmann et al. studying the stability of various SCs using human carboxylesterases (Wagmann et al. 2022). Furthermore, this finding is also consistent with a previous controlled in vivo pig study of the authors. In this study, no metabolite with a cleaved carboxamide moiety was detected in pig urine specimens (Walle et al. 2021).

Interestingly, to accurately describe the concentration of the NPA metabolite, transit compartments were necessary to account for the delay between the appearance of *cumyl*-5F-P7AICA and NPA in serum. Such a delay is typically not reported in TK modeling analyses involving metabolites. However, the formation of NPA from *cumyl*-5F-P7AICA requires several intermediate metabolism stages (Walle et al. 2021), which potentially explains its delayed appearance. Additionally, the sampling schedule of metabolites in TK studies is usually not as dense within the first min after dose administration as in our study. This might have prevented other analyses from identifying the time frame of metabolite formation within the first min. Interestingly, this delay differed between inhalative and i.v. application and amounted to 12 and 6.4 min. Additionally, the fraction metabolized differed with 12 and 24%, following inhalative and i.v. application, respectively. However, the origin of these differences remains unknown.

To sum up, the TK data obtained in the current study are in a rather good agreement with those reported in literature for several (fatal) intoxications. In comparison to the TK properties of JWH-210 and RCS-4, no substantial differences were detected for *cumyl*-5F-P7AICA. Therefore, structural modifications of SCs with the incorporation of a carboxamide moiety as a linker between the core structure and the bridge residue do not appear to have a relevant influence on the TK properties.

Conclusion

Based on concentration–time profiles of *cumyl*-5F-P7AICA and its NPA metabolite in pig serum, a popTK model was successfully developed. A three-compartment model with linear clearance describes best the pig serum concentration–time profiles of *cumyl*-5F-P7AICA, while a two-compartment model was better for the NPA metabolite. Following, the final popTK model was used for prediction of the human exposure of *cumyl*-5F-P7AICA and its NPA metabolite by allometric scaling. Compared to 'older' SCs (e.g. RCS-4 and JWH-210), which do not contain a carboxamide moiety, similar TK data were determined for *cumyl*-5F-P7AICA in the present study. Therefore, the incorporation of

a carboxamide moiety as a linker is a modification in the chemical structure of SCs that does not result in any relevant changes in the TK properties.

Supplementary Information The online version contains supplementary material available at https://doi.org/10.1007/s00204-024-03906-z.

Acknowledgements The authors would like to thank the Institute for Clinical & Experimental Surgery at Saarland University for their support and help during the study. We acknowledge the EU funded project ADEBAR (IZ25-5793-2016-27).

Funding Open Access funding enabled and organized by Projekt DEAL. This work was supported by the Deutsche Forschungsgemeinschaft (DFG, German Research Foundation, Grant number 508380150).

Data availability All data generated or analyzed during this study are included in this published article and its supplementary information files.

Declarations

Conflict of interest There are no financial or other relations that could lead to a conflict of interest.

Ethical approval All experiments were performed in accordance with the German legislation on protection of animals and the National Institutes of Health Guide for the Care and Use of Laboratory Animals (permission number: 44/2019).

References

Anzenbacher P, Soucek P, Anzenbacherová E et al (1998) Presence and activity of cytochrome P450 isoforms in minipig liver microsomes. Comparison with human liver samples. Drug Metab Dispos 26(1):56–59

Bakhle YS (1990) Pharmacokinetic and metabolic properties of lung. Br J Anaesth 65(1):79–93. https://doi.org/10.1093/bja/65.1.79

Banister SD, Adams A, Kevin RC et al (2019) Synthesis and pharmacology of new psychoactive substance 5F-CUMYL-P7AICA, a scaffold-hopping analog of synthetic cannabinoid receptor agonists 5F-CUMYL-PICA and 5F-CUMYL-PINACA. Drug Test Anal 11(2):279–291. https://doi.org/10.1002/dta.2491

Bend JR, Serabjit-Singh CJ, Philpot RM (1985) The pulmonary uptake, accumulation, and metabolism of xenobiotics. Annu Rev Pharmacol Toxicol 25:97–125. https://doi.org/10.1146/annurev.pa.25.040185.000525

Boer F (2003) Drug handling by the lungs. Br J Anaesth 91(1):50–60. https://doi.org/10.1093/bja/aeg117

Castaneto MS, Wohlfarth A, Desrosiers NA et al (2015) Synthetic cannabinoids pharmacokinetics and detection methods in biological matrices. Drug Metab Rev 47(2):124–174. https://doi.org/10.3109/03602532.2015.1029635

de Oliveira MC, Vides MC, Lassi DLS et al (2023) Toxicity of synthetic cannabinoids in K2/Spice: a systematic review. Brain Sci 13(7):990. https://doi.org/10.3390/brainsci13070990

Denney W, Duvvuri S, Buckeridge C (2015) Simple, automatic noncompartmental analysis: the PKNCA R package. J Pharmacokinet Pharmacodyn 42:S65–S65

Di L (2018) The impact of carboxylesterases in drug metabolism and pharmacokinetics. Curr Drug Metab 20(2):91–102. https://doi.org/10.2174/1389200219666180821094502

Doerr AA, Nordmeier F, Walle N et al (2021) Can a recently developed pig model be used for in vivo metabolism studies of 7-azaindole-derived synthetic cannabinoids? A study using 5F-MDMB-P7AICA. J Anal Toxicol 45(6):593–604. https://doi.org/10.1093/jat/bkaa122

Doerr AA, Dings C, Zaher O et al (2024a) Toxicokinetic modelling of the synthetic cannabinoid 5F-MDMB-P7AICA and its main metabolite in pigs following pulmonary administration. Br J Clin Pharmacol. (**submitted**)

Doerr AA, Nordmeier F, Walle N et al (2024b) Does a postmortem redistribution affect the concentrations of the 7 azaindole-derived synthetic cannabinoid 5F-MDMB-P7AICA in tissues and body fluids following pulmonary administration to pigs? Arch Toxicol 98(10):3289–3298. https://doi.org/10.1007/s00204-024-03815-1

Elliott S, Evans J (2014) A 3-year review of new psychoactive substances in casework. Forensic Sci Int 243:55–60. https://doi.org/10.1016/j.forsciint.2014.04.017

European Monitoring Centre for Drugs and Drug Addiction (EMCDDA)-Europol 2015 (2016) Annual report on the implementation of council decision 2005/387/JHA. http://www.emcdda.europa.eu/system/files/publications/2880/TDAS16001ENN.pdf. 13 Oktober 2024.

Eve & Rave (2012) The Swiss drug forum. https://www.eve-rave.ch/Forum/viewtopic.php?t=28044. Accessed 13 Oktober 2024

Ferrari Júnior E, Leite BHM, Gomes EB et al (2022) Fatal cases involving new psychoactive substances and trends in analytical techniques. Front Toxicol 25(4):1033733. https://doi.org/10.3389/ftox.2022.1033733

Franz F, Angerer V, Brandt SD et al (2017) In vitro metabolism of the synthetic cannabinoid 3,5-AB-CHMFUPPYCA and its 5,3-regioisomer and investigation of their thermal stability. Drug Test Anal 9(2):311–316. https://doi.org/10.1002/dta.1950

Giorgetti A, Busardò FP, Tittarelli R et al (2020) Post-mortem toxicology: a systematic review of death cases involving synthetic cannabinoid receptor agonists. Front Psychiatry 11:464. https://doi.org/10.3389/fpsyt.2020.00464

Guirguis A (2017) New psychoactive substances: a public health issue. Int J Pharm Pract 25(5):323–325. https://doi.org/10.1111/ijpp.12313

Halter S, Angerer V, Röhrich J et al (2019) Cumyl-PEGACLONE: a comparatively safe new synthetic cannabinoid receptor agonist entering the NPS market? Drug Test Anal 11(2):347–349. https://doi.org/10.1002/dta.2545

Hermanns-Clausen M, Kneisel S, Hutter M et al (2013) Acute intoxication by synthetic cannabinoids—four case reports. Drug Test Anal 5(9–10):790–794. https://doi.org/10.1002/dta.1483

Houston ML, Morgan J, Kelso C (2023) Narrative review of the pharmacodynamics, pharmacokinetics, and toxicities of illicit synthetic cannabinoid receptor agonists. Mini Rev Med Chem

24(1):92–109. https://doi.org/10.2174/1389557523666230515163107
Kaizaki-Mitsumoto A, Hataoka K (2017) Funada M et al Pyrolysis of UR-144, a synthetic cannabinoid, augments an affinity to human CB 1 receptor and cannabimimetic effects in mice. J Toxicol Sci 42(3):335–341. https://doi.org/10.2131/jts.42.335
Karlsson MO, Savic RM (2007) Diagnosing model diagnostics. Clin Pharmacol Ther 82(1):17–20. https://doi.org/10.1038/sj.clpt.6100241
Kleis J, Germerott T, Halter S et al (2020) The synthetic cannabinoid 5F-MDMB-PICA: a case series. Forensic Sci Int 314:110410. https://doi.org/10.1016/j.forsciint.2020.110410
Kraemer M, Boehmer A, Madea B, Maas A (2019) Death cases involving certain new psychoactive substances: a review of the literature. Forensic Sci Int 298:186–267. https://doi.org/10.1016/j.forsciint.2019.02.021
Meurens F, Summerfield A, Nauwynck H et al (2012) The pig: a model for human infectious diseases. Trends Microbiol 20(1):50–57. https://doi.org/10.1016/j.tim.2011.11.002
Meyer MR (2016) New psychoactive substances: an overview on recent publications on their toxicodynamics and toxicokinetics. Arch Toxicol 90(10):2421–2444. https://doi.org/10.1007/s00204-016-1812-x
Newman SP (2017) Drug delivery to the lungs: challenges and opportunities. Ther Deliv 8(8):647–661. https://doi.org/10.4155/tde-2017-0037
Nordmeier F, Sihinevich I, Doerr AA et al (2021) Toxicokinetics of U-47700, tramadol, and their main metabolites in pigs following intravenous administration: is a multiple species allometric scaling approach useful for the extrapolation of toxicokinetic parameters to humans? Arch Toxicol 95(12):3681–3693. https://doi.org/10.1007/s00204-021-03169-y
Nordmeier F, Doerr AA, Potente S et al (2022a) Perimortem distribution of U-47700, tramadol and their main metabolites in pigs following intravenous administration. J Anal Toxicol 46(5):479–486. https://doi.org/10.1093/jat/bkab044
Nordmeier F, Doerr AA, Potente S et al (2022b) Are the (new) synthetic Opioids U-47700, tramadol and their main metabolites prone to time-dependent postmortem redistribution?—a systematic study using an in vivo pig model. J Anal Toxicol 47(3):236–244. https://doi.org/10.1093/jat/bkac082
Oberhofer E (2018) Toedlicher Rauch aus der Eimer-Bong. MMW Fortschr Med 160(17):14. https://doi.org/10.1007/s15006-018-0960-8
Schaefer N, Kettner M, Laschke MW et al (2015) Simultaneous LC–MS/MS determination of JWH-210, RCS-4, Δ9-tetrahydrocannabinol, and their main metabolites in pig and human serum, whole blood, and urine for comparing pharmacokinetic data. Anal Bioanal Chem 407(13):3775–3786. https://doi.org/10.1007/s00216-015-8605-6
Schaefer N, Wojtyniak J-G, Kettner M et al (2016) Pharmacokinetics of (synthetic) cannabinoids in pigs and their relevance for clinical and forensic toxicology. Toxicol Lett 253:7–16. https://doi.org/10.1016/j.toxlet.2016.04.021
Schaefer N, Helfer AG, Kettner M et al (2017a) Metabolic patterns of JWH-210, RCS-4, and THC in pig urine elucidated using LC-HR-MS/MS: do they reflect patterns in humans? Drug Test Anal 9(4):613–625. https://doi.org/10.1002/dta.1995
Schaefer N, Kettner M, Laschke MW et al (2017b) Distribution of synthetic cannabinoids JWH-210, RCS-4 and Δ 9-tetrahydrocannabinol after intravenous administration to pigs. Curr Neuropharmacol 15(5):713–723. https://doi.org/10.2174/1570159X15666161111114214
Schaefer N, Wojtyniak J-G, Kroell AK et al (2018) Can toxicokinetics of (synthetic) cannabinoids in pigs after pulmonary administration be upscaled to humans by allometric techniques? Biochem Pharmacol 155:403–418. https://doi.org/10.1016/j.bcp.2018.07.029
Schaefer N, Kroell AK, Koerbel C et al (2019) Distribution of the (synthetic) cannabinoids JWH-210, RCS-4, as well as Δ9-tetrahydrocannabinol following pulmonary administration to pigs. Arch Toxicol 93(8):2211–2218. https://doi.org/10.1007/s00204-019-02493-8
Schaefer N, Kroell AK, Koerbel C et al (2020) Time- and temperature-dependent postmortem concentration changes of the (synthetic) cannabinoids JWH-210, RCS-4, as well as Δ9-tetrahydrocannabinol following pulmonary administration to pigs. Arch Toxicol 94(5):1585–1599. https://doi.org/10.1007/s00204-020-02707-4
Shafi A, Berry AJ, Sumnall H et al (2020) New psychoactive substances: a review and updates. Ther Adv Psychopharmacol 10:2045125320967197. https://doi.org/10.1177/2045125320967197
Soucek P, Zuber R, Anzenbacherová E et al (2001) Minipig cytochrome P450 3A, 2A and 2C enzymes have similar properties to human analogs. BMC Pharmacol 1:11. https://doi.org/10.1186/1471-2210-1-11
Swindle MM, Makin A, Herron AJ et al (2012) Swine as models in biomedical research and toxicology testing. Vet Pathol 49(2):344–356. https://doi.org/10.1177/0300985811402846
Upton RN, Mould DR (2014) Basic concepts in population modeling, simulation, and model-based drug development: Part 3—introduction to pharmacodynamic modeling methods. CPT Pharmacometr Syst Pharmacol 3(1):e88. https://doi.org/10.1038/psp.2013.71
Wagmann L, Stiller RG, Fischmann S et al (2022) Going deeper into the toxicokinetics of synthetic cannabinoids: in vitro contribution of human carboxylesterases. Arch Toxicol 96(10):2755–2766. https://doi.org/10.1007/s00204-022-03332-z
Walle N, Nordmeier F, Doerr AA et al (2021) Comparison of in vitro and in vivo models for the elucidation of metabolic patterns of 7-azaindole-derived synthetic cannabinoids exemplified using *cumyl*-5F-P7AICA. Drug Test Anal 13(1):74–90. https://doi.org/10.1002/dta.2899
Walle N, Doerr AA, Schmidt PH, Schaefer N (2023) 'Flying high?'—jump from a height in a "Spice" high?: a case report on the synthetic cannabinoid 5F-MDMB-P7AICA. Drug Test Anal 15(3):368–373. https://doi.org/10.1002/dta.3401
Walle N, Doerr AA, Peters B et al (2024) Are the postmortem concentration changes of the synthetic cannabinoid cumyl-5F-P7AICA and its *N*-pentanoic acid metabolite dependent on the environmental conditions?—a systematic study following pulmonary administration to pigs. Toxicol Lett. https://doi.org/10.1016/j.toxlet.2024.10.006
Zawadzki M, Chłopaś-Konowałek A, Nowak K et al (2021) Quantification of 5F-CUMYL-P7AICA in blood and urine from an authentic fatality associated with its consumption by UHPLC–MS/MS. Forensic Toxicol 39:240–247. https://doi.org/10.1007/s11419-020-00555-6

Archives of Toxicology

Supplementary Information

Does a carboxamide moiety alter the toxicokinetics of synthetic cannabinoids? - A study after pulmonary administration of cumyl-5F-P7AICA to pigs

Nadja Walle[1], Christiane Dings[2], Omar Zaher[2], Adrian A. Doerr[1], Benjamin Peters[1], Matthias W. Laschke[3], Thorsten Lehr[2], Michael D. Menger[3], Peter H. Schmidt[1], Markus R. Meyer[4] and Nadine Schaefer[1*]

---

[*]Correspondence to: Nadine Schaefer, Institute of Legal Medicine, Saarland University, Building 49.1, 66421 Homburg, Germany

Email: nadine.schaefer@uks.eu

[1]Institute of Legal Medicine, Saarland University, Building 49.1, 66421 Homburg, Germany

[2]Department of Clinical Pharmacy, Saarland University, Building C5 3, 66123 Saarbruecken, Germany

[3]Institute for Clinical & Experimental Surgery, Saarland University, Building 65/66, 66421 Homburg, Germany

[4]Department of Experimental and Clinical Toxicology, Center for Molecular Signaling (PZMS), Saarland University, Building 46, 66421 Homburg, Germany

Materials and methods

Chemicals and reagents

Ethylenediaminetetraacetic acid disodium salt (Na_2EDTA), glacial acetic acid, and di-potassium hydrogen phosphate were purchased by Merck (Darmstadt, Germany). Acetonitrile (Optima), formic acid (Optima), water (Optima), ethanol (HPLC grade), methanol (HPLC grade), and acetone p.a. were bought from Fisher Scientific (Loughborough, United Kingdom). For drug administration, *cumyl*-5F-P7AICA (purity 99.72 %; Fig. 1A) was offered by the German Federal Criminal Police Office (Wiesbaden, Germany). *Cumyl*-5F-P7AICA (1 mg, solid) for validation, its *N*-pentanoic acid metabolite (NPA; 1 mg; solid), 5F-MDMB-P7AICA (1 mg; solid), the standards RCS-4-d_9 (1 mg; solid) and AB-FUBINACA-d_4 (1 mg; solid), as well as AB-005, AB-FUBINACA, AM-694, AM-697, AM-1220, AM-1248, AM-2201, AM-2232, AM2233, EAM-2201, JWH-015, JWH-081, JWH-122, JWH182, JWH-200, JWH-203, JWH-210, JWH-250, MAM2201, 5F-MDMB-PINACA, PB-22, 5F-PB-22, Pravadoline, RCS-8, RCS-4, UR-144 and XLR-11 were obtained from Cayman Europe (Tallinn, Estonia). Additionally, Δ^9-tetrahydrocannabinol (THC), 11-hydroxy-THC (11-HO-THC), 11-nor-9-carboxy-THC (THC-COOH), cannabinol and cannabidiol were bought from Sigma-Aldrich (Munich, Germany), whilst JWH-018 was obtained by THC Pharm (Frankurt/Main, Germany).

Preparations

Buffer solution

Preparation of the phosphate buffer (0.1 M, pH 9) was performed in accordance to previous studies (Schaefer et al. 2015, 2017, 2019, 2020; Doerr et al. 2024b; Walle et al. 2024a). Analogously, 22.82 g di-potassium hydrogen phosphate was dissolved in 1 L HPLC grade water.

Blank whole blood and serum samples

For method validation as well as the preparation of calibration standards and quality control (QC) samples, blank whole blood specimens were obtained from drug free pigs (Swabian Hall strain, Emil Faerber GmbH & Co. KG, Zweibruecken, Germany), divided into two aliquots, and centrifuged at 1,476 x *g* for 15 min to obtain serum specimens, as already published in previous studies (Schaefer et

al. 2015; Nordmeier et al. 2021; Doerr et al. 2024a). To prevent coagulation, 1.64 mg/mL Na_2EDTA were added to the whole blood samples. Following, serum and whole blood specimens were stored at -20 °C.

Stock solutions, calibration standards, and QC samples

The solid substances *cumyl*-5F-P7AICA, its NPA metabolite, RCS-4-d_9, and AB-FUBINACA-d_4 were dissolved in ethanol to obtain standard stock solutions with conc. of 1000 µg/mL. Subsequently, the prepared standard stock solutions were dissolved with ethanol, to create working standard solutions containing 0.01 µg/mL, 0.1 µg/mL, 1 µg/mL, and 10 µg/mL of the respective substance. For preparation of the spiking solutions for calibration standards, the standard stock solutions were also diluted with ethanol, to receive final serum conc. of 0.1, 0.3, 0.5, 0.7, 0.9, and 1.1 ng/mL of the NPA metabolite and 0.5, 10, 20, 30, 40, and 50 ng/mL of *cumyl*-5F-P7AICA. The QC spiking solutions low and high, containing 0.2 ng/mL and 5 ng/mL or 0.8 ng/mL and 35 ng/mL of the NPA and *cumyl*-5F-P7AICA respectively, were prepared analogously. The prepared solutions were stored at – 20 °C.

In vitro drug delivery efficiency test

To assess the drug delivery efficiency of *cumyl*-5F-P7AICA after nebulization, an in vitro drug delivery efficiency test was performed in accordance to the setup already published by Schaefer et al. (Schaefer et al. 2018a) with a few modifications. In brief, 1 mL of a stock solution containing 0.5 mg/mL *cumyl*-5F-P7AICA was prepared by dissolving the solid substance in ethanol. Using the M-neb flow+ ventilation ultrasonic nebulizer MN-300/7 (Nebutec, Elsenfeld, Germany), the prepared solution was nebulized under ventilation applying the inspiration-triggered mode. The settings of the ventilation were in accordance to the in vivo pig studies (Schaefer et al. 2019; Walle et al. 2021; Doerr et al. 2021). After nebulization, the aerosol was transferred via the endotracheal tube, through a glass fiber filter (GFF) into a simulated pig lung (anesthesia bag). To ensure that only inhaled air and no exhaled breath can pass the GFF, two check valves have been installed in the experimental setup. The procedure was repeated six times. To assess the drug delivery efficiency, *cumyl*-5F-P7AICA was extracted from the components of the experimental setup in accordance to an already published study by Schaefer et al.

(Schaefer et al. 2018a), with slight modifications. Therefore, GFF were initially macerated by adding 5 mL acetone. The solution was ultrasonicated for 10 min and centrifuged at 2,898 x *g* for 8 min. Subsequently, the solution obtained was filtrated using chromafil filters (1.0 µm pore size, Macherey-Nagel, Düren, Germany). Afterwards, the solution was diluted 1:50 using ethanol in a first step. Secondly, the obtained dilution was further diluted 1:20 with a mixture (50:50, *v/v*) of mobile phases A (0.1% aqueous formic acid) and B (0.1% formic acid in acetonitrile). After the addition of 25 µL of a stable isotope-labeled internal standard (SIL-IS; AB-FUBINACA-d4, 50 ng/20 µL), 20 µL of the extracts were analysed by liquid chromatography (LC)-tandem mass spectrometry (MS). In order to calculate the drug delivery efficiency, the measured values were adjusted by the extraction efficiency of 90% using acetone as it was found in the context of another study (Walle et al. 2024b)

To determine the drug residues in the different experimental compounds, such as the endotracheal tube, the heat and moisture exchanger (HME) filter, the reservoir of the nebulizer, and the anesthesia bag, the respective part of the set up (n=6 each) was cut into pieces, mixed with ethanol, and macerated via ultrasonication for 10 min, respectively. As far as the reservoir of the nebulizer is concerned, the components (n=6) were only rinsed with ethanol. Subsequently, 20 or 25 µL of the SIL-IS (50 ng/25 µL for the reservoir of the nebulizer, and 5 ng/20 µL for the remaining components) and 25 µL of the respective solution were diluted 1:20 with a mixture (50:50, *v/v*) of mobile phases A and B. Following, 20 µL of the solutions were measured by LC-MS/MS.

The amount of the substance contained were determined by comparing the ratios with those of a reference solution measured at the same time.

In vivo study

Surgical procedures

The surgical procedures in the present work were in accordance to those already published in previous studies (Schaefer et al. 2019; Walle et al. 2021, 2024a; Doerr et al. 2021, 2024a, b; Nordmeier et al. 2022), with the modification, that 5 mg/kg body weight (BW) of carprofen (Rimadyl; Zoetis, Berlin, Germany) was additionally given to the pigs as a pain medication.

In brief, a mixed intramuscular injection of xylazine hydrochloride (2.5 mg/kg BW, Rompun®, Bayer, Leverkusen, Germany), ketamine hydrochloride (30 mg/kg BW, Ursotamin®; Serumwerke Bernburg, Bernburg, Germany), and atropine (1 mg, Braun, Melsungen, Germany) was administered to the animals for anesthetization. For sufficient fluid substitution (0.9% sodium chloride, 8 mL/kg/h, Braun, Melsungen, Germany), a 20G indwelling needle was inserted percutaneously in the left ear. The pigs were endotracheally intubated, mechanically ventilated with a volume-controlled ventilation with an oxygen and air mixture (1:2, *v/v*, FiO2 of 0.30, Respirator ABV-U; F. Stephan GmbH, Gackenbach, Germany) and a tidal volume of 10-12 mL/kg BW. Anesthesia was achieved by an inhalative administration of 2-4% isoflurane (Forene, AbbVie, Ludwigshafen, Germany). In addition, a triple-lumen 7F central venous catheter (Certofix Trio, Braun, Melsungen, Germany) was placed in the jugular vein for blood sampling, intravenous (i.v.) administration or monitoring of the mean central venous pressure. Additionally, a suprapubic bladder catheter (Cystofix, Braun, Melsungen, Germany) was placed in the bladder for continuous urine collection, and an arterial catheter (Leadercath Expert 14G, Vygon, Aachen, Germany) in the left formal artery for invasive blood pressure measurement. The animals were then allowed to stabilize for 10-15 min.

Sample preparation

For sample preparation, 500 µL serum or blood was added to 2.5 mL phosphate buffer (pH 9), 50 µL ethanol and 20 µL of the SIL-IS RCS-4-d_9 (1 ng/20 µL) and AB-FUBINACA-d_4 (0.25 ng/20 µL) each. After vortexing and centrifugation at 2,898 x *g* for 8 min, the solutions were loaded onto conditioned (2 x 3 mL methanol and 1 x 3 mL 0.1 M phosphate buffer pH 9) Strata C_{18} endcapped cartridges (200 mg/3 mL; Phenomenex LTD, Aschaffenburg, Germany) cartridges. After washing steps with 3 mL phosphate buffer, 3 mL acetic acid (0.25 M), and 3 mL water, 60 µL acetone were added and the cartridges were dried under a maximum vacuum of 10 inHg. Elution of the substances was carried out through the addition of 1.5 mL methanol-acetone (1:1, *v/v*) and the eluates were dried under a gentle stream of nitrogen at 60 °C. The dried residue was dissolved by adding 50 µL of a mixture (50:50, *v/v*) of mobile phases A and B. Afterwards, 5 µL were injected onto a LC quadrupole time-of-flight (TOF)-MS system.

Method validation

Method validation was performed in accordance to international guidelines (Peters et al. 2007) and the guidelines of the Society of Toxicological and Forensic Chemistry (Peters et al. 2009). Moreover, the procedure was already described in previous studies (Nordmeier et al. 2021; Walle et al. 2022). In this context, the analytical parameters selectivity, limits of detection (LODs), linearity, lower limits of quantification (LLOQs), recovery (RE), matrix effects (ME), process efficiency (PE), intra- and interday accuracy and precision tests, freeze/ thaw, long-term, and processed sample stability as well as carry-over effects were examined in order to achieve a full validation of the method for pig whole blood and serum samples.

First of all, selectivity of the method was checked. For this purpose, six blank pig serum or blood samples from different drug-free pigs were used. Additionally, two zero samples containing only the SIL-IS and one sample spiked with possible interfering substances (AB-005, AB-FUBINACA, AM-694, AM-697, AM1220, AM-1248, AM-2201, AM-2232, AM-2233, EAM2201, JWH-018, JWH-015, JWH-081, JWH-122, JWH-182, JWH-200, JWH-203, JWH-210, JWH-250, MAM-2201, 5F-MDMB-PINACA, PB-22, 5F-PB-22, Pravadoline, RCS-8, RCS-4, UR-144, XLR-11, THC, 11-THC-OH, THC-COOH, cannabidiol, cannabinol, and 5F-MDMB-P7AICA) in final concentrations (conc.) of 100 ng/mL each were prepared. After analyzing, the samples were checked for possible interfering signals at the multiple reaction monitoring (MRM) transitions of the SIL-IS, *cumyl*-5F-P7AICA and the NPA, respectively.

Following, LODs were examined. Therefore, blank pig serum and blood samples were spiked with different conc. of *cumyl*-5F-P7AICA and the NPA metabolite. The final blood and serum conc. of the substances investigated were as follows: 0.05, 0.1, 0.15, 0.2, 0.25, 0.3, 0.35, 0.4, 0.45, and 0.5 ng/mL as well as 0.001, 0.0025, 0.005, 0.01, 0.015, 0.02, 0.025, 0.03, 0.035, 0.04 ng/mL for the parent compound and the metabolite, respectively. Determination of the LODs was carried out by verifying the respective signal-to-noise ratios of the qualifier and quantifier MRM transitions (> 3:1).

For checking the linearity of the calibration, 500 µL blank pig blood or serum specimens were spiked with 25 µL of six different calibration standard conc., respectively. Final blood/ serum calibration

standard conc. were: 0.5, 10, 20, 30, 40, 50 ng/mL and 0.1, 0.3, 0.5, 0.7, 0.9, and 1.1 ng/mL for *cumyl*-5F-P7AICA and its metabolite respectively. Each calibrator was analyzed under repeated conditions six times. For evaluation, the peak area ratios (analyte/ SIL-IS) were calculated and plotted against the respective calibrator conc. Valistat 2.0 software (Arvecon, Walldorf, Germany) was used for linear regression applying a non-weighted, weighted [1/conc.], and a weighted least-square [1/(conc.)²] regression model was applied. Moreover, a Grubbs test, F test, and a Mandel test were performed. The LLOQ were set at the lowest calibrator in serum or blood, respectively.

To investigate the accuracy and precision of the method, 500 µL blank pig blood or serum were freshly extracted in duplicates on 8 different days using the standard extraction procedure. Before, 25 µL of each QC low or high solution, with final conc. of *cumyl*-5F-P7AICA or the NPA metabolite of 5 and 0.2 ng/mL or 35 and 0.8 ng/mL respectively, were added. The corresponding conc. of the QCs were finally determined by means of a daily calibration curve. For calculation of intermediate precision, repeatability, and bias values, Valistat 2.0 software was used.

To examine RE, ME, and PE, three different approaches were prepared in accordance to Matuszewski et al. applying drug-free pig blood or serum from five different pigs (Matuszewski et al. 2003). In this context, set 1 (spiked matrix samples) represents the standard sample preparation in which 25 µL of each QC low or high spiking solution of *cumyl*-5F-P7AICA and the NPA metabolite to 500 µL blank blood or serum before solid phase extraction (SPE). For preparation of set 2 (spiked extracts), the respective QC solutions were only added after the extraction procedure. Set 3 (control samples) represented the standard QC spiking solution without any extraction procedure or the addition of blank pig blood or serum, respectively. For evaluation of the ME, the absolute peak areas of the spiked extracts (set 2) were set into relation to those received after analyzing the control samples (set 3). Additionally, RE was evaluated by comparing the absolute peak areas of the spiked matrix samples (set 1) with those of the spiked extracts (set 2), whilst PE was obtained by comparing the results of the spiked matrix samples (set 1) with the control samples (set 3).

Regarding the stability of the substances in the matrices examined, various approaches were carried out. First, the freeze-thaw stability was investigated. Therefore, 500 µL blank pig blood or serum was spiked with 25 µL of the respective QC low or high spiking solution, whereby a sixfold preparation

was carried out for each QC level. Following, extraction and analysis of the respective samples was conducted after three freeze/ thaw cycles, with each cycle consisting of at least 20 h of freezing at – 20 °C with a following thawing of about 1 h at room temperature. The long-term stability was also examined by spiking 500 µL blank pig blood or serum with 25 µL of the respective QC low or high spiking solution (n=6 each). In contrast to the freeze-thaw stability, analysis of the samples was carried out 14 days after freezing at – 20 °C. To interpret the results, an additional daily extraction of six blank pig blood or serum samples was performed after the addition of 25 µL QC low or high, respectively. The remaining amount of the analytes in the treated matrices were calculated by means of a daily calibration curve. Furthermore, to investigate the processed sample stability, 500 µL blank pig blood or serum was spiked with 25 µL of the respective QC low or high spiking solution (n=6 each) and extracted by SPE. After the addition of a mixture (50:50, *v/v*) of mobile phases A and B, the respective solutions were pooled and six-fold aliquoted. Considering, that analysis of an authentic LC-TOF-MS sequence takes at least about 6 h, the prepared samples were evenly distributed over time, with time intervals of about 80 min. For calculation of the processed sample stability, the absolute peak areas of the respective analyte were plotted against the time of injection, and linear regression was performed using Valistat 2.0.

Finally, the carry over effects were checked during an authentic series of measurements, whilst one blank sample was analyzed between two authentic samples, containing high analyte conc.

LC-MS/MS apparatus

LC-triple-quadrupole MS

In accordance to previous studies (Schaefer et al. 2018a; Walle et al. 2022, 2024a), a high pressure LC system (Thermo Fisher, Dreieich, Germany) was used for analyses of the drug delivery efficiency test. The system was composed of one Allegro pump and an HTC PAL autosampler. For chromatographic separation, the system was equipped with a Gravity C18 column (150x2 mm, 5 µm, Macherey-Nagel, Dueren, Germany) and gradient elution was carried out using mobile phases A and B. Therefore, the system started with 25% mobile phase B (flow rate 0.5 mL/min). This setting was kept for 1 min.

Following, the amount of mobile phase B increased within 4 min to 100% and kept for 4 min. Finally, 25% mobile phase B were recovered and hold for 1 min. The total run time was set at about 10 min.

The LC system used was linked to a TF TSQ Quantum Ultra Accurate Mass triple stage MS, equipped with an electrospray ionization (ESI) interface. The source was set in positive mode. The settings of the MS were as follows: capillary temperature, 290 °C; vaporizer temperature, 380 °C; sheath gas, 40 arbitrary units (AU); auxiliary gas, 20 AU; ion sweep gas, 5 AU; spray voltage, 4.000 V; collision cell pressure, 1.5 mTorr. The MRM mode with three transitions per precursor ion was used for the detection of the substances and TF Xcalibur Version 2.0.7 SP 1 software was used for evaluation.

LC-TOF-MS

In accordance to previous studies (Walle et al. 2022, 2024a), a SCIEX TripleTOF 6600+ system (AB SCIEX, Concord, USA) was used for method validation and analysis of pig blood and serum samples. The system was connected to an Exion LC system (AB SCIEX), consisting of 2 AD pumps, an AD column oven as well as an AD autosampler. For chromatography a nucleoshell PFP column (100x2 mm, 2.7 µm; Macherey-Nagel, Dueren, Germany) was used. The column oven temperature has been 40 °C, the total runtime was set to 10 min with the following gradient elution settings: start with 25% mobile phase B with a flow rate of 0.5 mL/min and kept for 1 min. After a following increase to 99% mobile phase B over 3 min and holding for 3 min, the starting conditions were restored and hold for 2 min.

The instrumentation and settings of the MS were also according to the aforementioned studies. Analogously, the MS was equipped with a DuoSpray source running in positive ESI mode. The settings were: collision energy spread, 15 V; collision energy, 35 V; ion spray voltage, 4.500 V; declustering potential, 80 V; capillary temperature, 450 °C; ion source gas 1, 45 AU; ion source gas 2, 57 AU; curtain gas, 30 AU. After 5 runs, the system was mass calibrated using a calibrant delivery system. For detection and quantification of *cumyl*-5F-P7AICA and its NPA metabolite, the product ion scan mode was used. Sciex OS version 1.6.1.29803 software was used for evaluation.

Results

In vitro drug delivery efficiency

Drug delivery efficiency

To determine the drug delivery efficiency of *cumyl*-5F-P7AICA, the ratios of the nebulized drug were compared to those of the respective extracted drug using acetone as the extraction solvent, as already found in the context of a previous work (Walle et al. 2024b). This resulted in a drug delivery efficiency of 74 ± 10% for *cumyl*-5F-P7AICA.

Drug residues in the different components of the experimental setup

A small portion of approx. 10.3 ± 3.0% of the initial nebulized dose of *cumyl*-5F-P7AICA could be found in the remaining components of the experimental setup by separate refurbishment and analysis. Specifically, an amount of 6.3 ± 2.2%, 2.5 ± 0.54%, and 1.5 ± 0.23% of the drug could be found in the reservoir of the nebulizer, the endotracheal tube, and the HME filter (n=6 each), respectively. Analysis of the anesthesia bag (n=6) yielded negative results.

Method development and validation

In the present work, a SPE was performed in accordance to the method published by Schaefer et al. for other SCs (Schaefer et al. 2015, 2016, 2018b). However, slight modifications were made. First, 20 µL RCS-4-d_9 and AB-FUBINACA-d_4 each were used as SIL-IS for quantification of *cumyl*-5F-P7AICA and the NPA, respectively. In addition, a larger amount of ethanol (50 µL) was added. Moreover, after evaporation under nitrogen, the dry residues were dissolved in 50 µL of a mixture of mobile phases A and B (50:50, *v/v*) instead of 100 µL. The following analysis was performed using a LC-quadrupole TOF-MS system.

First of all, it had to be noted, that all of the validation parameters tested in the present work were in the specified range as recommended in the guidelines of the GTFCh (Peters et al. 2009). Regarding the selectivity of the method, no interfering signals were detected at the MRM transitions of the examined compounds when analyzing blank pig blood and serum or zero samples. Additionally, no similar MRM could be observed by the spiked substances.

The LOD was set at 0.06 ng/mL and 0.07 ng/mL for *cumyl*-5F-P7AICA as well as 0.006 ng/mL and 0.005 ng/mL for the NPA metabolite in blood and serum samples, respectively.

As far as the linearity of the calibration is concerned, a linear calibration was used with weighting factors of $1/x^2$ for the metabolite and 1/x for the parent substance. In both matrices examined, the calibration range was set to 0.1 – 1.1 ng/mL and 0.5 – 50 ng/mL for the metabolite and *cumyl*-5F-P7AICA, respectively. In addition, the lowest calibrator each was defined as LLOQ.

Regarding the accuracy and precision of the method, the bias values with the respective relative standard deviation (RSD) as well as the intermediate precision RSD for QC low and high in blood and serum samples are shown in Table SI 1. Regarding these data, accuracy and precision of the method is given, as the values fulfilled the criteria of the GTFCh guidelines pretending, that the bias values should be lay within 15% of the nominal conc. and the RSD values should be ≤15% (Peters et al. 2009).

The RE, ME, and PE values for QC low and high in blank pig blood and serum samples are depicted in Table SI 1. As can be seen here, the ME variability is < 25%, so that the requirements of the GTFCh guidelines are also complied here (Peters et al. 2009).

As far as the stability of the tested compounds is concerned, the freeze-thaw and long-term stability were initially tested. In both approaches, no relevant decrease in conc. of *cumyl*-5F-P7AICA and its NPA metabolite could be detected. Therefore, the validation criteria which say, that the mean conc. of the analyte after treatment has to be within ±10% of the control samples and the 90% confidence interval has to be in the range of ±20% of the control samples, was met. Subsequently, the processed sample stability of both analytes was tested at about 5 °C over 6h. Here, no relevant decrease in peak area could be detected over the time of an authentic sequence, showing, that an instability of *cumyl*-5F-P7AICA and its metabolite has not to be expected during this time.

Finally, no carry-over effects were detected.

Table SI 1 Limit of detection (LOD), calibration range, nominal concentration (conc.), accuracy, repeatability, intermediate precision as well as results of matrix effect (ME), recovery (RE), and process efficiency (PE) studies of quality control (QC) low and high samples containing *cumyl*-5F-P7AICA or its *N*-pentanoic acid metabolite (NPA) in pig serum and blood.

Validation parameter	***Cumyl*-5F-P7AICA**		**NPA**	
	Serum	**Blood**	**Serum**	**Blood**
LOD [ng/mL]	0.07	0.06	0.005	0.006
Calibration range [ng/mL]	0.5 - 50	0.5 - 50	0.1 – 1.1	0.1 – 1.1
QC low				
Nominal conc. [ng/mL]	5	5	0.2	0.2
Accuracy bias [%]	11	-7.4	3.0	-2.1
Repeatability RSD [%]	2.9	3.1	3.3	6.3
Intermediate Precision RSD [%]	4.8	5.0	6.2	6.3
ME % (RSD %)	78 (7.2)	76 (9.9)	86 (12)	88 (9.7)
RE % (RSD %)	90 (4.9)	86 (5.7)	92 (5.2)	87 (11)
PE % (RSD %)	71 (8.4)	66 (7.6)	79 (10)	77 (13)
QC high				
Nominal conc. [ng/mL]	35	35	0.8	0.8
Accuracy bias [%]	3.4	3.5	3.1	-1.3
Repeatability RSD [%]	4.9	6.8	3.3	5.0
Intermediate Precision RSD [%]	4.9	7.0	5.8	6.1
ME % (RSD %)	87 (7.3)	80 (5.0)	81 (10)	76 (5.2)
RE % (RSD %)	85 (4.8)	84 (3.1)	85 (6.8)	91 (5.6)
PE % (RSD %)	74 (4.1)	68 (6.1)	69 (5.7)	69 (8.3)

Discussion

In vitro drug delivery efficiency

Regarding the results of the in vitro drug delivery efficiency test, 74 ± 10% of the nebulized SC dose was found in the glass fiber filters, reflecting the deposition of the substance in the pig lung. Furthermore, a total amount of approx. 10.3 ± 3.0% of the initial nebulized SC dose was found in the remaining experimental components. Consequently, a loss of approx. 15% of the nebulized dose is not comprehensible.

If one has a look to the results published by Schafer et al for JWH-210, RCS-4 and THC (Schaefer et al. 2018a), a drug delivery efficiency of 70.5 – 78.8% of the nebulized dose was reported. Furthermore, approx. 10% of the nebulized dose were found by Schaefer et al in the nebulizer device and the endotracheal tube, resulting in an inexplicable loss of substance of about 10-20% (Schaefer et al. 2018a). Comparing these results with those obtained in the present work it can be noticed that similar findings were observed for *cumyl*-5F-P7AICA. However, compared to the herein published data, a slightly higher amount of the SCs was found in the endotracheal tube by Schaefer et al (Schaefer et al. 2018a). As it is already known, (synthetic) cannabinoids have a high tendency to affect to plastic surfaces due to their lipophilicity (Christophersen 1986; Kneisel et al. 2013). Hence, a possible explanation for the slightly higher amount of SCs deposition in the endotracheal tube reported by Schaefer et al as compared to the findings presented here might be in the lower lipophilicity of *cumyl*-5F-P7AICA (LogP = 4.20) as compared to JWH-210 (LogP = 7.5) or RCS-4 (LogP = 5.6) (Schaefer et al. 2019). However, analysis of the HME filter and the anesthesia bag were not carried out by Schaefer et al.

Overall, the findings of the present study for *cumyl*-5F-P7AICA are in good agreement to those published by Schaefer et al for JWH-210, RCS-4, and THC.

Final Model

Differential equations

Inhalation absorption and dosing compartment:

DADT(1) = -ka*A(1)

Central compartment *cumyl*-5F-P7AICA:

$DADT(2) = ka*A(2) – CL_i/V_i*A(2) – Q1_i/V_i*A(2) + Q1_i/V_{P1i}*A(4) – Q2_i/V_i*A(2) + Q2_i/V_{P2i}*A(5)$

Central compartment NPA:

$DADT(3) = ktr*(A(7)*AP + A(8)*(1-AP)) – CL_{Mi}/V_M*A(3) – QM_i/V_{Mi}*A(3) + QM_i/V_{PMi}*A(6)$

1st peripheral compartment *cumyl*-5F-P7AICA:

$DADT(4) = Q1_i/V_i*A(2) – Q1_i/V_{P1i}*A(4)$

2nd peripheral compartment *cumyl*-5F-P7AICA:

$DADT(5) = Q2_i/V_i*A(2) – Q2_i/V_{P2i}*A(5)$

1st peripheral compartment NPA:

$DADT(6) = QM_i/V_{Mi}*A(3) – QM_i/V_{PMi}*A(6)$

Metabolism delay compartment 1:

$DADT(7) = CL_i/V_i*A(2)*f_{MET}*(1+AP*f_{APP})*F\_WGT – ktr*A(7)$

Metabolism delay compartment 2:

$DADT(8) = ktr*A(7) – ktr*A(8)$

Parameter calculation

AP = 0 for inhalation and 1 for iv application

WGT = individual weight of the pig

$CL_i = CL* WGT**0.75$

$V_i = V2* WGT**0.75$

$Q1_i = Q1* WGT**0.75$

$V_{P1i} = V_{P1}* WGT**0.75$

$Q2_i = Q2 * WGT**0.75$

$V_{P2i} = V_{P2}* WGT**0.75$

$CL_{Mi} = CL_M * WGT**0.75$

$QM_i = QM * WGT**0.75$

$V_{PMi} = V_{PM} * WGT**0.75$

$V_{Mi} = V_i$

WGT_Parent = 367.5 → Molecular weight parent

WGT_Metabolite = 379.5 → Molecular weight metabolite

F_WGT = WGT_Metabolite/WGT_Parent

Concentration *cumyl*-5F-P7AICA: A(2)/V

Concentration NPA: A(3)/VM

Referenzen

Christophersen AS (1986) Tetrahydrocannabinol stability in whole blood: plastic versus glass containers. J Anal Toxicol 10(4):129-31. https://doi.org/10.1093/jat/10.4.129

Doerr AA, Nordmeier F, Walle N et al (2021) Can a recently developed pig model be used for in vivo metabolism studies of 7-azaindole-derived synthetic cannabinoids? A study using 5F-MDMB-P7AICA. J Anal Toxicol 45(6):593-604. https://doi.org/10.1093/jat/bkaa122

Doerr AA, Dings C, Zaher O et al (2024a) Toxicokinetic modelling of the synthetic cannabinoid 5F-MDMB-P7AICA and its main metabolite in pigs following pulmonary administration. Br J Clin Pharmacol, submitted.

Doerr AA, Nordmeier F, Walle N et al (2024b) Does a postmortem redistribution affect the concentrations of the 7 azaindole-derived synthetic cannabinoid 5F-MDMB-P7AICA in tissues and body fluids following pulmonary administration to pigs? Arch Toxicol 98(10):3289-3298. https://doi.org/10.1007/s00204-024-03815-1

Kneisel S, Speck M, Moosmann B, Auwaerter V (2013) Stability of 11 prevalent synthetic cannabinoids in authentic neat oral fluid samples: glass versus polypropylene containers at different temperatures. Drug Test Anal 5(7):602-6. https://doi.org/10.1002/dta.1497

Matuszewski BK, Constanzer ML, Chavez-Eng CM (2003) Strategies for the assessment of matrix effect in quantitative bioanalytical methods based on HPLC-MS/MS. Anal Chem 75(13):3019-30. https://doi.org/10.1021/ac020361s

Nordmeier F, Sihinevich I, Doerr AA et al (2021) Toxicokinetics of U-47700, tramadol, and their main metabolites in pigs following intravenous administration: is a multiple species allometric scaling approach useful for the extrapolation of toxicokinetic parameters to humans? Arch Toxicol 95(12):3681-3693. https://doi.org/10.1007/s00204-021-03169-y

Nordmeier F, Doerr AA, Potente S et al (2022a) Perimortem distribution of U-47700, tramadol and their main metabolites in pigs following intravenous administration. J Anal Toxicol 46(5):479-486. https://doi.org/10.1093/jat/bkab044

Peters FT, Drummer OH, Musshoff F (2007) Validation of new methods. Forensic Sci Int 165(2-3):216-24. https://doi.org/10.1016/j.forsciint.2006.05.021

Peters FT, Hartung M, Herbold M et al (2009) Anhang B zur Richtlinie der GTFCh zur Qualitätssicherung bei forensisch-toxikologischen Untersuchungen – Anforderungen an die Validierung von Analysenmethoden. Toxichem Krimtech 76, 185–208. https://www.gtfch.org/cms/images/stories/files/GTFCh_Richtlinie_Anhang%20B_Validierung_Version%201.pdf. Accessed Oktober 13, 2024.

Schaefer N, Kettner M, Laschke MW et al (2015) Simultaneous LC-MS/MS determination of JWH-210, RCS-4, Δ9-tetrahydrocannabinol, and their main metabolites in pig and human serum, whole blood, and urine for comparing pharmacokinetic data. Anal Bioanal Chem 407(13):3775-86. https://doi.org/10.1007/s00216-015-8605-6

Schaefer N, Wojtyniak J-G, Kettner M et al (2016) Pharmacokinetics of (synthetic) cannabinoids in pigs and their relevance for clinical and forensic toxicology. Toxicol Lett 253:7-16. https://doi.org/10.1016/j.toxlet.2016.04.021

Schaefer N, Kettner M, Laschke MW et al (2017) Distribution of synthetic cannabinoids JWH-210, RCS-4 and Δ 9-tetrahydrocannabinol after intravenous administration to pigs. Curr Neuropharmacol 15(5):713-723. https://doi.org/10.2174/1570159X15666161111114214

Schaefer N, Kroell AK, Laschke MW et al (2018a) Development of an in-vitro drug delivery efficiency test for a pulmonary toxicokinetic pig study. Curr Drug Deliv 15(8):1167-1171. https://doi.org/10.2174/1567201815666180214130014

Schaefer N, Wojtyniak J-G, Kroell AK et al (2018b) Can toxicokinetics of (synthetic) cannabinoids in pigs after pulmonary administration be upscaled to humans by allometric techniques? Biochem Pharmacol 155:403-418. https://doi.org/10.1016/j.bcp.2018.07.029

Schaefer N, Kroell AK, Koerbel C et al (2019) Distribution of the (synthetic) cannabinoids JWH-210, RCS-4, as well as Δ9-tetrahydrocannabinol following pulmonary administration to pigs. Arch Toxicol 93(8):2211-2218. https://doi.org/10.1007/s00204-019-02493-8

Schaefer N, Kroell AK, Koerbel C et al (2020) Time- and temperature-dependent postmortem concentration changes of the (synthetic) cannabinoids JWH-210, RCS-4, as well as Δ9-

tetrahydrocannabinol following pulmonary administration to pigs. Arch Toxicol 94(5):1585-1599. https://doi.org/10.1007/s00204-020-02707-4

Walle N, Nordmeier F, Doerr AA, et al (2021) Comparison of in vitro and in vivo models for the elucidation of metabolic patterns of 7-azaindole-derived synthetic cannabinoids exemplified using cumyl-5F-P7AICA. Drug Test Anal 13(1):74-90. https://doi.org/10.1002/dta.2899

Walle N, Doerr AA, Laschke MW et al (2022) Systematic studies on temperature-dependent in vitro stability during storage and smoking of the synthetic cannabinoid 5F-MDMB-P7AICA. J Anal Toxicol 46(4):374-382. https://doi.org/10.1093/jat/bkab022

Walle N, Doerr AA, Peters B et al (2024a) Are the postmortem concentration changes of the synthetic cannabinoid cumyl-5F-P7AICA and its N-pentanoic acid metabolite dependent on the environmental conditions? – A systematic study following pulmonary administration to pigs. Toxicol Lett S0378-4274(24)02040-X. https://doi.org/10.1016/j.toxlet.2024.10.006

Walle N, Doerr AA, Peters B et al (2024b) Development and method validation of a sampling technique for a reproducible detection of synthetic cannabinoids in exhaled breath using an in vitro pig lung model. J Anal Toxicol bkae078. https://doi.org/10.1093/jat/bkae078

Legend to figures

Fig. SI 1 Schematic representation of the final model structure. For intravenous application, only one transit compartment is used. For pulmonary application, two transit compartments are used.

Fig. SI 2 Goodness-of-fit plots stratified by analyte and application. Upper row: Observations vs. population model predictions, lower row: Observations vs. individual model predictions.

Fig. SI 3 Individual concentration-time profiles and model predictions. Points represent observations, dashed lines represent population predictions and full lines represent individual predictions.

Fig. SI 1 ~~2~~

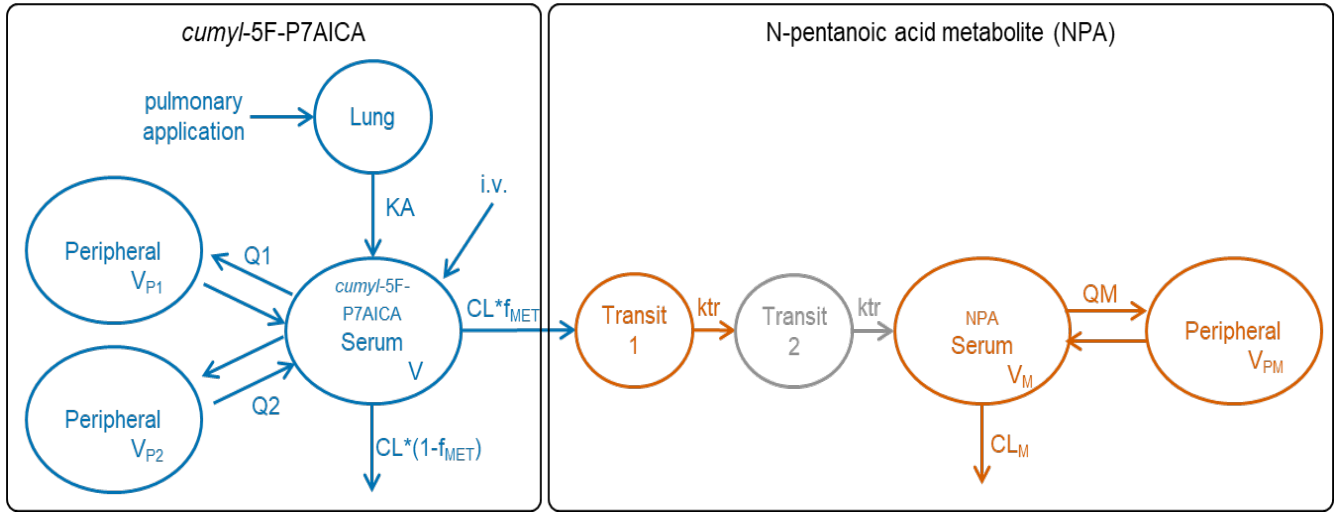
cumyl-5F-P7AICA
pulmonary application
Lung
KA
i.v.
Peripheral V_{P1}
Q1
cumyl-5F-P7AICA Serum V
$CL*f_{MET}$
Peripheral V_{P2}
Q2
$CL*(1-f_{MET})$
N-pentanoic acid metabolite (NPA)
Transit 1
ktr
Transit 2
ktr
NPA Serum V_M
QM
Peripheral V_{PM}
CL_M

Fig. SI ~~3~~ 2

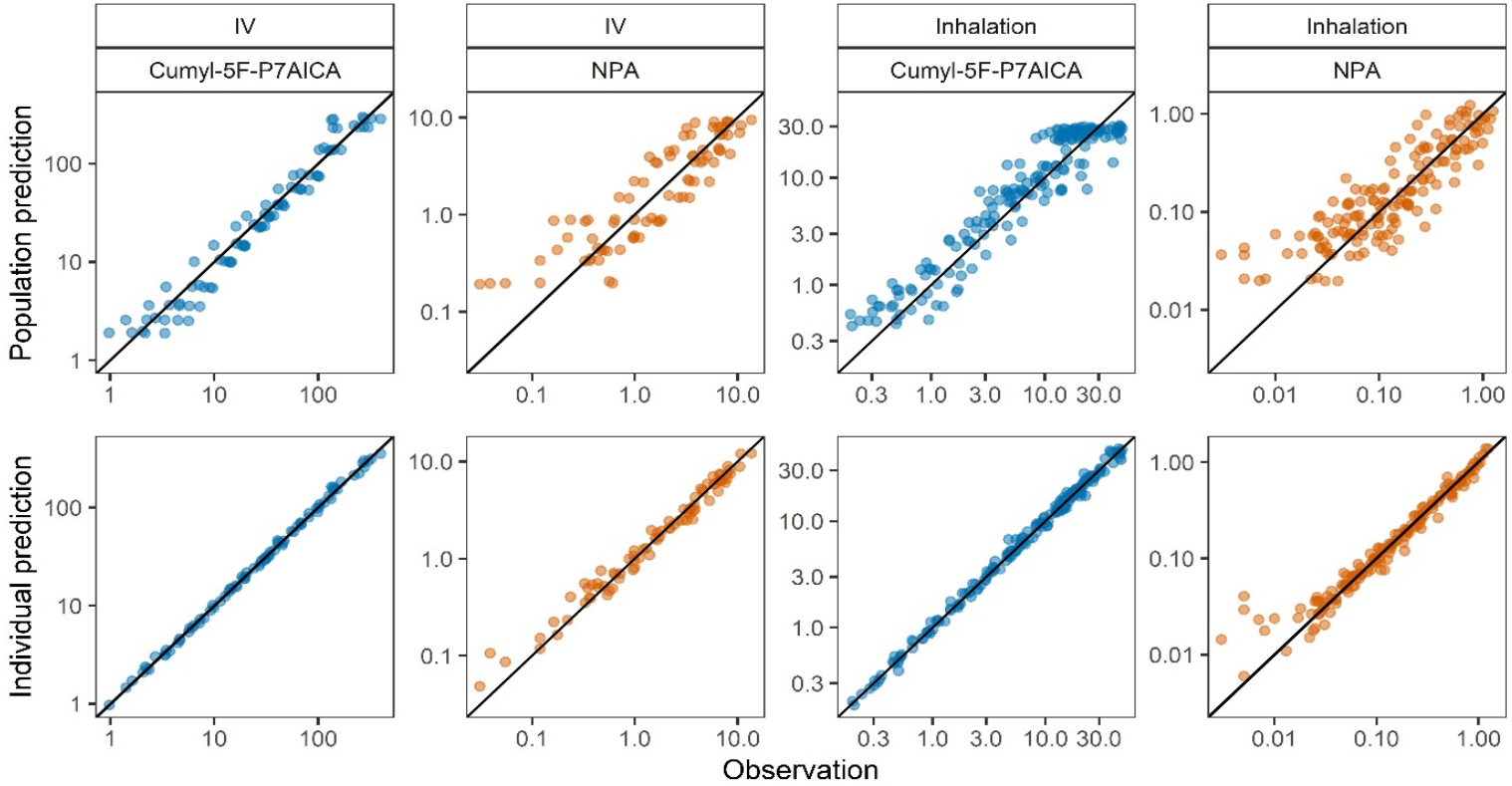
IV
Cumyl-5F-P7AICA
IV
NPA
Inhalation
Cumyl-5F-P7AICA
Inhalation
NPA
Population prediction
Individual prediction
Observation
1
10
100
0.1
1.0
10.0
0.3
3.0
30.0
0.01
0.10
1.00

Fig. SI 4-3

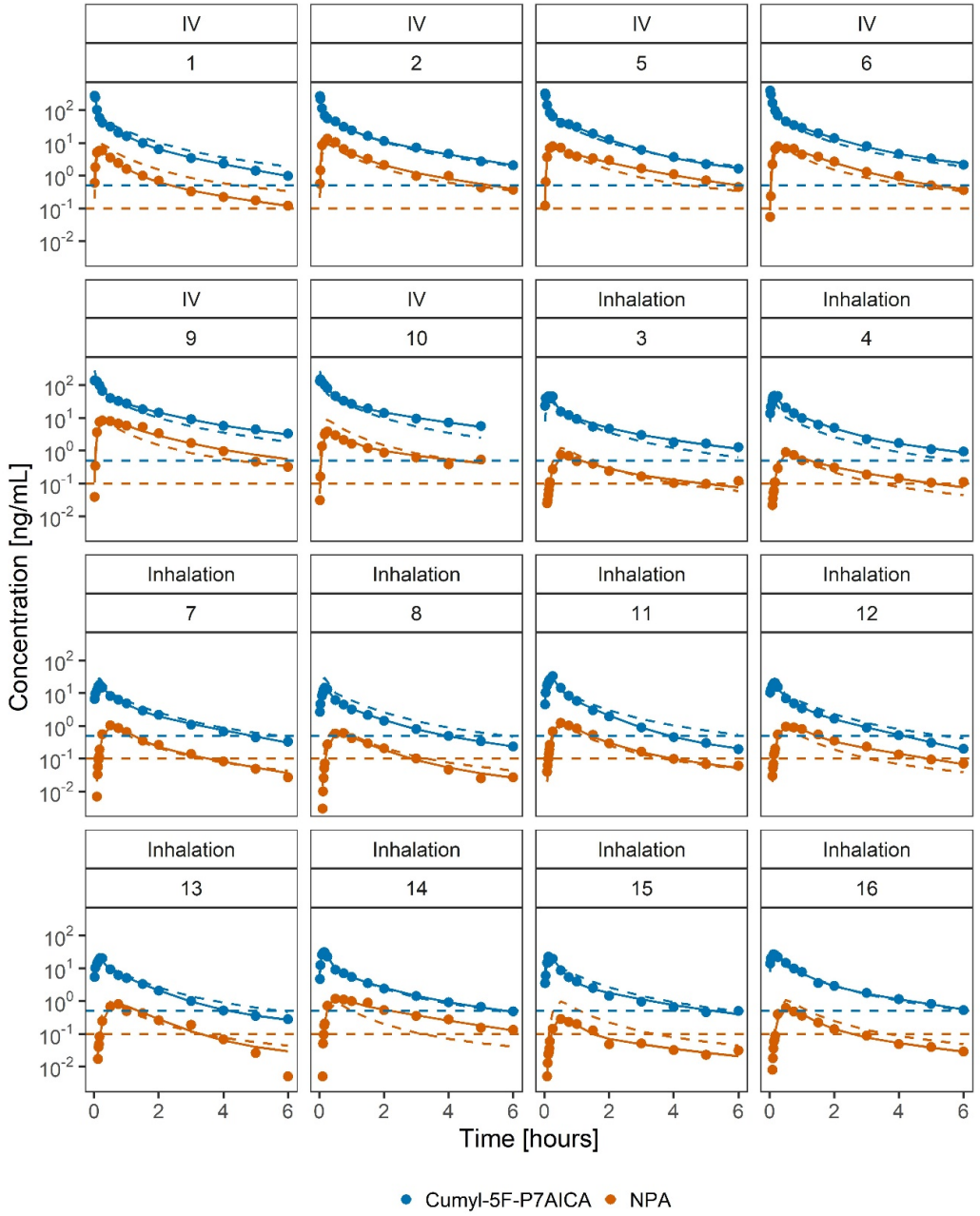
IV
1
IV
2
IV
5
IV
6
IV
9
IV
10
Inhalation
3
Inhalation
4
Inhalation
7
Inhalation
8
Inhalation
11
Inhalation
12
Inhalation
13
Inhalation
14
Inhalation
15
Inhalation
16
Concentration [ng/mL]
10^2
10^1
10^0
10^{-1}
10^{-2}
0
2
4
6
Time [hours]
Cumyl-5F-P7AICA
NPA

4. Discussion and Conclusion

Although the number of novel SCs reported by the EMCDDA slightly declined, they still represent the largest group of NPS. Minor modifications of the chemical structure of SCs results in novel compounds with often higher potencies. Due to the absence of preclinical safety studies, consumption of such compounds can lead to unpredictable effecs and side effecs. Hence, several intoxications with sometimes fatal outcomes after consumption of SCs have been reported in the last decades. Especially in the context of DUID cases, consumption of SCs can lead to an impairment of driving performance. As drug tests performed roadside do not cover NPS, there is often no initial suspicion of the consumption of e.g. SCs. In addition, the analytical detection of such SCs poses a major challenge in clinical and forensic toxicology. As the respective TK properties are often unknown, interpretation of analytical results is afflicted with several issues when an expert opinion on the fitness to drive is required. Furthermore, SCs are often subject to extensive metabolism. Hence, it is difficult to find the right analytical target, e.g. in the case of urine analyses as part of abstinence control programs. Overall, knowledge on the TK properties of structurally modified SCs is indispensable, as minor modifications of the chemical structure can potentially lead to altered TK.

Therefore, the present studies used a comprehensive controlled pig model after inhalative administration to assess the TK properties of SCs containing a 7-azaindole core and a carboxamide linker. Furthermore, a new EB sampling technique based on an *in vitro* pig lung model was developed that prospectively can be applied to anaesthetized and ventilated pigs to clarify the TK properties of SCs in EB.

In a first step, the metabolic pattern of *cumyl*-5F-P7AICA was elucidated using different *in vitro* (pHLM, PLM, pHS9) and *in vivo* (rat and pig model) assays. Subsequently, the findings were compared with each other as well as with already published *in vitro* (pHLM) and *in vivo* (human) metabolism data, to determine which approach represents the best and practicable one to investigate the metabolic pattern of SCs. Concerning the different *in vitro* assays conducted in the present work, the formed phase I metabolites were in a good agreement with each other. After performing pHLM and PLM incubations, besides the parent compound, a total of eleven phase I metabolites were detected each. Essential metabolic pathways in both *in vitro* incubations were

found to be *N*-dealkylation, monohydroxylation at the aryl moiety, monohydroxylation at the 5-fluoropentyl chain and ketone formation as well as an OF followed by a carboxylation representing the main metabolic step. However, dihydroxylation at the aryl moiety in the bridge residue could additionally be detected after incubation with pHLM. Due to the addition of cofactors, phase II metabolites were found in addition to phase I metabolites after pHS9 incubation. The main metabolic pathways after pHS9 incubation were consistent with those after pHLM or PLM incubation. In addition, phase II metabolites were formed by glucuronidation or sulfation of mono- or dihydroxylated metabolites, while sulfated compounds were detected more often. Comparison of the metabolic data obtained in the present study after pHLM incubation of *cumyl*-5F-P7AICA with those already published by Staeheli et al. showed a good agreement, as here also OF followed by carboxylation, monohydroxylation and dihydroxylation were identified as the main metabolic pathways after pHLM incubation.[145] In a next step, the metabolic excretion profile of *cumyl*-5F-P7AICA was elucidated in rat urine after oral administration. In general, only low abundances of metabolites were found in in rat urine. Here, phase I metabolites were mainly formed by OF followed by carboxylation, monohydroxylation at the aryl moiety, dihydroxylation at the 5-fluoropentyl side chain or the aryl moiety and the side chain as well as *N*-Desalkylation with a subsequent monohydroxylation at the 7-azaindole core or the aryl moiety. However, in rat urine, only two phase II metabolites were found, formed by glucuronidation or sulfation of the hydroxy group after *N*-desalkylation followed by monohydroxylation at the aryl moiety. In accordance with the results obtained by the *in vitro* approaches, besides the metabolites, *cumyl*-5F-P7AICA could additionally be detected in rat urine. Comparison of the metabolism pattern of *cumyl*-5F-P7AICA in rat urine with the obtained *in vitro* data showed that a generally lower number of metabolites could be detected in the *in vivo* model.

As pigs show a great similarity with human especially in terms of their enzyme equipment, physiological properties, and anatomical structure, the pig model represents a further *in vivo* approach to elucidate the TK properties of NPS.[100–103] Another advantage of this approach is that the substance can be administered inhalatively. As this route of administration reflects the generally authentic consumer habits, an *in vitro* setup has already been established.[111] Therefore, in a next step of the study, this *in vivo* approach was used in the context of a systematically controlled study after inhalative administration to obtain various TK data of the SC *cumyl*-5F-

P7AICA, as a representative for SCs containing a 7-azaindole core structure with a carboxamide linker. Initially, it should be mentioned that the parent substance could be detected in pig urine samples over a period of about 3 h after administration. Although it is known that SCs are highly metabolized, the detection of the parent substance in urine has already been described for other SCs with a 7-azaindole or an indole core structure.[146,147] Concerning the metabolism, a total of five metabolites were identified in pig urine samples. The only phase I metabolite found in every pig urine specimen throughout the whole duration of the experiment was formed by OF and a subsequent carboxylation. Besides that, *N*-dealkylation followed by monohydroxylation at the aryl moiety and monohydroxylation at the 5-fluoropentyl side chain or the aryl moiety could be deducted as phase I reaction. However, these more hydrophilic compounds were subject to a pronounced conjugation with glucuronic or sulfonic acid *in vivo*, so that only these conjugates were detected in the pig urine samples. These could also be detected up to the end of the experiment, with the aryl hydroxylated and subsequently glucuronidated metabolite consistently exhibiting the highest abundance. This intensive phase II metabolism in pigs was already described in the context of former studies on the TK of SCs.[93] Comparing the metabolic pattern of *cumyl*-5F-P7AICA obtained in the various *in vivo* experiments reveals that, apart from the parent compound, there are only similarities in the formation of the OF and carboxylated as well as the *N*-dealkylated followed by aryl monohydroxylated and sulfated metabolites. While phase I metabolites were mainly detected in rat urine after *N*-dealkylation with a subsequent hydroxylation, phase II metabolites were increasingly found in pig urine. However, it should be noted that both the dosage and the route of administration were different, making it difficult to compare the data obtained. In addition, interspecies differences e.g. in the CYP enzyme pattern as well as a possible insufficient absorption of *cumyl*-5F-P7AICA after oral administration due to its lipophilic properties, which may lead to an altered metabolic pattern, should be taken into consideration.[119,148,149] Summarizing the results of the *in vivo* approaches, rats seem to be less suitable than the pig model to elucidate the metabolic pattern of 7-azaindole-derived-SCs. Comparing the metabolites detected in pig urine with those obtained in the respective *in vitro* incubations, it could be stated that, due to the intensive phase II metabolism *in vivo*, pHS9 represents the most appropriate tool to elucidate the metabolic pattern of 7-azaindole-containing SCs.

However, a good match with human metabolism is required to ensure transferability. Regarding *cumyl*-5F-P7AICA, Staeheli et al. reported on OF followed by carboxylation as well as monohydroxylation at the aryl moiety followed by glucuronidation or sulfation as the major human biotransformation steps.[84] The respective metabolites of *cumyl*-5F-P7AICA were also found as the main metabolites in pig urine, so that the data showed a good agreement. As no dihydroxylated or corresponding phase II metabolites were found in both *in vivo* urine samples, it can be concluded that monohydroxylated metabolites seem to underlie a fast phase II conjugation. However, minor differences could be ascertained between pig and human urine specimens. First, as in pig urine *cumyl*-5F-P7AICA was detectable for about 3 h in urine specimens, no parent compound was found in authentic human urine.[84] However, no information is available on the dosage or the time of consumption in the authentic case. Hence, a longer time period between consumption of *cumyl*-5F-P7AICA and urine collection would be conceivable here. However, consistent with the data collected in pig urine, further studies on the human urinary excretion pattern of 7-azaindole-derived SCs also reported on the parent compound being detectable in human urine specimens after oral ingestion.[146] The results of the CYP activity screening using human CYP isoenzymes show that the main metabolic steps of *cumyl*-5F-P7AICA are predominantly catalyzed by the isoenzymes CYP2C19, CYP3A4 and CYP3A5. Hence, these three enzymes appear to be mainly responsible for the formation of the main metabolites in both humans and pigs.

Finally, it should be noted that due to only minor modifications in the chemical structure, the consumption of structurally similar SCs can lead to common metabolites. Therefore, a high specifity and sensitivity of the analytical targets are required. First, albeit *cumyl*-5F-P7AICA was not detected in authentic human urine specimens reported by Staeheli et al., accordingly to the obtained data in pig urine, the evidence of the parent compound was reported for other 7-azaindole-derived SCs.[146,147] Thus, the parent compound is highly recommended as a urinary analytical target to prove a recent consumption of 7-azaindole-derived SCs at least in the last 3 h prior to urine collection. Moreover, due to its high abundances in urine specimens, the OF and carboxylated metabolite should be used as a consumption marker. This metabolic reaction step was already reported for *cumyl*-5F-P7AICA in humans as well as for other fluorinated SCs.[71,84,150–152] Furthermore, as monohydroxylation represents a common metabolic phase I reaction for SCs[84,152–154] and the full parent structure is retained, the aryl-

monohydroxylated metabolite is also advocated as an analytical target. Indeed, as the aryl-monohydroxylated metabolite underlies a fast conjugation with glucuronic or sulfonic acid *in vivo*, conduction of an enzymatic hydrolysis is animated to enhance specifity. If none is feasible, the corresponding phase II metabolites should be used as consumption markers. Nevertheless, it should be considered that the aryl-monohydroxylated as well as the OF and carboxylated metabolite can also be formed after consumption of other SCs, e.g. *cumyl*-5F-PINACA.[19,145] However, an analytical assignment of the metabolites to the parent compound might be considered due to different physico-chemical properties and a resulting altered retention time.

To sum up, it can be stated that, due to the predominantly consistent metabolic pattern between pig and human urine specimens, this *in vivo* approach represents a suitable animal model to elucidate TK data of 7-azaindole-derived SCs.

Based on this result and the fact that the pig model has already proven to be suitable for the elucidation of the TK data of SCs, the next steps of the present work involved a comprehensive TK study using the pig model, in which, in addition to various TK parameters and their extrapolation to humans, the tissue distribution as well as the PM concentration changes of *cumyl*-5F-P7AICA and its NPA metabolite under various environmental conditions should be assessed.

In recent years EB has attracted enormous scientific interest as an alternative matrix besides others also in forensic toxicology. As this matrix can be easily obtained during the *in vivo* pig experiment without any further stress for the animal, the aim was to collect EB in the context of a prospective pig study to clarify the TK properties of SCs in EB in a systematically controlled and reproducible manner. Since commercially available EB sampling techniques such as ExaBreath® (SensAbues®, Västerås, Schweden) or Hound® Marijuana Breathalyzer (Hound Labs Inc., Oakland, CA, USA) are based on an active exhalation of the subject, they are not applicable to anesthetized and ventilated pigs.[60,69] Hence, in a next step of the present work, a new *in vitro* EB sampling technique was developed that can be applied in the context of future TK studies on the SC *cumyl*-5F-P7AICA using the *in vivo* pig model. In accordance to the *in vivo* approach, the SC was nebulized using the M-neb flow+ ventilation ultrasonic nebulizer MN-300/7 (Nebutec, Elsenfeld, Germany) coupled to a breathing tube and a ventilator, also used during surgeries. The aerosol was subsequently delivered via a tube into a simulated pig lung. In order to collect EB, a

BiVOC2V2 pump (Umweltanalytik Holbach GmbH, Wadern, Germany) originating from environmental analysis was connected to the breathing tube (expiratory limb), which transports the EB back to the ventilator. To collect substances contained in EB, a glass fiber filter (GFF) was inserted between the expiratory limb and the pump. The pump was then set to a fixed time interval (15 min) and a specified quantity of EB per minute (2 L/min) to ensure reproducibility. In total, about 40% of the nebulized *cumyl*-5F-P7AICA dose could be detected in the various components of the experimental setup, resulting in a 'loss' of about 60%. With regard to this finding, it should first be considered that a high affinity to plastic surfaces has already seen for other SCs.[111,155,156] Hence, a high drug deposition at the experimental components can result in lower drug concentrations in EB. This issue might also be transferred to the ventilation system used during the *in vitro* experiment. As this component constitutes an open ventilation system, an adsorption of *cumyl*-5F-P7AICA and thus a relevant loss of substance should be considered. However, as the experimental components as well as the ventilator are also part of the *in vivo* experiment, the amount of drug deposition could be transferred and might at least partly be neglected. As far as the comparatively low quantity of *cumyl*-5F-P7AICA (3.6 ± 1.3% accordingly 18 ± 6.5 µg/filter) detected in GFF is concerned, it should first be noted that the pump settings are limited to a maximum possible quantity of 2 L of EB per minute. Taking into account the ventilator settings (tidal volume of 500 ml and a respiratory rate of 12/min), this leads to about 33% of EB and therefore also contained substance that can be withheld by the GFF at all. As a consequence, around 67% of the substance contained in EB is lost in the setup. In this respect, the amount of 3.6 ± 1.3% detected in GFF is corrected to 11 ± 3.8% of the maximum detectable amount of substance, considering the nebulized dose of 0.5 mg of *cumyl*-5F-P7AICA. However, compared to commercially available EB collection devices, only a small portion of the substance contained in EB can be collected using the setup developed in the present study. Therefore, a more sensitive analytical method is required, especially when used in *in vivo* experiments. To sum up, a new *in vitro* EB sampling technique was successfully developed in the second part of the present work. Although only a small amount of the nebulized SC was detected in the developed *in vitro* setup, the low standard deviations indicate a controlled and reproducible detection of *cumyl*-5F-P7AICA using this experimental setup. To draw a conclusion, the developed EB sampling technique appears to be a

promising tool to elucidate the TK of SCs in EB in the context of *in vivo* studies using the pig model after inhalative administration.

In the next step of the present work, concentration-time profiles of the SC *cumyl*-5F-P7AICA and its NPA metabolite were established in blood and serum after inhalative as well as i.v. administration. For more details regarding the course of the respective concentration-time profiles see Chapter 3.4. Subsequently, a popTK model was successfully developed describing the serum concentration-time profiles, various TK parameters were generated, and the model was upscaled to humans using allometric scaling. The pop TK analysis yielded, that a three-compartment model describes the TK of *cumyl*-5F-P7AICA best, as a two-compartment model seems to be better for the NPA metabolite. In addition, transit compartments had to be incorporated to account for the time delay between the appearance of the parent substance and its metabolite. Following, the data obtained for *cumyl*-5F-P7AICA as well as its NPA metabolite were compared to those already published for JWH-210 and RCS-4, comprehending an indole core coupled to a carbonyl linker. In addition, the TK data of the SC 5F-MDMB-P7AICA, structurally comparable to *cumyl*-5F-P7AICA, but with a modified ester-containing bridge residue, were contrasted. First of all, the TK data obtained in the present work are in overall good agreement with those already reported for JWH-210 and RCS-4, their respective metabolites, as well as 5F-MDMB-P7AICA, albeit with differences in the substance concentrations detected.[97,157] However, the lowest concentrations were considerably lower for *cumyl*-5F-P7AICA as compared to JWH-210 and RCS-4. Hence, a faster *in vivo* elimination of *cumyl*-5F-P7AICA can be suggested. Concerning the TK parameters derived from the pop TK analysis, the data obtained were comparable with those reported for JWH-210 and RCS-4[97,157] Based on the overall comparable TK data for *cumyl*-5F-P7AICA and those reported for JWH-210 and RCS-4, it can therefore be assumed that no relevant cleavage of the carboxamide linker within the chemical structure of *cumyl*-5F-P7AICA occurs *in vivo*. This result can be substantiated by the data obtained in the present work regarding the metabolic pattern of *cumyl*-5F-P7AICA (see Chapter 3.1). Accordingly, no metabolite with a cleaved carboxamide moiety was found in pig urine specimens. In addition, this result is consistent with already published *in vitro* data studying the stability of various SCs using human carboxylesterases.[130] To date, only few data on intoxication cases involving *cumyl*-5F-P7AICA with a partly fatal outcome are available. However, in these cases the reported blood concentrations of *cumyl*-5F-P7AICA are in a good

agreement with the data obtained in the present work.[158–160] This further demonstrates the suitability of the pig model as an *in vivo* approach to elucidate the TK properties of structurally modified SCs. In summary, the exchange of a carbonyl linker towards a carboxamide moiety does not result in substantial different TK properties.

In a next step of the comprehensive study, samples of various relevant tissues, body fluids, and organs were initially drawn immediately after euthanasia of the animals to elucidate the initial perimortem distribution pattern of 7-azaindole containing SCs and the respective metabolite compared to indole-derived compounds. Here, highest concentrations of *cumyl*-5F-P7AICA were found in lung, bile fluid as well as AT specimens six hours after inhalative administration. These findings are in a good agreement with those published for JWH-210 and RCS-4.[72] Indeed, the sequestration of drugs in lung tissue, also called 'pulmonary first-pass uptake and metabolism', has already been described for several lipophilic drugs of abuse and could also be a reason for these results due to the lipophilic properties of SCs.[112–114] However, as the SCs investigated were administered inhalatively throughout the *in vivo* TK studies, a high drug concentration in the lungs is not really surprising. *Cumyl*-5F-P7AICA was also detected in central and peripheral blood specimens obtained perimortem, albeit in very low concentrations. Regarding the NPA metabolite, besides central and peripheral blood specimens, high concentrations could especially be found in organs involved in metabolism and elimination, such as liver, kidney, duodenum content and bile fluid, suggesting an enterohepatic circulation. These findings were also reported for JWH-210 and RCS-4.[72,161] Insofar, the perimortem distribution pattern of structurally modified SCs is comparable to that of 1st generation substances containing an indole-core structure with an attached carbonyl bridge.

In routine case work the corpses are are often exposed to different environmental conditions prior to forensic autopsy, e.g. under reduced oxygen availability after drowning. According to the 'Casper-rule', for example, storage under oxygen availability can lead to a faster onset of autolysis and putrefaction of the body compared to storage under oxygen-deficient conditions.[139,140] Since the PM stability, but also the tendency of a substance to exhibit a PMR, among other things, depends on the degree of autolysis, less PMR would be expected when corpses were exposed to oxygen-deficient conditions, such as drowned persons, as compared to oxygen-rich environments. Such factors should be considered when interpreting PM findings. Nevertheless, such data are lacking for SCs. Hence, in a last step of the present work,

the time-and oxygen-dependent influence of storage conditions on the PM stability and PMR of *cumyl*-5F-P7AICA as well as its NPA metabolite were investigated. For this purpose, one group of the animals (n=5) was stored in approximately 50 L water laying in a bath, while the second group (n=5) was kept at room temperature (RT). After 24 h (PMI 1), 48 h (PMI 2) and 72 h (PMI 3), the same set of specimens already sampled immediately after death was collected from the corpses again. In general, compared to the perimortem pattern, the PM distribution of *cumyl*-5F-P7AICA as well as its NPA metabolite was found to be rather stable over the observed period of 72 h independent of the storage conditions (only slight concentration changes). Thus, contrary to the expectations, *cumyl*-5F-P7AICA and its NPA metabolite seem to be quite stable in the respective analyzed specimens over a PMI of 72 h independent of the respective environmental conditions. Regarding PM specimens, highest concentrations of the parent compound were found in lung, liver and bile fluid, followed by kidney and duodenum content at both storage conditions. As already seen for other SCs, an accumulation in AT was also seen for *cumyl*-5F-P7AICA.[123] As far as central blood is concerned, comparable concentrations of *cumyl*-5F-P7AICA were found over the entire period, while the respective median concentrations in peripheral blood decreased over 72 h at both storage conditions. Regarding the NPA metabolite, highest PM concentrations were found in bile fluid and duodenum content followed by liver and kidney at both storage conditions with, besides duodenum content, comparatively stable concentrations over the PMI of 72 h. However, probably due to the physico-chemical properties of the NPA metabolite, being considerably more hydrophilic than the parent compound, analyses of AT specimens yielded negative results. Overall, only a slight tendency for a PMR was observed for *cumyl*-5F-P7AICA, with the metabolite not being susceptible to it under both environmental conditions. In order to conduct routine forensic toxicological analysis on PM specimens to investigate a possible influence of *cumyl*-5F-P7AICA on the occurrence of death, it is highly recommended that, besides the common specimens such as central and peripheral blood, also lung, bile fluid, and duodenum content are additionally drawn, especially in the case of a prolonged PMI. As *cumyl*-5F-P7AICA accumulates in AT, this also represents an appropriate matrix. Furthermore, if no peripheral blood is available, central blood can also be used for PM toxicological analysis as comparatively stable concentrations of the parent compound were observed over the entire PMI.

Taken together, the *in vivo* pig study provided many crucial and broad outcomes, especially in terms of the respective TK properties of strucuturally modified SCs containing a 7-azaindole core structure with a carboxamide linker. These findings might be very helpful to interpret toxicological findings among other things, also in the context of (fatal) intoxications and provide important assistance, in particular, if an expert opion, e.g. in DUID cases or after other criminal offenses, is required. Overall, the results presented show that, in contrast to 'older' SCs, in addition to phase I or II metabolites, the parent compound should also be implemented as a urinary target to prove the consumption of 7-azaindole-derived SCs. In comparison with various *in vitro* and *in vivo* models, pigs represent the most suitable model to elucidate the metabolic pattern of this class of SCs, as the metabolites formed are comparable to those found in human urine. After the development of a TK modeling approach, no relevant alteration in the TK properties were found for *cumyl*-5F-P7AICA with a carboxamide linker compared to those with a carbonyl moiety. Based on this TK model, the human exposure of *cumyl*-5F-P7AICA and its NPA metabolite were successfully predicted by allometric scaling. After elucidating the perimortem distribution pattern of *cumyl*-5F-P7AICA as well as its NPA metabolite, the time- and oxygen-dependent influence (water vs. air) on the PM stability and PMR of these two substances was investigated for the first time as part of the PM study carried out in the present work. Contrary to all expectations, only one statistically significant environment-dependent concentration change was found for *cumyl*-5F-P7AICA or the NPA metabolite each in the respective specimens indicating that both substances seem to be quite stable in PM specimens independent on the respective environmental conditions. In order to interpret PM toxicological findings of *cumyl*-5F-P7AICA that may have contributed to the occurrence of death, preservation of lung, bile fluid as well as duodenum content is highly recommended in addition to the standard specimens, such as peripheral blood, central blood, and urine. Furthermore, a controlled and reproducible *in vitro* EB sampling technique was successfully developed for the detection of *cumyl*-5F-P7AICA in EB based on the *in vivo* TK study setup. The developed sampling technique represents an auspicious approach to clarify the TK properties of NPS in EB in the context of TK studies using the pig model. However, the applicability should first be tested in a proof-of-concept study using the *in vivo* pig model.

5. References

1. Zou, S. & Kumar, U. Cannabinoid receptors and the endocannabinoid system: Signaling and function in the central nervous system. *Int J Mol Sci* **19**(3), 833, doi:10.3390/ijms19030833 (2018).
2. Alves, V. L., Gonçalves, J. L., Aguiar, J., Teixeira, H. M. & Câmara, J. S. The synthetic cannabinoids phenomenon: from structure to toxicological properties. A review. *Crit Rev Toxicol* **50**(5), 359–382, doi:10.1080/10408444.2020.1762539 (2020).
3. European Monitoring Centre for Drugs and Drug Addiction (EMCDDA). Synthetic cannabinoids in Europe. *Publications of the European Union* (2017). https://www.euda.europa.eu/publications/pods/synthetic-cannabinoids_en. (accessed June 2025)
4. European Monitoring Centre for Drugs and Drug Addiction (EMCDDA). European Drug Report 2024: Trends and Developments. *Publications of the European Union (2024).* https://www.emcdda.europa.eu/publications/european-drug-report/2024_en. (accessed June 2025)
5. Seely, K. A., Prather, P. L., James, L. P. & Moran, J. H. Marijuana-based drugs: innovative therapeutics or designer drugs of abuse? *Mol Interv* **11**(1), 36-51, doi:10.1124/mi.11.1.6 (2011).
6. Karila, L., Benyamina, A., Blecha, L., Cottencin, O. & Billieux, J. The synthetic cannabinoids phenomenon. *Curr Pharm Des* **22**(42), 6420–6425, doi:10.2174/1381612822666160919093450 (2016).
7. European Monitoring Centre for Drugs and Drug Addiction (EMCDDA). Understanding the 'Spice' Phenomenon. *Publications of the European Union* (2009). https://www.euda.europa.eu/publications/thematic-papers/understanding-spice-phenomenon_en. (accessed June 2025)
8. Fattore, L. & Fratta, W. Beyond THC: The new generation of cannabinoid designer drugs. *Front Behav Neurosci* **5**, 60, doi:10.3389/fnbeh.2011.00060 (2011).
9. Auwärter, V. *et al.* 'Spice' and other herbal blends: harmless incense or cannabinoid designer drugs? *J Mass Spectrom* **44**(5), 832–837, doi:10.1002/jms.1558 (2009).

10. Castaneto, M. S. *et al.* Synthetic cannabinoids: Epidemiology, pharmacodynamics, and clinical implications. *Drug Alcohol Depend* **144**, 12–41, doi:10.1016/j.drugalcdep.2014.08.005 (2014).
11. United Nations, Office on Drugs and Crime. Current NPS Threats Volume VII (2024). https://www.unodc.org/documents/scientific/Current_NPS_threats_VII.pdf. (accessed June 2025)
12. Diao, X. & Huestis, M. A. New synthetic cannabinoids metabolism and strategies to best identify optimal marker metabolites. *Front Chem* **7**, 109, doi:10.3389/fchem.2019.00109 (2019).
13. Shevyrin, V., Melkozerov, V., Endres, G. W., Shafran, Y. & Morzherin, Y. On a new cannabinoid classification system: A sight on the illegal market of novel psychoactive substances. *Cannabis Cannabinoid Res* **1**, 186–194, doi:10.1089/can.2016.0004 (2016).
14. Malaca, S., Busardò, F. P., Nittari, G., Sirignano, A. & Ricci, G. Fourth generation of synthetic cannabinoid receptor agonists: A review on the latest insights. *Curr Pharm Des* **28**(32), 2603–2617, doi:10.2174/1381612827666211115170521 (2021).
15. Andrews, R., Jorge, R., Christie, R. & Gallegos, A. From JWH-018 to OXIZIDS: Structural evolution of synthetic cannabinoids in the European Union from 2008 to present day. *Drug Test Anal* **15**(4), 378–387, doi:10.1002/dta.3422 (2023).
16. Debruyne, D. & Le Boisselier, R. Emerging drugs of abuse: current perspectives on synthetic cannabinoids. *Subst Abuse Rehabil* **6**, 113-129, doi:10.2147/SAR.S73586 (2015).
17. European Monitoring Centre for Drugs and Drug Addiction (EMCDDA) – Europol 2014. Report on the Implementation of Council Decision 2005/387/JHA. *Publications of the European Union* (2015). https://www.euda.europa.eu/publications/implementation-reports/2014_en. (accessed June 2025)
18. European Monitoring Centre for Drugs and Drug Addiction (EMCDDA) – Europol 2015. Report on the Implementation of Council Decision 2005/387/JHA. *Publications of the European Union* (2016). https://www.euda.europa.eu/publications/implementation-reports/2015_en. (accessed June 2025)

19. Angerer, V., Franz, F., Moosmann, B., Bisel, P. & Auwärter, V. 5F-Cumyl-PINACA in ‘e-liquids’ for electronic cigarettes: comprehensive characterization of a new type of synthetic cannabinoid in a trendy product including investigations on the in vitro and in vivo phase I metabolism of 5F-Cumyl-PINACA and its non-fluorinated analog Cumyl-PINACA. *Forensic Toxicol* **37**(1), 186–196, doi:10.1007/s11419-018-0451-8 (2019).
20. de Oliveira, M. C. *et al.* Toxicity of synthetic cannabinoids in K2/Spice: A systematic review. *Brain Sci* **13**(7), 990, doi:10.3390/brainsci13070990 (2023).
21. Giorgetti, A., Busardò, F. P., Tittarelli, R., Auwärter, V. & Giorgetti, R. Post-mortem toxicology: A systematic review of death cases involving synthetic cannabinoid receptor agonists. *Front Psychiatry* **11**, 464, doi:10.3389/fpsyt.2020.00464 (2020).
22. Ferrari Júnior, E. *et al.* Fatal cases involving new psychoactive substances and trends in analytical techniques. *Front Toxicol* **4**, 1033733, doi:10.3389/ftox.2022.1033733 (2022).
23. Mills, B., Yepes, A. & Nugent, K. Synthetic cannabinoids. *Am J Med Sci* **350**(1), 59-62 doi:10.1097/MAJ.0000000000000466 (2015).
24. Akram, H., Mokrysz, C. & Curran, H. V. What are the psychological effects of using synthetic cannabinoids? A systematic review. *J Psychopharmacol* **33**(3), 271–283, doi:10.1177/0269881119826592 (2019).
25. Prete, M. M., Feitosa, G. T. B., Ribeiro, M. A. T., Fidalgo, T. M. & Sanchez, Z. M. Adverse clinical effects associated with the use of synthetic cannabinoids: A systematic review. *Drug Alcohol Depend* **272**, 112698, doi:10.1016/j.drugalcdep.2025.112698 (2025).
26. Di, L. The impact of carboxylesterases in drug metabolism and pharmacokinetics. *Curr Drug Metab* **20**(2), 91–102, doi:10.2174/1389200219666180821094502 (2019).
27. Tamama, K. Advances in drugs of abuse testing. *Clin Chim Acta* **514**, 40–47, doi:10.1016/j.cca.2020.12.010 (2021).
28. Gorynski, K. A critical review of solid-phase microextraction applied in drugs of abuse determinations and potential applications for targeted doping testing. *Trends Anal Chem* **112**, 135–146, doi:10.1016/j.trac.2018.12.029 (2019).

29. Meyer, M. R. Trends in analyzing emerging drugs of abuse – from seized samples to body samples. *Anal Bioanal Chem* **406**(25), 6105–6110, doi:10.1007/s00216-014-8082-3 (2014).
30. Frederick, D. L. Toxicology testing in alternative specimen matrices. *Clin Lab Med* **32**(3), 467–492, doi:10.1016/j.cll.2012.06.009 (2012).
31. Manousi, N. & Samanidou, V. Green sample preparation of alternative biosamples in forensic toxicology. *Sustain Chem Pharm* **20**, 100388, doi:10.1016/j.scp.2021.100388 (2021).
32. Beck, O., Ullah, S. & Kronstrand, R. First evaluation of the possibility of testing for drugged driving using exhaled breath sampling. *Traffic Inj Prev* **20**(3), 238–243, doi:10.1080/15389588.2019.1584397 (2019).
33. da Costa, B. R. B. & De Martinis, B. S. Analysis of urinary VOCs using mass spectrometric methods to diagnose cancer: A review. *Clin Mass Spectrom* **18**, 27–37, doi:10.1016/j.clinms.2020.10.004 (2020).
34. Kintz, P., Villain, M. & Cirimele, V. Hair analysis for drug detection. *Ther Drug Monit* **28**(3), 442-446, doi:10.1097/01.ftd.0000211811.27558.b5 (2006).
35. Wada, M., Ikeda, R., Kuroda, N. & Nakashima, K. Analytical methods for abused drugs in hair and their applications. *Anal Bioanal Chem* **397**(3), 1039-1067, doi:10.1007/s00216-010-3569-z (2010).
36. Kintz, P. Hair analysis in forensic toxicology: An updated review with a special focus on pitfalls. *Curr Pharm Des* **23**(36), 5480-5486, doi:10.2174/1381612823666170929155628 (2017).
37. Kuwayama, K. *et al.* Development of the “selective concentration” analytical method for drug-containing hair regions based on micro-segmental analysis to identify a trace amount of drug in hair: hair analysis following single-dose ingestion of midazolam. *Forensic Toxicol* **39**, 156–166, doi:10.1007/s11419-020-00553-8 (2021).
38. Cuypers, E. & Flanagan, R. J. The interpretation of hair analysis for drugs and drug metabolites. *Clin Toxicol* **56**(2), 90–100, doi:10.1080/15563650.2017.1379603 (2018).
39. Vogliardi, S., Tucci, M., Stocchero, G., Ferrara, S. D. & Favretto, D. Sample preparation methods for determination of drugs of abuse in hair samples: A review. *Anal Chim Acta* **857**, 1–27, doi:10.1016/j.aca.2014.06.053 (2015).

40. Gallardo, E. & Queiroz, J. A. The role of alternative specimens in toxicological analysis. *Biomed Chromatogr* **22**(8), 795–821, doi:10.1002/bmc.1009 (2008).
41. Sobolesky, P. M. *et al.* Validation of a liquid chromatography-tandem mass spectrometry method for analyzing cannabinoids in oral fluid. *Clin Chim Acta* **491**, 30–38, doi:10.1016/j.cca.2019.01.002 (2019).
42. Aps, J. K. M. & Martens, L. C. Review: The physiology of saliva and transfer of drugs into saliva. *Forensic Sci Int* **150**(2-3), 119–131, doi: 10.1016/j.forsciint.2004.10.026 (2005).
43. Lee, D. & Huestis, M. A. Current knowledge on cannabinoids in oral fluid. *Drug Test Anal* **6**(1-2), 88–111, doi:10.1002/dta.1514 (2014).
44. Jacobs, C. M., Wagmann, L. & Meyer, M. R. Sample matrices for mass spectrometry-based adherence monitoring: A systematic critical review. *Ther Drug Monit* **46**(1), 6-15, doi: 10.1097/FTD.0000000000001145 (2023).
45. Fabritius, M., Staub, C., Mangin, P. & Giroud, C. Analysis of cannabinoids in oral fluid by liquid chromatography–tandem mass spectrometry. *Forensic Toxicol* **31**, 151–163, doi:10.1007/s11419-012-0168-z (2013).
46. Concheiro, M., Lee, D., Lendoiro, E. & Huestis, M. A. Simultaneous quantification of Δ9-tetrahydrocannabinol, 11-nor-9-carboxy-tetrahydrocannabinol, cannabidiol and cannabinol in oral fluid by microflow-liquid chromatography–high resolution mass spectrometry. *J Chromatogr A* **1297**, 123–130, doi:10.1016/j.chroma.2013.04.071 (2013).
47. Patton, J. S. & Byron, P. R. Inhaling medicines: delivering drugs to the body through the lungs. *Nat Rev Drug Discov* **6**(1), 67–74, doi:10.1038/nrd2153 (2007).
48. Hermans, C. & Bernard, A. Lung epithelium–specific proteins: characteristics and potential applications as markers. *Am J Respir Crit Care Med* **159**(2), 646–678, doi:10.1164/ajrccm.159.2.9806064 (1999).
49. López-Lorente, C. I., Awchi, M., Sinues, P. & García-Gómez, D. Real-time pharmacokinetics via online analysis of exhaled breath. *J Pharm Biomed Anal* **205**, 114311, doi:10.1016/j.jpba.2021.114311 (2021).
50. Issitt, T. *et al.* Volatile compounds in human breath: critical review and meta-analysis. *J Breath Res* **16**(2), 024001, doi:10.1088/1752-7163/ac5230 (2022).

51. Moura, P. C., Raposo, M. & Vassilenko, V. Breath volatile organic compounds (VOCs) as biomarkers for the diagnosis of pathological conditions: A review. *Biomed J* **46**(4), 100623, doi:10.1016/j.bj.2023.100623 (2023).
52. Kubáň, P. & Foret, F. Exhaled breath condensate: Determination of non-volatile compounds and their potential for clinical diagnosis and monitoring. A review. *Anal Chim Acta* **805**, 1–18, doi:10.1016/j.aca.2013.07.049 (2013).
53. van Velzen, P. *et al.* Exhaled breath profiles before, during and after exacerbation of COPD: A prospective follow-Up study. *COPD* **16**(5-6), 330–337, doi:10.1080/15412555.2019.1669550 (2019).
54. Sarbach, C. *et al.* Evidence of endogenous volatile organic compounds as biomarkers of diseases in alveolar breath. *Ann Pharm Fr* **71**(4), 203–215, doi:10.1016/j.pharma.2013.05.002 (2013).
55. Neerincx, A. H. *et al.* Breathomics from exhaled volatile organic compounds in pediatric asthma. *Pediatr Pulmonol* **52**(12), 1616–1627, doi: 10.1002/ppul.23785 (2017).
56. Beck, O., Sandqvist, S., Eriksen, P., Franck, J. & Palmskog, G. Method for determination of methadone in exhaled breath collected from subjects undergoing methadone maintenance treatment. *J Chromatogr B Analyt Technol Biomed Life Sci* **878**(24), 2255–2259, doi:10.1016/j.jchromb.2010.06.035 (2010).
57. Beck, O., Leine, K., Palmskog, G. & Franck, J. Amphetamines detected in exhaled breath from drug addicts: A new possible method for drugs-of-abuse testing. *J Anal Toxicol* **34**(5), 233–237, doi:10.1093/jat/34.5.233 (2010).
58. Beck, O., Sandqvist, S., Dubbelboer, I. & Franck, J. Detection of Δ9-tetrahydrocannabinol in exhaled breath collected from cannabis users. *J Anal Toxicol* **35**(8), 541–544, doi:10.1093/anatox/35.8.541 (2011).
59. Beck, O., Stephanson, N., Sandqvist, S. & Franck, J. Detection of drugs of abuse in exhaled breath from users following recovery from intoxication. *J Anal Toxicol* **36**(9), 638–646, doi:10.1093/jat/bks079 (2012).
60. Beck, O., Stephanson, N., Sandqvist, S. & Franck, J. Detection of drugs of abuse in exhaled breath using a device for rapid collection: comparison with plasma, urine and self-reporting in 47 drug users. *J Breath Res* **7**(2), 026006, doi:10.1088/1752-7155/7/2/026006 (2013).

61. Kintz, P., Mura, P., Jamey, C. & Raul, J.-S. Detection of ∆9-tetrahydrocannabinol in exhaled breath after cannabis smoking and comparison with oral fluid. *Forensic Toxicol* **35**, 173–178, doi:10.1007/s11419-016-0333-x (2017).
62. Arvidsson, M. *et al.* Pharmacokinetics of methylphenidate and ritalinic acid in plasma correlations with exhaled breath and oral fluid in healthy volunteers. *Eur J Clin Pharmacol* **76**(2), 229–237, doi:10.1007/s00228-019-02787-x (2020).
63. Meyer, M. R., Rosenborg, S., Stenberg, M. & Beck, O. First report on the pharmacokinetics of tramadol and O-desmethyltramadol in exhaled breath compared to plasma and oral fluid after a single oral dose. *Biochem Pharmacol* **98**(3), 502–510, doi:10.1016/j.bcp.2015.09.008 (2015).
64. Ellefsen, K. N. *et al.* Quantification of cocaine and metabolites in exhaled breath by liquid chromatography-high-resolution mass spectrometry following controlled administration of intravenous cocaine. *Anal Bioanal Chem* **406**(25), 6213–6223, doi:10.1007/s00216-014-8051-x (2014).
65. Himes, S. K. *et al.* Cannabinoids in exhaled breath following controlled administration of smoked cannabis. *Clin Chem* **59**(12), 1780–1789, doi:10.1373/clinchem.2013.207407 (2013).
66. Coucke, L., Massarini, E., Ostijn, Z., Beck, O. & Verstraete, A. G. Δ(9)-Tetrahydrocannabinol concentrations in exhaled breath and physiological effects following cannabis intake - A pilot study using illicit cannabis. *Clin Biochem* **49**(13-14), 1072–1077, doi:10.1016/j.clinbiochem.2016.06.003 (2016).
67. Lynch, K. L., Luo, Y. R., Hooshfar, S. & Yun, C. Correlation of breath and blood Δ(9)-tetrahydrocannabinol concentrations and release kinetics following controlled administration of smoked cannabis. *Clin Chem* **65**(9), 1171–1179, doi:10.1373/clinchem.2019.304501 (2019).
68. Manolis, A., McBurney, L. J. & Bobbie, B. A. The detection of Δ9-tetrahydrocannabinol in the breath of human subjects. *Clin Biochem* **16**(4), 229–233, doi:10.1016/s0009-9120(83)90070-x (1983).
69. Tinglev, Å. D. *et al.* Characterization of exhaled breath particles collected by an electret filter technique. *J Breath Res* **10**(2), 026001, doi:10.1088/1752-7155/10/2/026001 (2016).
70. Schaefer, N. *et al.* Time- and temperature-dependent postmortem concentration changes of the (synthetic) cannabinoids JWH-210, RCS-4, as well as ∆9-

tetrahydrocannabinol following pulmonary administration to pigs. *Arch Toxicol* **94**(5), 1585–1599, doi:10.1007/s00204-020-02707-4 (2020).

71. Doerr, A. A. *et al.* Can a recently developed pig model be used for in vivo metabolism studies of 7-azaindole-derived synthetic cannabinoids? A study using 5F-MDMB-P7AICA. *J Anal Toxicol* **45**(6), 593–604, doi:10.1093/jat/bkaa122 (2021).
72. Schaefer, N. *et al.* Distribution of the (synthetic) cannabinoids JWH-210, RCS-4, as well as ∆9-tetrahydrocannabinol following pulmonary administration to pigs. *Arch Toxicol* **93**(8), 2211–2218, doi:10.1007/s00204-019-02493-8 (2019).
73. Adamowicz, P., Zuba, D. & Sekuła, K. Analysis of UR-144 and its pyrolysis product in blood and their metabolites in urine. *Forensic Sci Int* **233**(1-3), 320–327, doi:10.1016/j.forsciint.2013.10.005 (2013).
74. McCain, K. R. *et al.* Impaired driving associated with the synthetic cannabinoid 5F-ADB. *J Forensic Sci Criminol* **6**(1), 105, doi:10.15744/2348-9804.6.105 (2018).
75. Scheidweiler, K. B., Jarvis, M. J. Y. & Huestis, M. A. Nontargeted SWATH acquisition for identifying 47 synthetic cannabinoid metabolites in human urine by liquid chromatography-high-resolution tandem mass spectrometry. *Anal Bioanal Chem* **407**(3), 883–897, doi:10.1007/s00216-014-8118-8 (2015).
76. Adamowicz, P. Blood concentrations of synthetic cannabinoids. *Clin Toxicol* **59**(3), 246–251, doi:10.1080/15563650.2020.1787429 (2021).
77. Brandon, E. F. A., Raap, C. D., Meijerman, I., Beijnen, J. H. & Schellens, J. H. M. An update on in vitro test methods in human hepatic drug biotransformation research: pros and cons. *Toxicol Appl Pharmacol* **189**(3), 233–246, doi:10.1016/s0041-008x(03)00128-5 (2003).
78. Guengerich, F. P. Common and uncommon cytochrome P450 reactions related to metabolism and chemical toxicity. *Chem Res Toxicol* **14**(6), 611–650, doi:10.1021/tx0002583 (2001).
79. Josephy, P. D., Guengerich, F. P. & Miners, J. O. “Phase I and Phase II” drug metabolism: Terminology that we should phase out? *Drug Metab Rev* **37**(4), 575–580, doi:10.1080/03602530500251220 (2005).
80. Jancova, P., Anzenbacher, P. & Anzenbacherova, E. Phase II drug metabolizing enzymes. *Biomed Pap Med Fac Univ Palacky Olomouc Czech Repub* **154**(2), 103–116, doi:10.5507/bp.2010.017 (2010).

81. Castaneto, M. S. *et al.* Synthetic cannabinoids pharmacokinetics and detection methods in biological matrices. *Drug Metab Rev* **47**(2), 124–174, doi:10.3109/03602532.2015.1029635 (2015).
82. Peters, F. T. Recent developments in urinalysis of metabolites of new psychoactive substances using LC-MS. *Bioanalysis* **6**(15), 2083–2107, doi:10.4155/bio.14.168 (2014).
83. Haschimi, B. *et al.* The novel psychoactive substance cumyl-CH-MEGACLONE: Human phase-I metabolism, basic pharmacological characterization and comparison to other synthetic cannabinoid receptor agonists with a γ-carboline-1-one core. *J Anal Toxicol* **45**(3), 277–290, doi:10.1093/jat/bkaa065 (2021).
84. Staeheli, S. N., Steuer, A. E. & Kraemer, T. Identification of urinary metabolites of the synthetic cannabinoid 5F-CUMYL-P7AICA in human casework. *Forensic Sci Int* **294**, 76–79, doi:10.1016/j.forsciint.2018.11.002 (2019).
85. Hutter, M. *et al.* Metabolism of nine synthetic cannabinoid receptor agonists encountered in clinical casework: Major in vivo phase I metabolites of AM-694, AM-2201, JWH-007, JWH-019, JWH-203, JWH-307, MAM-2201, UR-144 and XLR-11 in human urine using LC-MS/MS. *Curr Pharm Biotechnol* **19**(2), 144–162, doi:10.2174/1389201019666180509163114 (2018).
86. Su, M. K., Seely, K. A., Moran, J. H. & Hoffman, R. S. Metabolism of classical cannabinoids and the synthetic cannabinoid JWH-018. *Clin Pharmacol Ther* **97**(6), 562–564, doi:10.1002/cpt.114 (2015).
87. Nordmeier, F., Richter, L. H. J., Schmidt, P. H., Schaefer, N. & Meyer, M. R. Studies on the in vitro and in vivo metabolism of the synthetic opioids U-51754, U-47931E, and methoxyacetylfentanyl using hyphenated high-resolution mass spectrometry. *Sci Rep* **9**(1), 13774, doi:10.1038/s41598-019-50196-y (2019).
88. Richter, L. H. J., Flockerzi, V., Maurer, H. H. & Meyer, M. R. Pooled human liver preparations, HepaRG, or HepG2 cell lines for metabolism studies of new psychoactive substances? A study using MDMA, MDBD, butylone, MDPPP, MDPV, MDPB, 5-MAPB, and 5-API as examples. *J Pharm Biomed Anal* **143**, 32–42, doi:10.1016/j.jpba.2017.05.028 (2017).
89. Richter, L. H. J. *et al.* Tools for studying the metabolism of new psychoactive substances for toxicological screening purposes – A comparative study using pooled human liver S9, HepaRG cells, and zebrafish larvae. *Toxicol Lett* **305**, 73–80, doi:10.1016/j.toxlet.2019.01.010 (2019).

90. De Brabanter, N. *et al.* In vivo and in vitro metabolism of the synthetic cannabinoid JWH-200. *Rapid Commun Mass Spectrom* **27**(18), 2115–2126, doi: 10.1002/rcm.6673 (2013).
91. Gampfer, T. M. *et al.* Metabolism and cytotoxicity studies of the two hallucinogens 1cP-LSD and 4-AcO-DET in human liver and zebrafish larvae models using LC-HRMS/MS and a high-content screening assay. *J Pharm Biomed Anal* **245**, 116187, doi:10.1016/j.jpba.2024.116187 (2024).
92. Wagmann, L., Gampfer, T. M. & Meyer, M. R. Recent trends in drugs of abuse metabolism studies for mass spectrometry–based analytical screening procedures. *Anal Bioanal Chem* **413**(22), 5551–5559, doi:10.1007/s00216-021-03311-w (2021).
93. Schaefer, N. *et al.* Metabolic patterns of JWH-210, RCS-4, and THC in pig urine elucidated using LC-HR-MS/MS: Do they reflect patterns in humans? *Drug Test Anal* **9**(4), 613–625, doi:10.1002/dta.1995 (2017).
94. Park, Y. M., Meyer, M. R., Müller, R. & Herrmann, J. Drug administration routes impact the metabolism of a synthetic cannabinoid in the zebrafish larvae model. *Molecules* **25**(19), 4474, doi:10.3390/molecules25194474 (2020).
95. Hsin-Hung Chen, M. *et al.* Detection and characterization of the effect of AB-FUBINACA and its metabolites in a rat model. *J Cell Biochem* **117**(4), 1033–1043, doi:10.1002/jcb.25421 (2016).
96. Pasanen, M. Species differences in CYP enzymes. Monografías de la Real Academia Nacional de Farmacia (2004).
97. Schaefer, N. *et al.* Pharmacokinetics of (synthetic) cannabinoids in pigs and their relevance for clinical and forensic toxicology. *Toxicol Lett* **253**, 7–16, doi:10.1016/j.toxlet.2016.04.021 (2016).
98. Nordmeier, F. *et al.* Toxicokinetics of U-47700, tramadol, and their main metabolites in pigs following intravenous administration: is a multiple species allometric scaling approach useful for the extrapolation of toxicokinetic parameters to humans? *Arch Toxicol* **95**(12), 3681–3693, doi:10.1007/s00204-021-03169-y (2021).
99. Bode, G. *et al.* The utility of the minipig as an animal model in regulatory toxicology. *J Pharmacol Toxicol Methods* **62**(3), 196–220, doi:10.1016/j.vascn.2010.05.009 (2010).

100. Swindle, M. M., Makin, A., Herron, A. J., Clubb Jr, F. J. J. & Frazier, K. S. Swine as models in biomedical research and toxicology testing. *Vet Pathol* **49**(2), 344–356, doi:10.1177/0300985811402846 (2012).
101. Meurens, F., Summerfield, A., Nauwynck, H., Saif, L. & Gerdts, V. The pig: a model for human infectious diseases. *Trends Microbiol* **20**(1), 50–57, doi:10.1016/j.tim.2011.11.002 (2012).
102. Anzenbacher, P. *et al.* Presence and activity of cytochrome P450 isoforms in minipig liver microsomes. Comparison with human liver samples. *Drug Metab Dispos* **26**(1), 56–59, doi:10.1124/dmd.26.1.56 (1998).
103. Soucek, P., Zuber, R., Anzenbacherová, E., Anzenbacher, P. & Guengerich, F. P. Minipig cytochrome P450 3A, 2A and 2C enzymes have similar properties to human analogs. *BMC Pharmacol* **1**, 11, doi:10.1186/1471-2210-1-11 (2001).
104. Brunet, B. *et al.* Validation of large white pig as an animal model for the study of cannabinoids metabolism: Application to the study of THC distribution in tissues. *Forensic Sci Int* **161**(2-3), 169–174, doi:10.1016/j.forsciint.2006.04.018 (2006).
105. Sjögren, E., Bredberg, U. & Lennernäs, H. The pharmacokinetics and hepatic disposition of repaglinide in pigs: Mechanistic modeling of metabolism and transport. *Mol Pharm* **9**(4), 823–841, doi:10.1021/mp200218p (2012).
106. Nordmeier, F. *et al.* Are pigs a suitable animal model for in vivo metabolism studies of new psychoactive substances? A comparison study using different in vitro/in vivo tools and U-47700 as model drug. *Toxicol Lett* **329**, 12–19, doi:10.1016/j.toxlet.2020.04.001 (2020).
107. Doerr, A. A. *et al.* Toxicokinetic modelling of the synthetic cannabinoid 5F-MDMB-P7AICA and its main metabolite in pigs following pulmonary administration. *Br J Clin Pharmacol*, doi:10.1111/bcp.16340 (2024).
108. Franz, F. *et al.* In vitro metabolism of the synthetic cannabinoid 3,5-AB-CHMFUPPYCA and its 5,3-regioisomer and investigation of their thermal stability. *Drug Test Anal* **9**(2), 311–316, doi:10.1002/dta.1950 (2017).
109. Franz, F., Angerer, V., Moosmann, B. & Auwärter, V. Phase I metabolism of the highly potent synthetic cannabinoid MDMB-CHMICA and detection in human urine samples. *Drug Test Anal* **9**(5), 744–753, doi:10.1002/dta.2049 (2017).
110. Lobato-Freitas, C. *et al.* Overview of synthetic cannabinoids adb-fubinaca and amb-fubinaca: Clinical, analytical, and forensic implications. *Pharmaceuticals* **14**(3), 186, doi:10.3390/ph14030186 (2021).

111. Schaefer, N. *et al.* Development of an in-vitro drug delivery efficiency test for a pulmonary toxicokinetic pig study. *Curr Drug Deliv* **15**(8), 1167–1171, doi:10.2174/1567201815666180214130014 (2018).
112. Bend, J. R., Serabjit-Singh, C. J. & Philpot, R. M. The pulmonary uptake, accumulation, and metabolism of xenobiotics. *Annu Rev Pharmacol Toxicol* **25**, 97–125, doi:10.1146/annurev.pa.25.040185.000525 (1985).
113. Bakhle, Y. S. Pharmacokinetic and metabolic properties of lung. *Br J Anaesth* **65**(1), 79–93, doi:10.1093/bja/65.1.79 (1990).
114. Boer, F. Drug handling by the lungs. *Br J Anaesth* **91**(1), 50–60, doi:10.1093/bja/aeg117 (2003).
115. Newman, S. P. Drug delivery to the lungs: challenges and opportunities. *Ther Deliv* **8**(8), 647–661, doi:10.4155/tde-2017-0037 (2017).
116. Derendorf H, Gramatté T, Schaefer H. G. & Staab A. Pharmakokinetik Kompakt. Grundlagen und Praxisrelevanz. Wissenschaftliche Verlagsgesellschaft Stuttgart, Stuttgart (2011).
117. Benet, L. Z. & Zia-Amirhosseini, P. Basic principles of pharmacokinetics. *Toxicol Pathol* **23**(2), 115–123, doi:10.1177/019262339502300203 (1995).
118. Ahmed, T. A. Chapter 3: Pharmacokinetics of drugs following IV bolus, IV infusion, and oral administration. *In: Basic Pharmacokinetic Concepts and Some Clinical Applications* IntechOpen, London, United Kingdom, doi:10.5772/61573 (2015).
119. Martignoni, M., Groothuis, G. M. M. & de Kanter, R. Species differences between mouse, rat, dog, monkey and human CYP-mediated drug metabolism, inhibition and induction. *Expert Opin Drug Metab Toxicol* **2**(6), 875–894, doi:10.1517/17425255.2.6.875 (2006).
120. Allucent. What is Population Pharmacokinetic (popPK) Analysis? https://www.allucent.com/resources/blog/what-population-pharmacokinetic-poppk-analysis. (accessed June 2025)
121. Mould, D. R. & Upton, R. N. Basic concepts in population modeling, simulation, and model-based drug development—Part 2: Introduction to pharmacokinetic modeling methods. *CPT Pharmacometrics Syst Pharmacol* **2**(4), e38, doi:10.1038/psp.2013.14 (2013).

122. Kneisel, S., Teske, J. & Auwärter, V. Analysis of synthetic cannabinoids in abstinence control: long drug detection windows in serum and implications for practitioners. *Drug Test Anal* **6**(1-2), 135–136, doi:10.1002/dta.1445 (2014).
123. Schaefer, N. *et al.* Is adipose tissue suitable for detection of (synthetic) cannabinoids? A comparative study analyzing antemortem and postmortem specimens following pulmonary administration of JWH-210, RCS-4, as well as ∆9-tetrahydrocannabinol to pigs. *Arch Toxicol* **94**(10), 3421–3431, doi:10.1007/s00204-020-02843-x (2020).
124. Gurney, S. M. R., Scott, K. S., Kacinko, S. L., Presley, B. C. & Logan, B. K. Pharmacology, toxicology, and adverse effects of synthetic cannabinoid drugs. *Forensic Sci Rev* **26**(1), 53–78 (2014).
125. Shanks, K. G., Clark, W. & Behonick, G. Death associated with the use of the synthetic cannabinoid ADB-FUBINACA. *J Anal Toxicol* **40**(3), 236–239, doi:10.1093/jat/bkv142 (2016).
126. Adamowicz, P. Fatal intoxication with synthetic cannabinoid MDMB-CHMICA. *Forensic Sci Int* **261**, e5–e10, doi:10.1016/j.forsciint.2016.02.024 (2016).
127. Abouchedid, R. *et al.* Acute toxicity associated with use of 5F-derivations of synthetic cannabinoid receptor agonists with analytical confirmation. *J Med Toxicol* **12**(4), 396–401, doi:10.1007/s13181-016-0571-7 (2016).
128. Tait, R. J., Caldicott, D., Mountain, D., Hill, S. L. & Lenton, S. A systematic review of adverse events arising from the use of synthetic cannabinoids and their associated treatment. *Clin Toxicol* **54**(1), 1–13, doi:10.3109/15563650.2015.1110590 (2016).
129. Hutter, M., Moosmann, B., Kneisel, S. & Auwärter, V. Characteristics of the designer drug and synthetic cannabinoid receptor agonist AM-2201 regarding its chemistry and metabolism. *J Mass Spectrom* **48**(7), 885–894, doi:10.1002/jms.3229 (2013).
130. Wagmann, L., Stiller, R. G., Fischmann, S., Westphal, F. & Meyer, M. R. Going deeper into the toxicokinetics of synthetic cannabinoids: in vitro contribution of human carboxylesterases. *Arch Toxicol* **96**(10), 2755–2766, doi:10.1007/s00204-022-03332-z (2022).
131. Doerr, A. A. *et al.* Does a postmortem redistribution affect the concentrations of the 7 azaindole-derived synthetic cannabinoid 5F-MDMB-P7AICA in tissues and

body fluids following pulmonary administration to pigs? *Arch Toxicol* **98**(10), 3289– 3298, doi:10.1007/s00204-024-03815-1 (2024).

132. Skopp, G. Postmortem toxicology. *Forensic Sci Med Pathol* **6**(4), 314–325, doi:10.1007/s12024-010-9150-4 (2010).
133. Kennedy, M. C. Post-mortem drug concentrations. *Intern Med J* **40**(3), 183–187, doi:10.1111/j.1445-5994.2009.02111.x (2010).
134. Brockbals, L. *et al.* Time-dependent postmortem redistribution of opioids in blood and alternative matrices. *J Anal Toxicol* **42**(6), 365–374, doi:10.1093/jat/bky017 (2018).
135. Drummer, O. H. & Gerostamoulos, J. Postmortem drug analysis: Analytical and toxicological aspects. *Ther Drug Moni*t **24**(2), 199– 209, doi:10.1097/00007691-200204000-00002 (2002).
136. Gerostamoulos, D. *et al.* The effect of the postmortem interval on the redistribution of drugs: A comparison of mortuary admission and autopsy blood specimens. *Forensic Sci Med Pathol* **8**(4), 373–379, doi:10.1007/s12024-012-9341-2 (2012).
137. Pélissier-Alicot, A.-L., Gaulier, J.-M., Champsaur, P. & Marquet, P. Mechanisms underlying postmortem redistribution of drugs: a review. *J Anal Toxicol* **27**(8), 533–544, doi:10.1093/jat/27.8.533 (2003).
138. Leikin, J. B. & Watson, W. A. Post-mortem Toxicology: What the dead can and cannot tell us. *J Toxicol Clin Toxicol* **41**(1), 47–56, doi:10.1081/clt-120018270 (2003).
139. Dettmeyer, R. B., Schuetz, H. F. & Verhoff, M. A. Thanatologie. In: Schuetz, Verhoff, Dettmeyer (Ed.), Rechtsmedizin,2nd edn. Springer-Verlag, Berlin Heidelberg, p.19 (2014).
140. Vennemann, B. & Brinkmann, B. Der Tod im Wasser. *Rechtsmedizin* **13**, 201–215, doi:10.1007/s00194-003-0212-8 (2003).
141. Walle, N. *et al.* Comparison of in vitro and in vivo models for the elucidation of metabolic patterns of 7-azaindole-derived synthetic cannabinoids exemplified using cumyl-5F-P7AICA. *Drug Test Anal* **13**(1), 74–90, doi:10.1002/dta.2899 (2021).
142. Walle, N. *et al.* Development and method validation of a sampling technique for a reproducible detection of synthetic cannabinoids in exhaled breath using an in

vitro pig lung model. *J Anal Toxicol* **48**(9), 659– 666, doi:10.1093/jat/bkae078 (2024).

143. Walle, N. *et al.* Are the postmortem concentration changes of the synthetic cannabinoid cumyl-5F-P7AICA and its N-pentanoic acid metabolite dependent on the environmental conditions? – A systematic study following pulmonary administration to pigs. *Toxicol Lett* **401**, 170–180, doi:10.1016/j.toxlet.2024.10.006 (2024).
144. Walle, N. *et al.* Does a carboxamide moiety alter the toxicokinetics of synthetic cannabinoids? A study after pulmonary and intravenous administration of cumyl-5F-P7AICA to pigs. *Arch Toxicol* **99**(2), 633– 643, doi:10.1007/s00204-024-03906-z (2025).
145. Staeheli, S. N. *et al.* In vitro metabolism of the synthetic cannabinoids CUMYL-PINACA, 5F–CUMYL-PINACA, CUMYL-4CN-BINACA, 5F–CUMYL-P7AICA and CUMYL-4CN-B7AICA. *Drug Test Anal* **10**(1), 148–157, doi:10.1002/dta.2298 (2018).
146. Giorgetti, A. *et al.* Detection and phase I metabolism of the 7-azaindole-derived synthetic cannabinoid 5F-AB-P7AICA including a preliminary pharmacokinetic evaluation. *Drug Test Anal* **12**(1), 78–91, doi:10.1002/dta.2692 (2020).
147. Yeter, O. & Ozturk, Y. E. Metabolic profiling of synthetic cannabinoid 5F-ADB by human liver microsome incubations and urine samples using high-resolution mass spectrometry. *Drug Test Anal* **11**(6), 847–858, doi:10.1002/dta.2566 (2019).
148. Turpeinen, M. *et al.* Predictive value of animal models for human cytochrome P450 (CYP)-mediated metabolism: A comparative study in vitro. *Xenobiotica* **37**(12), 1367–1377, doi:10.1080/00498250701658312 (2007).
149. Taneja, I. *et al.* Species differences between rat and human in vitro metabolite profile, in vivo predicted clearance, CYP450 inhibition and CYP450 isoforms that metabolize benzanthrone: Implications in risk assessment. *Food Chem Toxicol* **111**, 94–101, doi:10.1016/j.fct.2017.11.009 (2018).
150. Watanabe, S., Kuzhiumparambil, U., Nguyen, M. A., Cameron, J. & Fu, S. Metabolic profile of synthetic cannabinoids 5F-PB-22, PB-22, XLR-11 and UR-144 by cunninghamella elegans. *AAPS J* **19**(4), 1148–1162, doi:10.1208/s12248-017-0078-4 (2017).

151. Wohlfarth, A. *et al.* Metabolism of synthetic cannabinoids PB-22 and its 5-fluoro analog, 5F-PB-22, by human hepatocyte incubation and high-resolution mass spectrometry. *Anal Bioanal Chem* **406**(6), 1763–1780, doi:10.1007/s00216-014-7668-0 (2014).
152. Wohlfarth, A. *et al.* First metabolic profile of XLR-11, a novel synthetic cannabinoid, obtained by using human hepatocytes and high-resolution mass spectrometry. *Clin Chem* **59**(11), 1638–1648, doi:10.1373/clinchem.2013.209965 (2013).
153. Mogler, L. *et al.* Phase I metabolism of the recently emerged synthetic cannabinoid CUMYL-PEGACLONE and detection in human urine samples. *Drug Test Anal* **10**(5), 886–891, doi:10.1002/dta.2352 (2018).
154. Erratico, C. *et al.* In vitro and in vivo human metabolism of the synthetic cannabinoid AB-CHMINACA. *Drug Test Anal* **7**(10), 866–876, doi:10.1002/dta.1796 (2015).
155. Christophersen, A. S. Tetrahydrocannabinol stability in whole blood: plastic versus glass containers. *J Anal Toxicol* **10**(4), 129–131, doi:10.1093/jat/10.4.129 (1986).
156. Kneisel, S., Speck, M., Moosmann, B. & Auwärter, V. Stability of 11 prevalent synthetic cannabinoids in authentic neat oral fluid samples: glass versus polypropylene containers at different temperatures. *Drug Test Anal* **5**(7), 602–606, doi:10.1002/dta.1497 (2013).
157. Schaefer, N. *et al.* Can toxicokinetics of (synthetic) cannabinoids in pigs after pulmonary administration be upscaled to humans by allometric techniques? *Biochem Pharmacol* **155**, 403–418, doi:10.1016/j.bcp.2018.07.029 (2018).
158. Kleis, J. *et al.* The synthetic cannabinoid 5F-MDMB-PICA: A case series. *Forensic Sci Int* **314**, 110410, doi:10.1016/j.forsciint.2020.110410 (2020).
159. Zawadzki, M., Chłopaś-Konowałek, A., Nowak, K., Wachełko, O. & Szpot, P. Quantification of 5F-CUMYL-P7AICA in blood and urine from an authentic fatality associated with its consumption by UHPLC–MS/MS. *Forensic Toxicol* **39**, 240–247, doi:10.1007/s11419-020-00555-6 (2021).
160. Halter, S. *et al.* Cumyl-PEGACLONE: A comparatively safe new synthetic cannabinoid receptor agonist entering the NPS market? *Drug Test Anal* **11**(2), 347–349, doi:10.1002/dta.2545 (2019).

161. Schaefer, N. *et al.* Distribution of synthetic cannabinoids JWH-210, RCS-4 and Δ 9-tetrahydrocannabinol after intravenous administration to pigs. *Curr Neuropharmacol* **15**(5), 713–723, doi:10.2174/1570159X15666161111114214 (2017).

6. Abbreviations

5F-MDMB-P7AICA	methyl 2-{[1-(5-fluoropentyl)-1H-pyrrolo[2,3-b]pyridin-3-yl]formamido}-3,3-dimethylbutanoate
AT	adipose tissue
AUC	area under the curve
CB	cannabinoid
Cl	clearance
cumyl-5F-PICA	1-(5-fluoropentyl)-N-(2-phenylpropan-2-yl)-1H-indole-3-carboxamide
cumyl-5F-PINACA	1-(5-fluoropentyl)-N-(2-phenylpropan-2-yl)-1H-indazole-3-carboxamide
cumyl-5F-P7AICA	1-(5-fluoropentyl)-N-(2-phenylpropan-2-yl)-1H-pyrrolo[2,3-b]pyridine-3-carboxamide
CYP	cytochrome P450 monooxygenase
DUID	driving under the influence of drugs
EB	exhaled breath
EMCDDA	European Monitoring Center for Drugs and Drug Addiction
GFF	glass fiber filter
i.v.	intravenous
JWH	John W. Huffman
JWH-018	1-Naphthyl-(1-pentylindol-3-yl)methanon
JWH-210	4-ethylnaphthalen-1-yl-(1-pentylindol-3-yl)methanone
LC-MS/MS	liquid chromatography-tandem mass spectrometry
NPA	*N*-pentanoic acid
NPS	new psychoactive substances
OF	oxidative defluorination
pHLM	pooled human liver microsomes
pHS9	pooled human liver S9 fraction
PLM	pig liver microsomes
PM	postmortem
PMI	postmortem interval
PMR	postmortem redistribution

pop	population
RCS-4	2-(4-methoxyphenyl)-1-(1-pentylindol-3-yl)methanone
RT	room temperature
SCs	synthetic cannabinoids
$t_{½}$	elimination half-life time
THC	Δ9-tetrahydrocannabinol
TK	toxicokinetic
V_d	volume of distribution
VOCs	volatile organic compounds